NBSIR 84-2943

New Concepts for Measuring Flame Spread Properties

J.G. Quintiere and
M. Harkleroad

U.S. DEPARTMENT OF COMMERCE
National Bureau of Standards
National Engineering Laboratory
Center for Fire Research
Gaithersburg, MD 20899

November 1984

Sponsored in part by:
U.S. Department of Transportation
Federal Aviation Administration
Technical Center
Atlantic City Airport, NJ 08405

NBSIR 84-2943

NEW CONCEPTS FOR MEASURING FLAME SPREAD PROPERTIES

J.G. Quintiere and
M. Harkleroad

U.S. DEPARTMENT OF COMMERCE
National Bureau of Standards
National Engineering Laboratory
Center for Fire Research
Gaithersburg, MD 20899

November 1984

Sponsored in part by:
U.S. Department of Transportation
Federal Aviation Administration
Technical Center
Atlantic City Airport, NJ 08405

U.S. DEPARTMENT OF COMMERCE, Malcolm Baldrige, *Secretary*
NATIONAL BUREAU OF STANDARDS, Ernest Ambler, *Director*

TABLE OF CONTENTS

LIST OF TABLES

LIST OF FIGURES

LIST OF FIGURES (continued)

LIST OF FIGURES (continued)

LIST OF FIGURES (continued)

LIST OF FIGURES (continued)

LIST OF FIGURES (continued)

NOMENCLATURE

b	parameter in eq. (5)
c	specific heat
C	parameter in eq. (12)
D	Damkohler number (see reference 1, 11, 12)
$F(t)$	thermal response function, eqns. (1, 2, 5)
g	gravitational acceleration
h	heat loss coefficient
h_c	convective heat transfer coefficient
k	thermal conductivity
ℓ	length scale
$\dot{q}''$	heat transfer per unit time and per unit area
$\dot{q}''_{o,ig}$	critical flux for ignition
$\dot{q}''_{o,s}$	critical flux for spread
$\dot{q}''_e$	external radiant flux
t	time
t_m	characteristic equilibrium time, eq. (5)
T	temperature
T_f	adiabatic flame temperature
T_∞	ambient and initial temperature
T_s	surface temperature before flame effects
T_{ig}	ignition temperature
$T_{s,min}$	minimum temperature for spread
V	flame (pyrolysis front) velocity
V_a	opposed gas velocity
x	distance along sample

y	coordinate normal to sample exposed surface
$Y_{ox,\infty}$	mass fraction of oxygen in ambient
ρ	density
Φ	flame heating parameter, eq. (8)
δ_f	flame length
σ	Stefan-Boltzmann constant

NEW CONCEPTS FOR MEASURING FLAME SPREAD PROPERTIES

J.G. Quintiere and M. Harkleroad

Abstract

An experimental procedure is described which can be used to derive data relevant to the prediction of ignition and flame spread on materials. It offers a direct method for determining material property data suitable for use in mathematical fire models. The apparatus utilizes a radiant heat source capable of supplying up to 6.5 W/cm^2 to a vertically oriented specimen. The test results pertain to piloted ignition of a vertical sample under constant and uniform irradiation, and to lateral flame spread on a vertical surface due to an external applied radiant heat flux. The results can be used to display the maximum velocity and ignition time as a function of irradiance. Critical or minimum irradiances for spread and ignition are determined. An empirical correlation, based on heat conduction principles, is found to correlate the ignition data and also provides a more general interpretation for the flame spread results. Further analyses of the data yield effective values for the thermal inertia of the material ($k\rho c$), its ignition temperature, and a parameter related to flame temperature. These parameters appear to be phenomenological constants for each material, rather than factors dependent on the apparatus. Results are presented for a wide range of materials. Suggestions for extending the results to other flame spread conditions are presented.

Key words: carpets; composites materials; fire tests; flame spread; ignition; material properties; measurements; plastics; wood

1. INTRODUCTION

Test methods for the flammability of materials differ widely among and within countries. Yet research on flame spread and ignition has developed to permit, at least conceptually, a universal framework for their description. Moreover, certain essential material data are needed to enable the researcher to assess his theories and correlations against experimental results. Consequently, it appears logical to organize that process so that material flammability tests might supply the data needed in theoretical models of ignition and flame spread. This paper will present such a process.

In considering flame spread it is realized that it depends on the orientation of the material and on the conditions of the surrounding fluid. It is interesting that several principal standard flammability tests consider distinct modes of flame spread. Generally, flame spread can be divided into spread in an opposed gas flow (i.e., the ambient gas flow is in the opposite direction to the propagating flame front) and spread in a concurrent flow (i.e., the local gas flow is in the same direction as the propagating flame). The opposed flow case is typified by ASTM E162, Standard Test Method for Surface Flammability of Materials Using a Radiant Heat Energy Source, in which the flame spread is downward on an inclined sample and the opposed flow is buoyancy-induced primarily by the flame. In contrast, ASTM E84, Standard Test Method for Surface Burning Characteristic of Burning Materials, is an example of concurrent spread along a ceiling-mounted material in which the ambient flow is held fixed. Also ASTM E648, Standard Test Method for Critical Radiant Flux of Floor-Covering Systems Using a Radiant Heat Energy Source, is another example of opposed flow spread under natural convection for an upward facing

horizontal surface. Except for ASTM E648, these test results are expressed in terms of indices which have no relationship to particular physical or chemical data. However, this does not preclude the possibility of an interpretation of these data in more scientific terms. To derive these scientific results mathematical solutions of the flame spread processes are needed.

The literature on flame spread and ignition is abundant, and reviews on flame spread by Fernandez-Pello and Hirano [1] and on ignition by Kanury [2] provide good sources of information. From results found there, and in particular from analyses by deRis [3] on opposed-flow spread and Sibulkin and Kim [4] on upward (concurrent) spread it can be shown that common combustible materials respond to flame spread and to ignition (for exposures >2 W/cm^2) as thermally thick materials for thicknesses greater than approximately 1 mm. Thus, the semi-infinite-solid solutions for ignition and spread will most often apply, and may even apply to thin materials on a thick substrate where some effective properties of the composite solid must be considered. Yet, under low heat transfer conditions, as would occur in the early development of compartment fires, the thickness of the solid and the conditions at its back surface are important to its temperature rise. Thus, under these developing fire conditions, the upstream surface temperature can be assumed to be the initial temperature of the solid. In other words, even when a temperature gradient is present in the solid only about 1 mm of its depth responds to the flame heat transfer and the temperature over that depth represents the initial temperature. Fernandez-Pello [5] has shown that this is a valid representation for downward spread under external radiant heating.

From an examination of the simplest solutions for flame spread [3,4] under the thermally thick assumption, several common parameters emerge. One is the product of the solid's conductivity, density and specific heat ($k\rho c$); another is a critical surface temperature to produce fuel vapors from the solid - this can be considered as an "ignition temperature". Since the theoretical results do not consider melting, charring, regression, or temperature effects on the solid's properties, the parameter $k\rho c$ must be considered as an effective property when such theories are applied to realistic flame spread conditions. Also, the ignition temperature must be viewed as a modeling parameter in the formula, rather than the exact surface temperature of the solid when a flammable mixture is produced. Moreover, both of these parameters occur in the simplest models for ignition [2]. Hence the determination of these quantities offer a consistent way of relating test data to theoretical models. For flame spread, however, these two parameters are not sufficient to describe the various modes of spread. From deRis' result for opposed flow spread, at least a flame temperature is required; and for concurrent spread, the downstream flame length and flame heat transfer to the surface are required [4]. The former case is perhaps resolvable, and will be examined here. The prospects of resolving the latter case will be discussed later.

The present work considers a method for deriving the parameters: $k\rho c$, ignition temperature, and a flame temperature factor, suitable for use in models for piloted ignition and opposed flow flame spread. The apparatus used here was developed by Robertson [6]; subsequent studies [7,8,9] describe the evolution of the use of the apparatus and the interpretation of its results. Here, we attempt to provide a more general interpretation of these previous results, a compilation of results for a wide range of materials, and a guide for others who wish to explore this procedure.

2. EXPERIMENTAL PROCEDURE

The apparatus consists basically of a gas-fired (air-natural gas) radiant panel and a framed sample-holder assembly to contain a vertically oriented sample. A schematic of the arrangement is shown in figure 1. The radiant panel is inclined from the sample orientation so as to yield an incident heat flux distribution along the center of the sample as shown in figure 2. By varying the fuel-air flow rate to the panel, the incident heat flux at 50 mm could be varied from 1.5 to 7 W/cm^2. Thus, the normalized heat flux result in figure 2 represents the geometric radiation factor for this apparatus, and served as a calibration reference in subsequent flame spread measurements.

2.1 Ignition

Ignition results were obtained for small samples mounted over the 0 to 110 mm region of nearly uniform heat flux as shown in figures 1 and 2. Initially the incident heat flux was measured at the 50 mm position. Once stable conditions were recorded, the sensor was removed and the sample was mechanically mounted in place. The mounting process could be done in several seconds or less, so that ignition times of this magnitude will be subject to uncertainty. It was found important to upwardly extend the plane of the sample surface with a steel plate. This enabled the boundary layer containing the pyrolyzed gases and the induced air flow to be maintained above the sample. An acetylene-air pilot flame located approximately 25 mm from the top of the sample and 5 mm from the steel extension plate interrupted this boundary layer mixture. This plate and pilot arrangement insured a sustained pilot flame, ignition based on the mixture concentration generated at the

sample, and a propensity for flame propagation upstream through the boundary layer to the sample face. Sustained ignition was noted and its time recorded when continuous combustion was visible at the center of the specimen. In most cases this was unambiguous, but on approaching the minimum flux for ignition ($\dot{q}''_{o,ig}$), oscillatory or incomplete surface combustion was sometimes observed. In some cases of, for example, melting or delaminating materials, judgement was necessary in deciding on a primary ignition time when spurious effects occurred. The data were recorded for a series of decreasing flux conditions until a minimum flux, below which ignition would not occur, was found. An example of a typical set of results is shown in figure 3 for fiber insulation board. Here, no ignition would occur below 1.4 W/cm^2.

2.2 Flame Spread

A test for flame spread was initiated by selecting the proper external heat flux at the 50 mm position. If the ignition pilot flame was used, the external heat flux was required to exceed the minimum flux for ignition. The optimum procedure is to adjust $\dot{q}''(50)$ to be slightly greater than $\dot{q}''_{o,ig}$. In obtaining the flame spread data, it should be realized that the ignition process itself is unimportant, but $\dot{q}''(50)$ must be greater than $\dot{q}''_{o,ig}$. Indeed, several ignition techniques were explored and two distinct processes will be illustrated.

The sample size for flame spread spans the frame length as shown in figure 1. Once the external heat flux was set and stabilized, the calibration board was removed and the sample was inserted in place. This was done manually and took several seconds. Following sample ignition, a flame propa-

gated in the direction of decreasing external flux (figure 2). Its position (x) was recorded as a function of time measured from the instant of sample insertion. Varying degrees of curvature of the flame front were observed so that the flame position was based on the centerline of the sample. The curvature of the propagating front was primarily caused by the nature of its initial shape following ignition. It was not obviously dependent on sample edge or air flow effects. Except near extinction, the curved front advanced uniformly. These mid-front positions were recorded until the flame stopped. Two examples of results are shown in figures 4 and 5. Figure 4 illustrates results for a fiberglass-based roofing shingle in which $\dot{q}''_e(50)$ was set at 3.0 W/cm^2 compared to its $\dot{q}''_{o,ig}$ of 2.1 W/cm^2. The ignition pilot was used and ignited the sample in slightly more than one minute. The results in figure 5 are for a hardboard wood product which was exposed to a heat flux distribution of $\dot{q}''_e(50)$ = 3.0 W/cm^2 for more than 11 minutes before a pilot flame initiated ignition. This long pre-heating method was used to insure that thermal equilibrium would exist under flame spread conditions. Although considerable charring and gasification occurs under long preheat conditions over the region where $\dot{q}''_e(x) > \dot{q}''_{o,ig}$, this should not affect the flame spread results. To ignite the sample in this case a small diffusion flame was slowly moved along the bottom edge of the sample in the x-direction until ignition occurred. The idea was to initiate the flame spread process at $T_s(x) = T_{ig}$. Regardless of the ignition process, surface flame spread will only occur where the external heating conditions cause surface temperatures less than the ignition temperature. Once ignition temperature is reached at the surface this implies that sufficient degradation (volatilization, charring, etc.) is present to sustain ignition. Hence the introduction of a pilot flame at these conditions will cause surface ignition. Although rapid gas-phase propagation is perceived in

the preheating operational mode, it does not relate to "surface" flame spread and the data are not recorded or are applicable as such. Most of the data were taken when either of these two ignition techniques was used to initiate flame spread. In both cases a preheating time at a position x was achieved before the arrival of the flame front. It will be shown that the analysis of the data can account for these variations in preheat times.

2.3 Sample Preparation

All samples tested were conditioned at approximately 55% relative humidity and 20-22°C. Aluminum foil was wrapped around the edges and back to prevent the release of volatiles from these surfaces. The samples were supported in the spring-loaded frame by a calcium silicate board 13 mm thick. Other backing materials of lower density and conductivity were employed to a limited extent and were found to have an insignificant effect on the results.

3. ANALYSIS

The objectives in analyzing the data have been to seek consistent results for a material, to simplify the process of analysis, and to generalize the results beyond the context of the test apparatus. Since a test procedure has evolved with practice, no attempt has been made to standardize testing, to automate the data analysis, or to evaluate statistical deviations. The emphasis has been on describing the physical significance of the data and streamlining the procedure. The following analysis forms the bare essence of the general features of ignition and flame spread. It is intended as a framework for interpreting data in a generally useable form for prediction. It

does not purport to address all possible factors that could represent a specific material. Where features, such as melting, variable properties, and diathermancy, are present they would be accounted for by effective values of the properties in the simple inert thermal model described subsequently.

3.1 Ignition

The framework for analyzing and interpreting the ignition data is the thermal conduction model for ignition with a critical surface temperature. This is fully discussed by Kanury [2] and was utilized successfully by Simms [10] in ignition studies of wood materials. Those results suggest that the form of solution for the surface temperature (T_s) under constant external radiant heat flux ($\dot{q}''_e$) can be given as

$$T_s - T_\infty = \frac{\dot{q}''_e}{h} F(t) \tag{1}$$

where T_∞ is the ambient and initial temperature, h is the surface heat loss coefficient, and F(t) is a function of time and thermal properties of the solid. Although an exact expression can be given for F(t) under conditions of constant properties and a thermally thick (semi-infinite) or a finite thick solid, it will be determined empirically. This approach is motivated by the limits of the thermally thick solid solution, and by the preponderant form of the ignition results in these tests. For the semi-infinite solid under these heating conditions it can be shown [7] that

$$F(t) = \begin{cases} \dfrac{2h\sqrt{t}}{\sqrt{\pi k \rho c}}, & t \to \text{small} \\ 1, & t \to \text{large} \end{cases} \tag{2}$$

The thermal model for ignition is that $T_s = T_{ig}$ at ignition, and thus the ignition time can be determined from an expression of the form of eq. (1). Moreover, the critical radiant flux is found at long time where F(t) becomes asymptotic to unity. Thus, from eq. (1)

$$\dot{q}''_{o,ig} = h\left(T_{ig} - T_\infty\right) \tag{3}$$

when $F(t) \to 1$. Here, the heat loss coefficient is understood to include both radiative and convective effects. In general, the steady-state energy balance which holds after long heating time can be written as follows:

$$\dot{q}''_e - \dot{q}''_k = \varepsilon\sigma\left(T_s^4 - T_\infty^4\right) + h_c\left(T_s - T_\infty\right) \equiv h\left(T_s - T_\infty\right) \tag{4}$$

where $\dot{q}''_k$ is the conductive loss into the solid due to its finite thickness, ε is the surface emissivity which is usually greater than 0.8 for common combustibles under infra-red conditions, and h_c is the convective heat transfer coefficient. For the conditions and materials used in this study it can be estimated that $\dot{q}''_k$ is less than ten percent of $\dot{q}''_e$.

Surface temperature measurements as a function of external radiant flux are shown in figure 6 for several materials. The idealized material represents $\dot{q}''_k = 0$ and $\varepsilon \approx 1$ while a low bulk density aircraft panel and a wood particle board demonstrate departure from the ideal conditions. A theoretical result based on $\varepsilon = 1$ and $h_c = 15$ W/m^{2}K, characteristic of the natural convection conditions in the test apparatus, provides a good overall fit to the idealized data. It is assumed that this theoretical curve, applicable to the test apparatus, can be used to infer surface temperature for a material under

long-time heating conditions. Thus, from an experimental determination of $\dot{q}''_{o,ig}$, T_{ig} can be found from the theoretical curve in figure 6 and h can be subsequently computed from eq. (3). The data in figure 6 suggest that the true surface temperature can be as much as 50°C below the inferred idealized temperature.

Within the framework of eqns. (1-3), an empirical result has been found to successfully describe all of the ignition results from the apparatus. The results have been correlated by the expression

$$\frac{\dot{q}''_{o,ig}}{\dot{q}''_e} = F(t) = \begin{cases} b\sqrt{t}, & t \leq t_m \\ 1, & t \geq t_m \end{cases} \qquad (5)$$

where, for each material, b is a constant, and t_m is a characteristic time indicative of the time to reach thermal equilibrium since $F(t) = 1$ at $t = t_m$. An example of a typical fit to the data is shown in figure 7 for the results of the fiber insulation board (figure 3). The parameters b and t_m are found from the slope and intercept, respectively. This correlation, although not theoretically justified, must account for variable property effects which are significant for the range of temperatures encountered; and must account for the effect of heat losses from the back of the sample and the backing board. Thus this result is characteristic of the apparatus to some extent.

Having obtained eq. (5) to represent the ignition results, it can be related to the thermally thick result in eq. (2). Since eq. (5) implies the results hold for small times as well as up to t_m, then the parameter b can be related to $k\rho c$. Hence an effective $k\rho c$ can be computed:

$$k\rho c = \frac{4}{\pi}\left(\frac{h}{b}\right)^2. \tag{6}$$

Here, the value for h is determined at T_{ig} from eq. (3).

3.2 Flame Spread

The formula derived by deRis [3] for the thermally thick case can be used as a framework to analyze and generalize the flame spread data. That result, modified to account for an elevated solid temperature, is given as

$$V = \frac{V_a\,(k\rho c)_g\,(T_f - T_{ig})^2}{k\rho c\,(T_{ig} - T_s)^2} \tag{7}$$

where $(k\rho c)_g$ refers to the gas-phase properties, T_f is the flame temperature, and V_a is the opposed flow gas velocity. Several studies, both experimental and theoretical [1], have used this formula to correlate results for a wide range of conditions including chemical kinetic effects which reduce the spread velocity to a point where extinction occurs. Notable among them are the work of Fernandez-Pello et al [11] who examined the affect of ambient oxygen concentration and opposed velocity on flame spread over horizontal PMMA, and the work of Altenkirch et al [12] who examined the effects of oxygen, gravity, and pressure on the downward spread over PMMA. These studies show that the spread velocity normalized by the value given in eq. (7), for which T_f is computed as the stoichiometric adiabatic flame temperature, is solely a function of a Damkohler number (D) which represents the ratio of the residence time of the gas in the flame to the chemical reaction time. Thus, they find that this dimensionless spread velocity decreases from a value of approximately one to some finite value at extinction as D decreases, or in other

words, as chemical kinetic effects become relatively more important. These results provide important guidance for generalizing opposed flow spread results for a wide range of conditions, but do not address their applicability to different materials.

In order to deal with differences among materials, eq. (7) is represented in this analysis as

$$V = \frac{\Phi}{k\rho c \left(T_{ig} - T_s\right)^2} \tag{8}$$

where Φ can be considered to represent the numerator of eq. (7) and any effects of the Damkohler number under the test conditions. Thus Φ depends on the test conditions, but some insight can be given to extending it. For example, under the lateral (or downward) spread conditions in the apparatus, V_a, is induced by natural convection, and that characteristic velocity is given by [3]

$$V_a = \left[\frac{\left(\frac{k}{\rho c}\right)_g g \left(T_f - T_\infty\right)}{T_\infty}\right]^{1/3} . \tag{9}$$

For typical values in air (e.g., $T_f = 2080°C$, $T_\infty = 22°C$, $(k/\rho c)_g = 0.216 \times 10^4$ m^2/s, $g = 9.8$ m/s^2), it is found that V_a is 11 cm/s, a value consistent with measurements [2]. Also, opposed flow speeds of this magnitude or less tend to have an insignificant effect on the spread rate [11]. Thus, this suggests that the natural convection conditions of the apparatus configuration mitigate effects of V_a on the results, in contrast to the sensitivity of spread rate to V_a at high oxygen concentrations. But extension to higher flow speeds in air must require a modification of Φ based

on its dependence on V_a in accordance with the correlations of Fernandez-Pello et al [11].

Another factor influencing Φ is seen to be the flame temperature. Under stoichiometric and adiabatic conditions it can be shown [12] that this temperature is approximately given by

$$T_f = \frac{Y_{ox,\infty} \Delta H_{ox}}{c_g} \tag{10}$$

where $Y_{ox,\infty}$ is the ambient oxygen concentration, c_g is the specific heat of the gas, and ΔH_{ox} is the heat of combustion per unit mass of oxygen which is generally a constant (13 kJ/g) for most fuels. Equations (7), (8) and (10) suggest that Φ depends on $Y^n_{ox,\infty}$ where $n \geq 2$, and in fact it is found that n increases as extinction conditions are approached [1]. Moreover, the effects of non-adiabaticity, decreasing Damkohler number, and other departures from the ideal conditions assumed in eq. (7) should decrease Φ. Under natural convection conditions with values for PMMA at $Y_{ox,\infty} = 0.23$ with an adiabatic flame temperature of 2080°C and an ignition temperature of 390°C [11], Φ was computed as 10. $(kW)^2/m^3$. Thus it is expected that Φ should range from this order of magnitude to smaller values for materials tested in air under natural convection conditions. For other conditions the value of Φ must be modified accordingly.

Eq. (8) then forms the basis for analyzing the test data. For direct application it must be put in terms of the heating conditions encountered in the apparatus. Several assumptions are necessary. First, it is assumed that one dimensional conduction applies at any position x as shown in figure 2.

From figure 2, an appropriate length scale in the x-direction which accounts for the flux distribution was taken as

$$\ell_x = \frac{\dot{q}''_e(x)/\dot{q}''(50)}{\frac{d}{dx}\left[\dot{q}''_e(x)/\dot{q}''(50)\right]} \tag{11}$$

which can be greater than 200 mm. If ℓ_y is taken as the thickness of the material, say $\ell_y \leq 10$ mm; then conduction in the x-direction compared to conduction in the y-direction is $(\ell_y/\ell_x)^2 \leq 1/400$. Hence the one dimensional assumption is justifiable. Second, the surface temperature rise is assumed to be given by eq. (1) where F(t) is given by eq. (5). This is an empirical, but reasonable approximation, as illustrated by the results shown in figure 8 for particle board and in figure 9 for an aircraft honeycomb multi-layered panel. The measured values for F(t) were computed from surface temperatures using eq. (1) for several $\dot{q}''_e$ conditions. These are the same materials illustrated in figure 6 at steady-state conditions. With these assumptions, (i.e., using eqs. (1) and (3)) eq. (8) is expressed as

$$V^{-1/2} = C\left(\dot{q}''_{o,ig} - \dot{q}''_e(x) \cdot F(t)\right), \tag{12}$$

where C is a constant related to Φ. This equation can be used to analyze the flame spread data as illustrated in figures 4 and 5. Although F(t) must be determined from the ignition data, $\dot{q}''_{o,ig}$ can be found directly from the spread data as well as from the ignition data. The process proceeds as follows. The local slope of the position-time data is computed to yield the velocity as a function of x or equivalently $\dot{q}''_e(x)$. Herein, a three-point running least-squares fit was used to find V. The function F(t) is applied to $\dot{q}''_e$ at the corresponding flame position and elapsed time from the initiation of heating.

By plotting these results as $V^{-1/2}$ against $\dot{q}''_e$ F(t), both C, the slope, and $\dot{q}''_{o,ig}$, the intercept, can be found. Figures 10 and 11 illustrate this process for the data corresponding to the fiberglass shingle of figure 4 and the hardboard of figure 5, respectively. For the shingle F(t) < 1 for most of the data, while F(t) = 1 for all of the data from the hardboard test. Although not clearly shown by these data, it is common to find departures from this $V^{-1/2}$ relationship at large values of $V^{-1/2}$ where extinction sometimes appears to cause a greater negative slope, and at small values of $V^{-1/2}$ where greater uncertainties are likely in the data. Nevertheless, this analysis yields $\dot{q}''_{o,ig}$, C and $\dot{q}''_{o,s}$, the minimum external flux for spread.

Agreement between $\dot{q}''_{o,ig}$ found from this process and $\dot{q}''_{o,ig}$ found from the ignition experiments demonstrates consistency and the complementary relationship between piloted ignition and flame spread. Having found these values, their counterparts in the temperature formulation can be computed. It follows from eqns. (1), (3), (6), (8) and (12) that

$$\Phi = \frac{4}{\pi} /(Cb)^2. \tag{13}$$

A minimum surface temperature for spread ($T_{s,min}$) can be found from figure 6 and $\dot{q}''_{o,s}$, the irradiance at the position the flame stops.

4. RESULTS

Although the parameters Φ, $k\rho c$, T_{ig} and $T_{s,min}$ are the most useful in generalizing these results, it is interesting to consider the maximum spread velocity (F(t) = 1) and the ignition time as a function of the external

radiant heat flux. This might be considered as a "flammability diagram" for the material over the range of heating conditions in the apparatus. It applies under conditions of constant irradiance and for flame spread under long heating times. Several of these diagrams are shown for a varied set of materials: plywood (figure 12), rigid polyurethane foam (figure 13), gypsum board (figure 14), an asphalt shingle (figure 15), and a polycast polymethylmethacrylate (PMMA) (figure 16). All are shown at the same coordinate scales, the analytical curves according to the values of C, b, etc. are shown with the data, and only velocity data for which $F(t) = 1$ or $t \geq t_m$ is plotted. These results show a range of heating conditions, $\dot{q}''_{o,s} \leq \dot{q}''_e \leq \dot{q}''_{o,ig}$, over which only opposed flow flame spread can occur; and a domain, $\dot{q}''_e > \dot{q}''_{o,ig}$, for which only piloted ignition is possible. Of course, flame spread can occur for $\dot{q}''_e > \dot{q}''_{o,ig}$, but only for heating times below which $T_s < T_{ig}$. Since $\dot{q}''_{o,ig}$ is considered to be the same for ignition and flame spread in the theory, the vertical asymptotic values of the spread and ignition results should coincide. The extent to which they do indicates the consistency in the results and perhaps their accuracy as well.

A more extensive listing of results is given in table 1. It should be pointed out that the materials tested came from several sources, all of whom were interested in the performance of these materials in fire. In many cases, therefore, additional measurements were made for these materials. In table 1 the materials have been listed by their generic names and grouped into categories of woods, plastics, carpets and composites (laminates). Painted surfaces have been included with the wood materials. Except for the hardboard painted with nitrocellulose paint, all of the laminated materials displayed a single flame front. However, delamination of the surface coating preceded

flame spread for some laminates. The case of the nitrocellulose paint displayed an initial rapid surface spread due to the paint. This was then followed by a slower spread with continued burning behind the front. Only this latter result has been reported due to the rapidity of the first phenomenon. The results presented in table 1 can be used to construct the flammability diagrams as shown in figures 12-16. The applicability of these diagrams depends on the heating conditions. In contrast, table 2 lists results that are more general and can be construed as "flame spread properties". There, the results are ordered in terms of ignition temperature. These results, the ignition temperature, the minimum temperature for spread, the effective $k\rho c$, and the Φ value, all can be used to predict piloted ignition and opposed flow spread under natural convection conditions regardless of the heating conditions. Only the surface temperature need be computed for the specific heating conditions. Also it is recognized that an estimation of $k\rho c$ from eq. (2) and the ignition data reported may be too approximate to be acceptable. Consequently, $\Phi/k\rho c$ is reported to skirt this possible uncertainty since $\Phi/k\rho c$ is the primary parameter needed anyway. Moreover, when ignition data were not recorded for a material, the ignition temperature and $\Phi/k\rho c$ values were derived for table 2 by using the flame spread data alone. In all other cases T_{ig} was derived from the ignition data. In many cases the flame spread results were derived from several tests in which the heating conditions varied with respect to irradiance and pre-heating times.

5. DISCUSSION

Although no direct check on the kρc values was attempted, a compilation of thermal properties for common materials under normal environmental conditions is given in table 3. Those values for kρc appear to be generally lower than the correspondingly similar materials listed in table 2. Several reasons can be offered to explain why kρc derived from ignition data and eq. (2) will be higher than the associated ambient value for kρc. Firstly, both k and c increase with temperature, and thus some higher than ambient temperature value must be used to compute temperature rise to ignition. Secondly, ignition requires the production of a gaseous fuel from the heated solid. Thus, the enthalpy changes required in pyrolysis, vaporization, and melting in some instances must be included in the derived kρc values. These endothermic effects will be reflected in an increase in the kρc parameter for an inert thermal ignition model. Thirdly, the kρc values may be higher due to effects of sample thickness and the heat sink effects of the support board behind the sample. Except for these last sources of error, which should be further examined, it would appear that the derived kρc values are the proper values to use in the flame spread models that utilize an inert-ignition temperature model for the solid. In summary the kρc values of table 2 appear somewhat high but credible under the circumstances of the models.

The results tabulated for the ignition temperatures appear plausible since values quoted in the literature for PMMA and cellulosics range from 300 to 400°C for piloted conditions [1,2]. Of course, these values should not necessarily be construed as precise surface temperatures, just approximate indications thereof. This follows because T_{ig} is a derived temperature from

an approximate model. As long as the piloting conditions and models of ignition and flame spread are consistent with inert solid models, it is probably a good general value to use. Moreover, since the ignition temperature is just a surrogate condition for a gas-phase flammability limit, it is possible to expect that it may depend to some extent on sample size and orientation and on oxygen concentration. For example, it may increase somewhat for charring materials as the oxygen concentration is reduced since more fuel will be necessary to produce a combustible mixture, but solid oxidation effects may offset this increase.

The values for Φ are particularly intriguing. If one examines the correlations of Fernandez-Pello et al [11] and Altenkirch et al [12], Φ can be expressed as

$$\Phi = V_a (k\rho c)_g (T_f - T_{ig})^2 f(D) \qquad (14)$$

where f(D) is a function of the Damkohler number. The flame temperature (T_f) represents the energy available and although the adiabatic flame temperature is nearly constant for most hydrocarbons, it will decrease with a reduction of oxgyen in the atmosphere or an addition of an inert diluent to the solid. The f(D) will contain the chemical kinetic effects and the gas transport times available for combustion as dependent on V_a. As the oxygen concentration is reduced, D, and also f(D) at least for PMMA [1], are sharply reduced. Previously, a reference value for Φ was computed as 10 $(kW)^2/m^3$ based on T_f = 2080°C, T_{ig} = 390°C, V_a = 11 cm/s and $Y_{ox,\infty}$ = 0.23 nominally representative of PMMA spreading under opposed flow natural convection conditions. The results in table 2 show Φ ranges from roughly 1 to 15 $(kW)^2/m^3$.

Sufficient data are not available to assess these results against the dimensionless correlations for spread rate in terms of D since they are only available for PMMA [11,12]. Nevertheless, the range of values inferred for Φ from the PMMA correlations appears consistent with the results for all the materials in table 2 since f(D) for PMMA ranges from approximately 0.1 to slightly greater than 1. Although this consistency may be fortuitous it does offer some credibility and perhaps insight into the magnitude of Φ. Of course, the computation of Φ does depend on the estimate for kpc (or b) so that any uncertainties in that estimation will affect the value for Φ.

Table 2 also lists the minimum surface temperature ($T_{s,min}$) required for spread under the conditions of the experiment. It was computed using figure 6 from the critical external irradiance at the position at which the flame stopped. This generally occurred at a finite spread velocity, or in other words, the flame spread velocity does not approach zero continuously as the surface temperature approaches $T_{s,min}$. Borgeson and Tien [13] have developed a theoretical model for a thin fuel which shows these same characteristics. They found that as the surface temperature is decreased, the gas phase combustion zone at the leading edge of the flame recedes in the direction of the opposed air flow. The reduction in forward heat transfer and a decrease in the pyrolysis zone appears responsible for the cessation of flame spread. Of course, for the range of fuels listed in tables 1 and 2, other effects could be responsible for extinction. Indeed, surface heat losses in charring materials, and significant regression effects for some of the foam plastics could be contributory. In any case, this temperature limit is a significant characteristic, and in fact, is related to the measurement of results in ASTM E648. It should be noted, however, that due to the limits of the flux condi-

tions in the apparatus, values of $T_{s,min} < 80°C$ could apply to much lower temperatures.

Extended use of the results in table 2 might be considered in practical engineering analyses of fire spread. Current knowledge must be used to guide the necessary assumptions. For example, the results here show that the same ignition temperature can be used to describe piloted ignition and opposed flow flame spread. Thus, it might be assumed that the same value would be applicable under concurrent spread conditions. If the ambient oxygen or flow velocity varies, it is necessary to infer resultant changes in opposed flow spread from the Damkohler-number correlations [11,12]. As a first approximation, for natural convection conditions in room fires, the values of Φ in table 2 might be modified by $\left(Y_{ox,\infty}/0.233\right)^2$ to account for vitiation conditions. Under concurrent flow spread conditions, Sibulkin and Kim [4] derived an approximate expression for spread velocity over a thermally thick solid which is given as

$$V = \frac{(\dot{q}")^2 \ \delta_f}{k\rho c \ (T_{ig} - T_s)^2} \tag{15}$$

where $\dot{q}"$ is the average flame heat flux over the surface downstream of the pyrolysis zone, and δ_f represents the flame length over this heated region. Thus, to utilize this formula in an analysis of fire growth it will be necessary to understand the behavior of $\dot{q}"$ and δ_f in terms of material properties and environmental conditions. Although this is feasible, it has not yet been demonstrated. Nevertheless, the denominator can be estimated from the current results of table 2.

6. CONCLUSIONS

It has been shown that it is feasible to derive ignition and flame spread properties for a wide range of materials. Ignition temperatures range from about 250 to 600°C, may be overestimated by 50°C at most, and consistent values were found for piloted ignition and flame spread. The derived $k\rho c$ values applicable to flame spread over thermally thick solids tend to be higher, but in relative agreement, with literature values for similar materials under normal room conditions. A parameter Φ has been defined which is representative of the available flame energy, and applies to opposed flow flame spread. These three parameters respectively correspond to (1) the conditions necessary for combustion (T_{ig}), (2) the time response of the material to heat ($k\rho c$), and (3) the energy available for spread (Φ). Evidence suggests that these properties, although not fundamental, can be generally used in mathematical models to predict the performance of materials. Although the results given here only apply to natural convection conditions in opposed air flow, extension to other environmental conditions or to concurrent flow spread is possible.

7. ACKNOWLEDGMENTS

The authors are indebted to Dr. A.F. Robertson for the basic design of the apparatus. Mr. D. Walton was responsible for obtaining much of the heat transfer data for the apparatus. Various people and organizations contributed materials for analysis. They include the following: (1) A.F. Robertson, materials tested by ISO (International Standards Organization); (2) Bjorn Sundstrom (National Testing Institute, Boras, Sweden) materials used in room

fire studies; (3) E. Braun, materials used in solar energy applications; (4) B. Lee, materials used in evaluating a standard room fire test; (5) J. White of Weyerhauser; and (6) T. Eklund of the Federal Aviation Administration (FAA) Technical Center. Several others assisted in gathering and processing the data; namely, D. Corley, R. Sumner, and B. Cooper.

This work was partially supported by the FAA Technical Center, Atlantic City, NJ.

8. REFERENCES

[1] Fernandez-Pello, A.C. and Hirano, T., Combustion Science Technology, Vol. 32, Nos. 1-4, June 1983, pp. 1-31.

[2] Kanury, A. Murty, "Ignition of Cellulosic Solids - A Review", Fire Research Abstracts and Reviews, Factory Mutual Research Corporation, Vol. 14, No. 1, 1972, pp. 24-72.

[3] DeRis, J.N., Twelth Symposium (International) on Combustion, The Combustion Institute, 1969, pp. 241-252.

[4] Sibulkin, M. and Kim, J., Combustion Science and Technology, Vol. 17, 1977, pp. 39-49.

[5] Fernandez-Pello, A.C., Combustion Science and Technology, Vol. 17, 1977, pp. 1-9.

[6] Robertson, A.F., "A Flammability Test Based on Proposed ISO Spread of Flame Test", Third Progress Report, Intergovernmental Maritime Consultative Organization, IMCO FP/215, 1979.

[7] Quintiere, J., Fire and Materials, Vol. 5, No. 2, 1981, pp. 52-60.

[8] Quintiere, J., Harkleroad, M. and Walton, D., Combustion Science and Technology, Vol. 32, 1983, pp. 67-89.

[9] Harkleroad, M., Quintiere, J. and Walton, D., "Radiative Ignition and Opposed Flow Flame Spread Measurements on Materials", DOT/FAA/CT-83/28, Atlantic City Airport, NJ, August 1983.

[10] Simms, D.L., Combustion and Flame, Vol. 7, September 1963, pp. 253-261.

[11] Fernandez-Pello, A.C., Ray, S.R. and Glassman, I., Eighteenth Symposium (International) on Combustion, The Combustion Institute, Pittsburg, PA, 1981, p. 519.

[12] Altenkirch, R.A., Eichhorn, R. and Rigvi, A.R., Combustion Science and Technology, Vol. 32, 1983, pp. 49-66.

[13] Borgeson, R.A. and Tien, J.S., Combustion Science and Technology, Vol. 32, 1983, pp. 125-136.

Table 1

Ignition and Flame Spread Characteristics Under Constant Irradiance Conditions

Material	$q_{o,s}$ (W/cm^2)	C $\left(\frac{s}{mm}\right)^{1/2}\left(\frac{cm^2}{W}\right)$	$q_{o,ig}$ [1] (W/cm^2)	$q_{o,ig}$ [2] (W/cm^2)	b ($s^{-1/2}$)	t_m (s)
Plywood, Plain (0.635cm)	0.4	1.8	1.2	1.6	0.07	190.
Plywood, Plain (1.27cm)	0.3	1.5	1.4	1.6	0.07	225.
Plywood, FR (1.27cm)	*	*	*	4.4	0.10	110.
Hardboard (6.35mm)	0.4	5.8	1.0	1.0	0.03	1190.
Hardboard (3.175mm)	0.1	2.2	1.3	1.4	0.05	420.
Hardboard (S159M)	0.1	1.8	1.5	--	--	--
Hardboard (gloss paint), (3.4mm)	1.1	4.1	1.8	1.7	0.05	468.
Hardboard (nitrocellulose paint)	0.4	2.0	2.1	1.7	0.06	306.
Particle Board (1.27cm stock)	0.9	3.2	1.7	1.8	0.05	342.
Douglas Fir Particle Board (1.27cm)	0.6	2.0	1.7	1.6	0.05	395.
Chipboard (S118M)	0.4	2.2	1.6	—	--	--
Wood Panel (S178M)	0.4	1.1	1.6	--	--	--
Fiber Insulation Board	0.6	3.4	1.4	1.4	0.07	205.
Fiberboard, low density (S119M)	0.1	1.3	1.2	--	--	--
Polyisocyanurate (5.08cm)	0.9	0.4	1.7	2.1	0.36	8.
Polystyrene (5.08cm)	*	*	*	4.6	0.14	53.

Material	$q_{o,s}$ (W/cm^2)	C $\left(\frac{s}{mm}\right)^{1/2}\left(\frac{cm^2}{W}\right)$	$q_{o,ig}$ [1] (W/cm^2)	$q_{o,ig}$ [2] (W/cm^2)	b ($s^{-1/2}$)	t_m (s)
Polyurethane (S353M)	0.2	1.0	0.9	--	--	--
Polycarbonate (1.52mm)	2.2	1.5	3.0	3.0	0.06	260.
Foam, Rigid (2.54cm)	0.6	0.6	2.0	2.0	0.32	100.
Foam, Flexible (2.54cm)	0.2	1.2	1.2	1.6	0.09	132.
PMMA Type G (1.27cm)	0.1	2.0	1.6	1.5	0.05	456.
PMMA Polycast (1.59mm)	0.3	3.4	1.0	0.9	0.04	462.
Carpet #1 (wool, stock)	2.1	1.5	2.5	2.3	0.18	32.
Carpet #2 (wool, untreated)	1.2	1.2	1.6	2.0	0.11	83.
Carpet #2 (wool, treated)	1.4	3.2	1.6	2.2	0.12	72.
Carpet (nylon/wood blend)	0.8	1.7	1.8	1.8	0.06	248.
Carpet (acrylic)	0.4	1.8	1.1	1.0	0.06	250.
Gypsum Board, (common) (1.27mm)	1.9	0.9	3.5	3.5	0.11	87.
Gypsum Board, FR (1.27cm)	1.0	1.1	2.1	2.8	0.10	95.
Gypsum Board, Wall Paper (S142M)	0.7	5.8	1.0	1.8	0.07	208.
Mineral Wool, Textile Paper (S160M)	0.2	1.2	1.7	--	--	--
Asphalt Shingle	0.3	2.7	1.6	1.5	0.06	306.
Fiberglass Shingle	1.8	1.5	2.7	2.1	0.08	161.
GRP (2.24mm)	0.1	1.3	2.0	1.6	0.09	132.
GRP (1.14mm)	1.4	2.9	1.6	1.7	0.06	279.
Aircraft Panel Epoxy Fiberite	*	*	*	2.8	0.13	57.

1. From spread data
2. From ignition data

* Flame spread was not measureable

-- Data were not taken

Note: Values are only significant to two places

Table 2

Flame Spread Properties

Material	(T_{ig}) (°C)	$(k\rho c)$ $(kW/m^2K)^2s$	(Φ) $(kW)^2/m^3$	$(T_{s,min})$ (°C)	$(\Phi/k\rho c)$ (mK^2/s)
PMMA Polycast (1.59mm)	278.	0.73	5.45	120.	8.
Polyurethane (S353M)	280.	—	—	105.	82.
Hardboard (6.35mm)	298.	1.87	4.51	170.	2.
Carpet (acrylic)	300.	0.42	9.92	165.	24.
Fiberboard, low density (S119M)	330.	—	—	90.	42.
Fiber Insulation Board	355.	0.46	2.25	210.	5.
Hardboard (3.175mm)	365.	0.88	10.97	40.	12.
Hardboard (S159M)	372.	—	—	80.	18.
PMMA Type G (1.27cm)	378.	1.02	14.43	90.	14.
Asphalt Shingle	378.	0.70	5.38	140.	8.
Douglas Fir Particle Board (1.27cm)	382.	0.94	12.75	210.	14.
Wood Panel (S178M)	385.	—	—	155.	43.
Plywood, Plain (1.27cm)	390.	0.54	12.91	120.	24.
Chipboard (S118M)	390.	—	—	180.	11.
Plywood, Plain (0.635cm)	390.	0.46	7.49	170.	16.
Foam, Flexible (2.54cm)	390.	0.32	11.70	120.	37.
GRP (2.24mm)	390.	0.32	9.97	80.	31.
Mineral Wool, Textile Paper (S160M)	400.	—	—	105.	34.
Hardboard (gloss paint), (3.4mm)	400.	1.22	3.58	320.	3.
Hardboard (nitrocellulose paint)	400.	0.79	9.81	180.	12.
GRP (1.14mm)	400.	0.72	4.21	365.	6.

Table 2 cont'd

Material	(T_{ig}) (°C)	$(k\rho c)$ $(kW/m^2K)^2s$	(Φ) $(kW)^2/m^3$	$(T_{s,min})$ (°C)	$(\Phi/k\rho c)$ (mK^2/s)
Particle Board (1.27cm stock)	412.	0.93	4.27	275.	5.
Gypsum Board, Wall Paper (S142M)	412.	0.57	0.79	240.	1.
Carpet (Nylon/Wool Blend)	412.	0.68	11.12	265.	16.
Carpet #2 (Wool, untreated)	435.	0.25	7.32	335.	30.
Foam, Rigid (2.54cm)	435.	0.03	4.09	215.	141.
Polyisocyanurate (5.08cm)	445.	0.02	4.94	275.	201.
Fiberglass Shingle	445.	0.50	9.08	415.	18.
Carpet #2 (Wool, treated)	455.	0.24	0.89	365.	4.
Carpet #1 (Wool, stock)	465.	0.11	1.83	450.	17.
Aircraft Panel Epoxy Fiberite	505.	0.24	*	505.	*
Gypsum Board, FR (1.27cm)	510.	0.40	9.25	300.	23.
Polycarbonate (1.52mm)	528.	1.16	14.74	455.	13.
Gypsum Board, (common) (1.27mm)	565.	0.45	14.44	425.	32.
Plywood, FR (1.27 cm)	620.	0.76	*	620.	*
Polystyrene (5.08cm)	630.	0.38	*	630.	*

* Flame spread was not measureable

— Data were not taken

Note: Values are only significant to two places

Table 3. Properties of Common Materials*

Material	Density ρ (kg/m^3)	Conductivity $k \times 10^3$ (kW/m-K)	Specific Heat c (kJ/kg-K)	$k\rho c$ $(kW/m^2-K)^2 s$
Concrete, stone	2200	1.7	0.75	2.8
Polymethylmethacrylate (PMMA)	1200	0.26	2.1	0.66
Gypsum board	950	0.17	1.1	0.18
Calcium silicate board	700	0.11	1.1	0.085
Particle board	650	0.11	2.0	0.14
Plywood	540	0.12	2.5	0.16
Cork board	200	0.040	1.9	0.015
Balsa wood	160	0.050	2.9	0.023
Polyurethane, rigid	32	0.020	1.3	0.0008
Polystyrene, expanded	20	0.034	1.5	0.0010

*Compiled from various sources.

APPARATUS

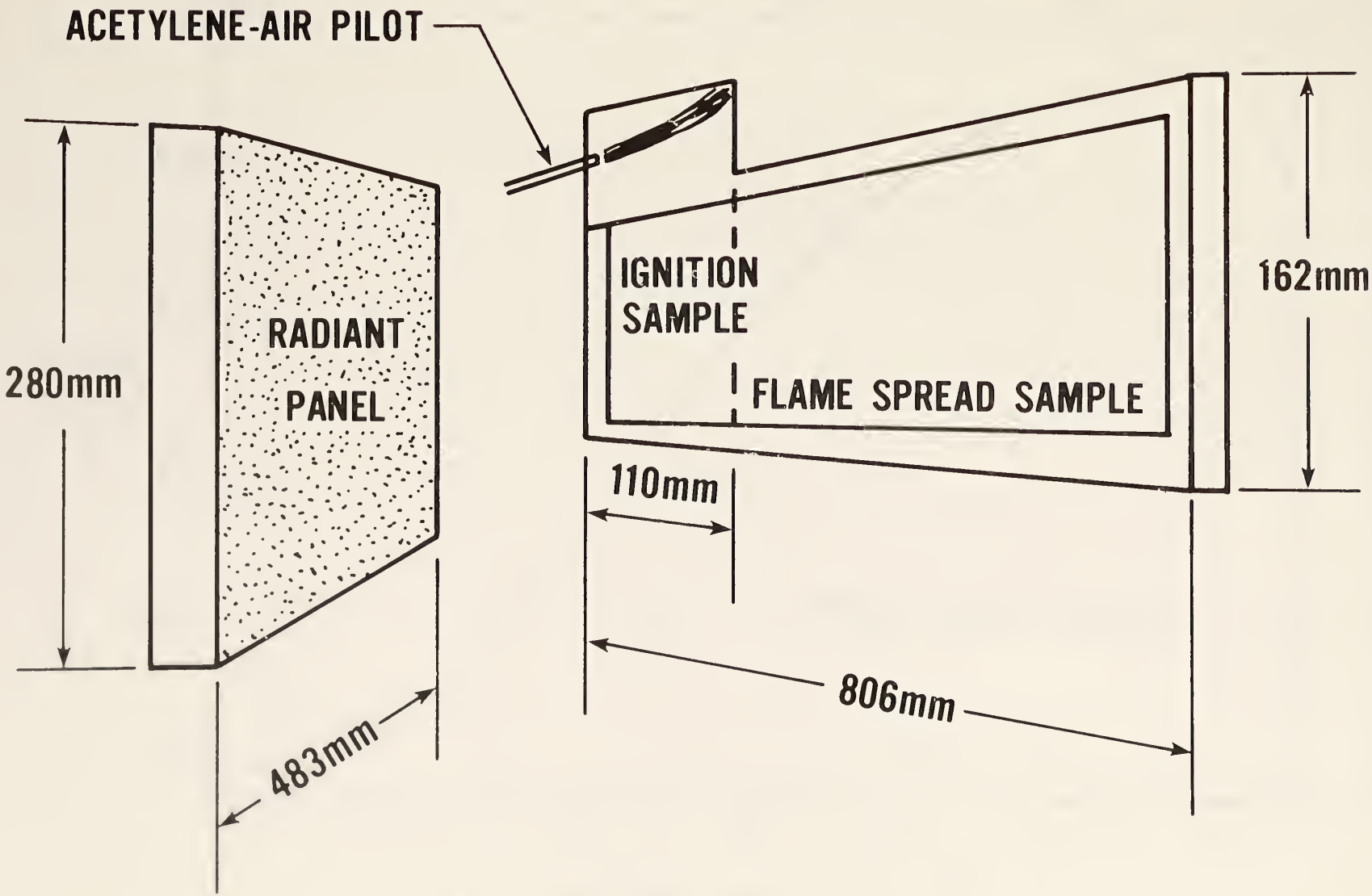

Figure 1. Schematic of test apparatus.

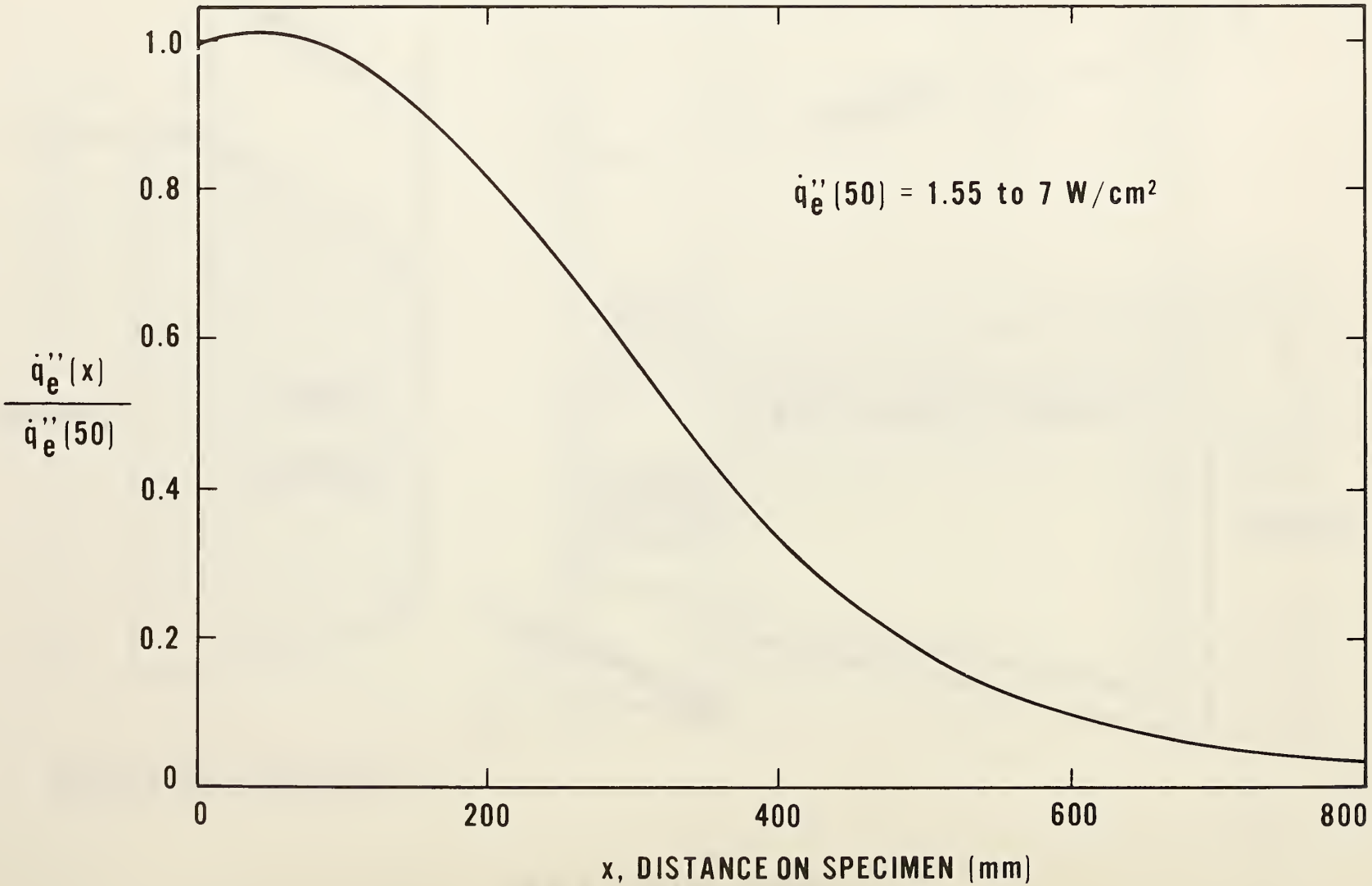

Figure 2. Normalized irradiance over the sample.

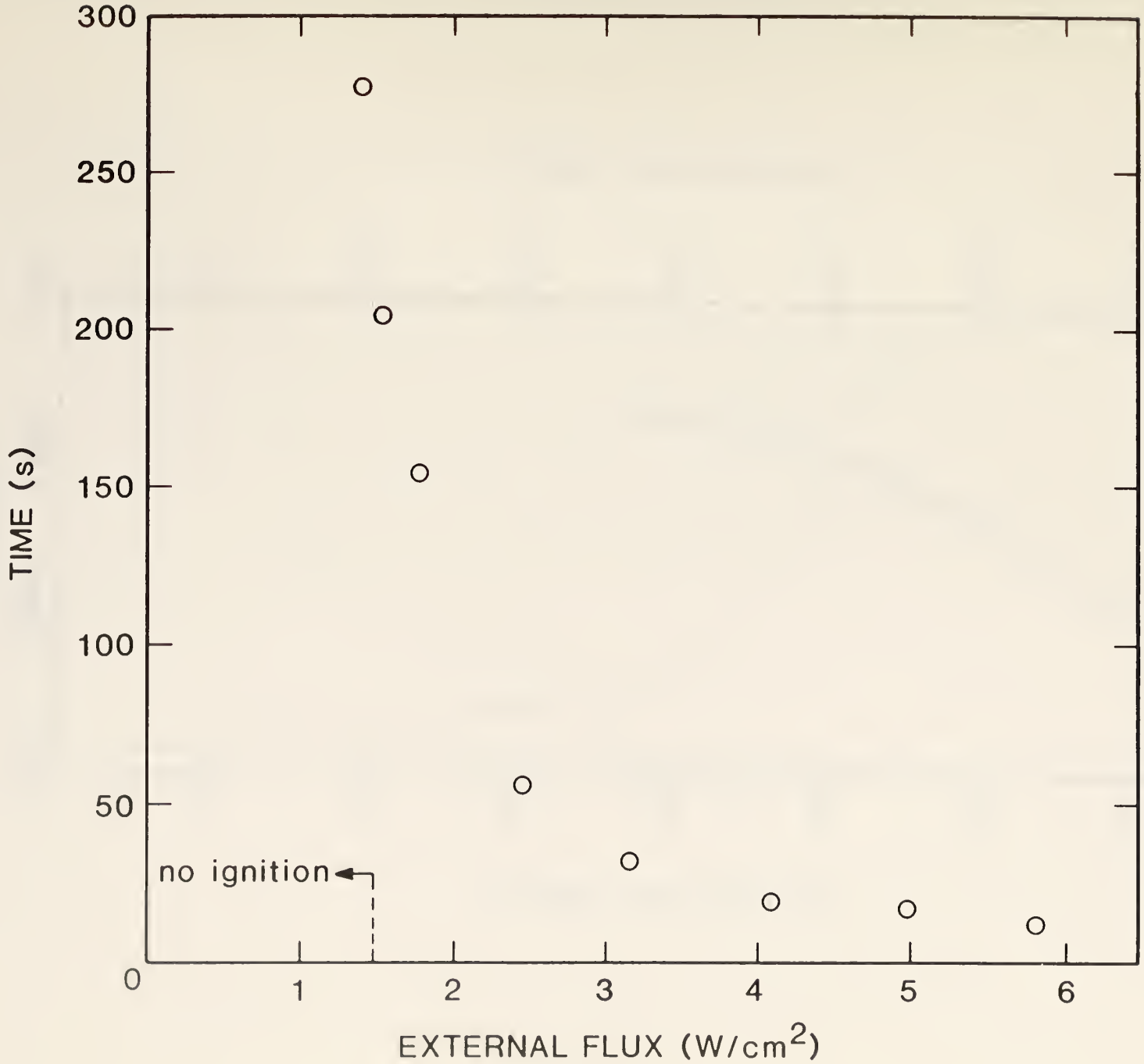

Figure 3. Ignition results for fiberboard.

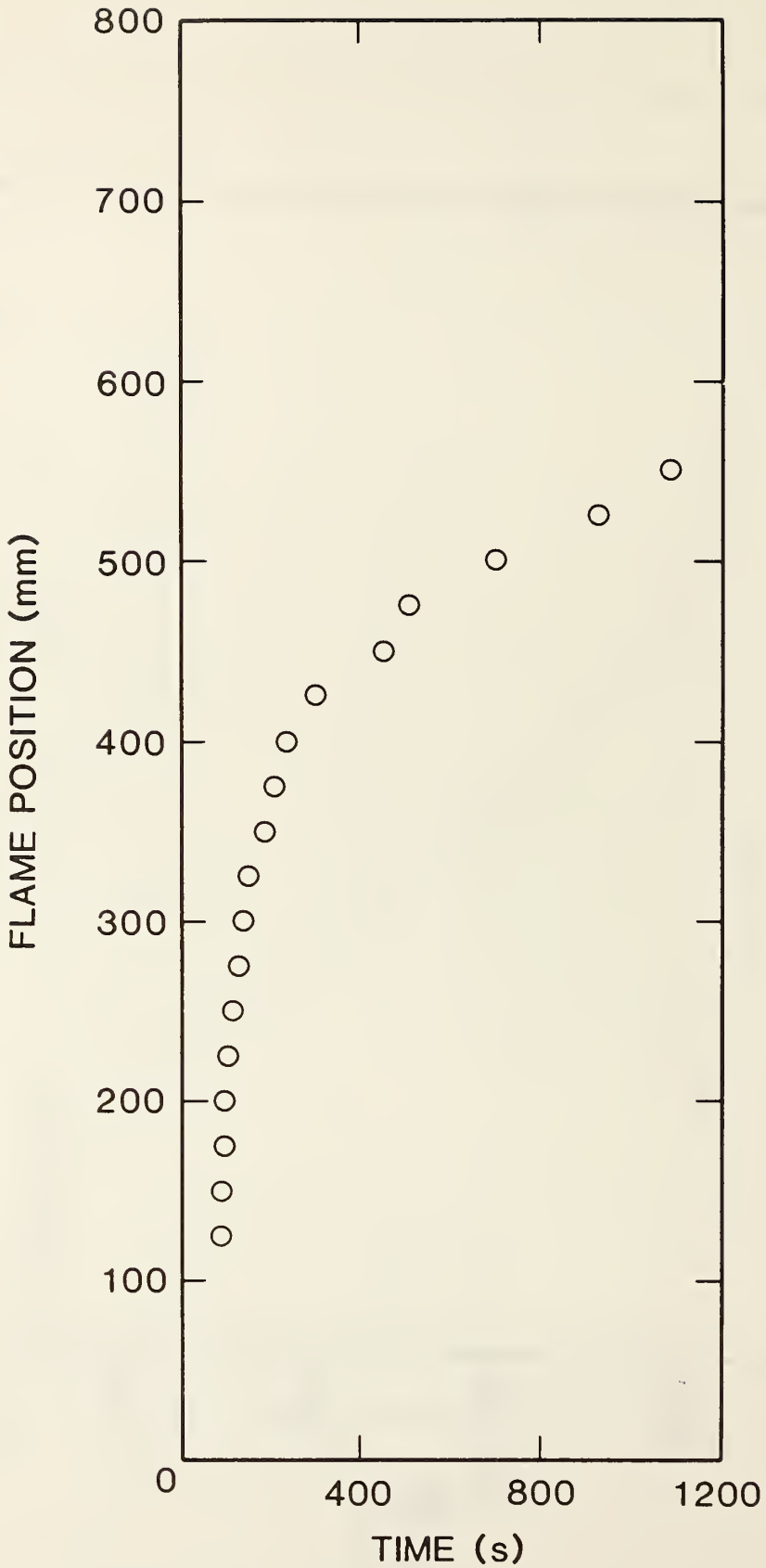

Figure 4. Flame position as a function of time for a fiberglass roofing shingle.

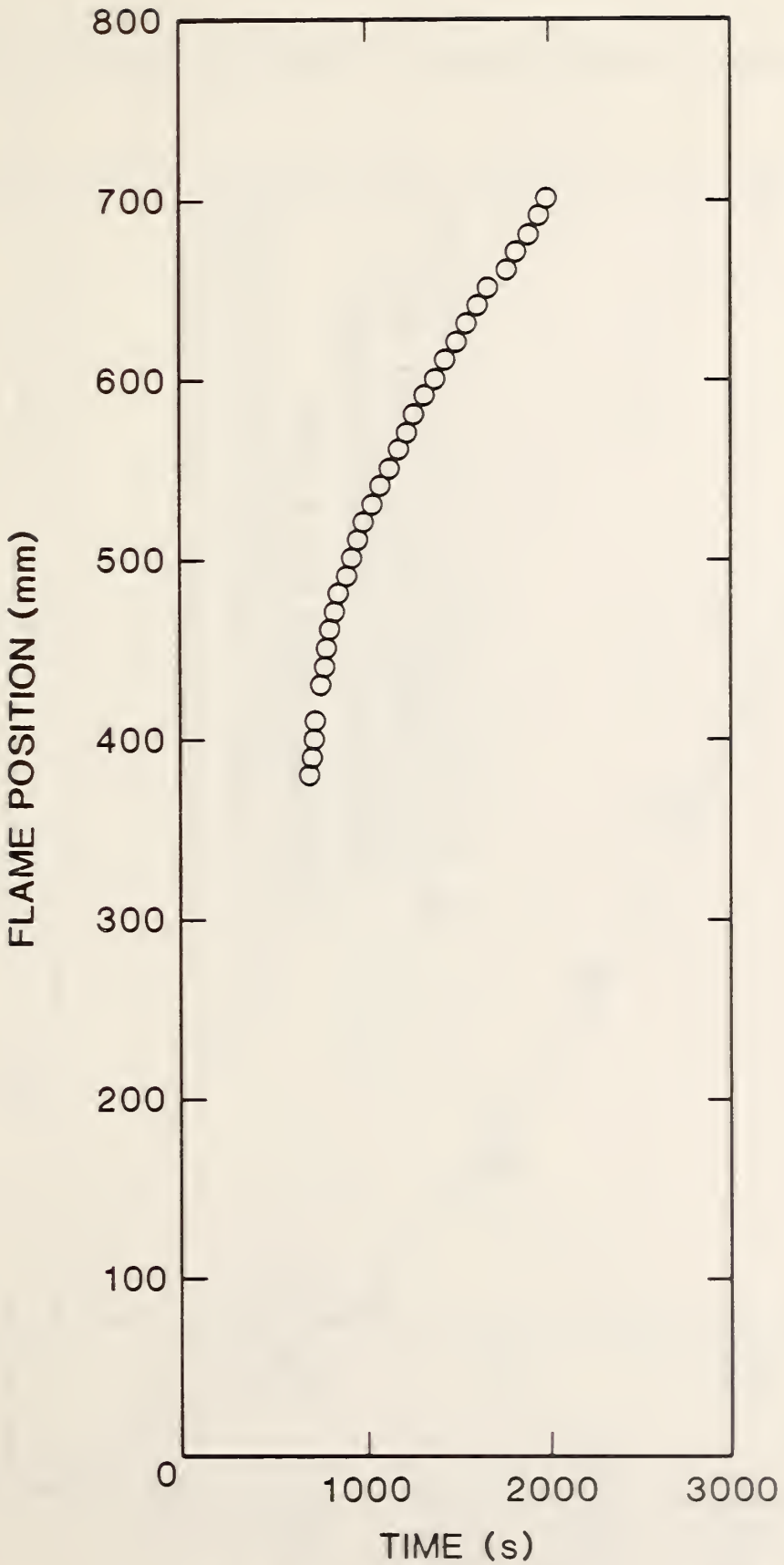

Figure 5. Flame position after delayed ignition of hardboard.

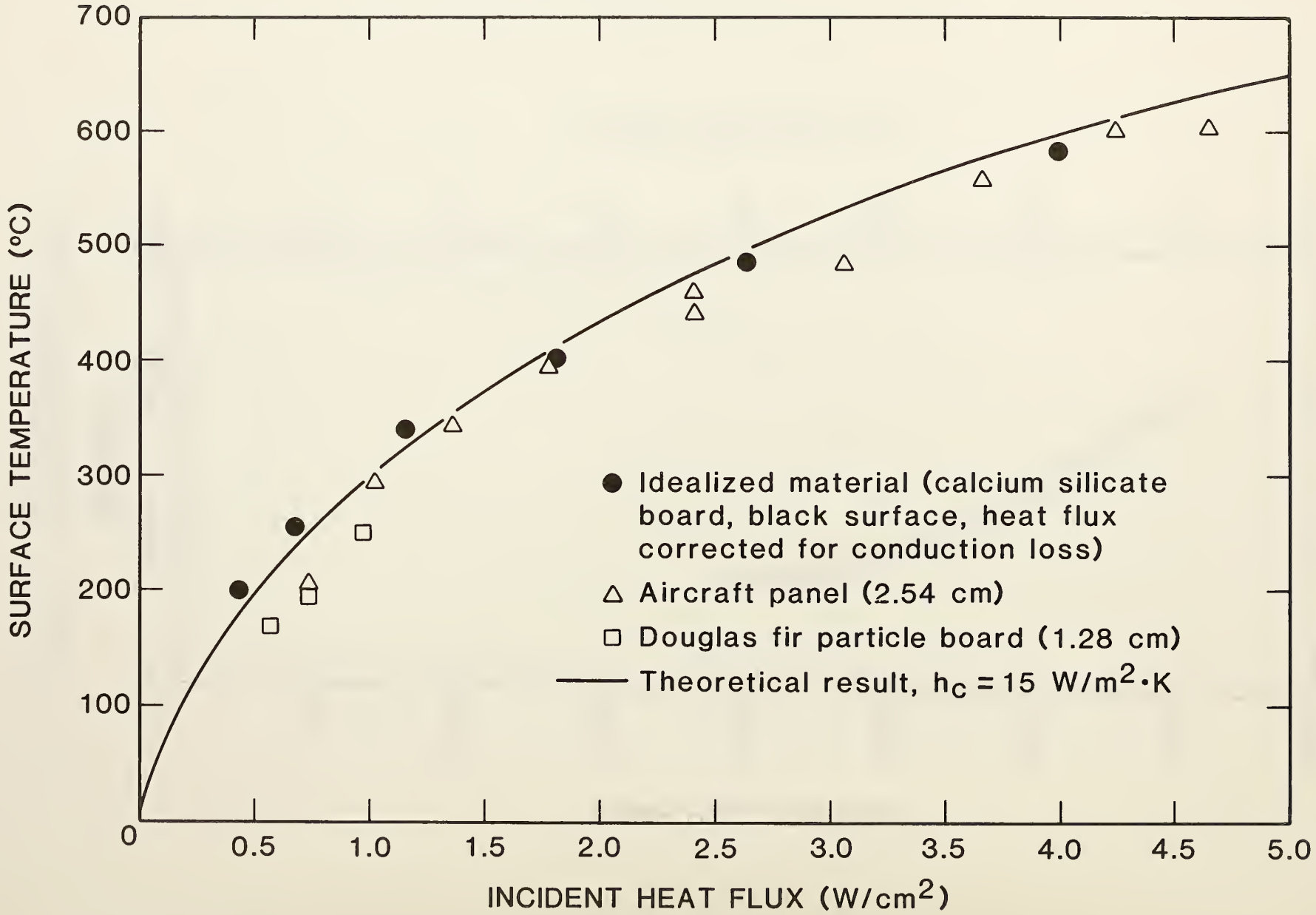

Figure 6. Equilibrium surface temperatures as a function of external radiant heating in the test apparatus.

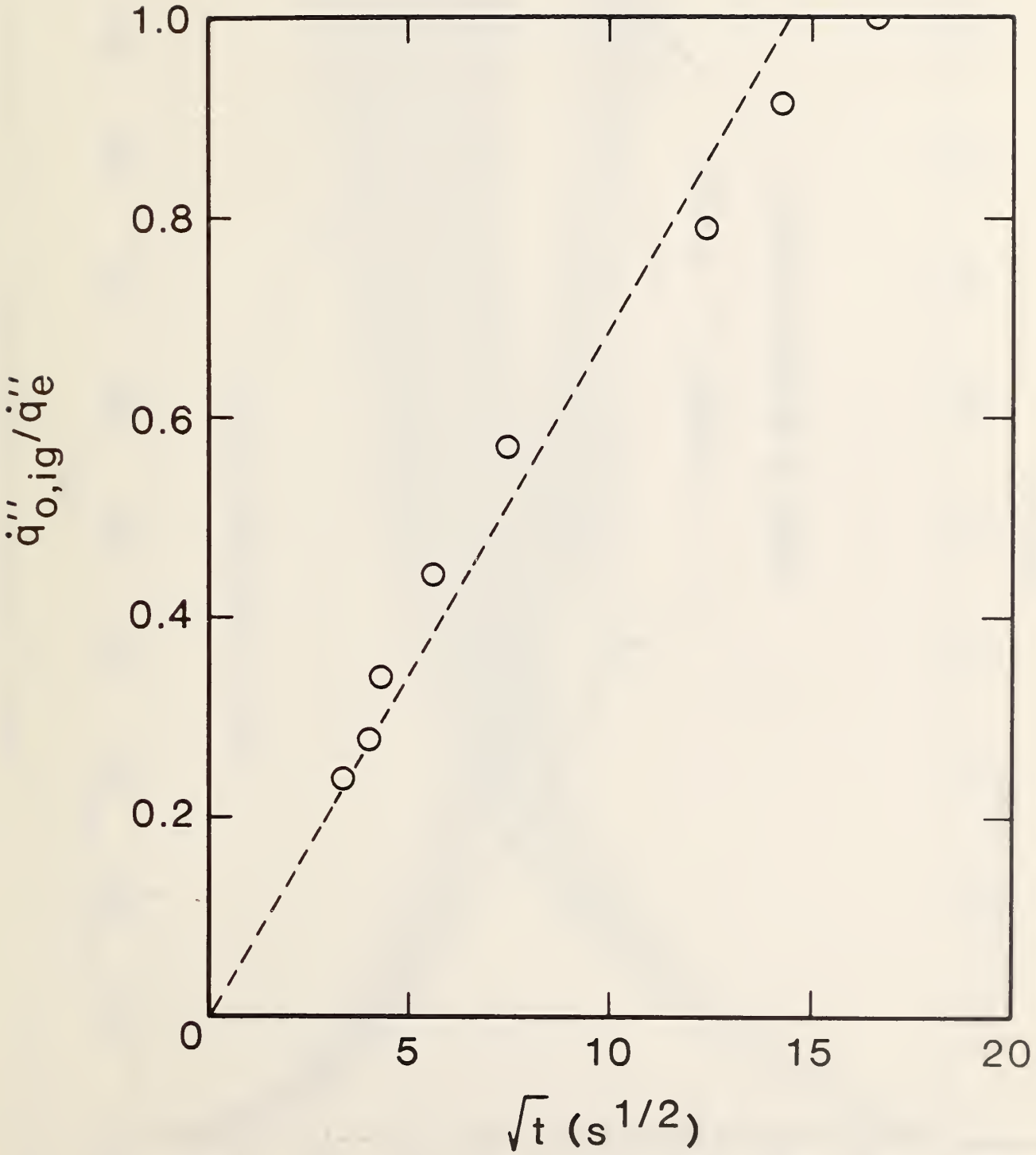

Figure 7. Correlation of ignition results for fiberboard (see Fig. 2).

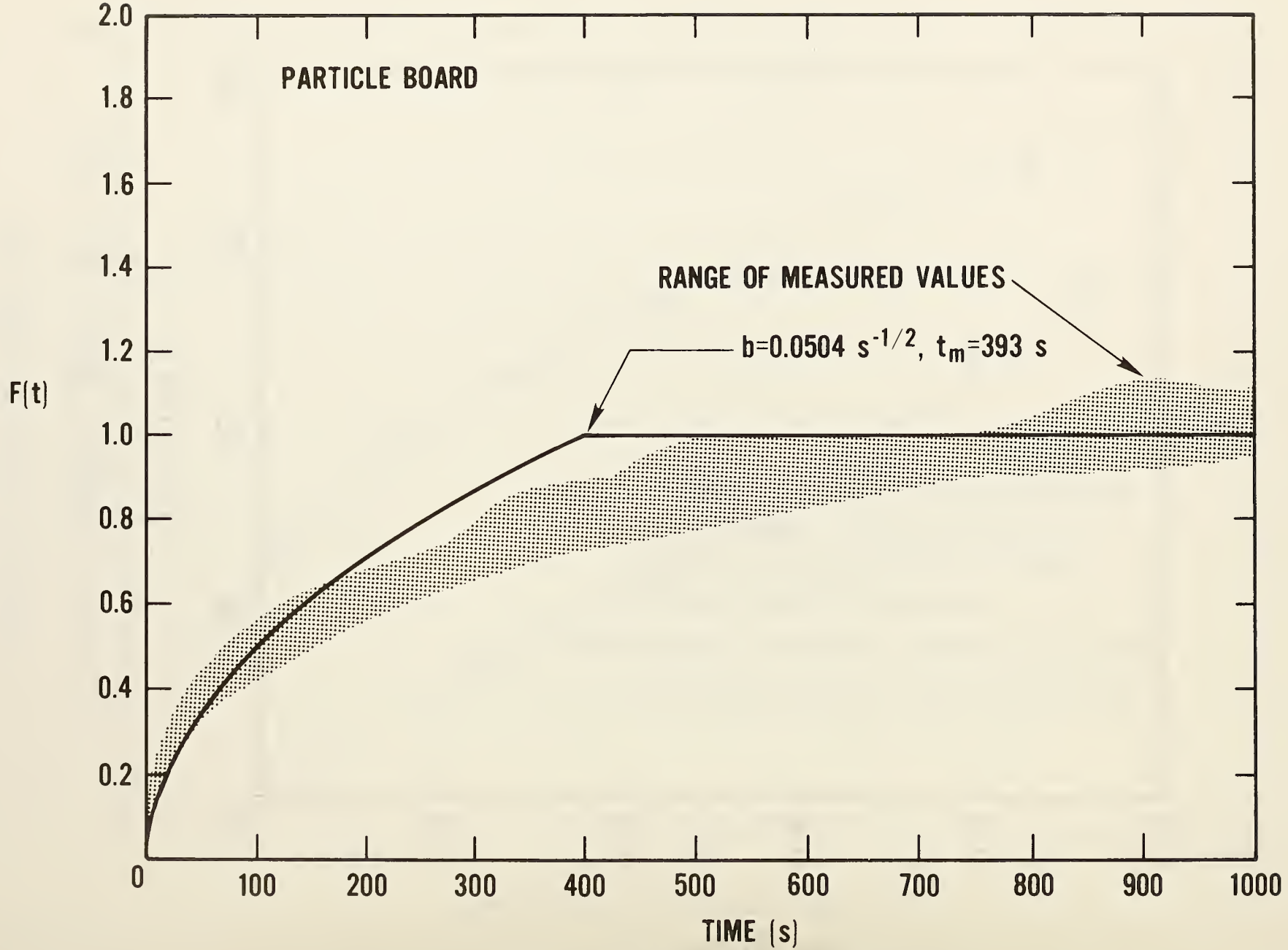

Figure 8. Comparison of measured and approximate values for F(t): particle board.

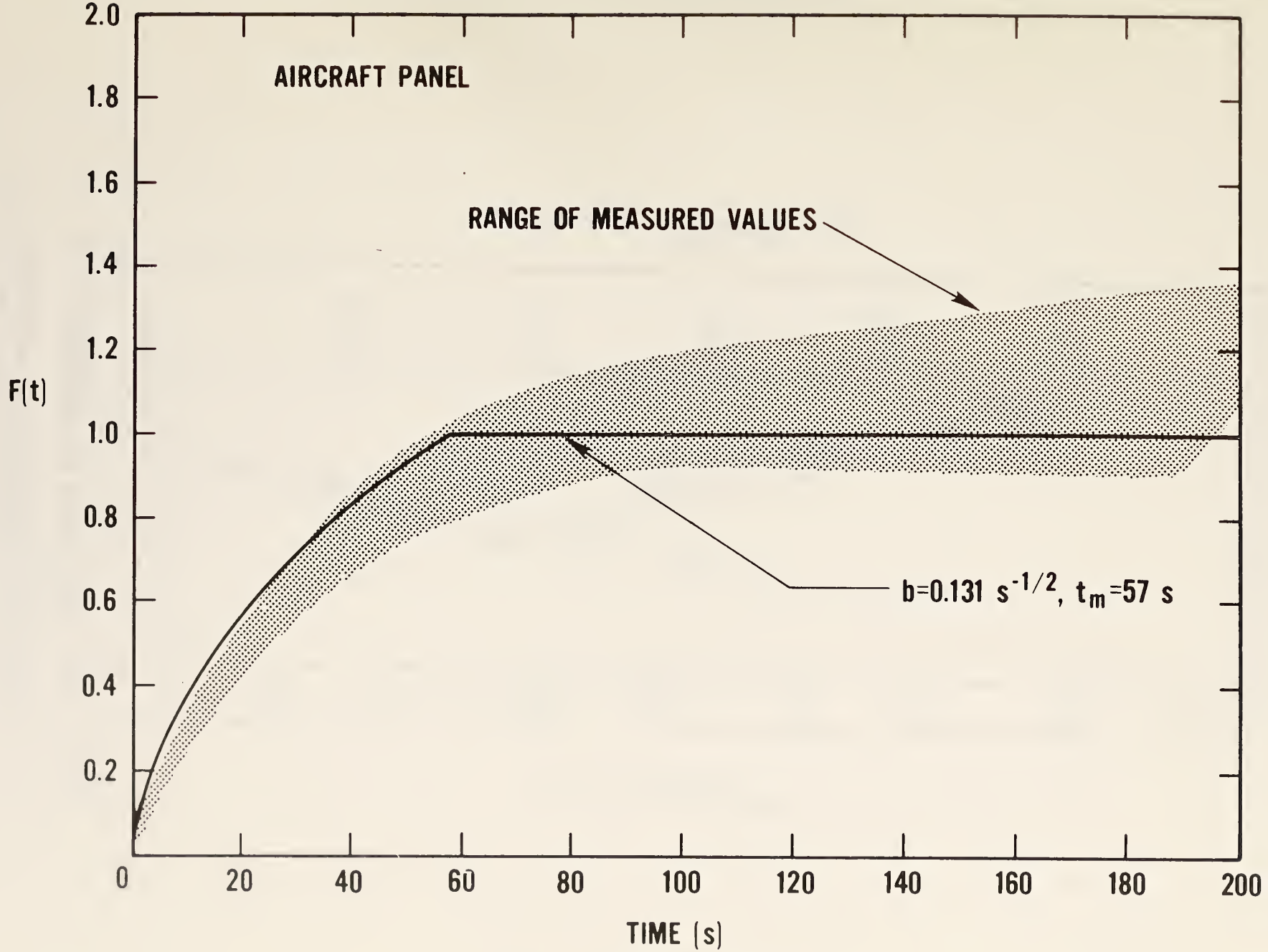

Figure 9. Comparison of measured and approximate values for F(t): aircraft panel.

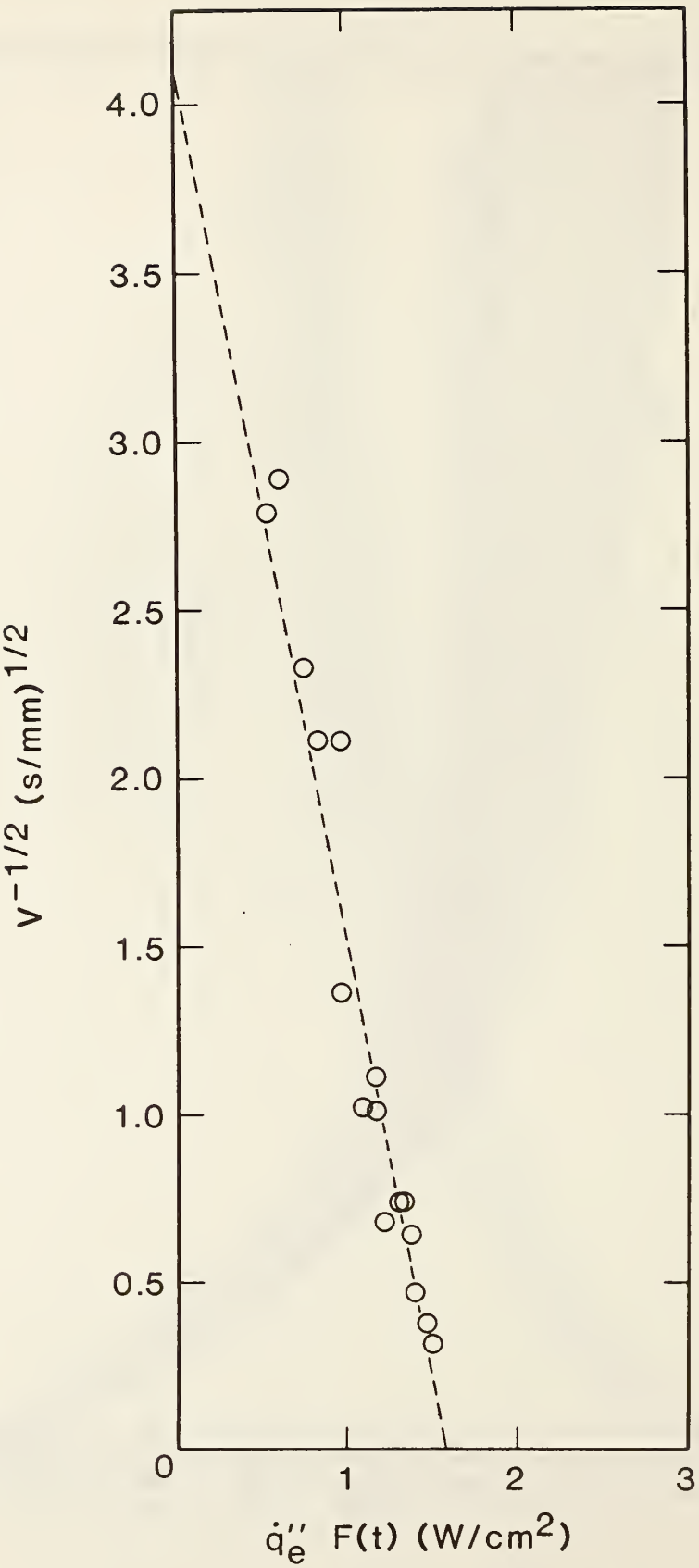

Figure 10. Correlation of spread velocity for a fiberglass shingle (see Fig. 4).

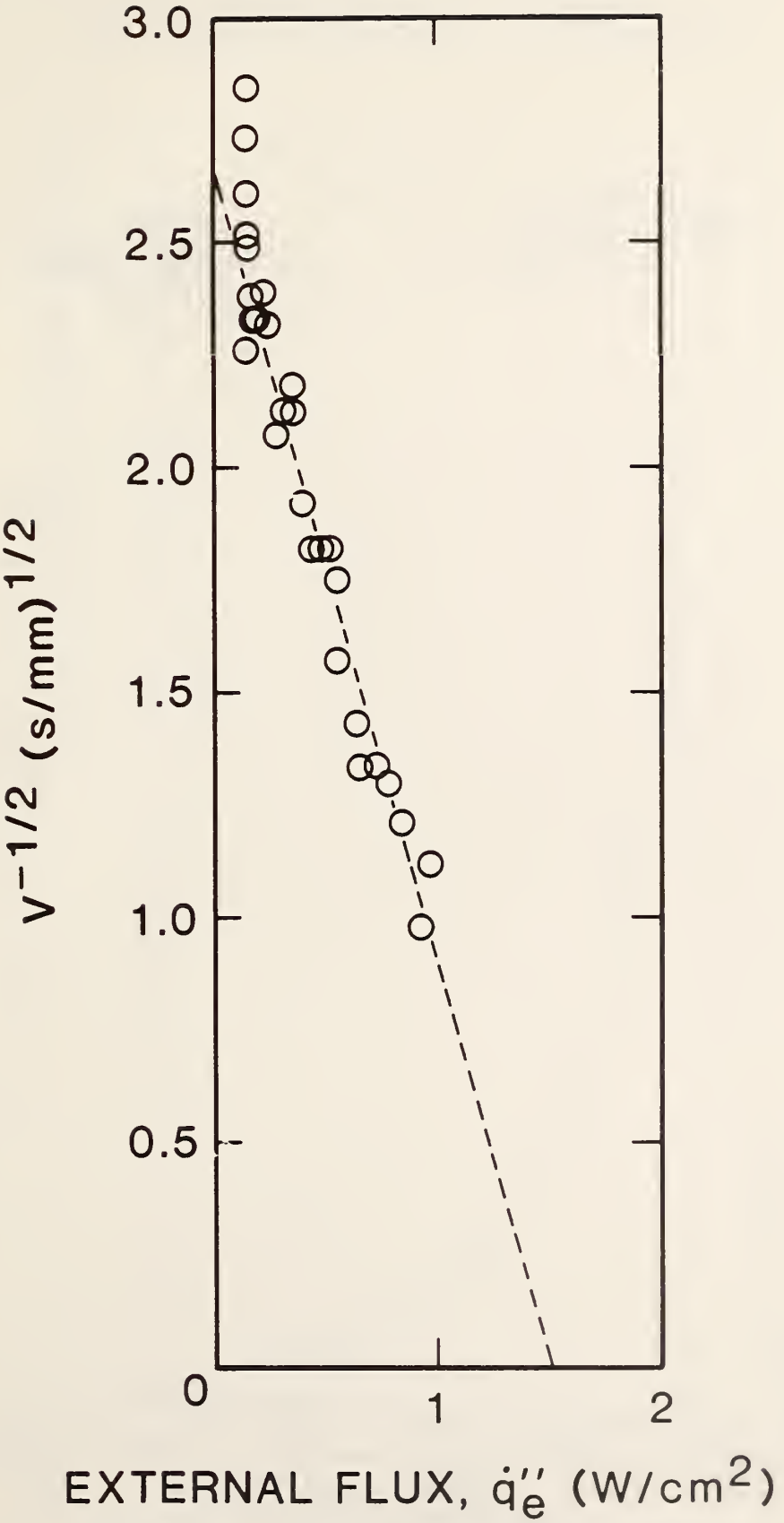

Figure 11. Correlation of spread velocity for hardboard (see Fig. 5).

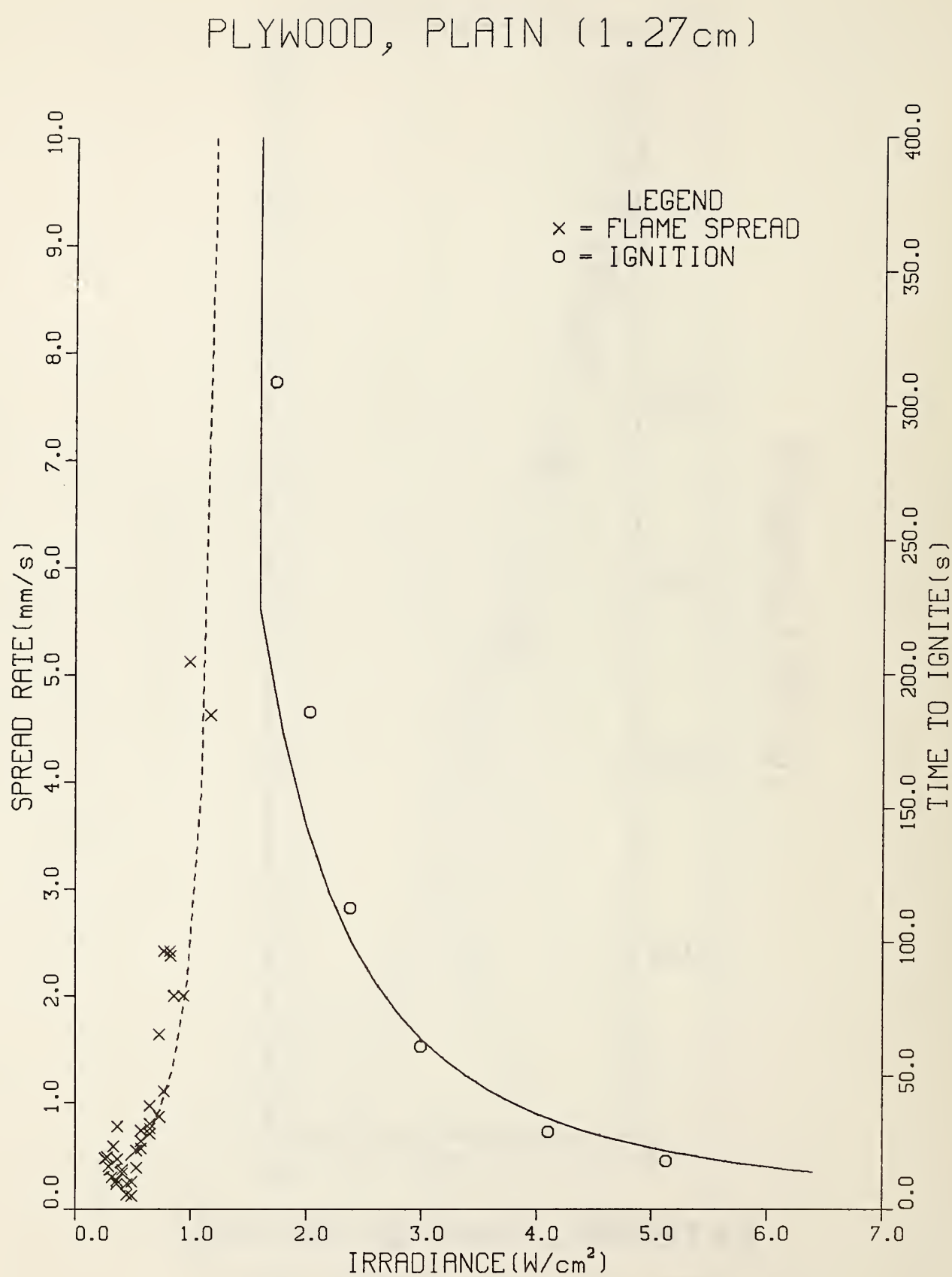

Figure 12. Spread and ignition results for plywood.

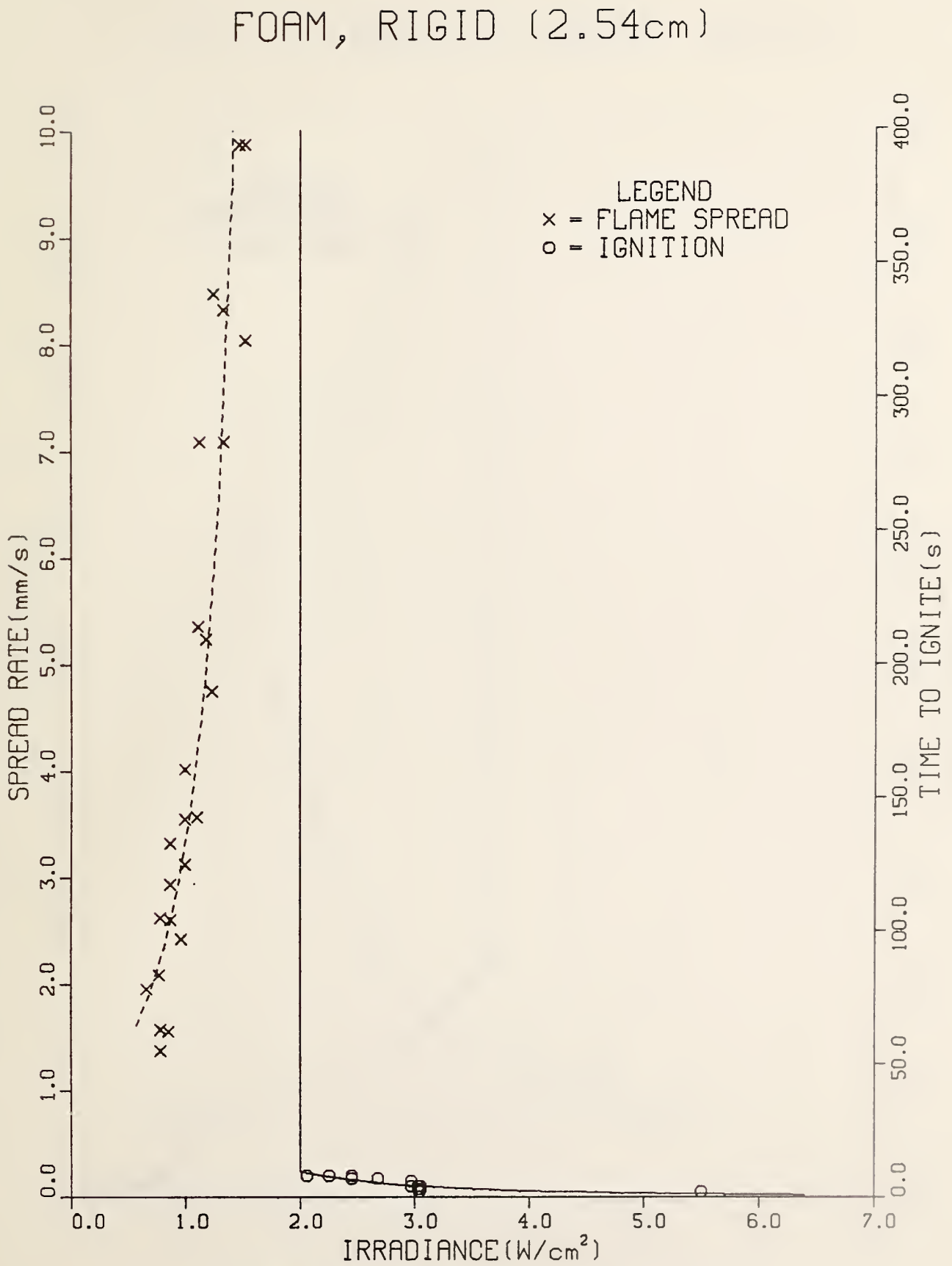

Figure 13. Spread and ignition results for rigid polyurethane foam.

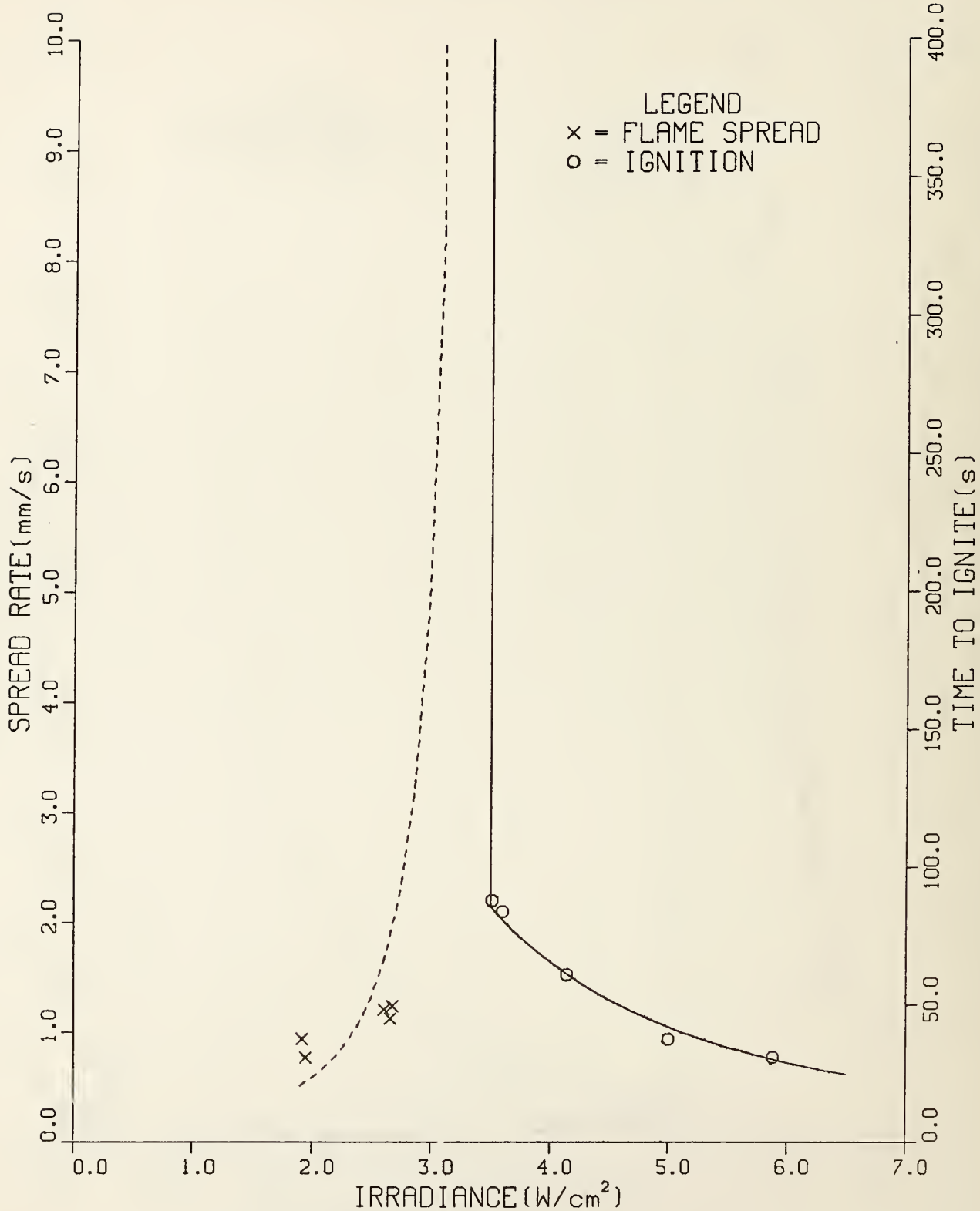

Figure 14. Spread and ignition results for gypsum board.

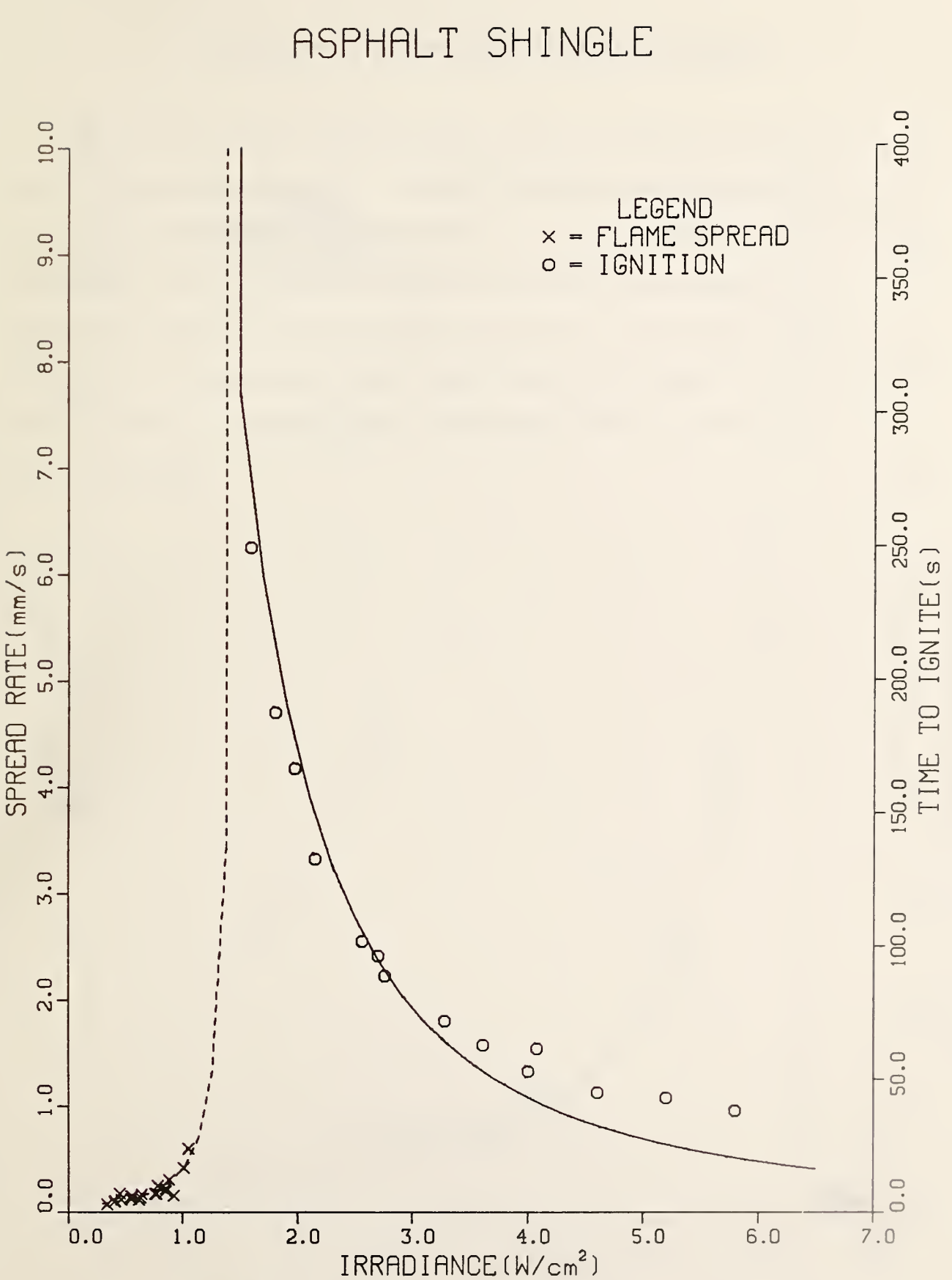

Figure 15. Spread and ignition results for an asphalt shingle.

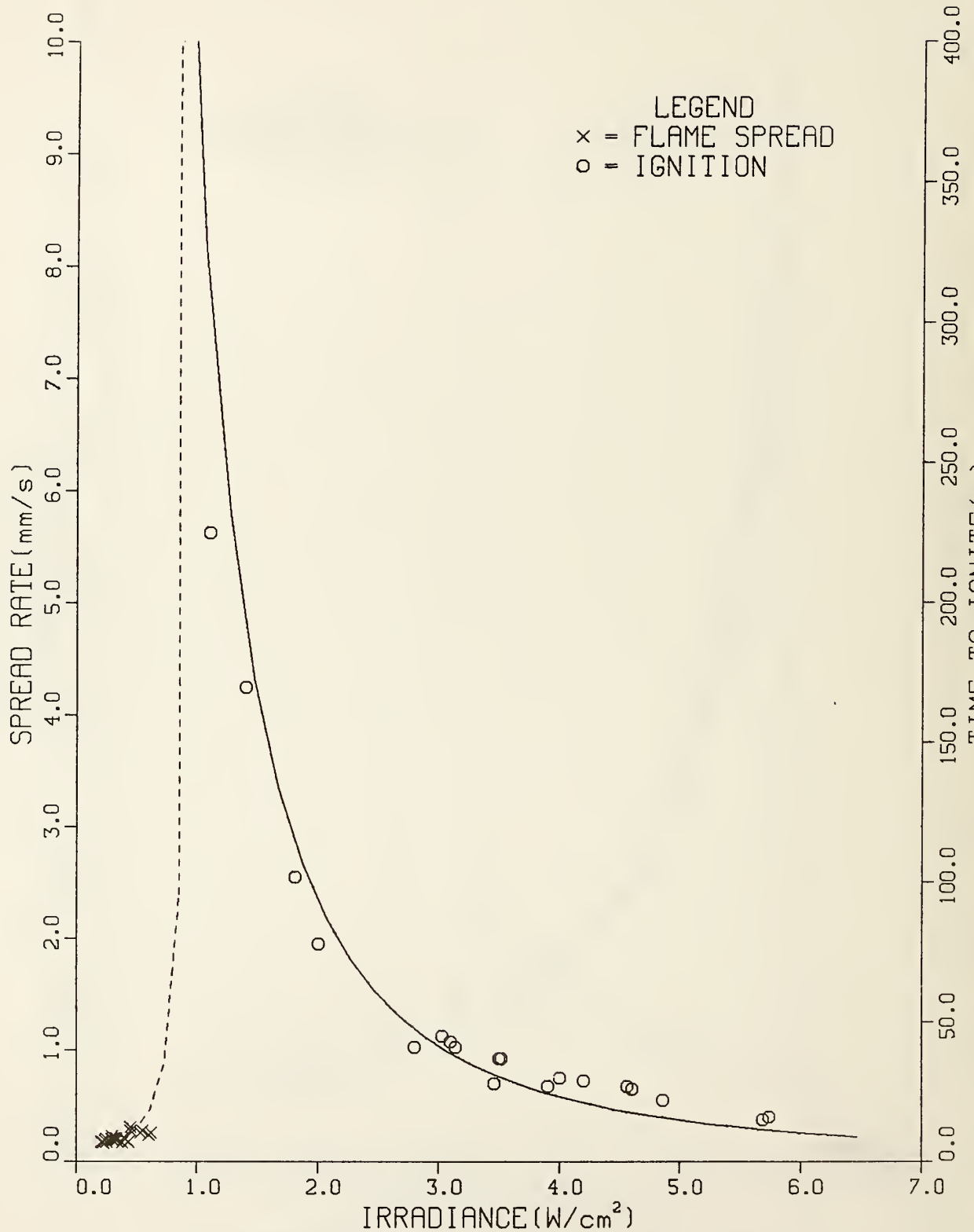

Figure 16. Spread and ignition results for PMMA.

Appendix A. Correlation of Ignition Results

Ignition tests were conducted for a variety of materials including plastics, woods and composites. The fit of these data correlated by eq. (5) to the empirically derived function F(t) is shown in figures A-1 to A-30. The illustrated line fit favors the shorter times where the assumption of an infinitely thick solid would be more valid [8,9]. For layered composite materials, the data reflect results applicable to the ignition of the first layer. However, it was not always obvious what role the underlayment materials played.

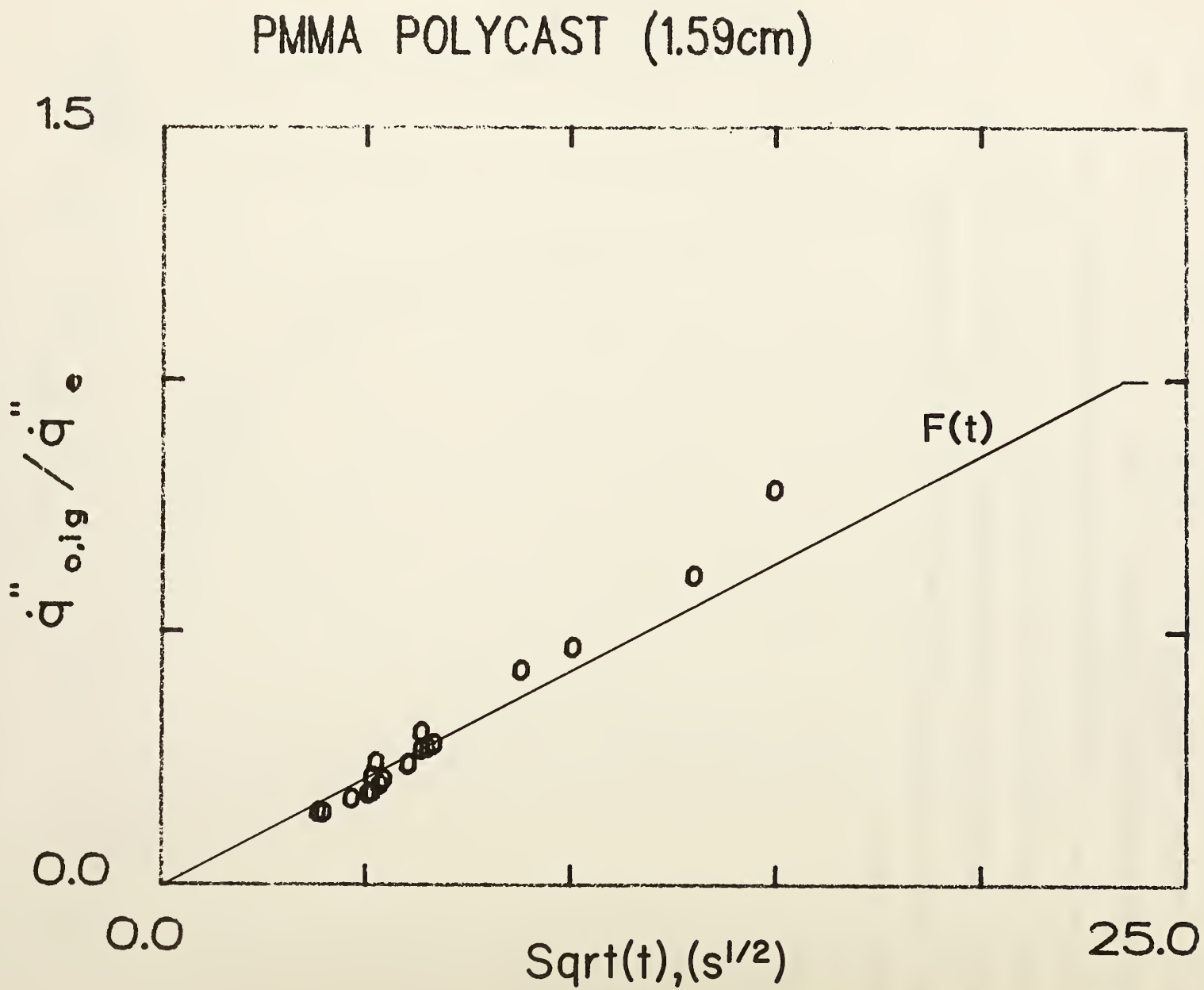

Figure A-1. Correlation of ignition results for PMMA Polycast (1.59 mm).

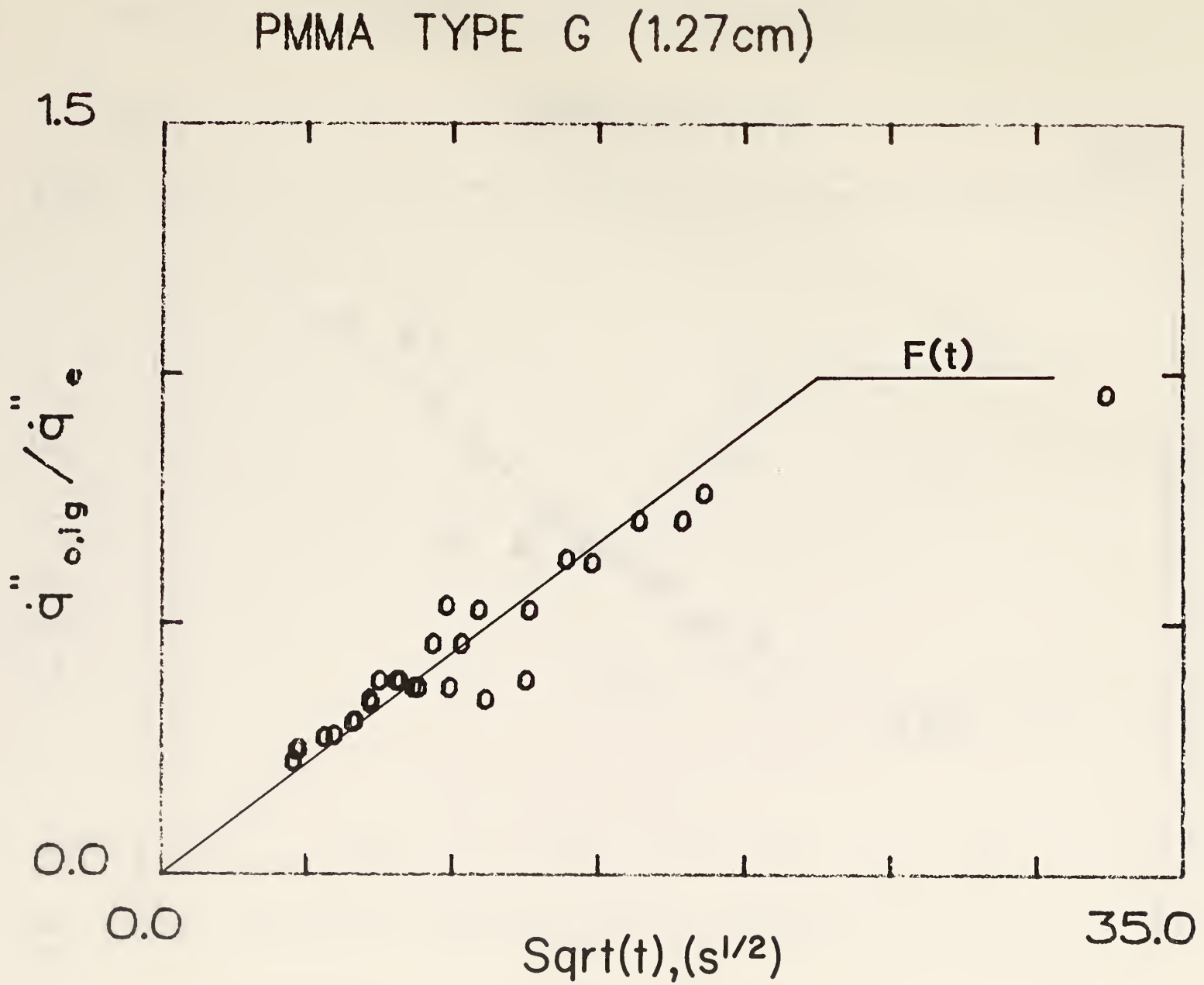

Figure A-2. Correlation of ignition results for PMMA Type G (1.27 cm).

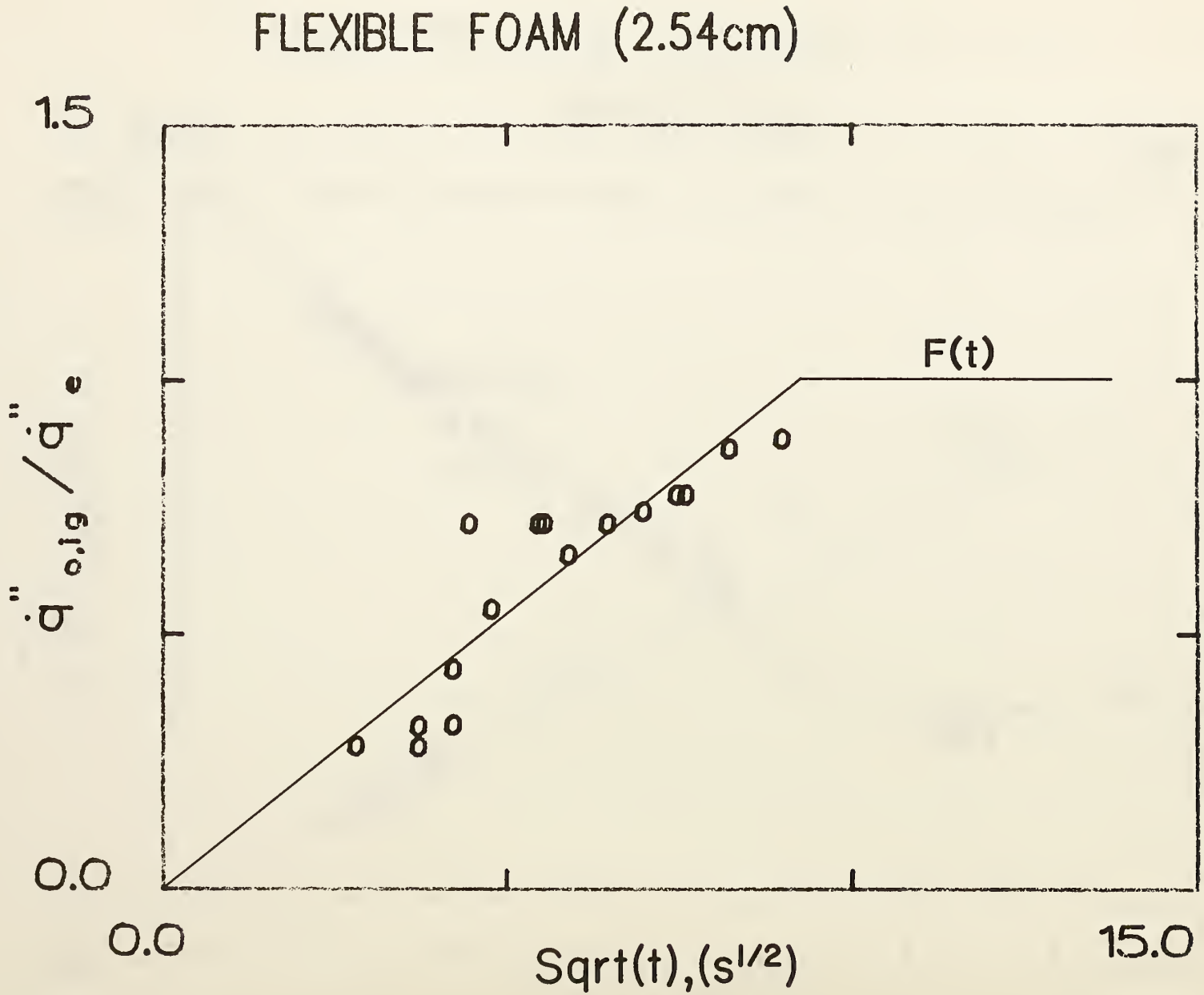

Figure A-3. Correlation of ignition results for flexible foam (2.54 cm).

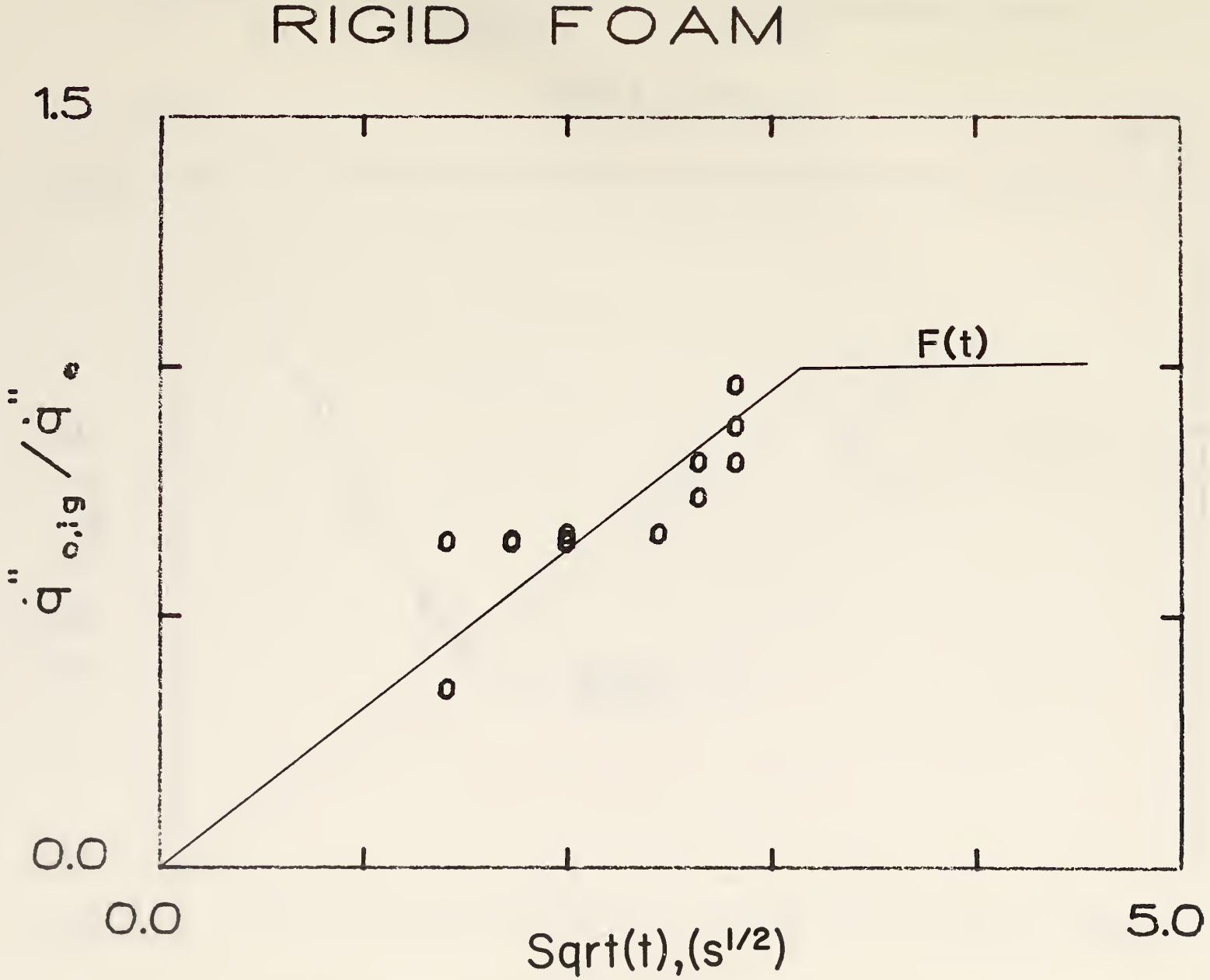

Figure A-4. Correlation of ignition results for rigid foam (2.54 cm).

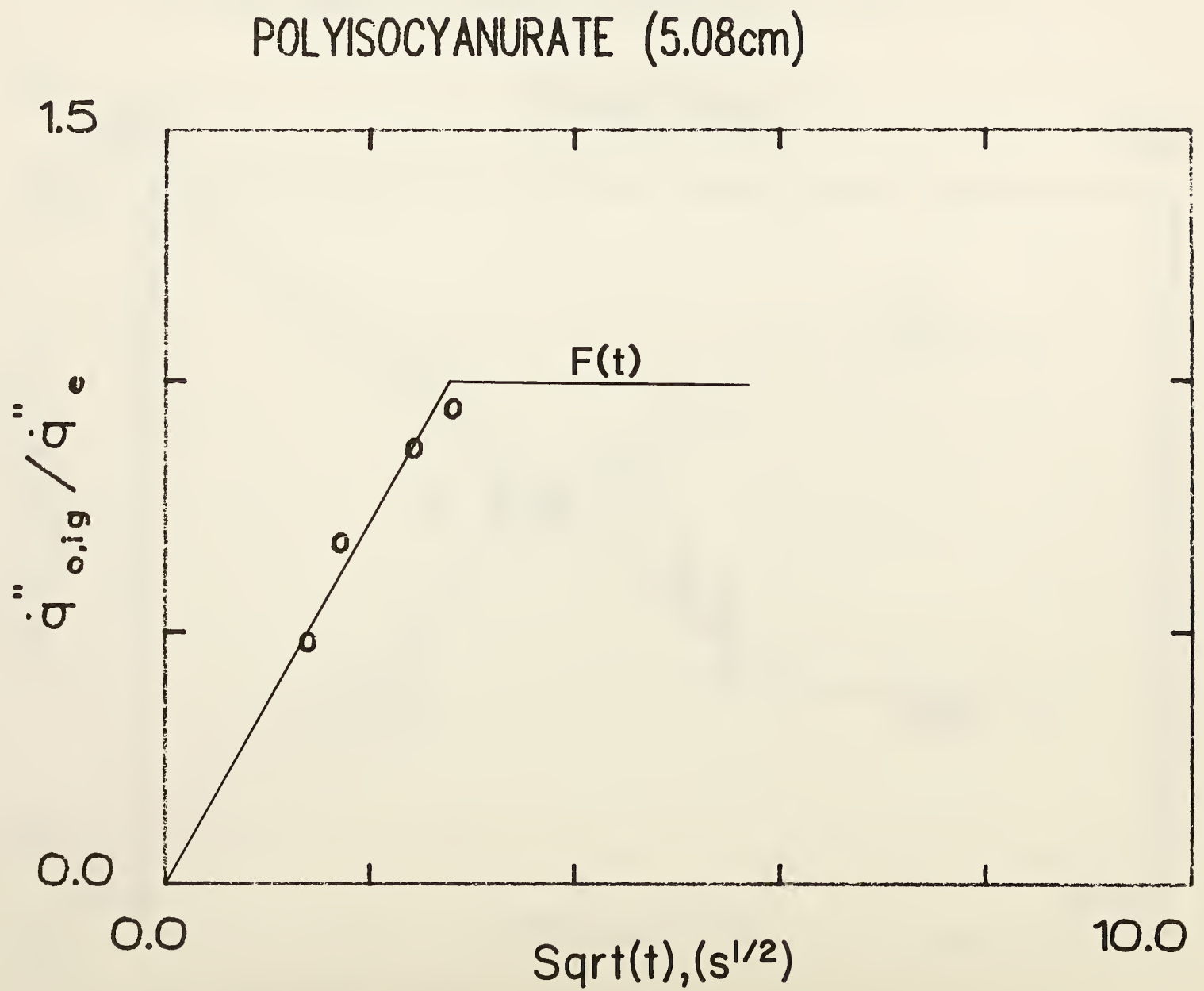

Figure A-5. Correlation of ignition results for polyisocyanurate (5.08 cm).

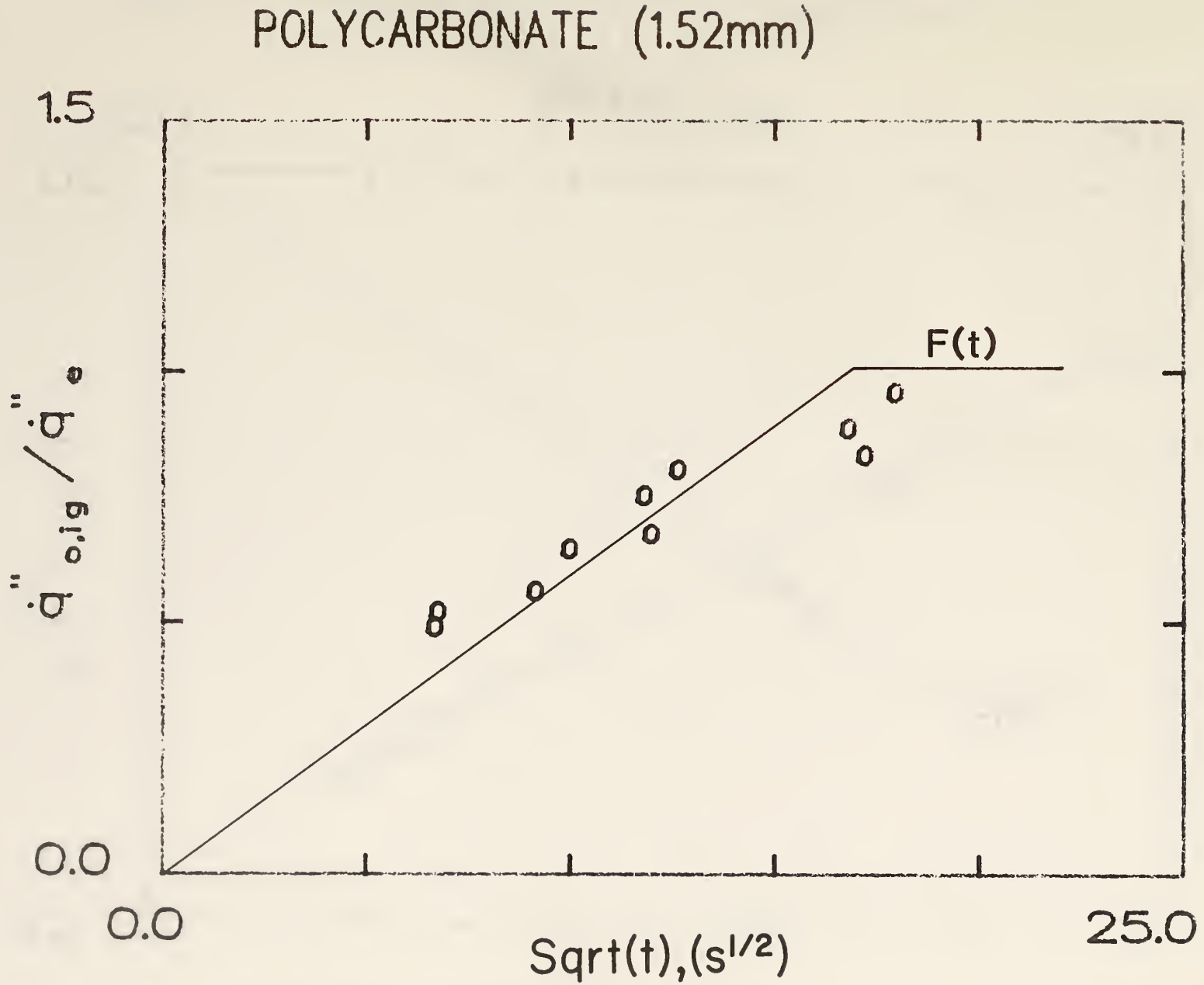

Figure A-6. Correlation of ignition results for polycarbonate (1.52 mm).

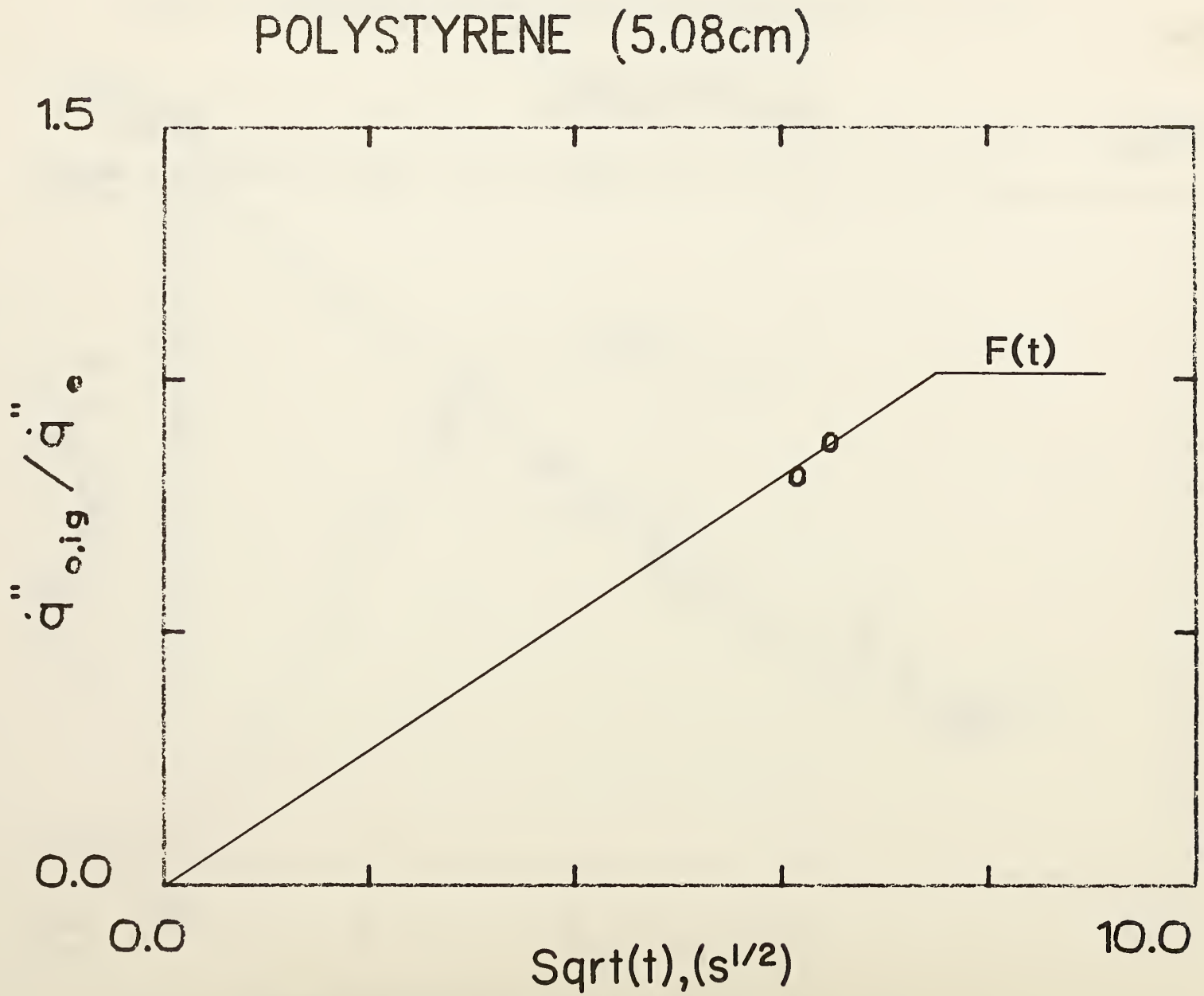

Figure A-7. Correlation of ignition results for polystyrene (5.08 cm).

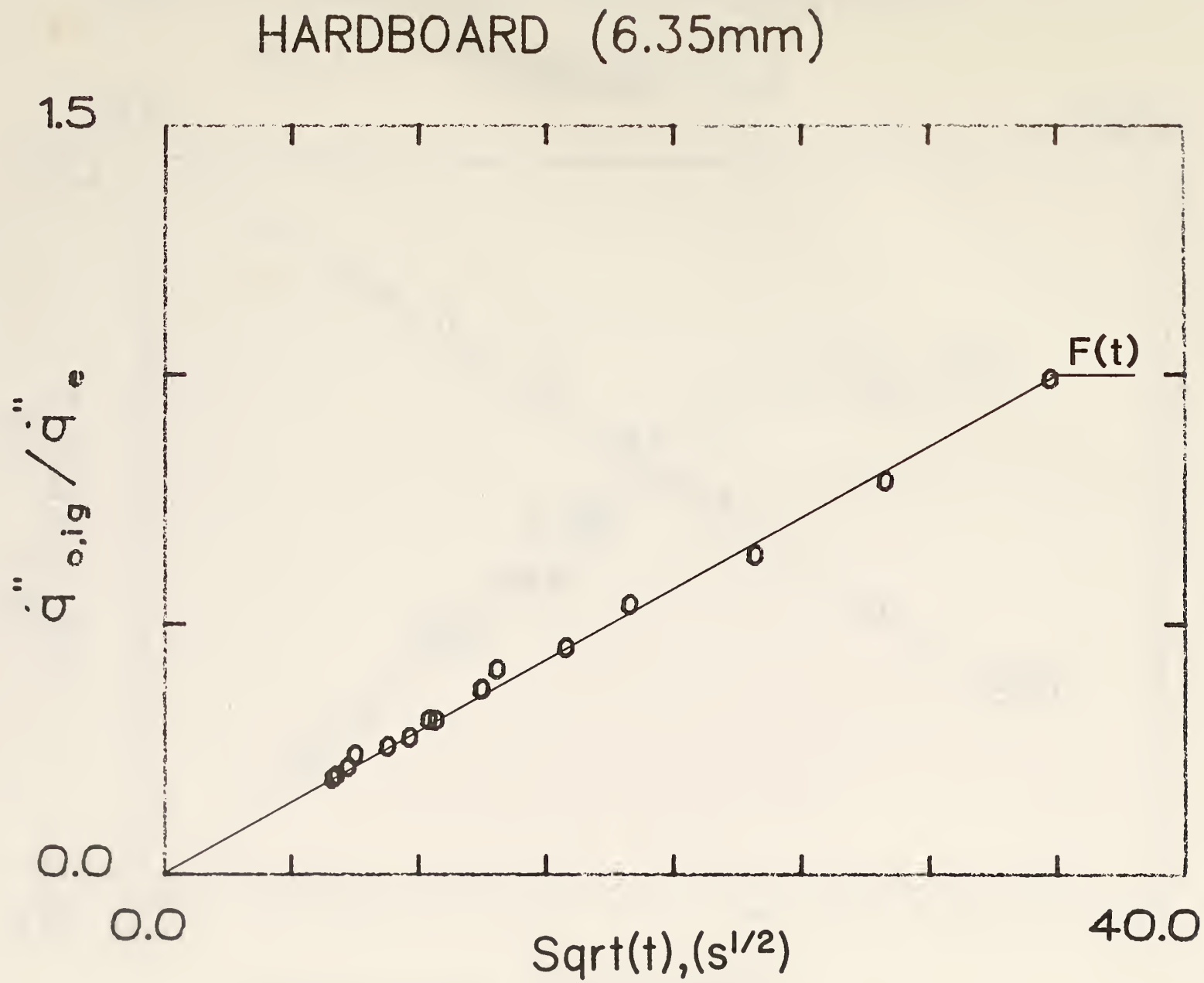

Figure A-8. Correlation of ignition results for hardborad (6.35 mm).

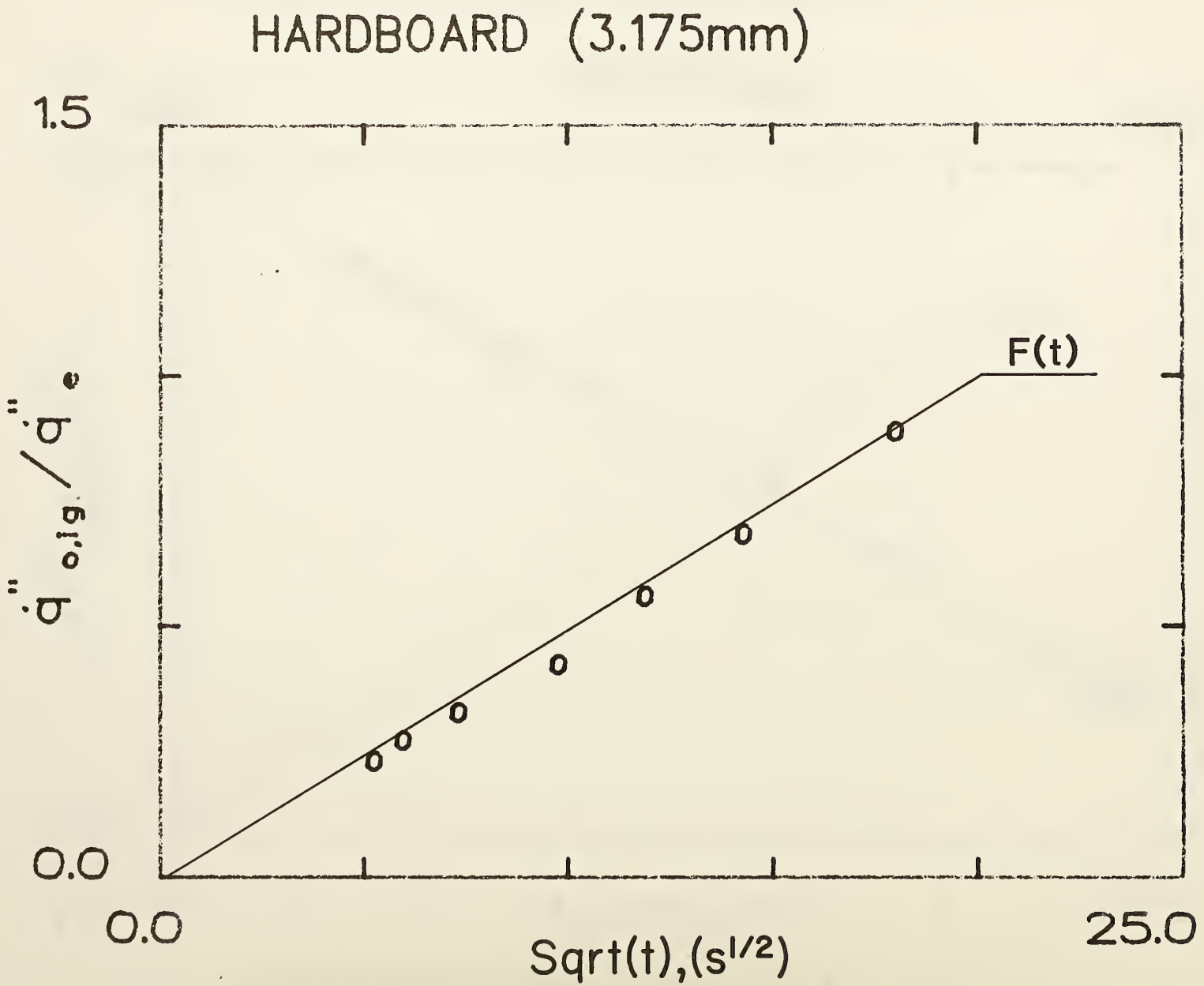

Figure A-9. Correlation of ignition results for hardboard (3.175 mm).

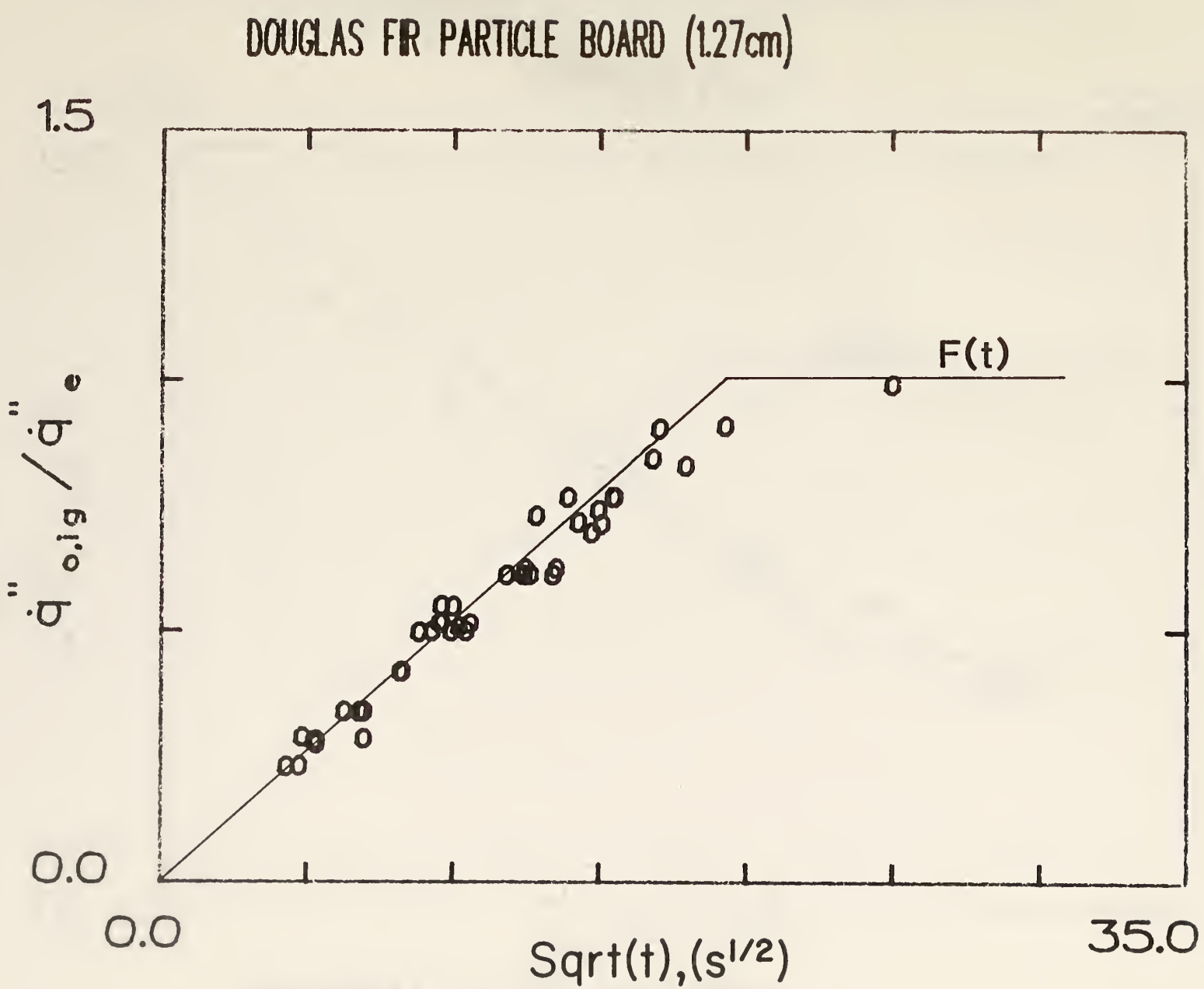

Figure A-10. Correlation of ignition results for Douglas fir particle board (1.27 cm).

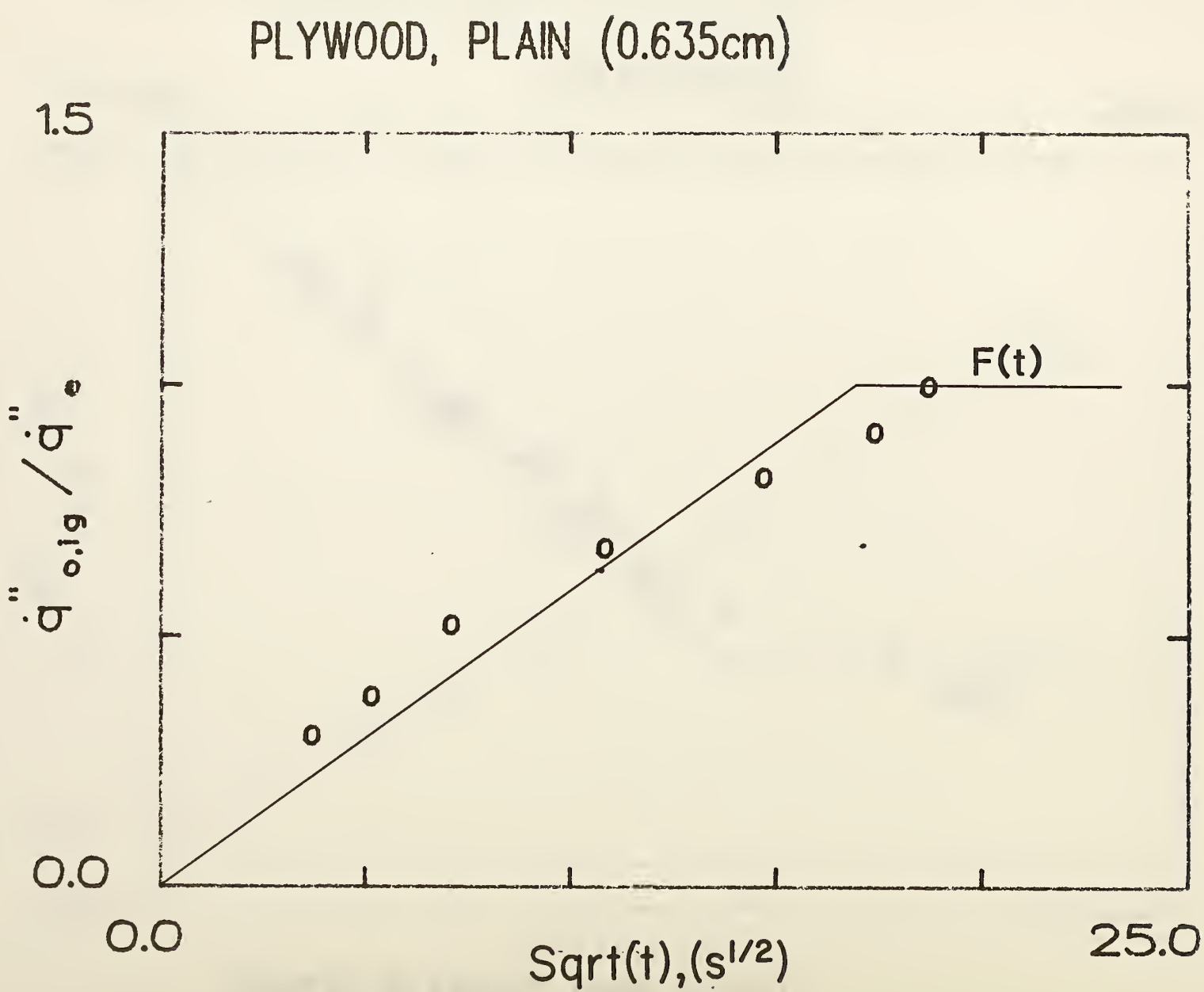

Figure A-11. Correlation of ignition results for plywood, plain (0.635 cm).

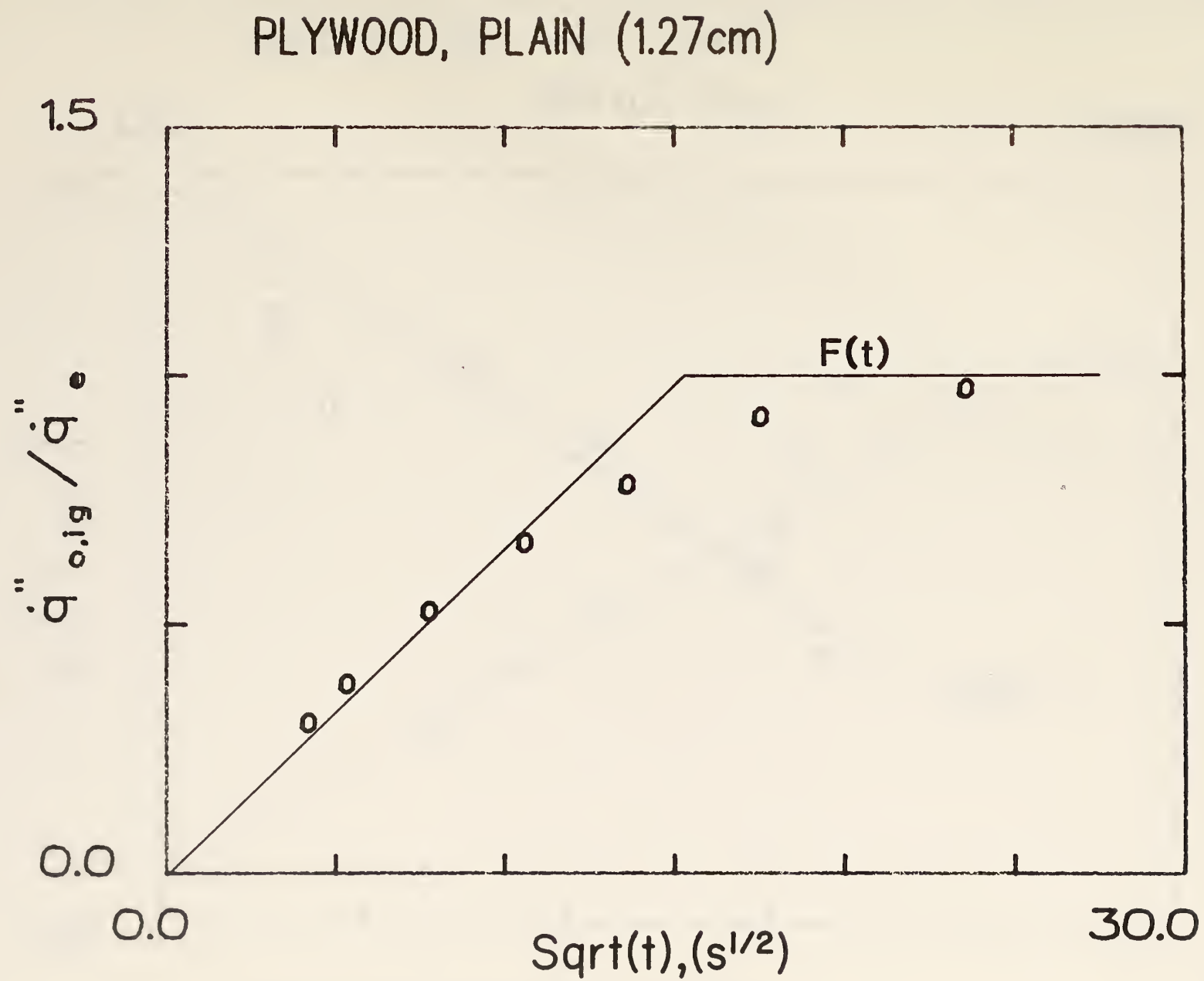

Figure A-12. Correlation of ignition results for plywood, plain (1.27 cm).

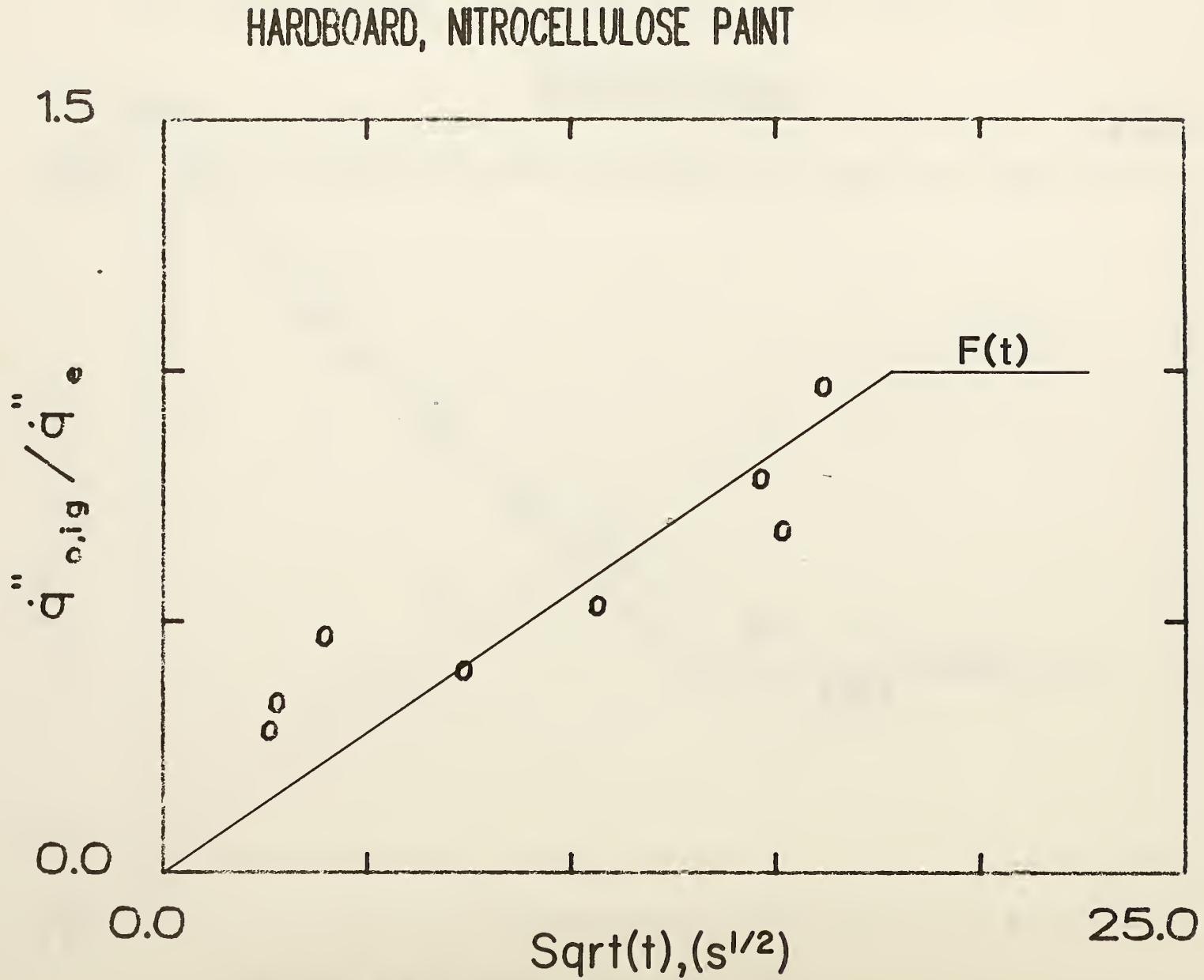

Figure A-13. Correlation of ignition results for hardboard (3.4 mm, nitrocellulose paint).

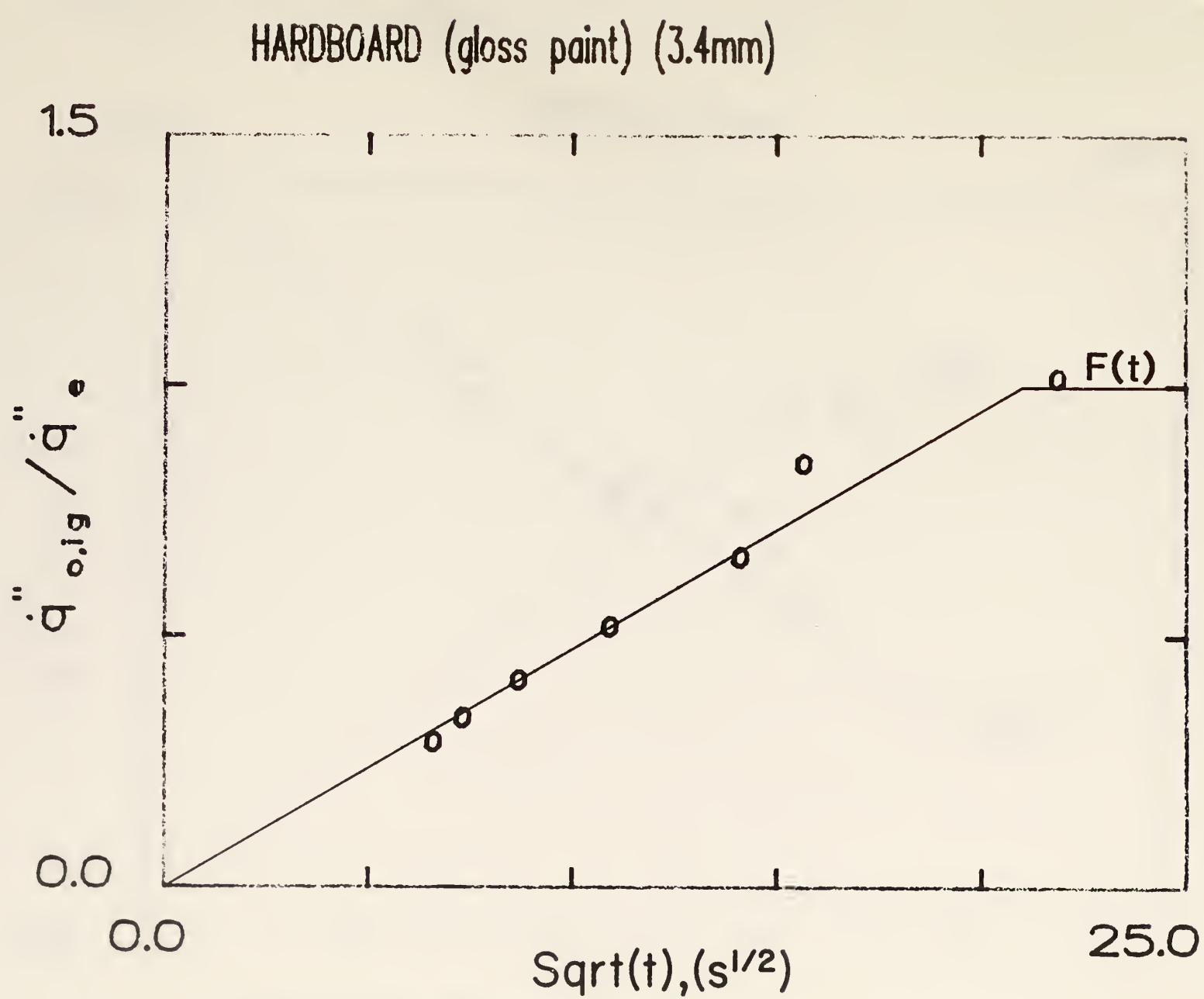

Figure A-14. Correlation of ignition results for hardboard (3.4 mm, gloss paint).

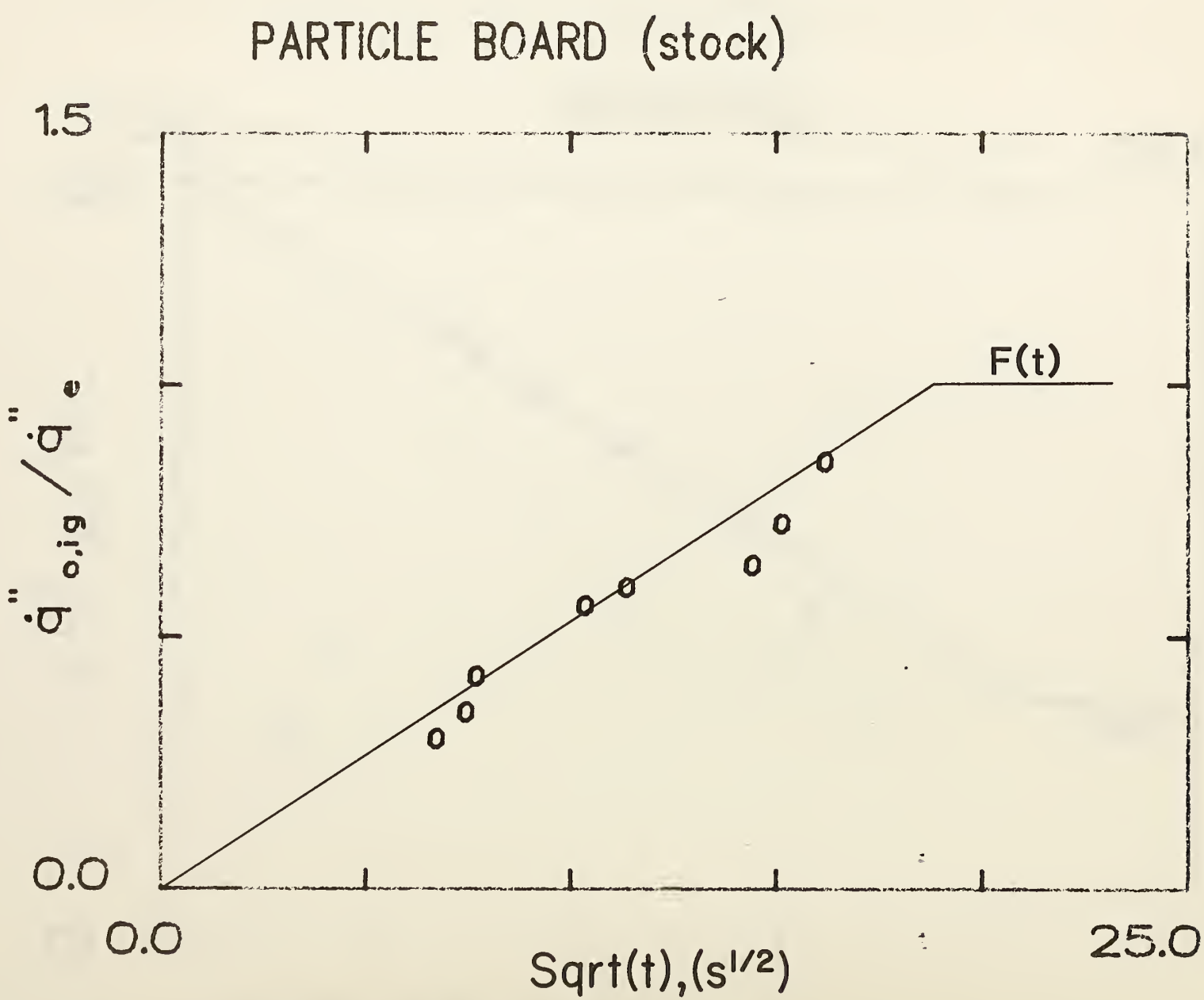

Figure A-15. Correlation of ignition results for particle board (1.27 cm, stock).

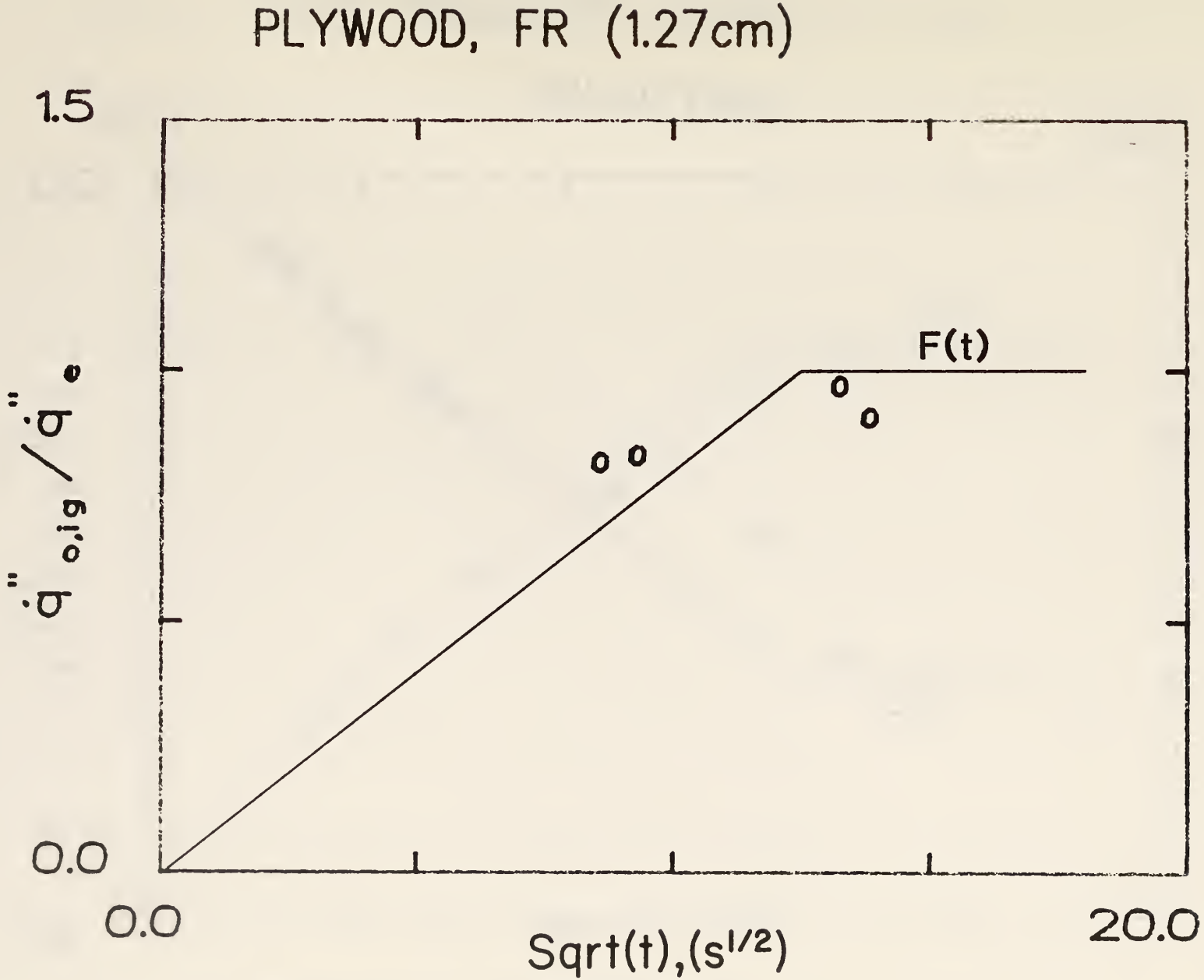

Figure A-16. Correlation of ignition results for plywood, FR (1.27 cm).

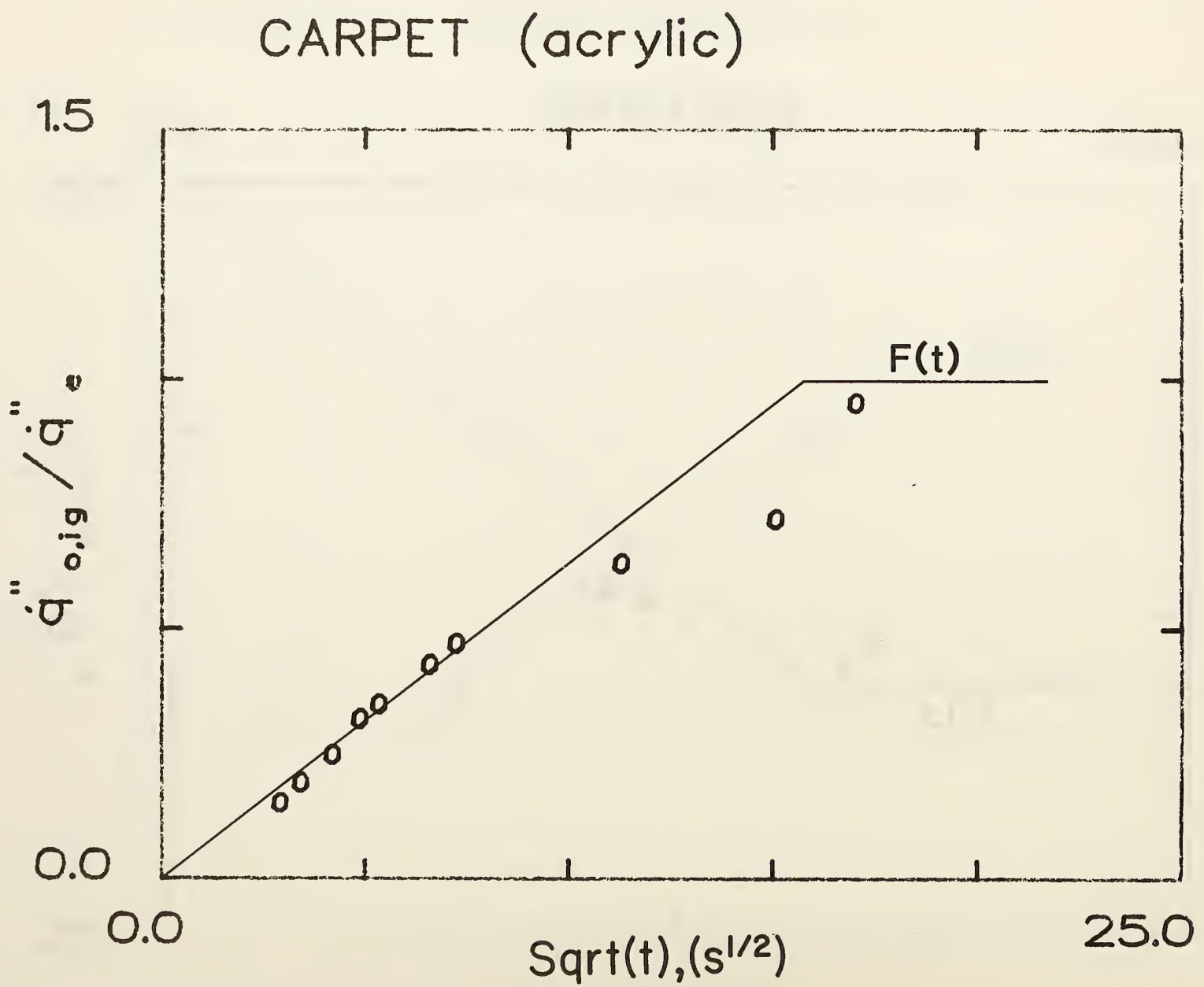

Figure A-17. Correlation of ignition results for carpet (acrylic) (S119M).

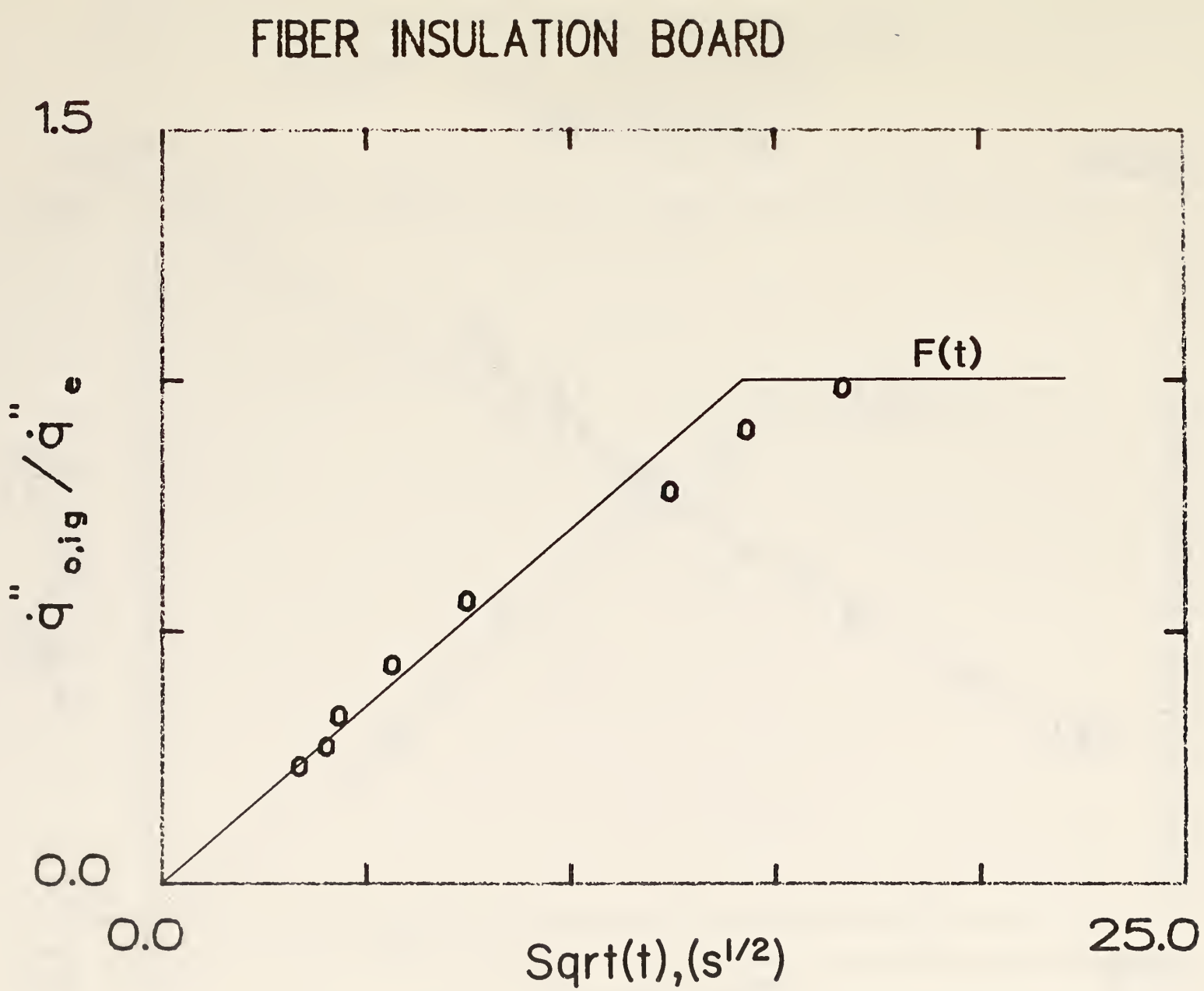

Figure A-18. Correlation of ignition results for fiber insulation board.

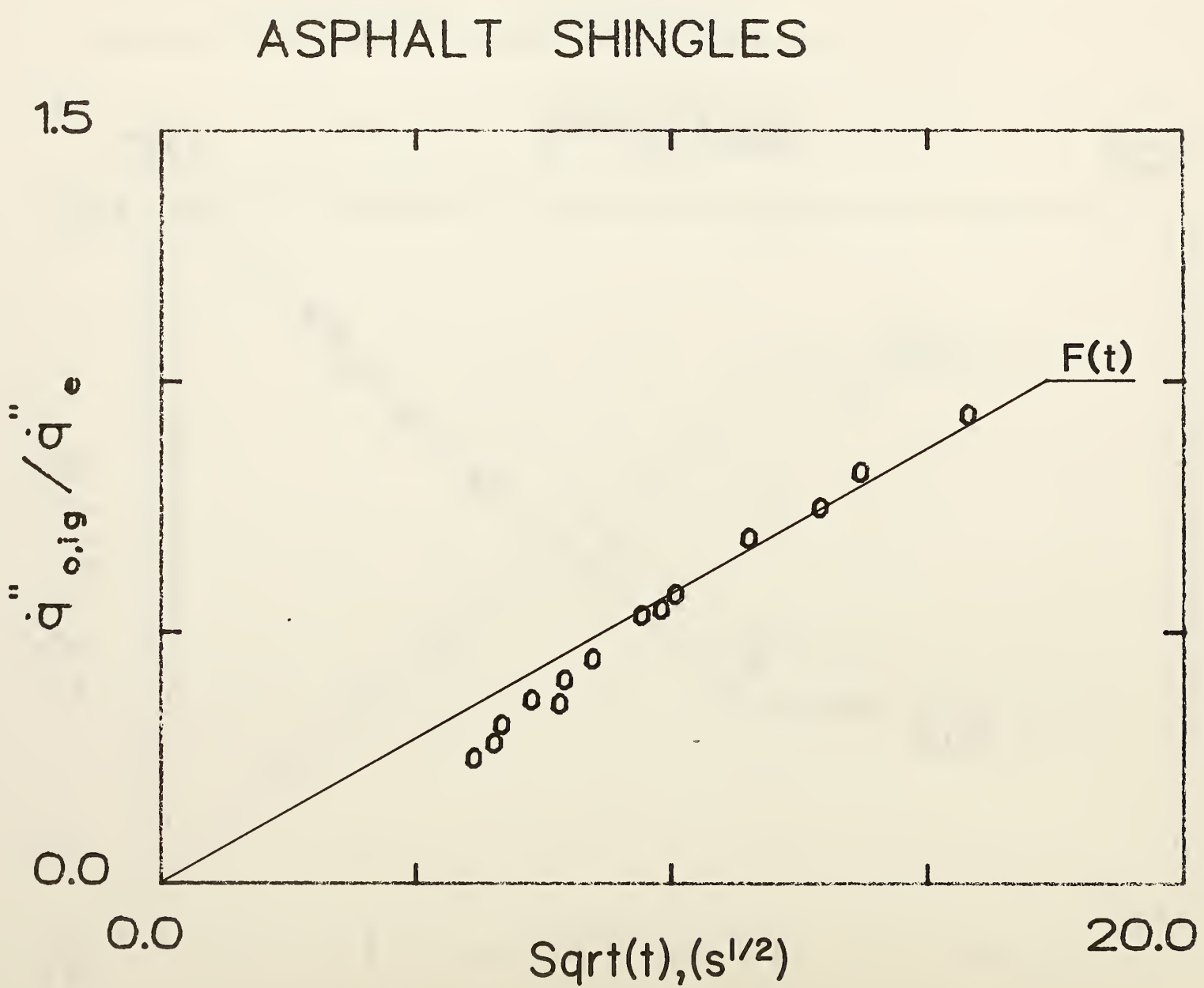

Figure A-19. Correlation of ignition results for asphalt shingle.

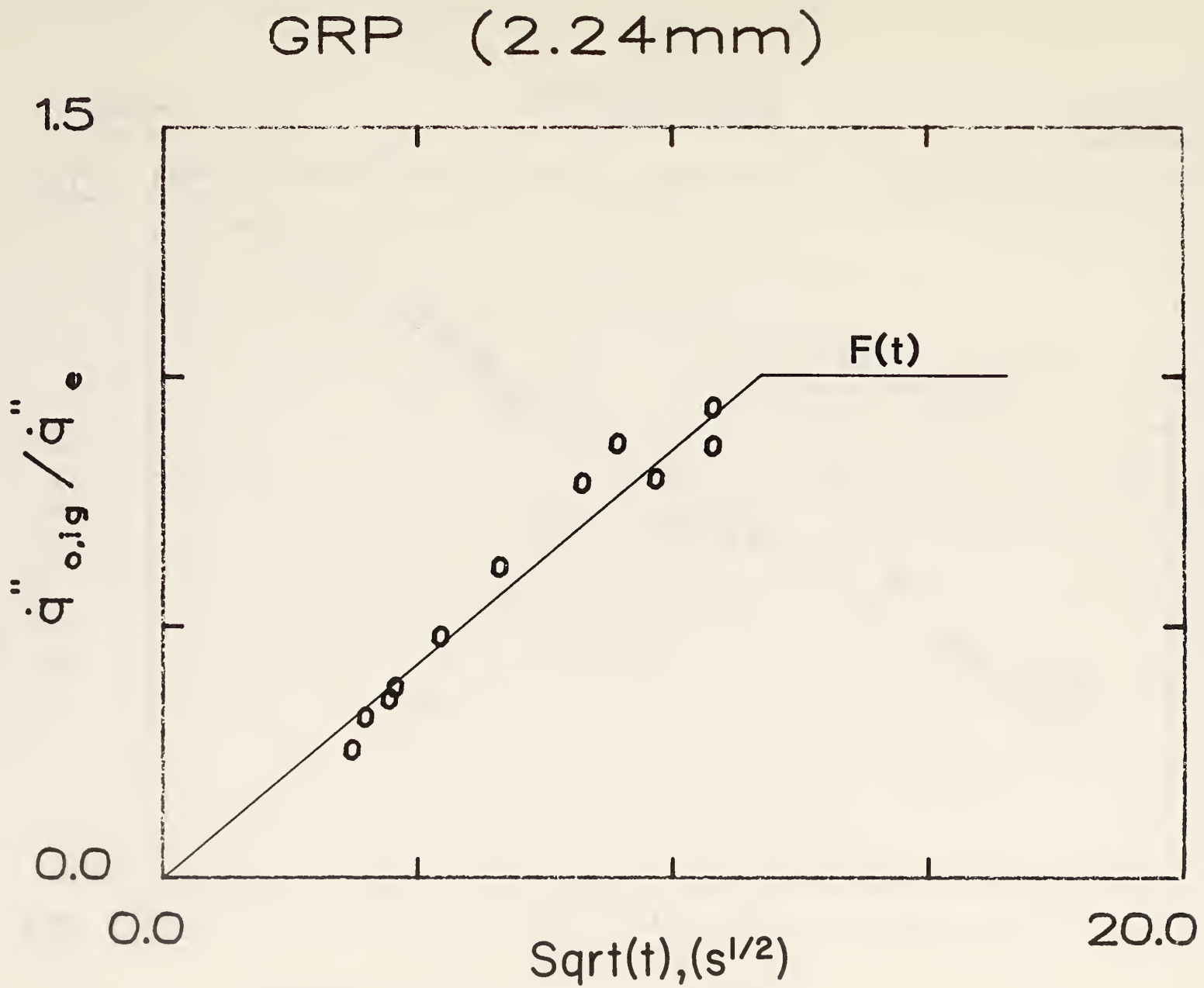

Figure A-20. Correlation of ignition results for GRP (2.24 mm).

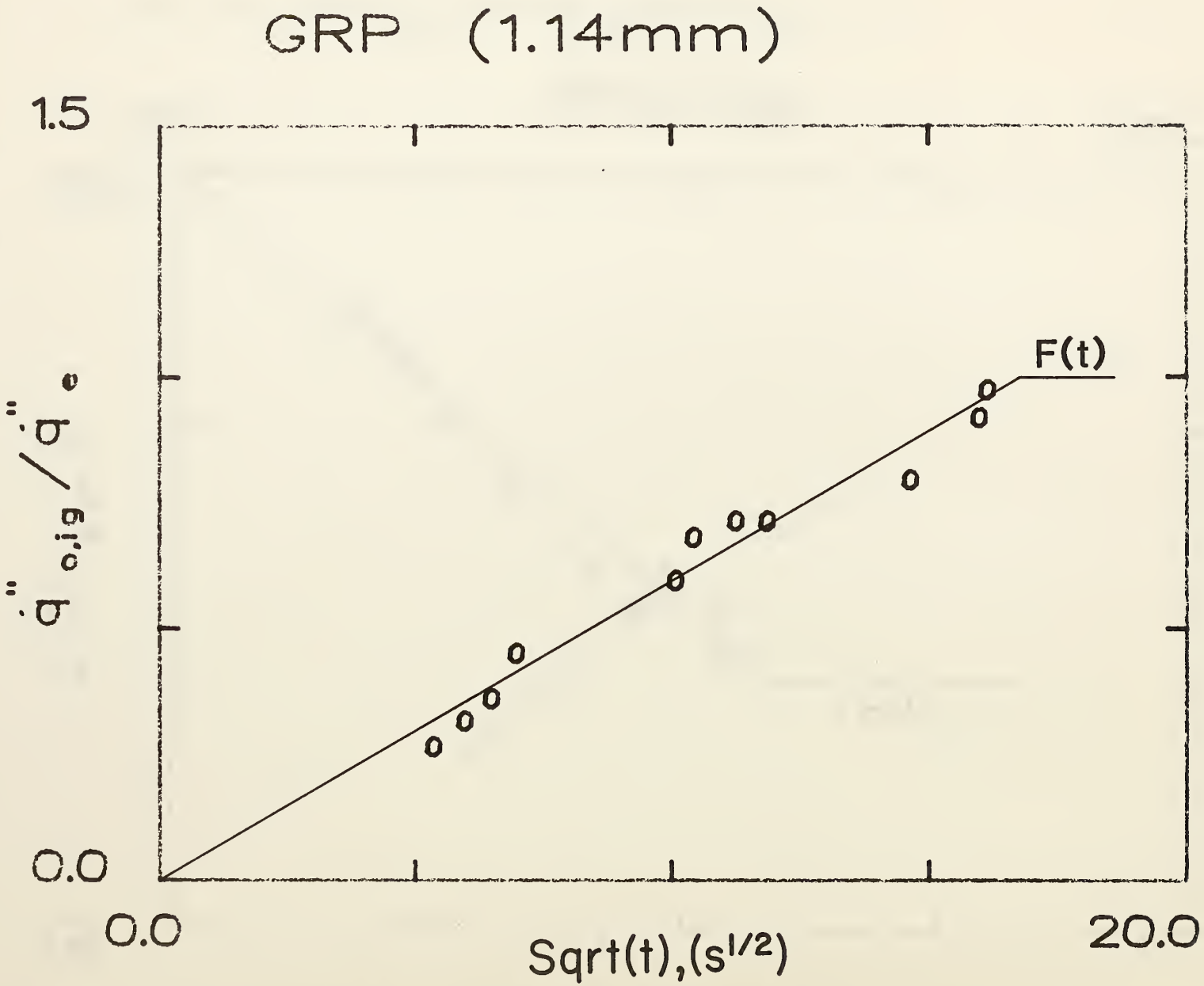

Figure A-21. Correlation of ignition results for GRP (1.14 mm)

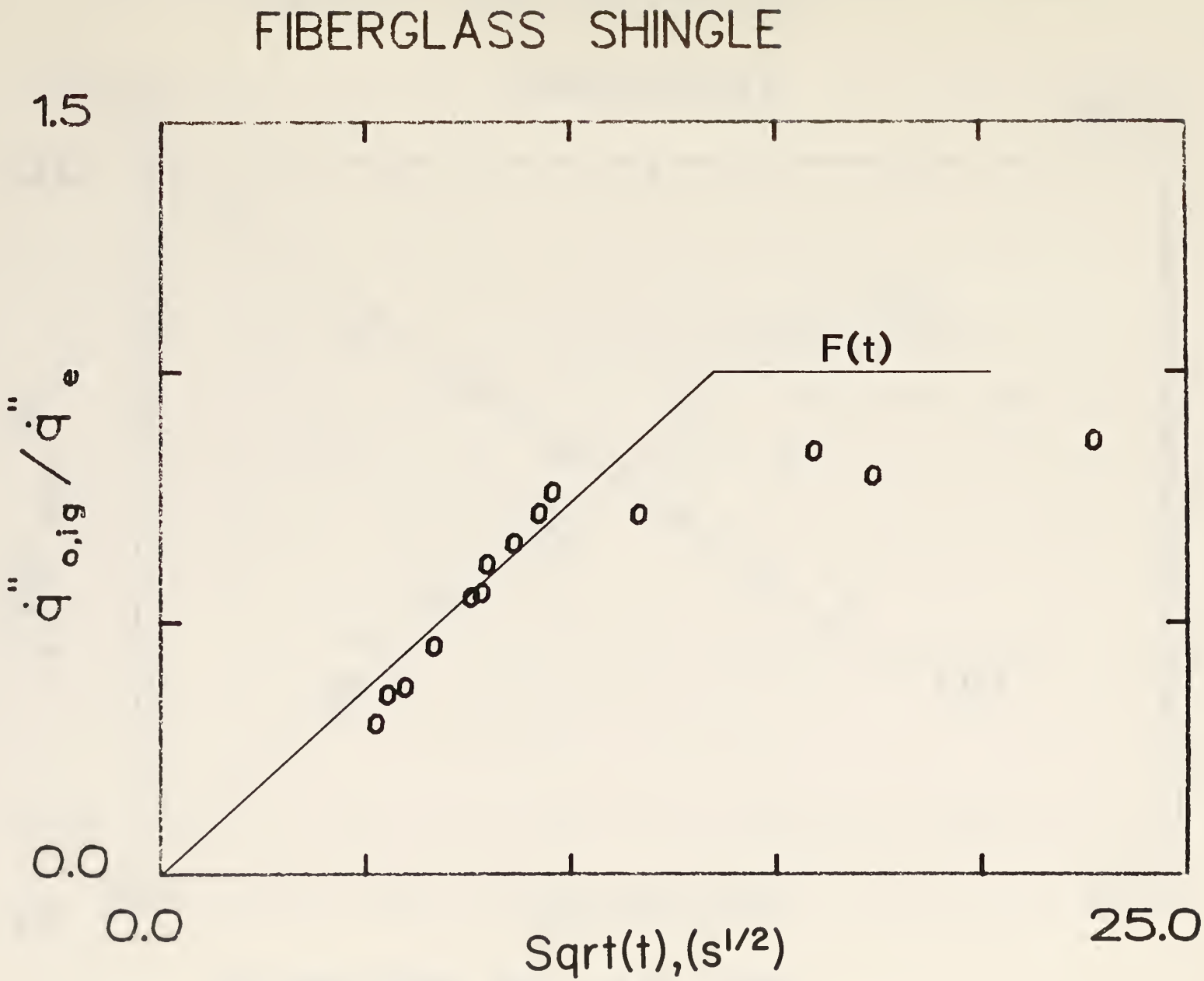

Figure A-22. Correlation of ignition results for fiberglass shingle.

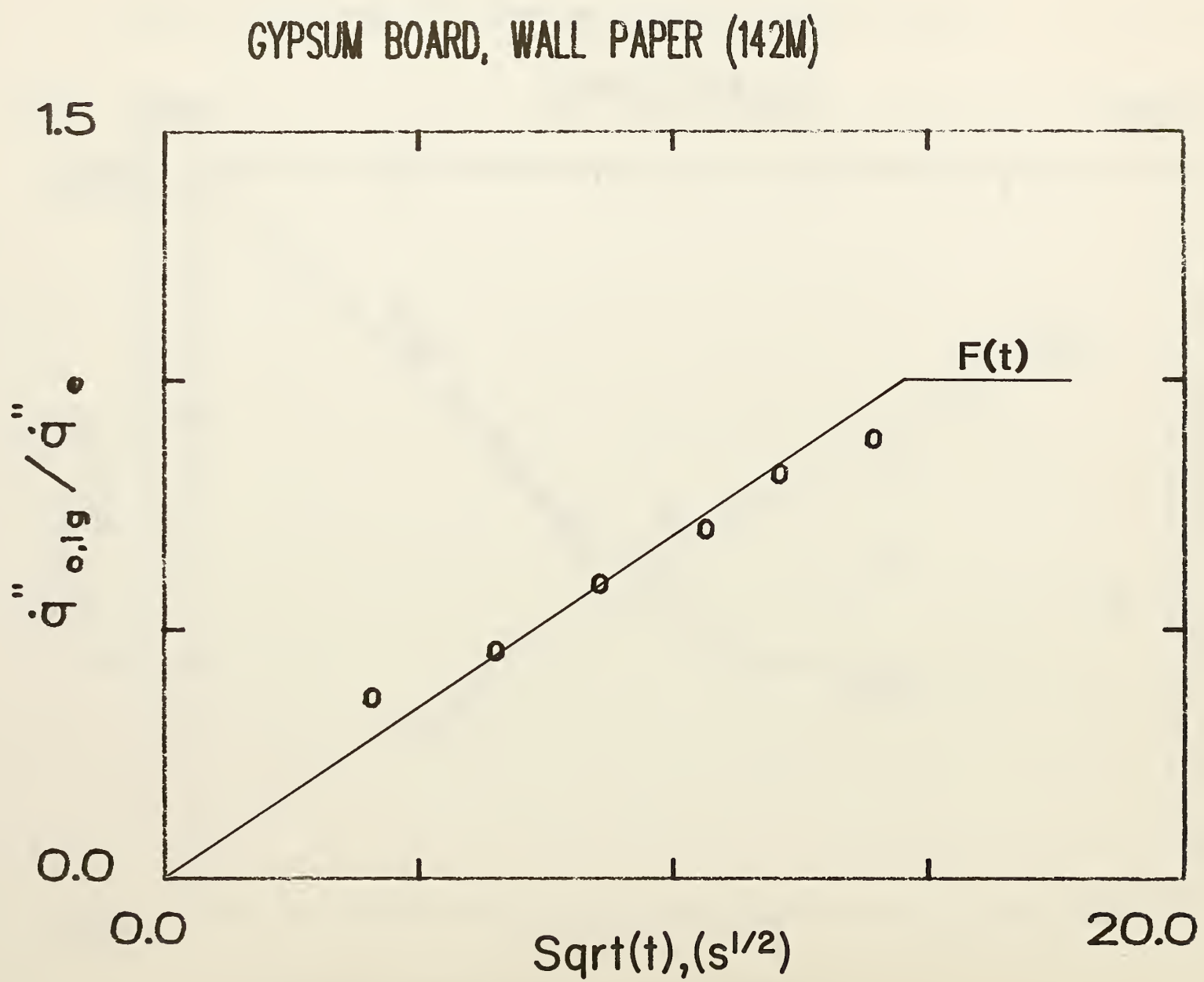

Figure A-23. Correlation of ignition results for gypsum board wallpaper (S142M).

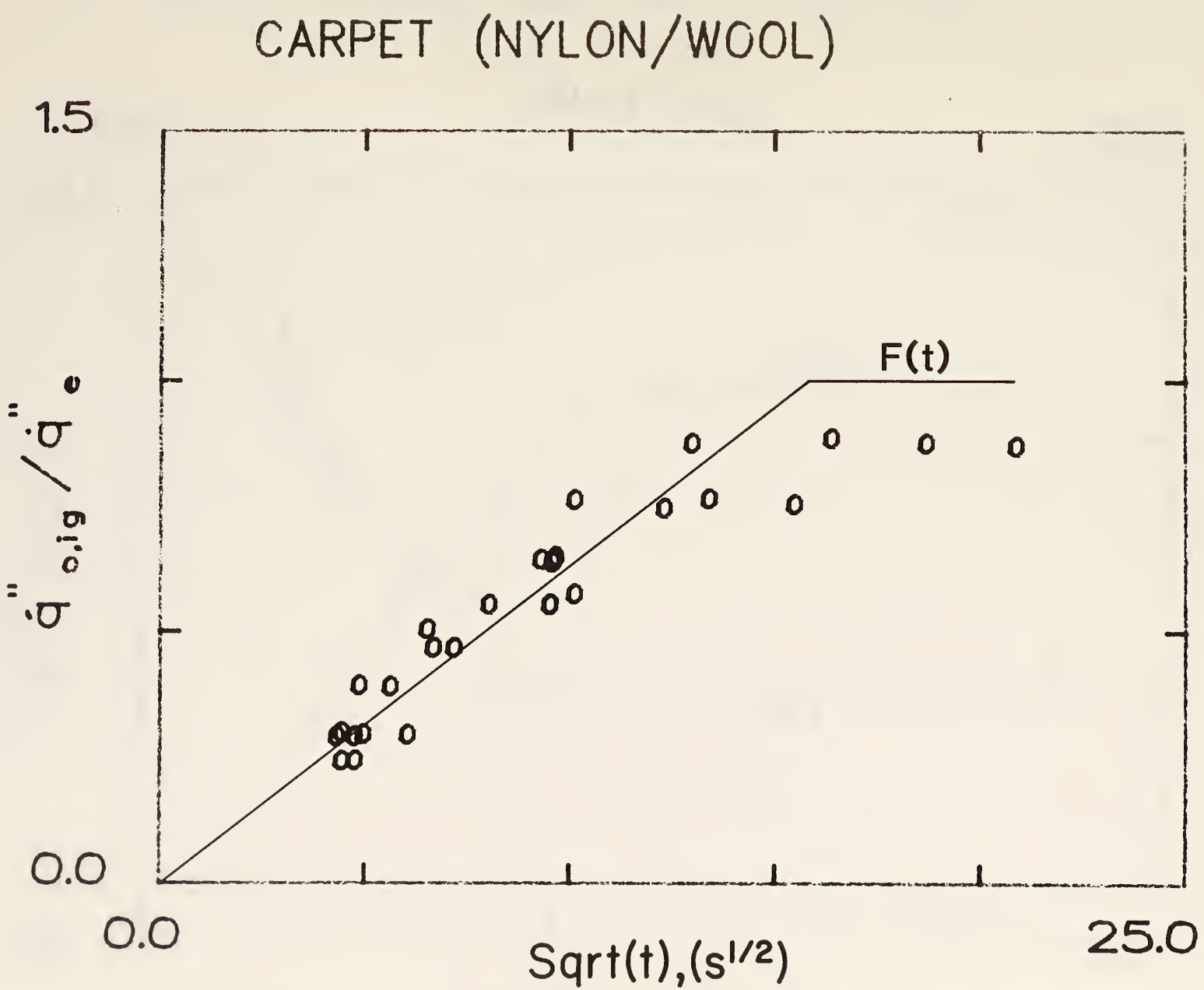

Figure A-24. Correlation of ignition results for carpet (nylon/wool).

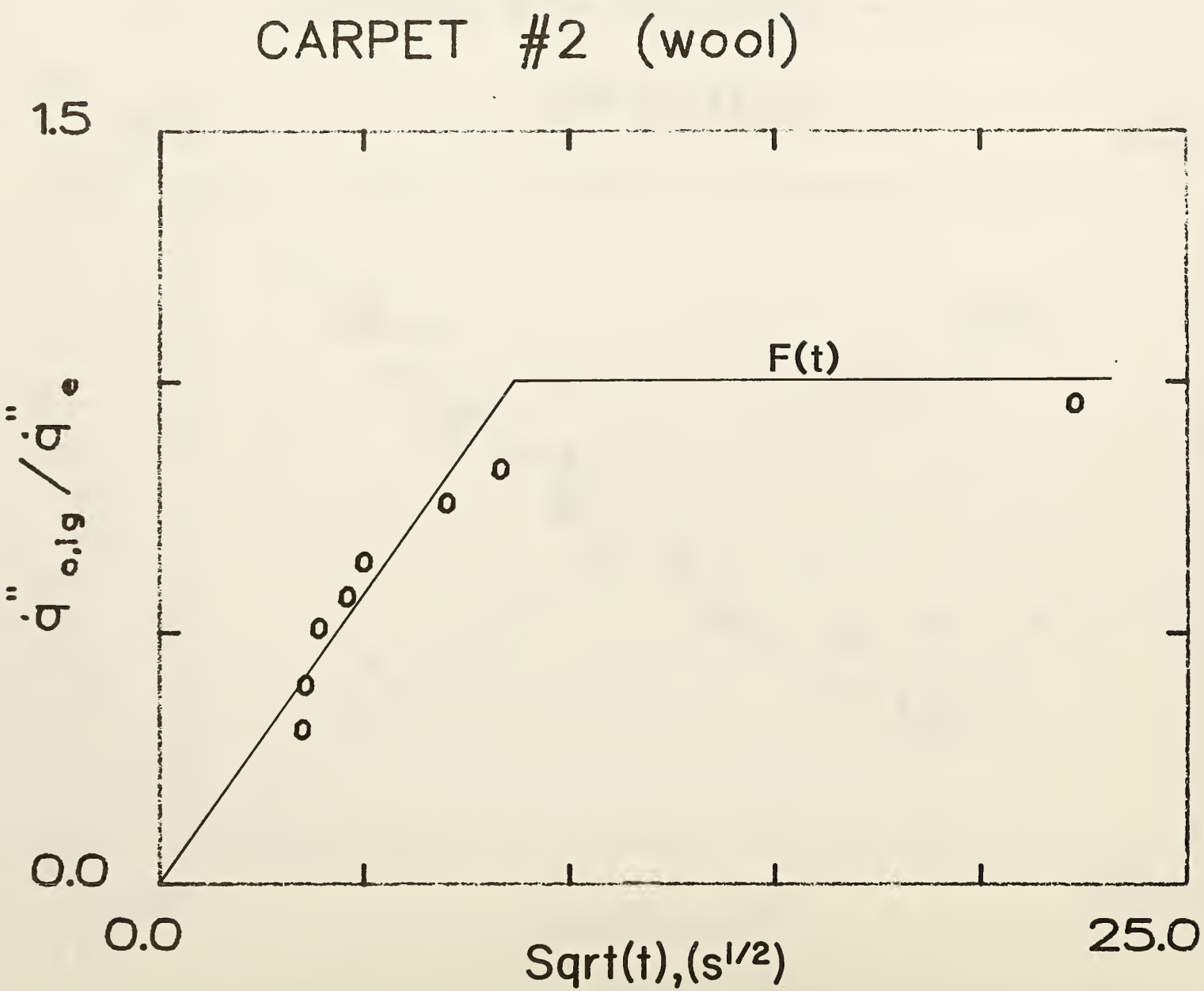

Figure A-25. Correlation of ignition results for carpet #2 (wool).

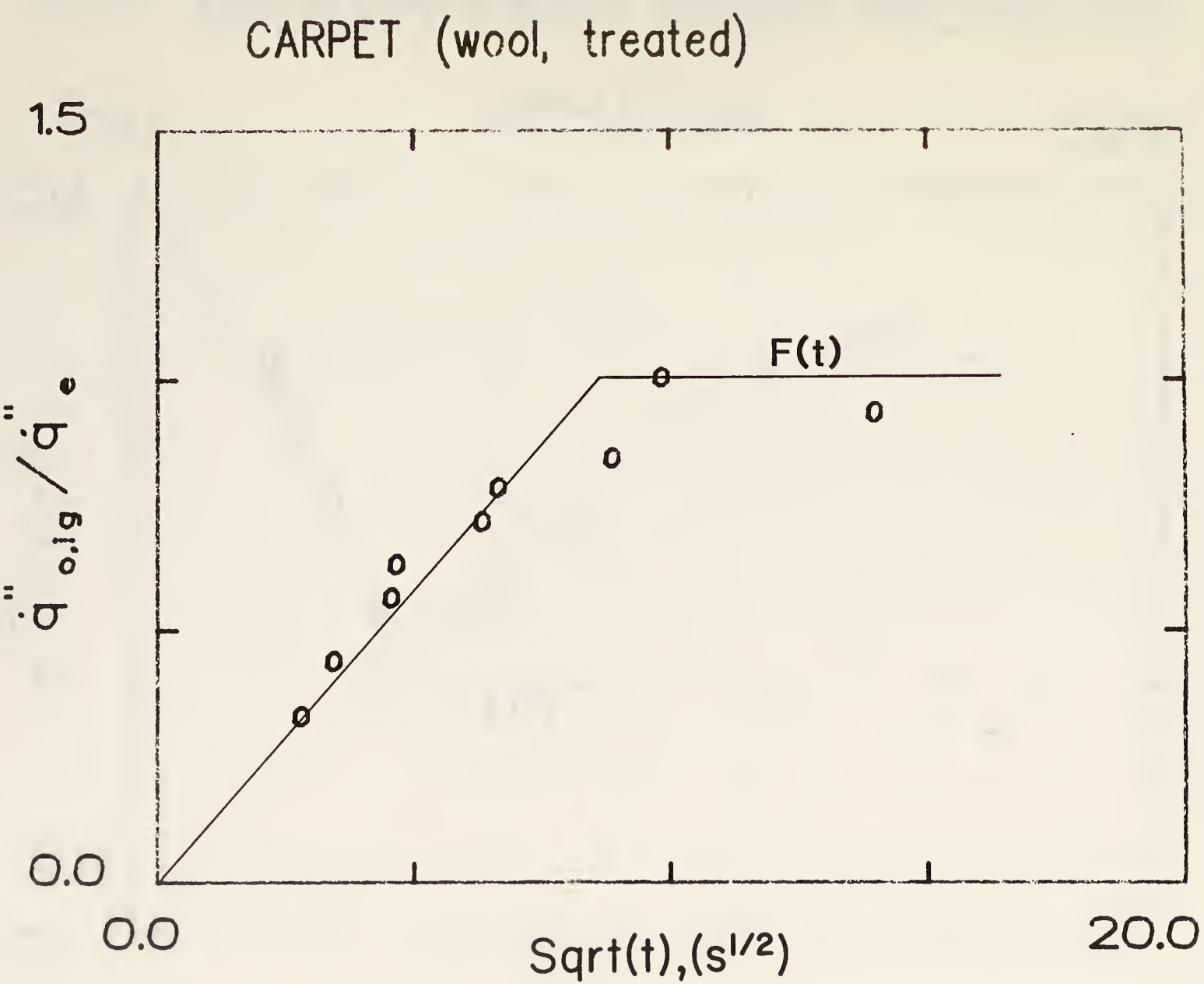

Figure A-26. Correlation of ignition results for carpet #2 (wool, treated).

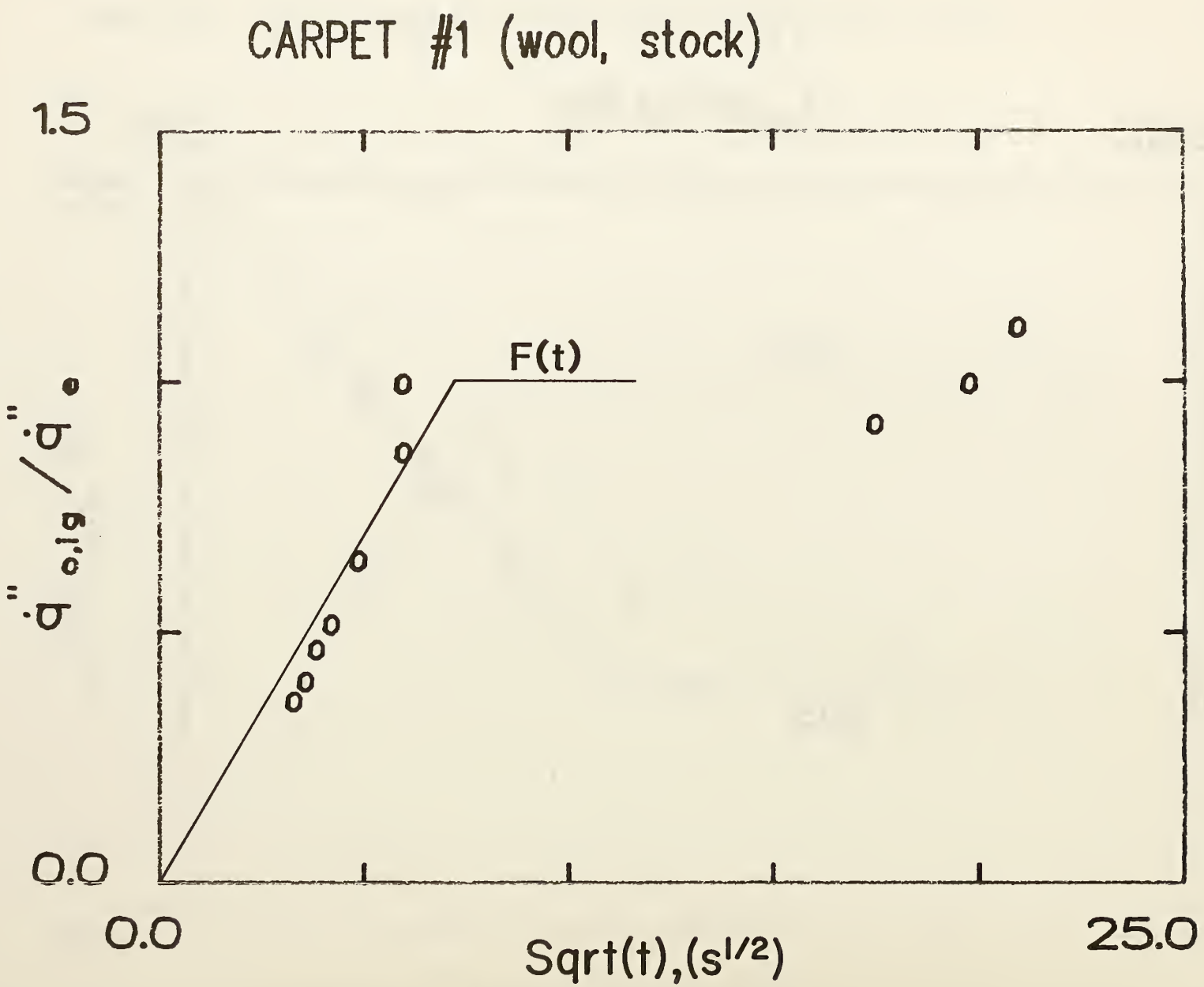

Figure A-27. Correlation of ignition results for carpet #1 (wool, stock).

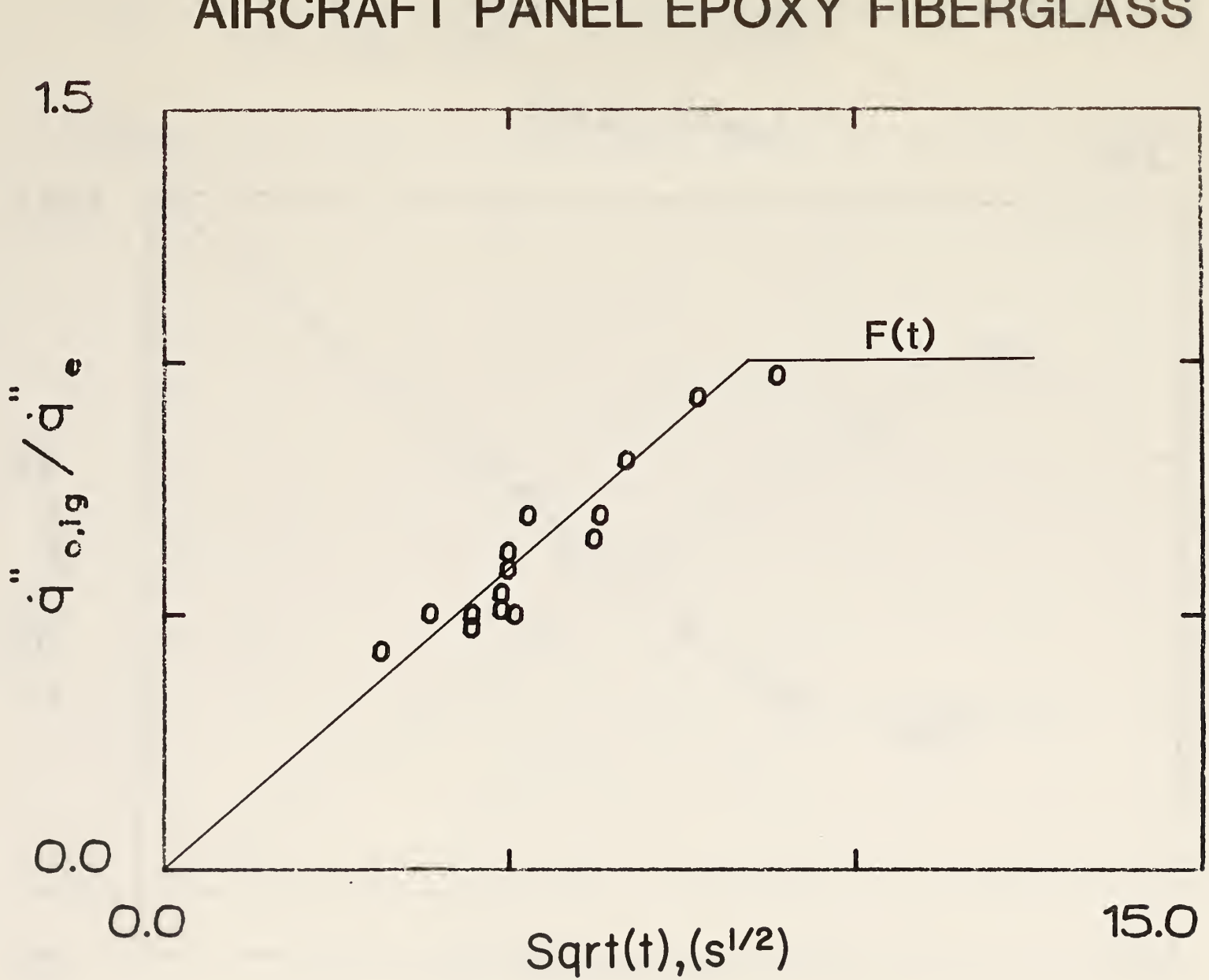

Figure A-28. Correlation of ignition results for aircraft panel (epoxy fiberglass).

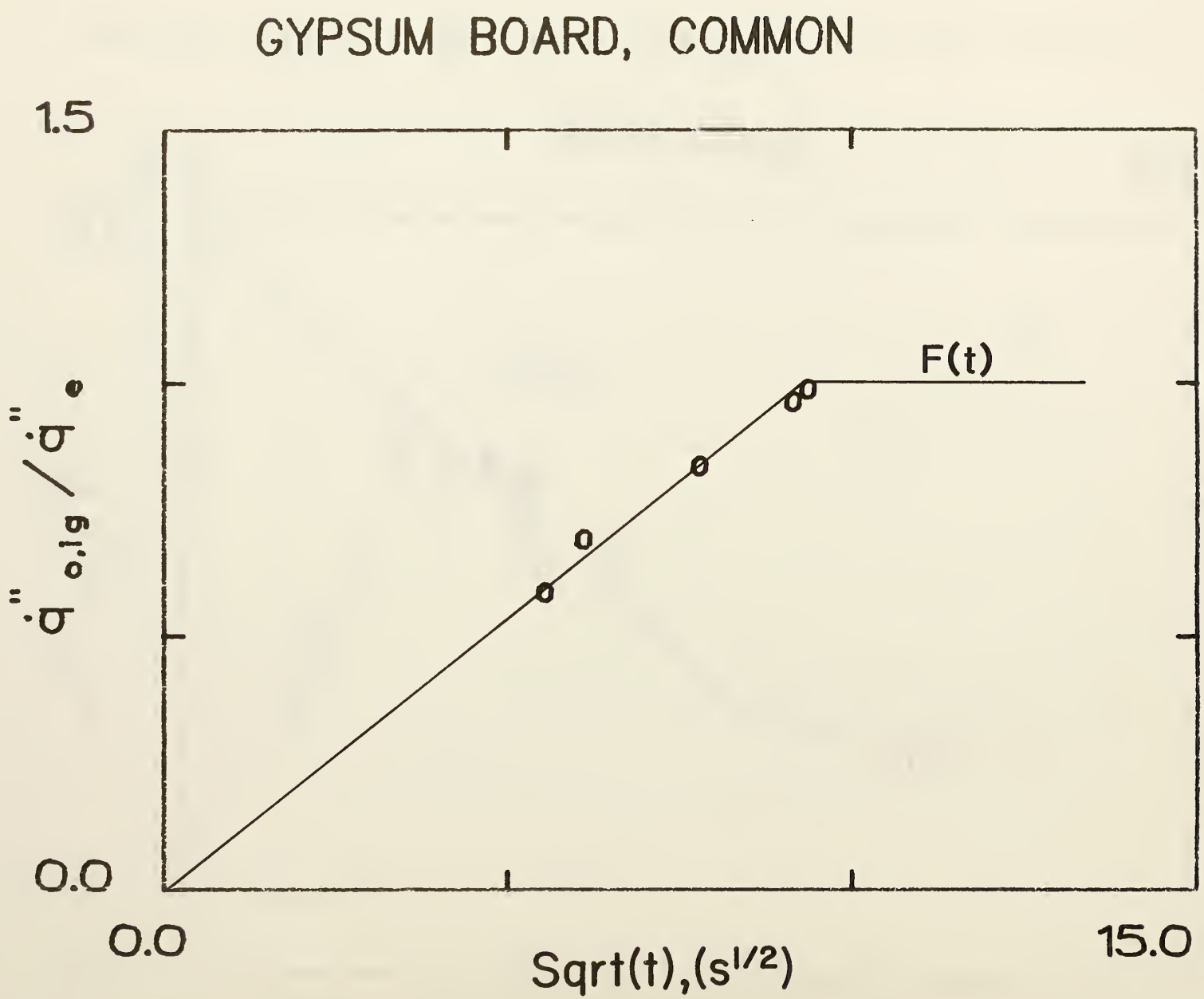

Figure A-29. Correlation of ignition results for gypsum board (1.27 mm, common).

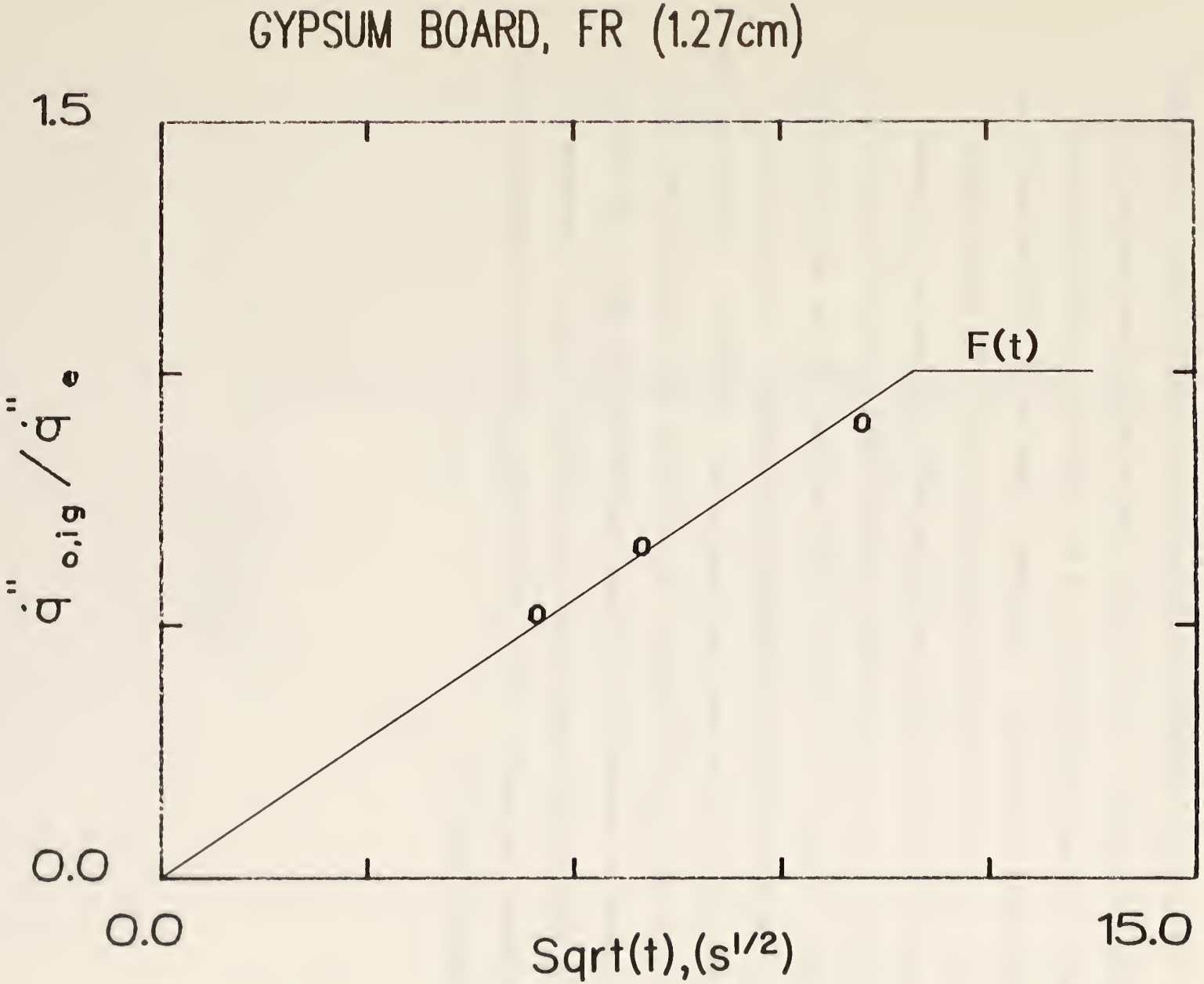

Figure A-30. Correlation of ignition results for gypsum board, FR (1.27 cm).

Appendix B. Correlation of Spread Results

Flame spread tests were conducted for a variety of plastic, wood and composite materials. The materials flame velocities were computed from a running 3-point least square fit of the slope of the position-time data. These computed velocities, correlated in terms of eq. (12) and plotted as V-1/2 vs q''_e F(t) are shown in figures B-1 to B-33. The data represents results for varied external irradiances for no pre-heat and pre-heated materials. Table B-1 lists these external radiant fluxes to the material surface at the 50 mm position $(q''_e (50))$ and indicates the ignition procedure, i.e., no pre-heat and/or pre-heating of the specimen. The solid line, indicating the slope, was drawn based on the core-data set, ignoring the ends at high and low $\dot{q}''_e$ F(t) values. The low end is near extinction and other phenomena are suspected to influence the flame spread speed. The high end is near ignition where spread velocities are high and ignition phenomena can influence this speed. Figures B-3, B-4, B-5, B-11 and B-32 include data for downward spread (9).

Table B-1.
External irradiance and ignition procedure for spread velocity tests

Figure #	$\dot{q}''_e(50)$ W/cm^2	No Preheat	Preheat
1	3.0		x
2	3.0		x
3	3.0	x	x
4	2.0	x	x
5	3.0	x	x
6	2.0		x
7	4.0		x
8	3.0		x
9	2.7 to 5.0	x	
10	3.0		x
11	1.7 to 5.0	x	x
12	3.0	x	x
13	3.0		x
14	3.0		x
15	3.0		x
16	5.0	x	
17	5.0	x	
18	5.0	x	
19	5.0	x	
20	3.5		x
21	2.1 to 5.0	x	
22	3.0		x
23	3.0 to 4.0		x
24	3.0		x
25	3.0		x
26	2.1 to 3.0		x
27	2.0		x
28	2.3 to 3.8		x
29	5.0	x	
30	5.0	x	
31	5.0	x	
32	5.0		x
33	3.0		x
34	5.0	x	

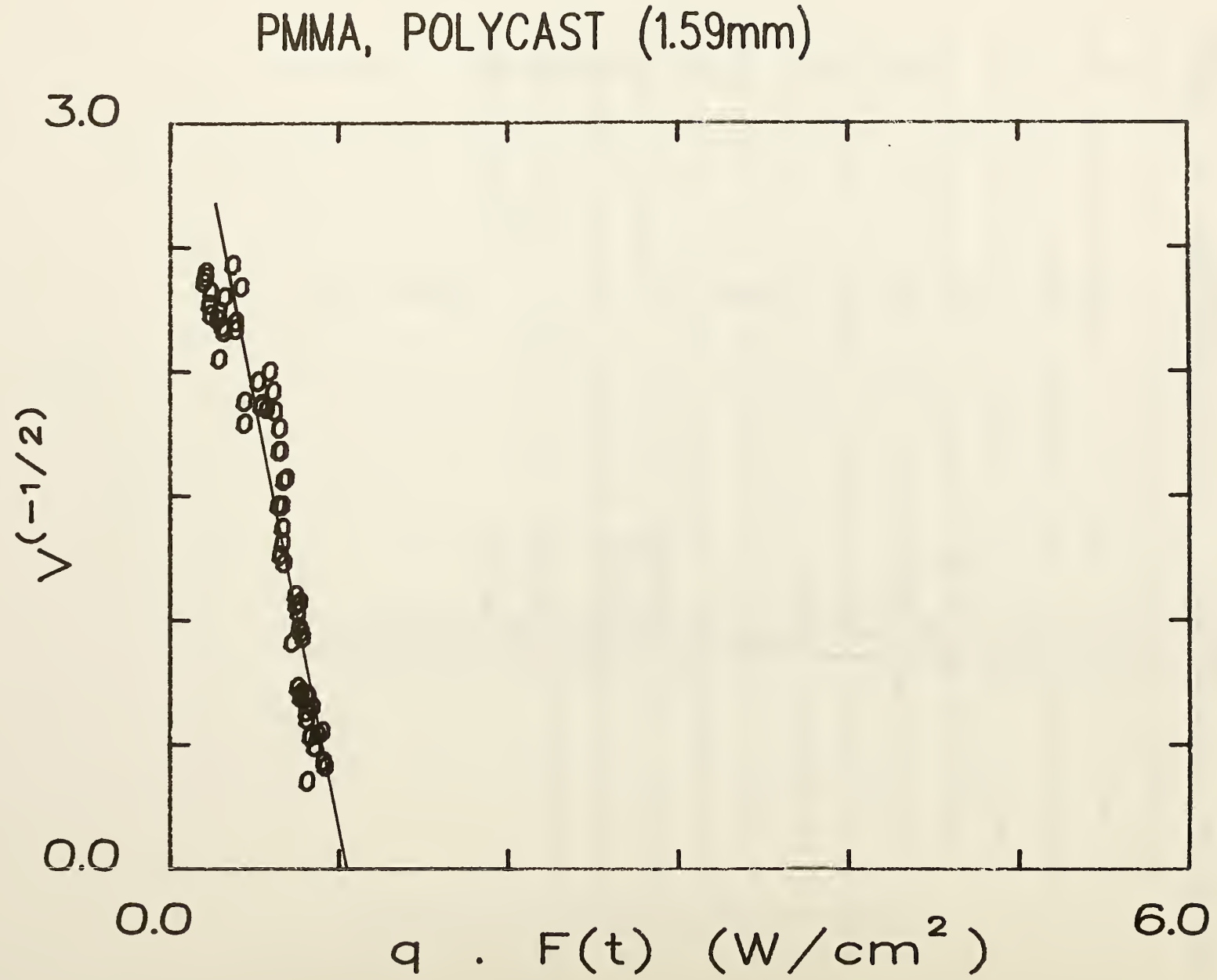

Figure B-1. Correlation of spread velocity for PMMA polycast (1.59 mm).

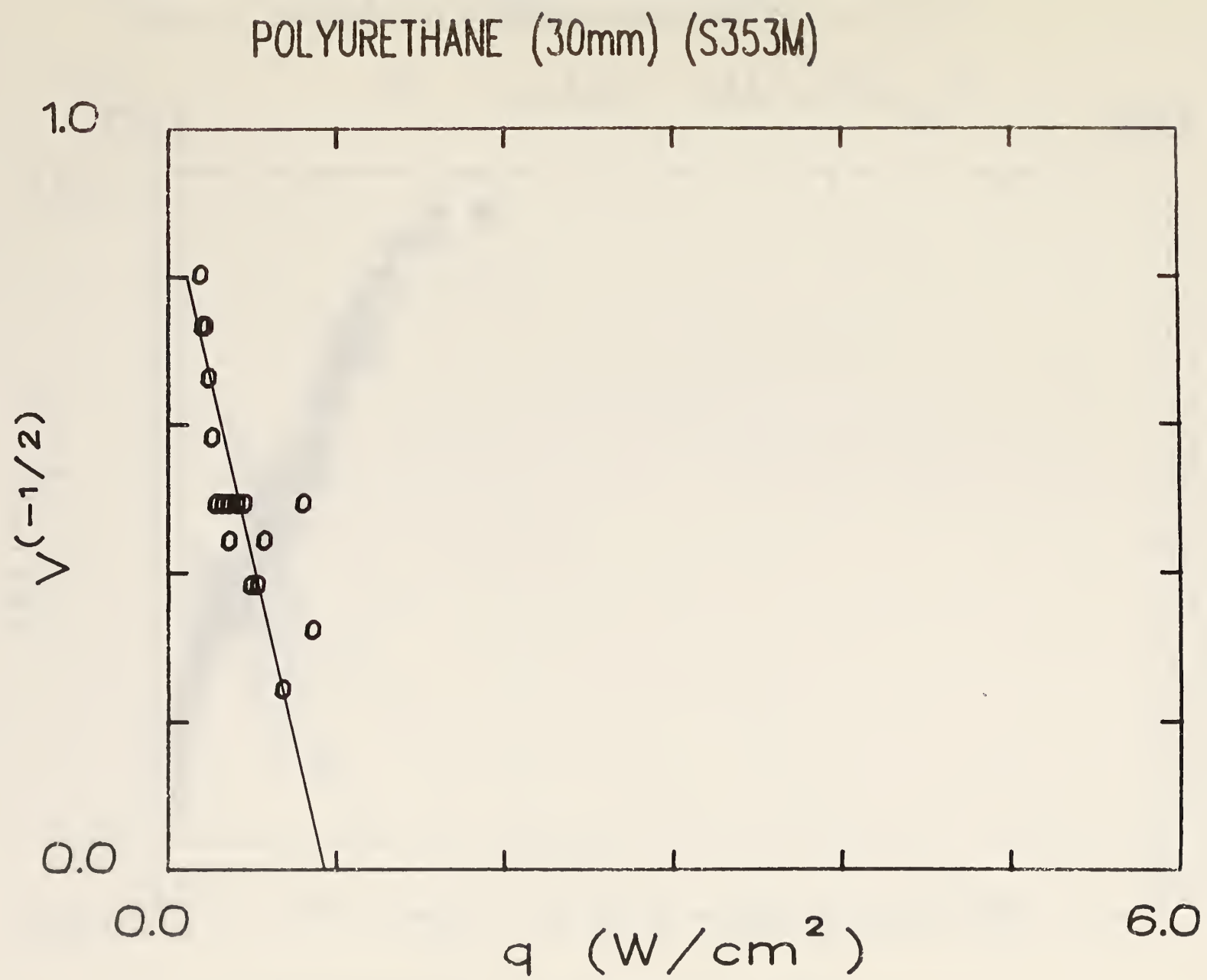

Figure B-2. Correlation of spread velocity for polyurethane (S353M, 30 mm).

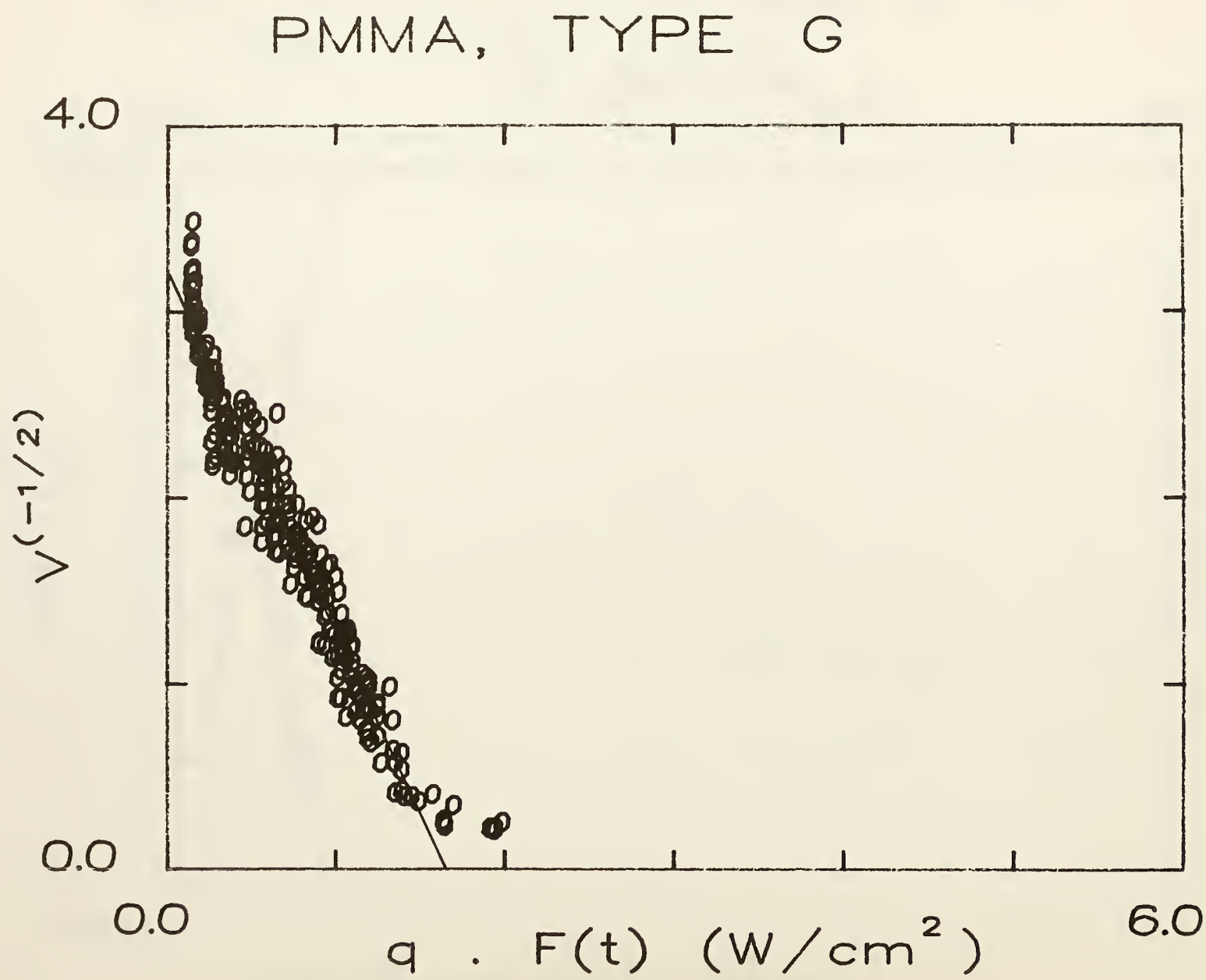

Figure B-3. Correlation of spread velocity for PMMA Type G (1.27 cm).

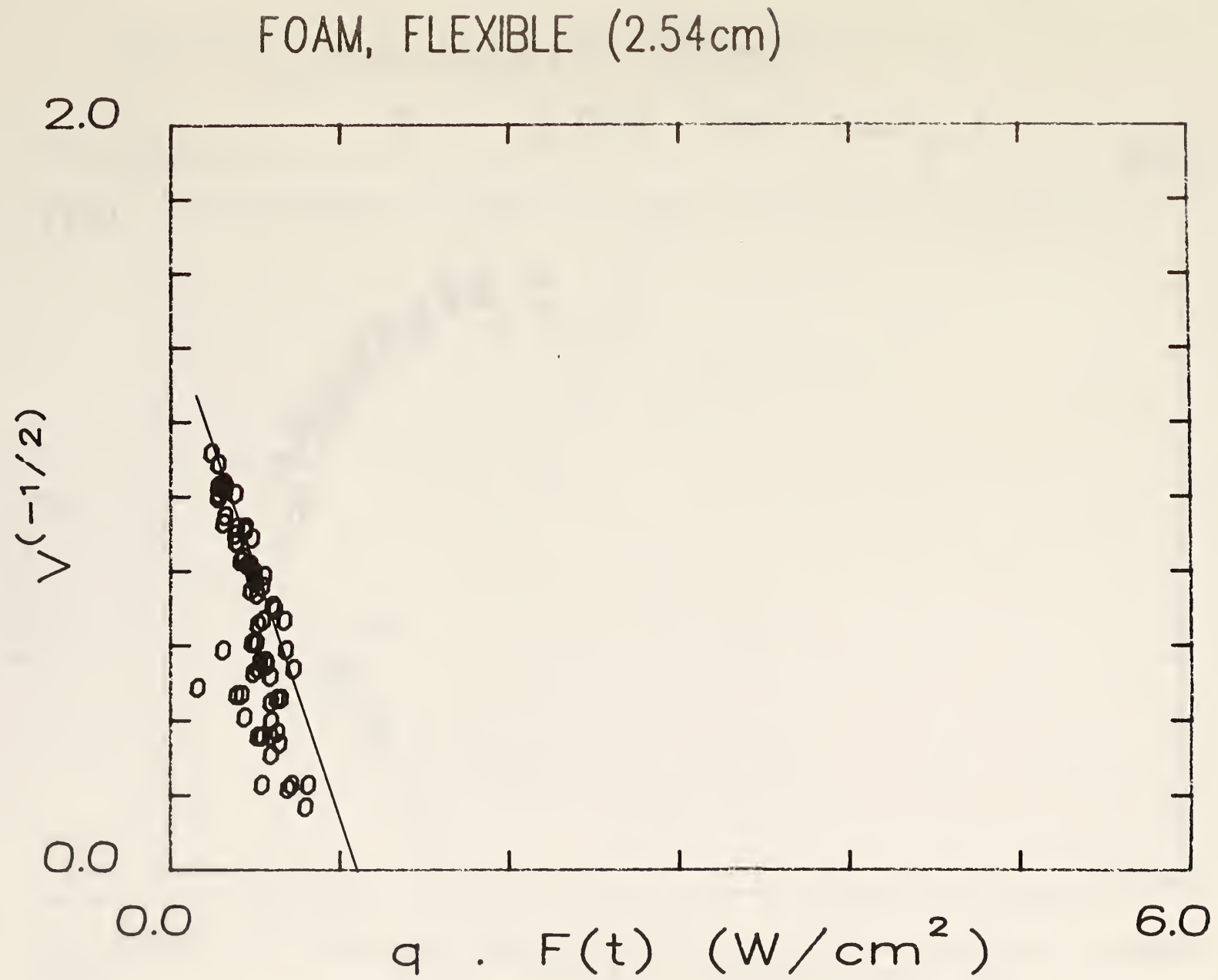

Figure B-4. Correlation of spread velocity for flexible foam (2.54 cm).

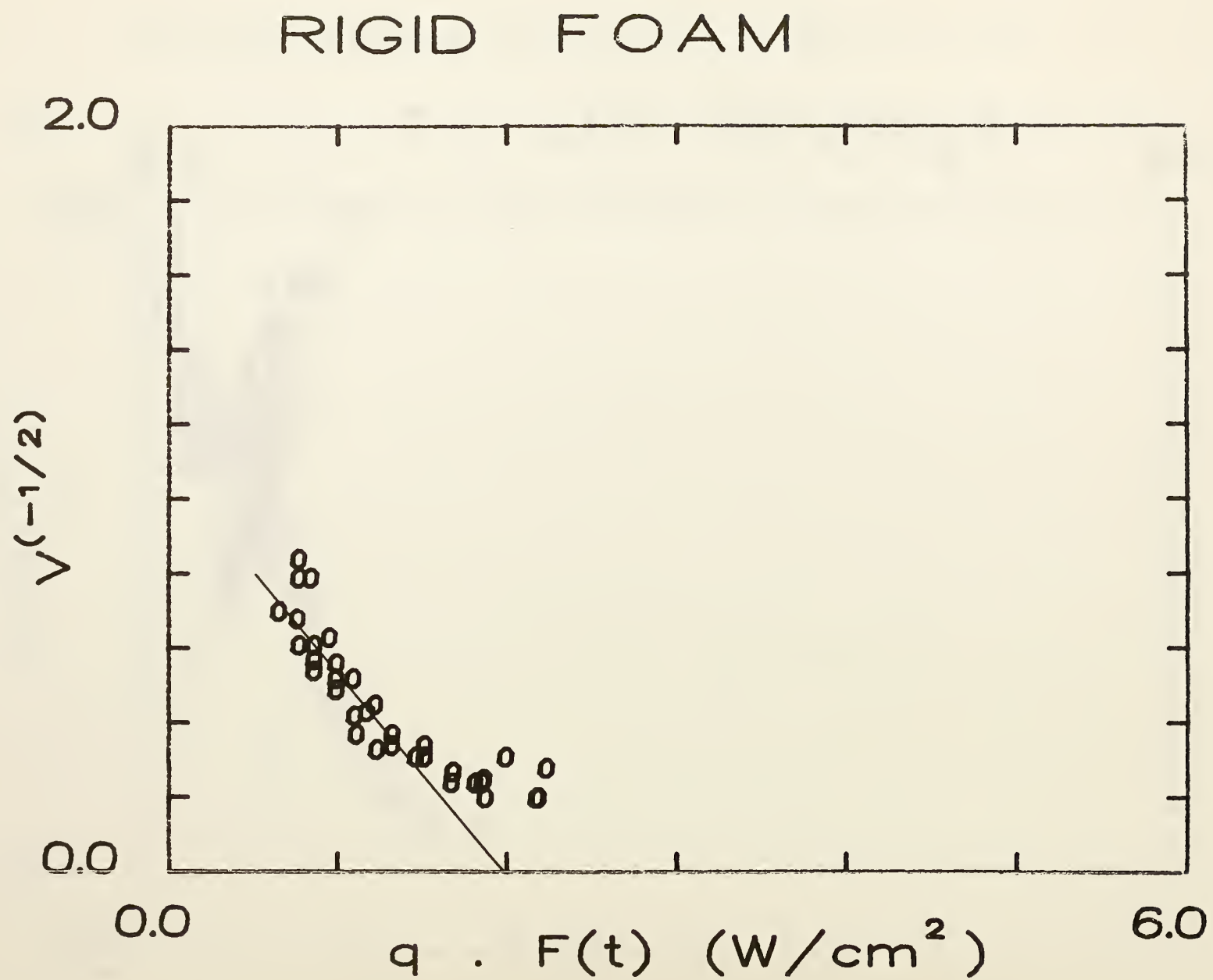

Figure B-5. Correlation of spread velocity for rigid foam (2.54 cm).

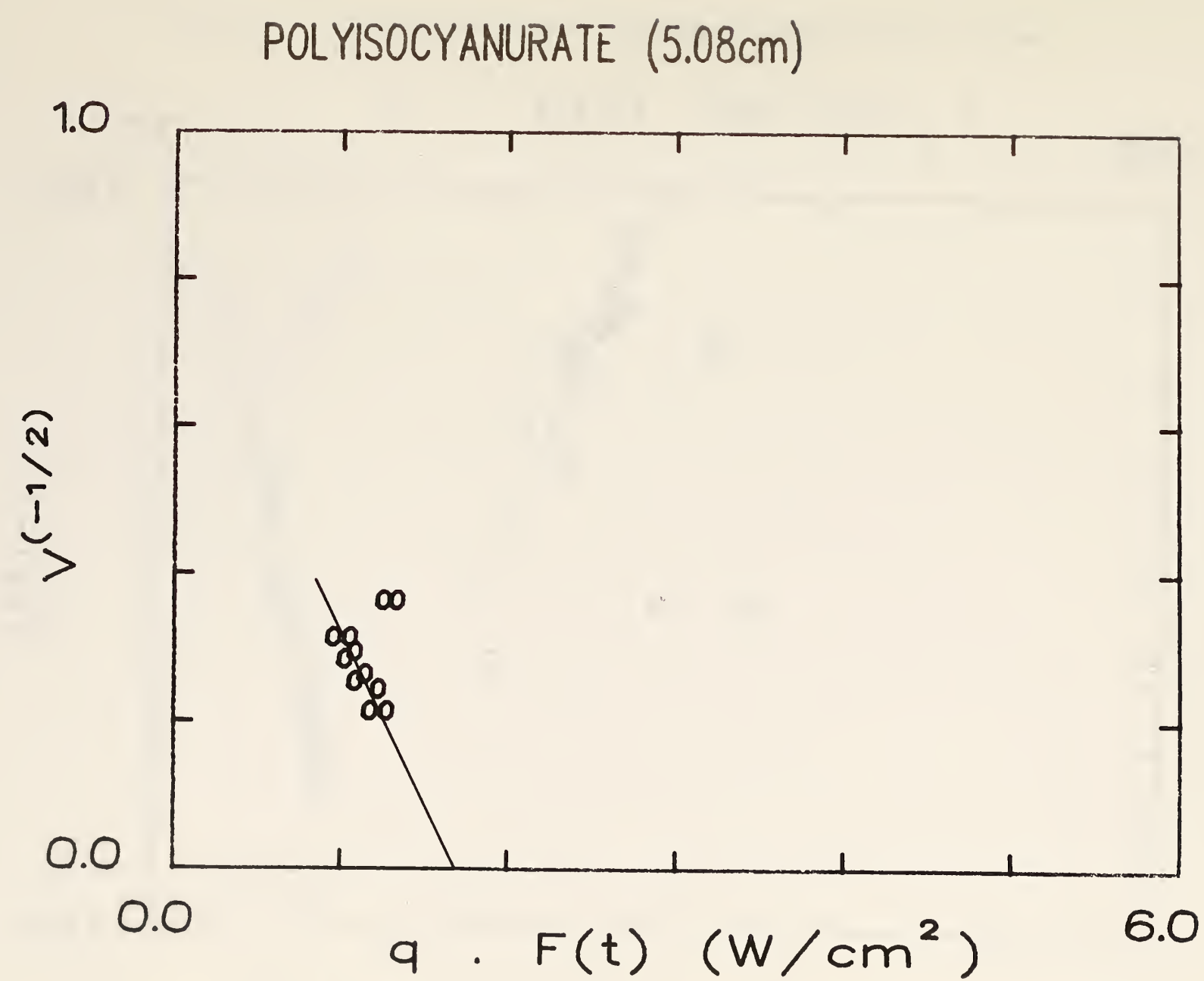

Figure B-6. Correlation of spread velocity for polyisocyanurate (5.08 cm).

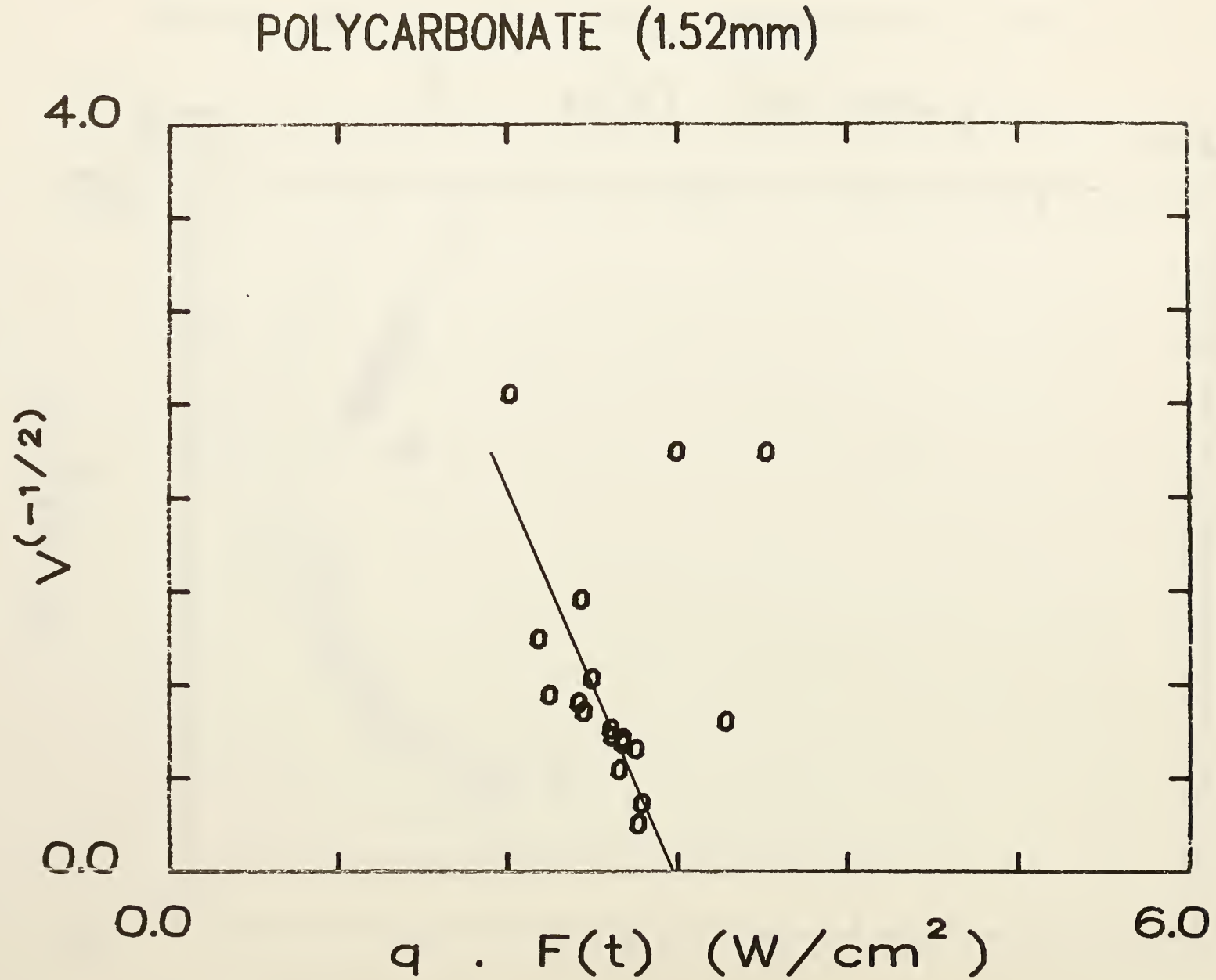

Figure B-7. Correlation of spread velocity for polycarbonate (1.52 mm).

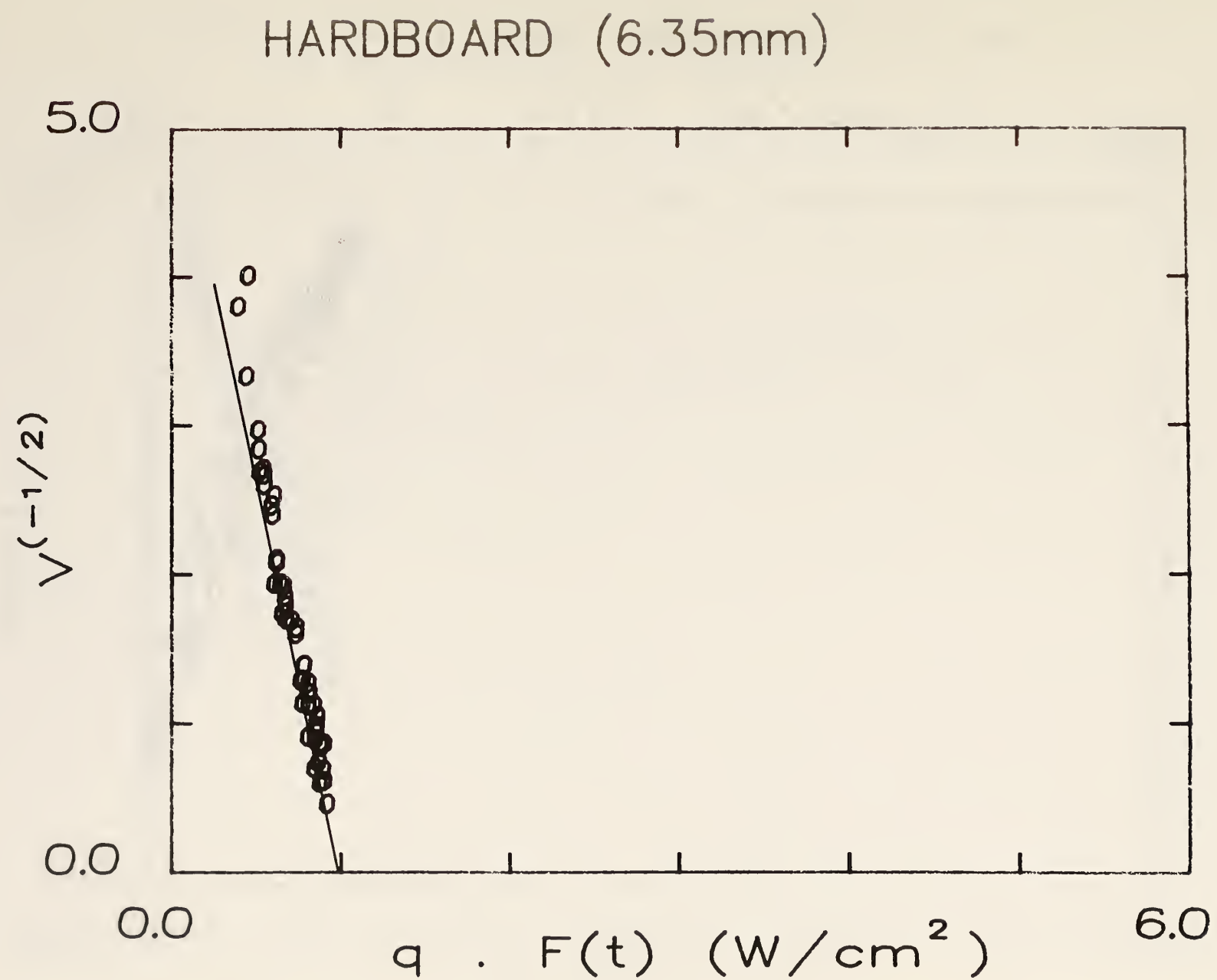

Figure B-8. Correlation of spread velocity for hardboard (6.35 mm).

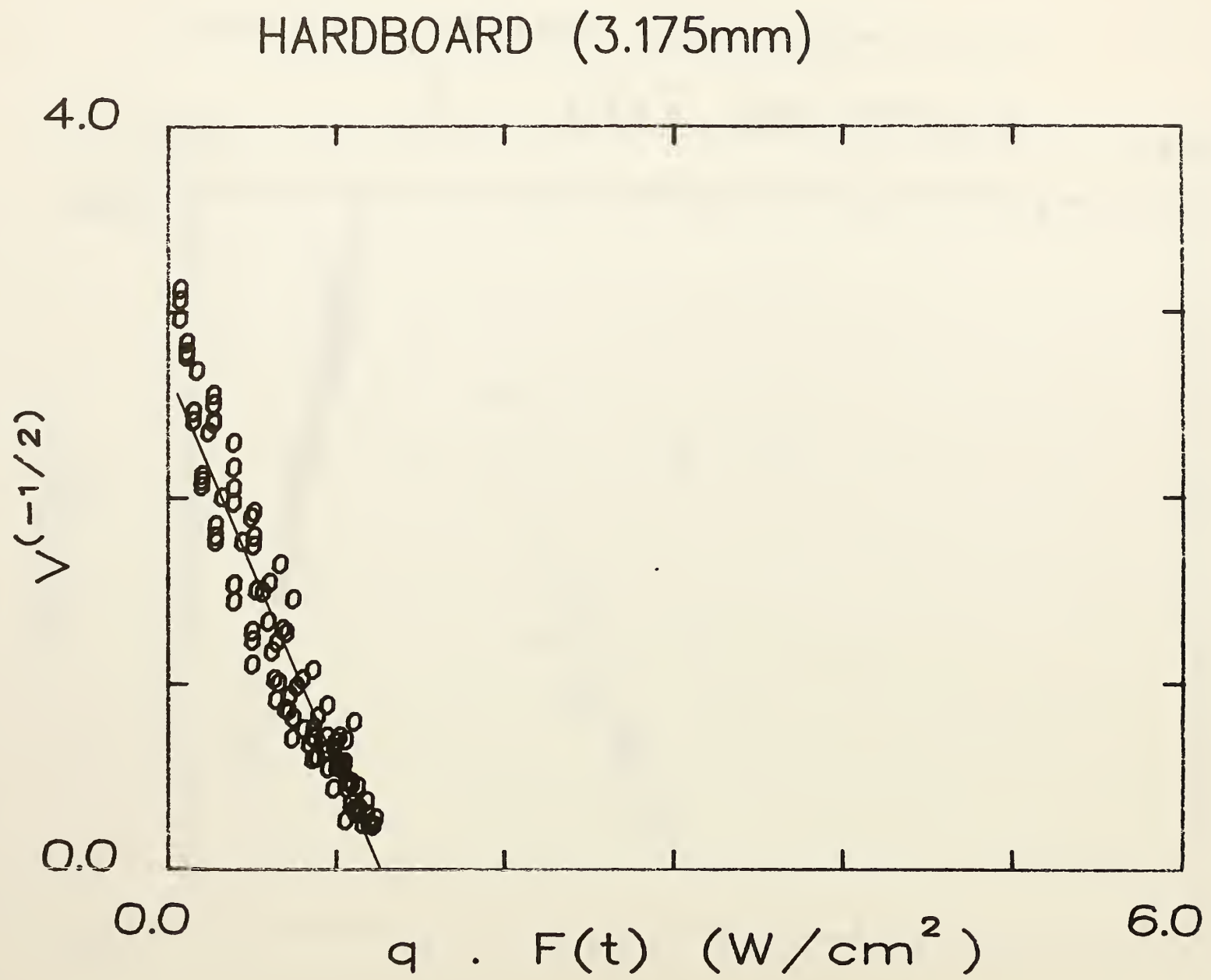

Figure B-9. Correlation of spread velocity for hardboard (3.175 mm).

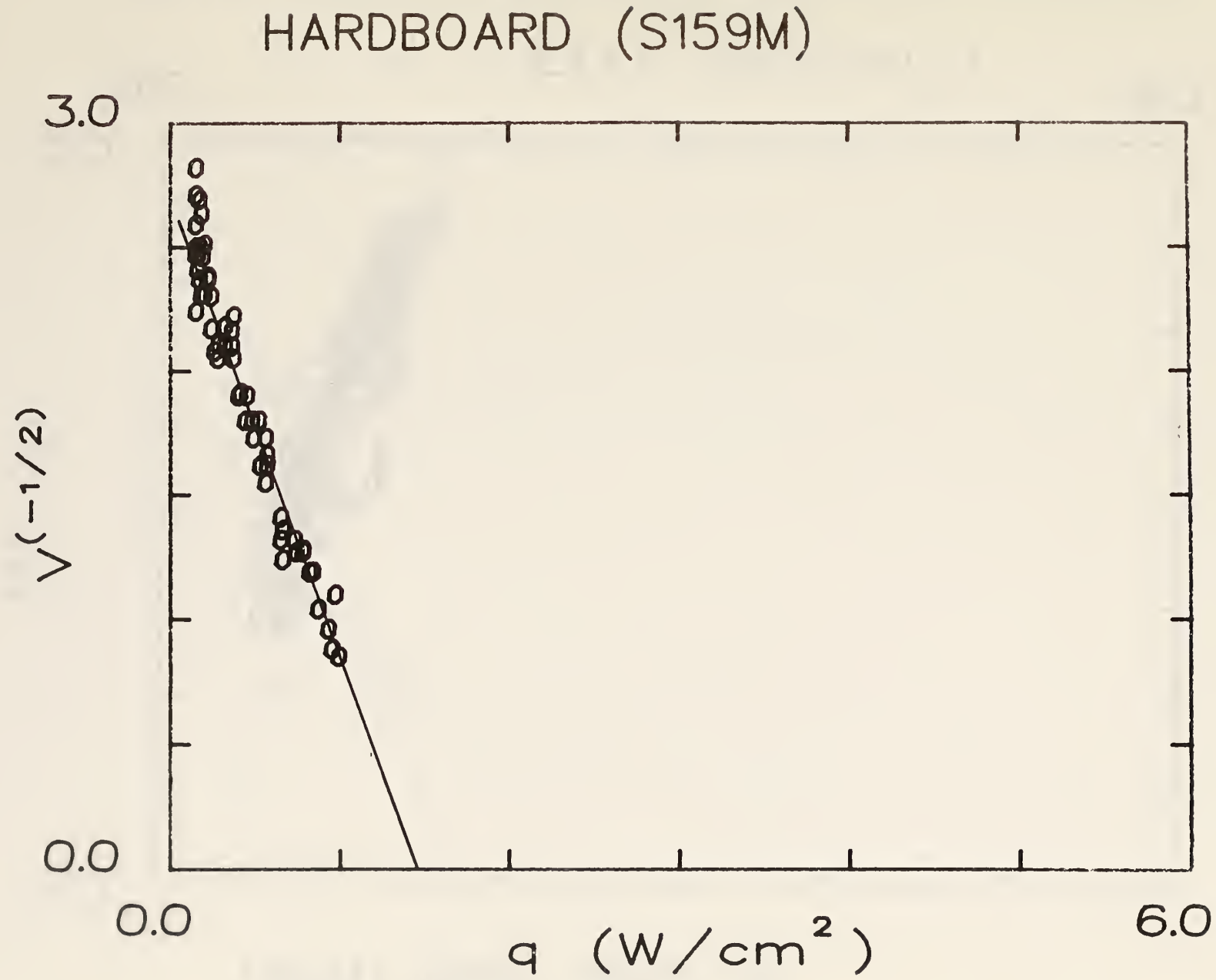

Figure B-10. Correlation of spread velocity for hardboard (S159M, 1.0 cm).

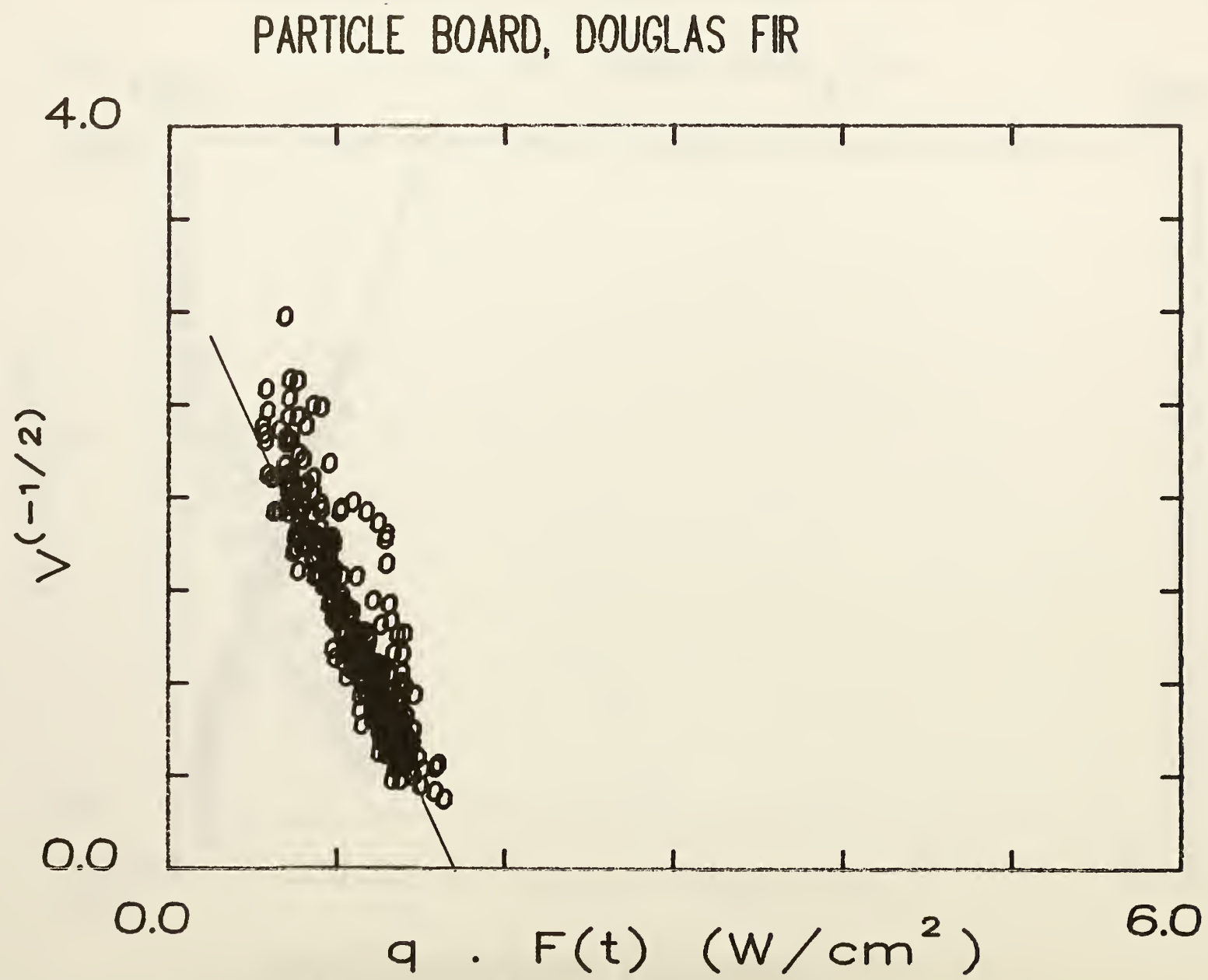

Figure B-11. Correlation of spread velocity for Douglas fir particle board (1.27 cm).

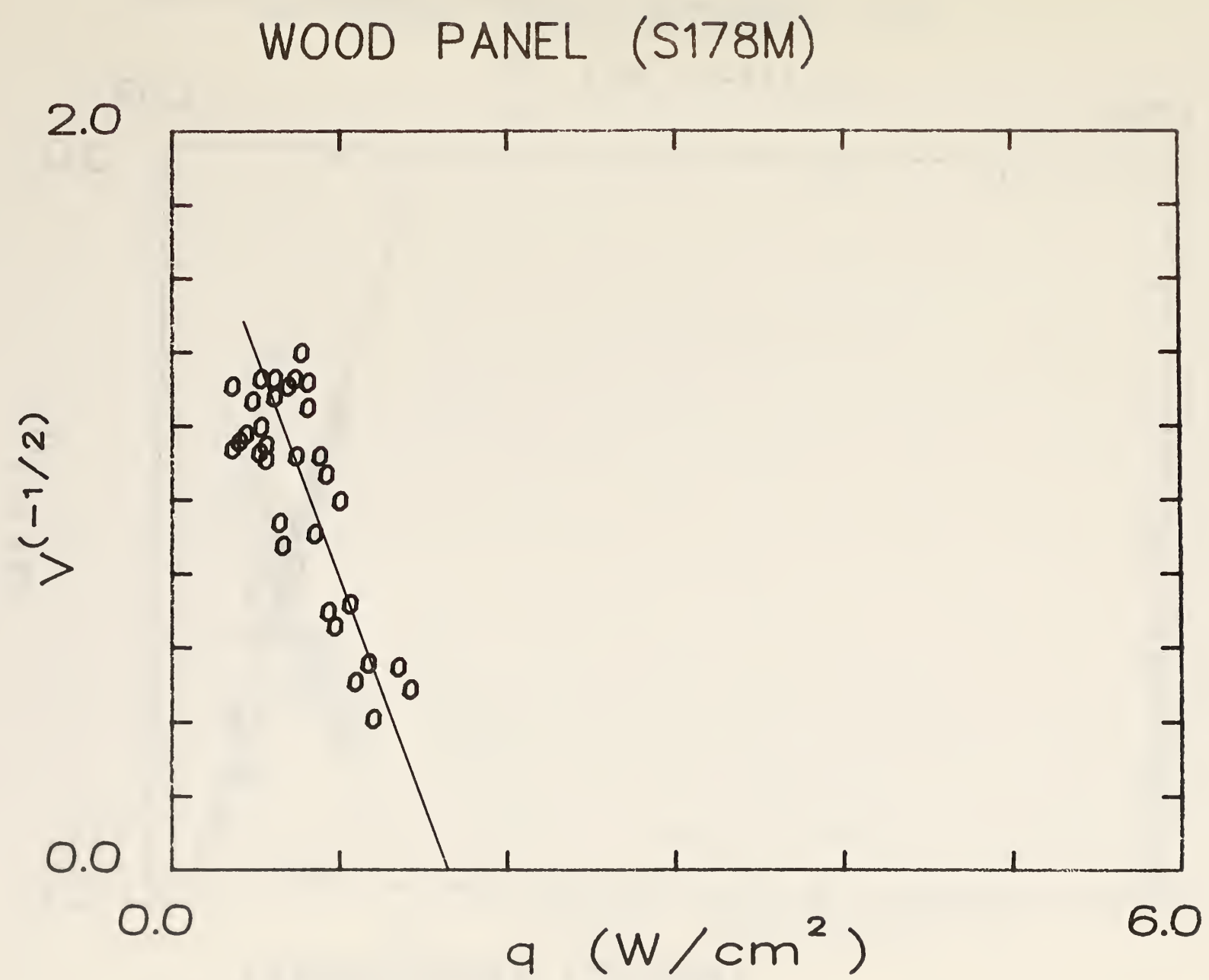

Figure B-12. Correlation of spread velocity for wood panel (S178M).

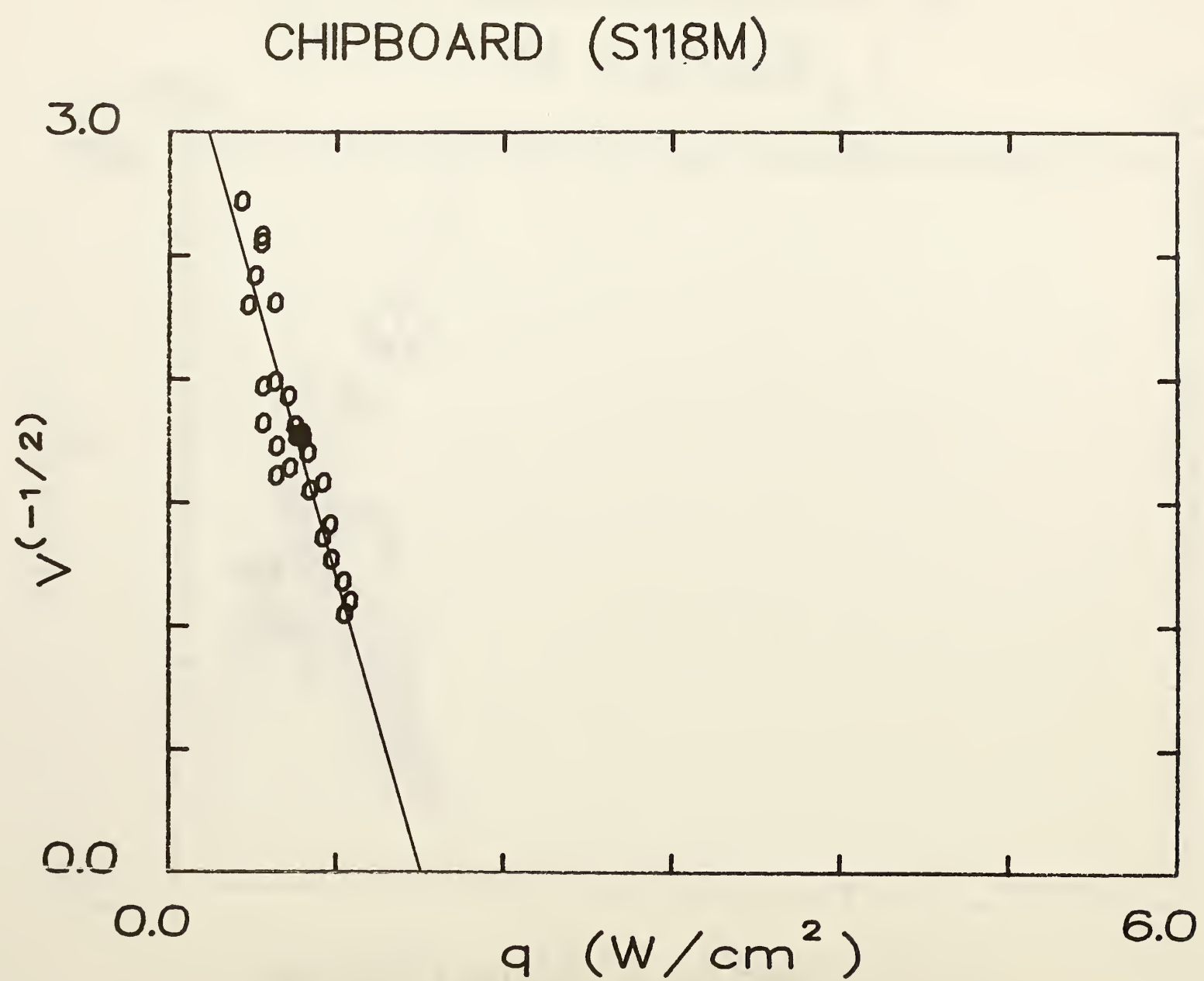

Figure B-13. Correlation of spread velocity for chipboard (S118M).

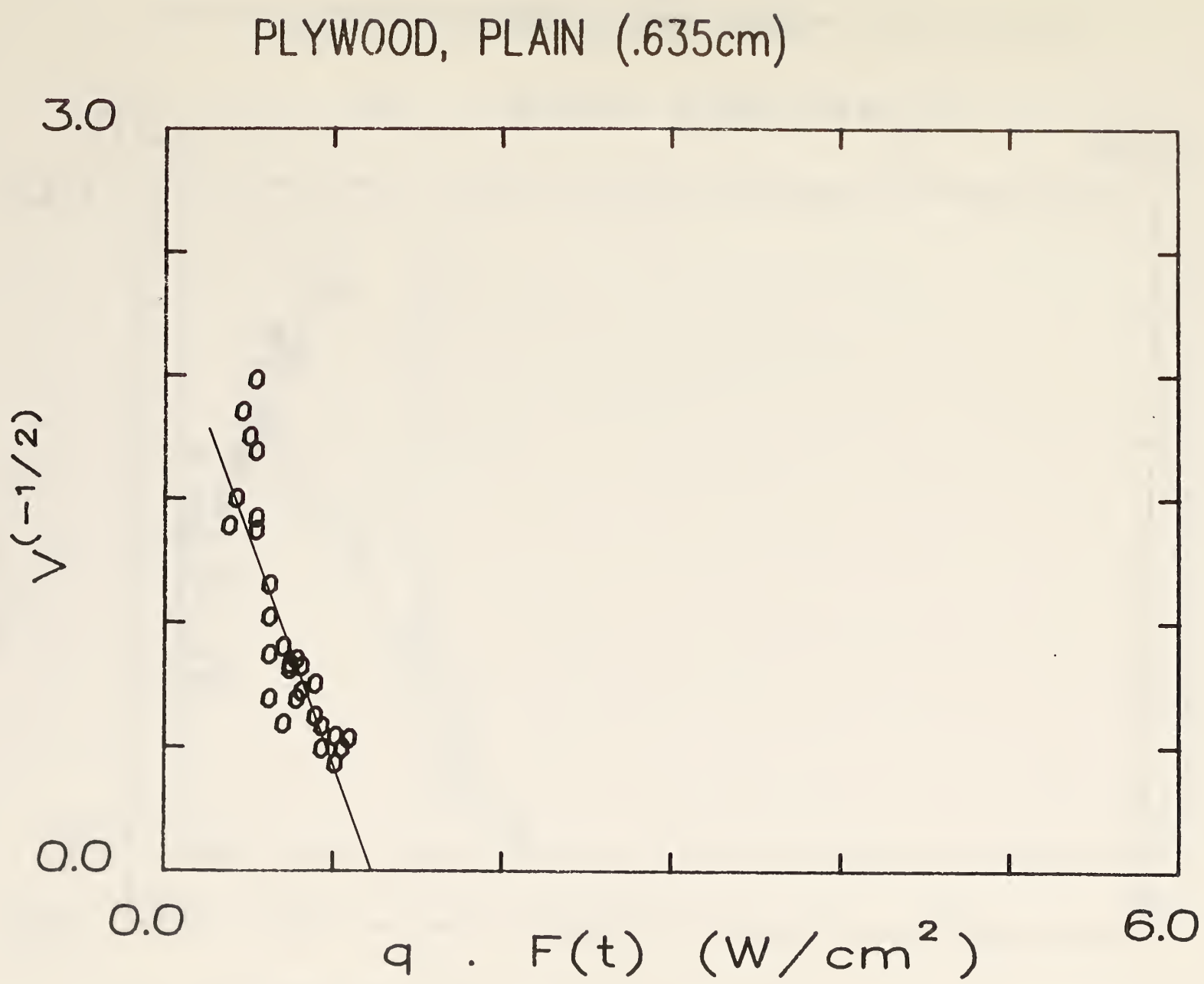

Figure B-14. Correlation of spread velocity for plywood, plain (0.635 cm).

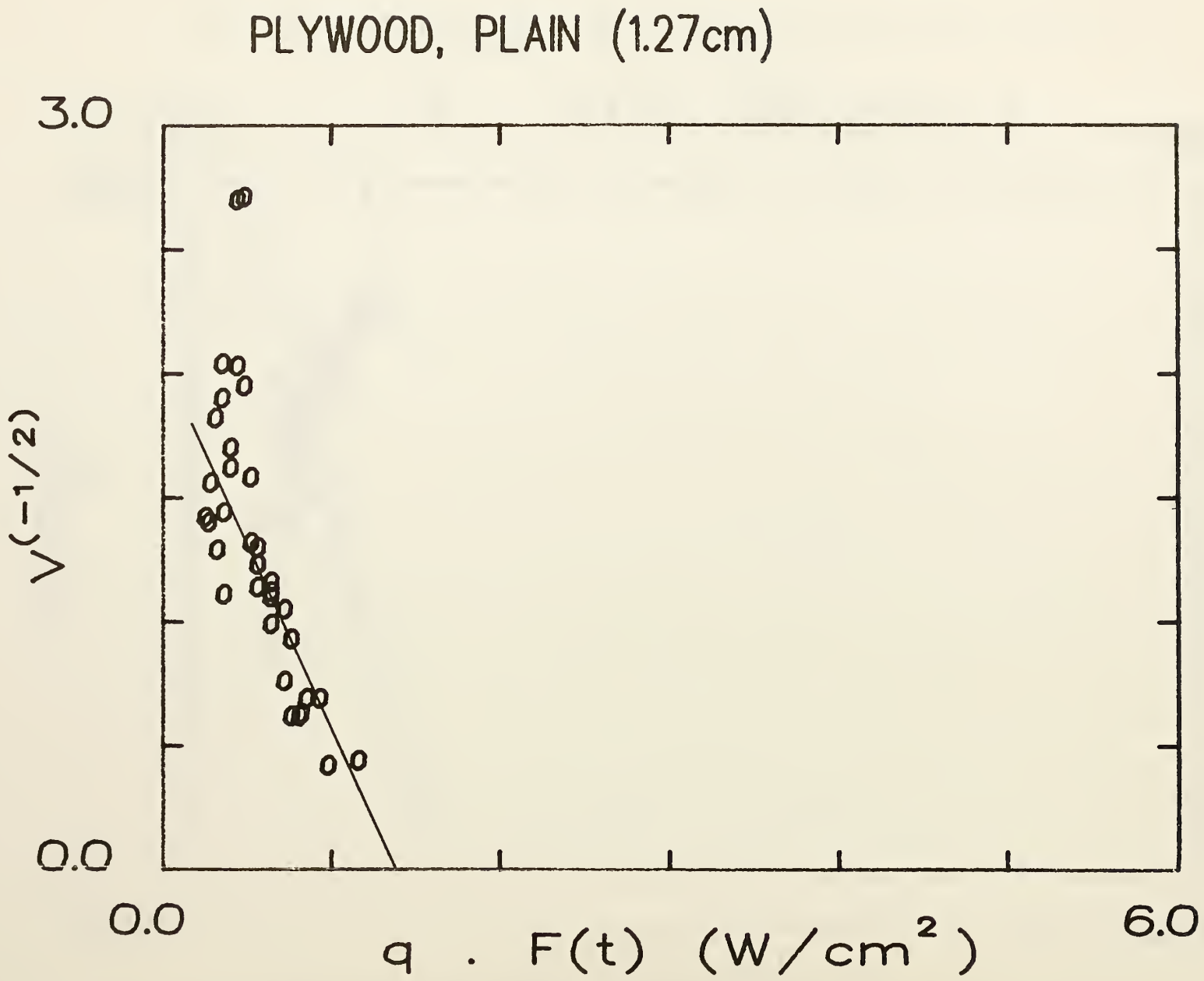

Figure B-15. Correlation of spread velocity for plywood, plain (1.27 cm).

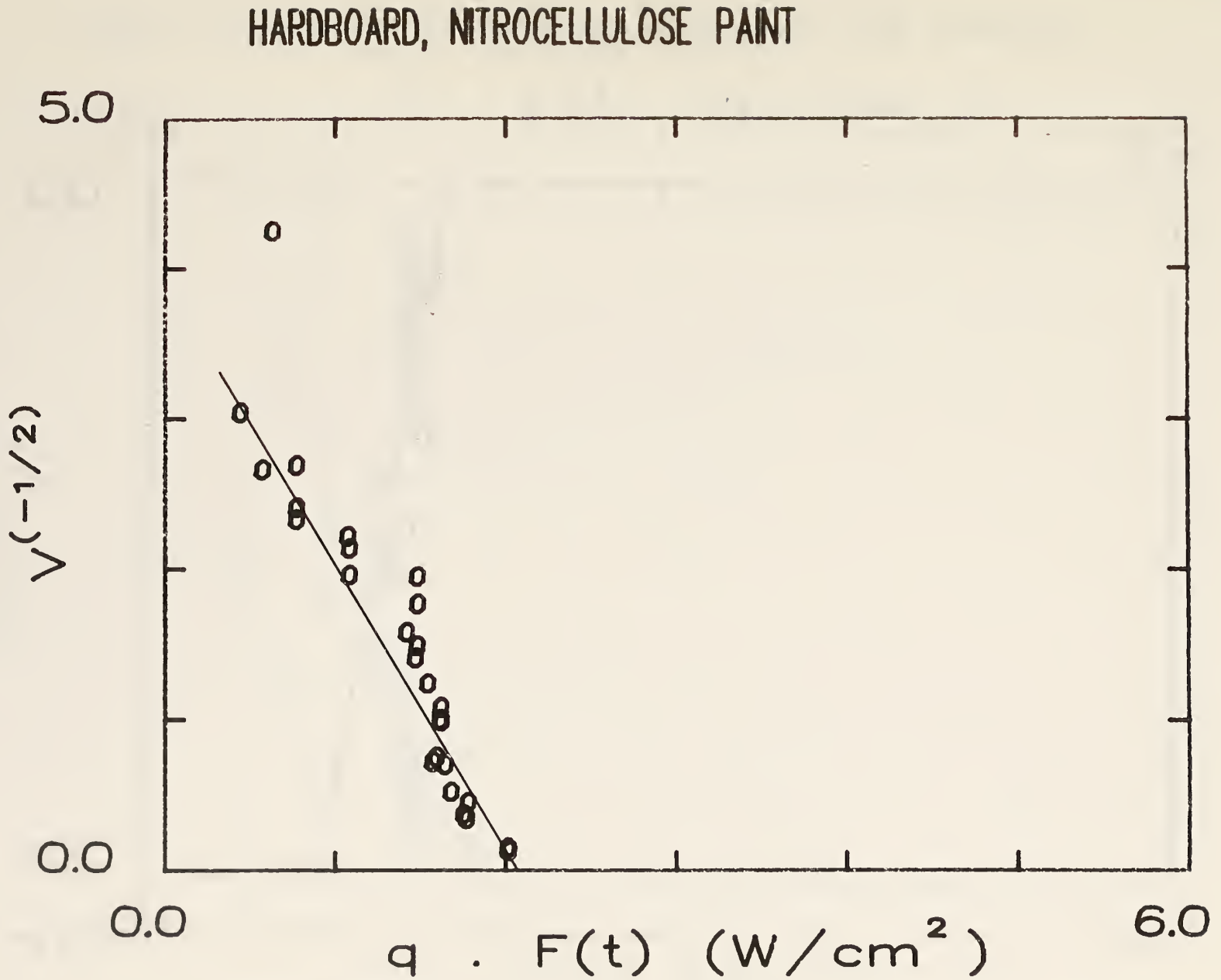

Figure B-16. Correlation of spread velocity for hardboard (3.4 mm, nitrocellulose paint).

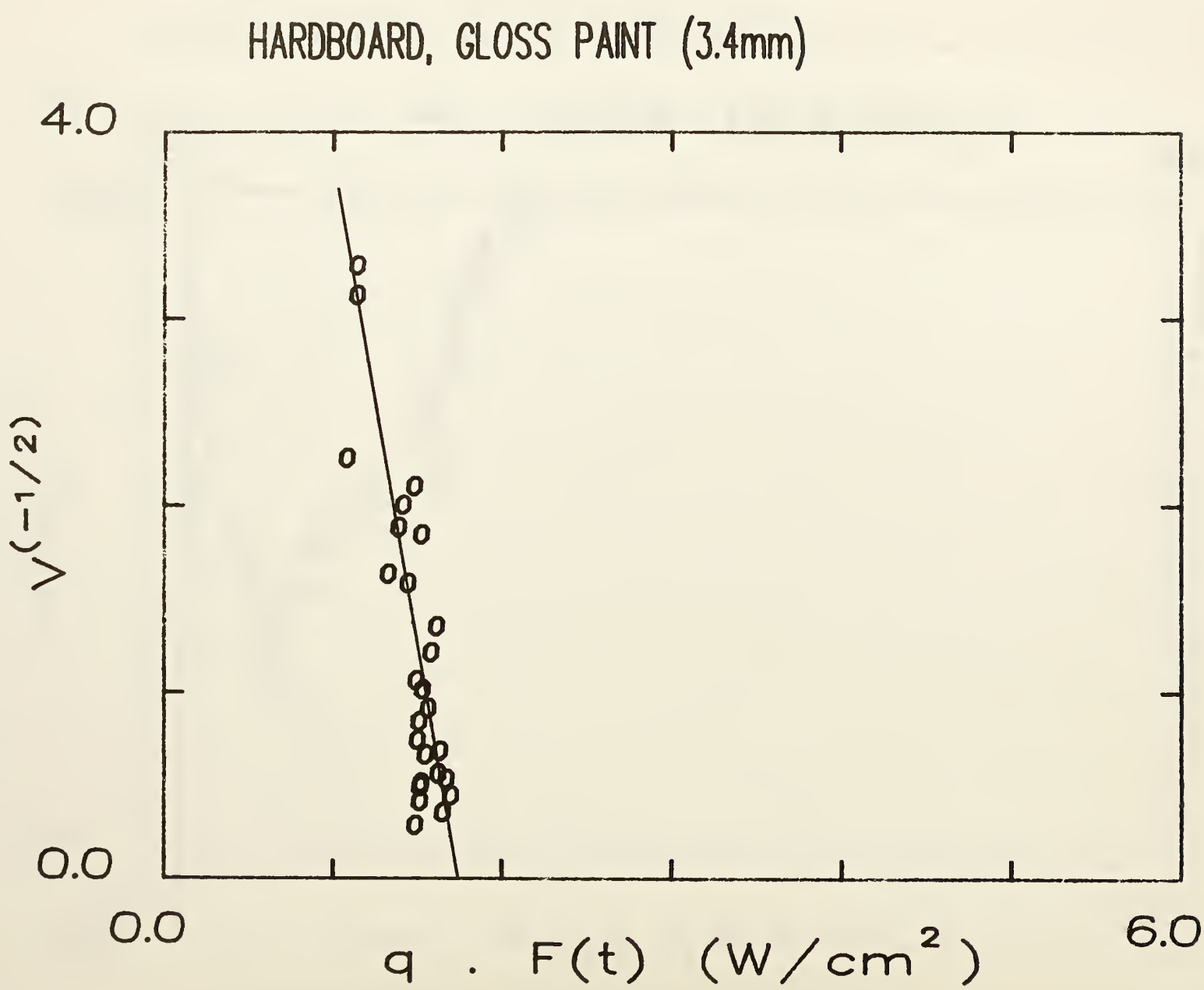

Figure B-17. Correlation of spread velocity for hardboard (3.4 mm, gloss paint).

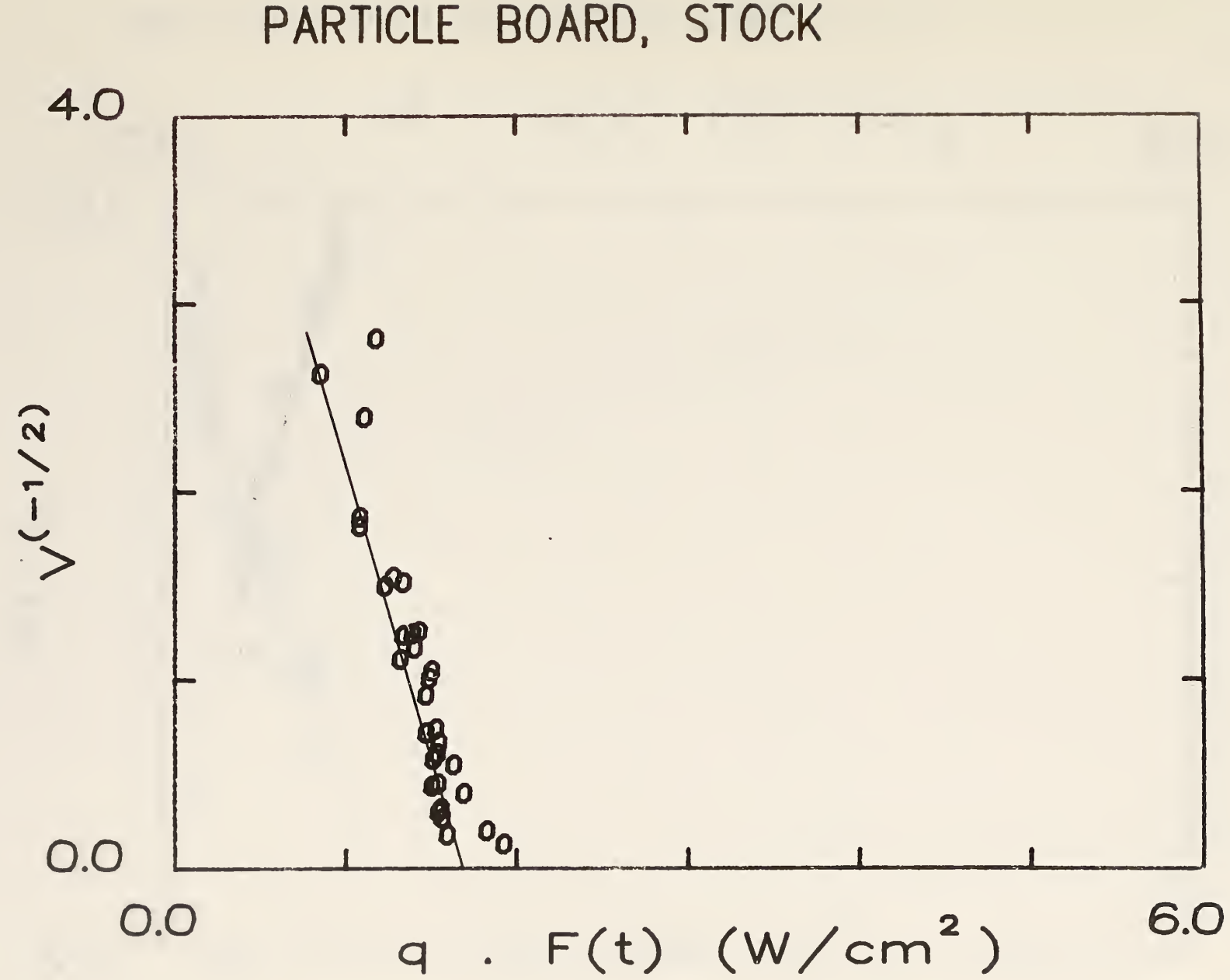

Figure B-18. Correlation of spread velocity for particle board (1.27 cm, stock).

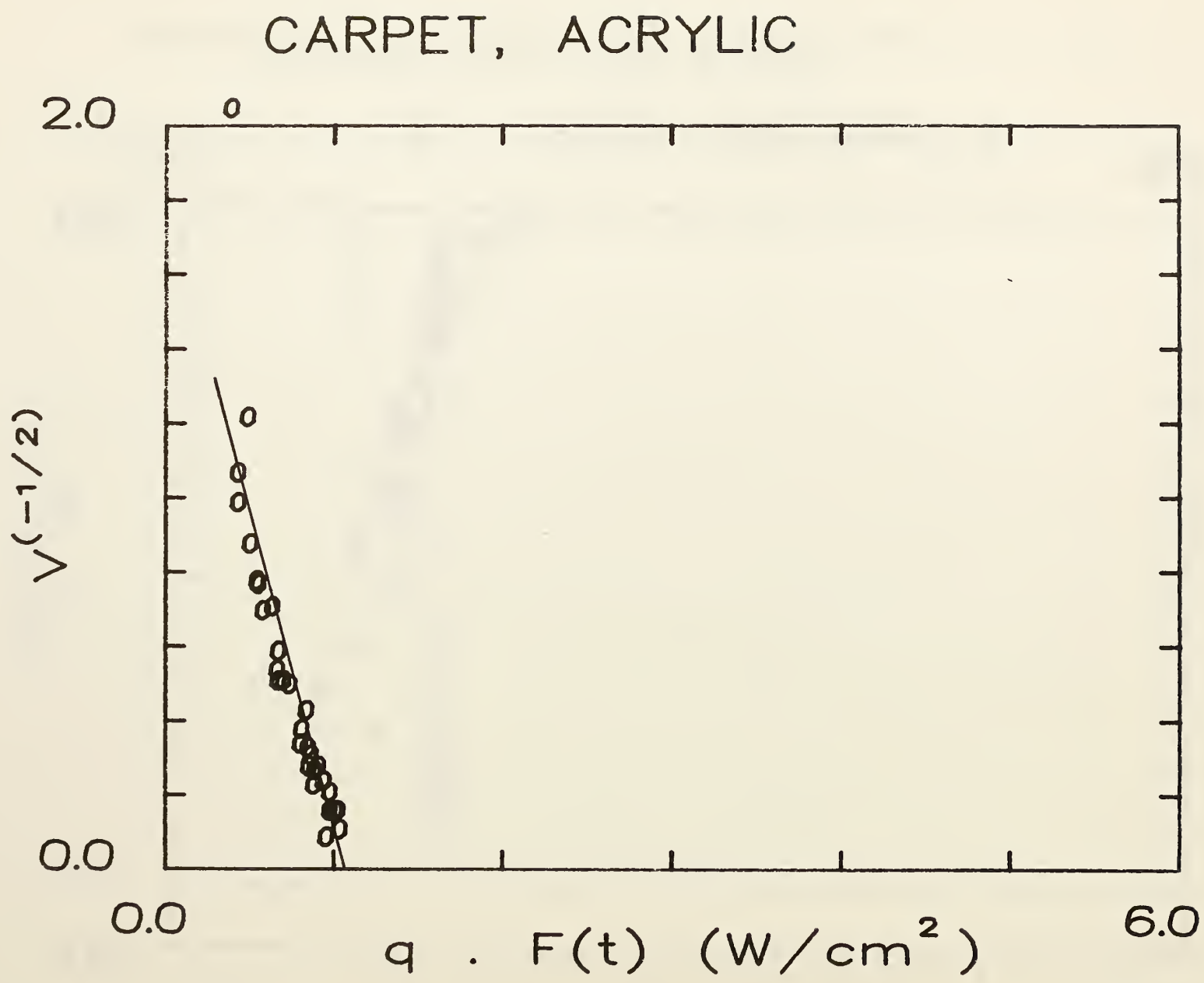

Figure B-19. Correlation of spread velocity for carpet (acrylic).

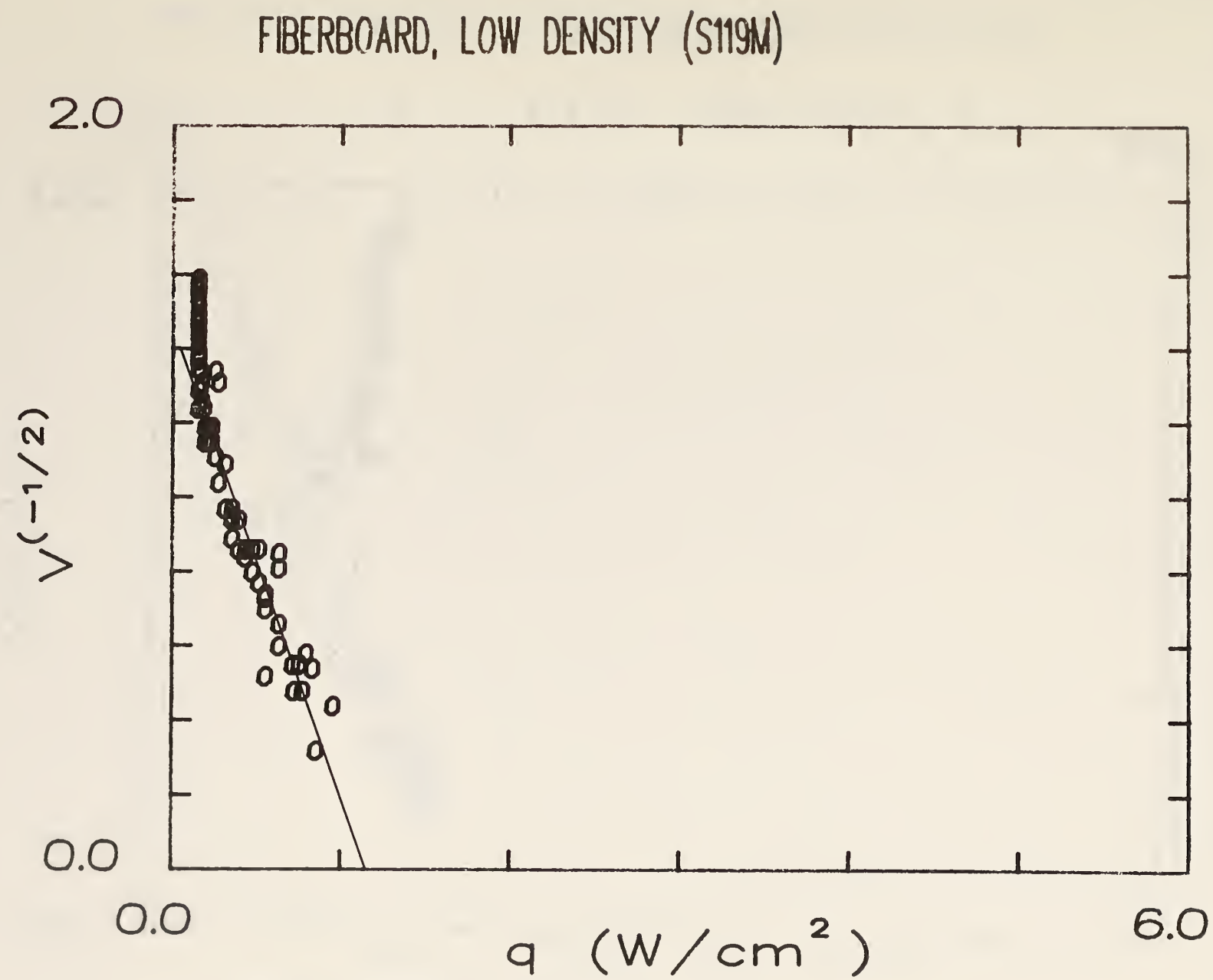

Figure B-20. Correlation of spread velocity for fiberboard, low density (S119M).

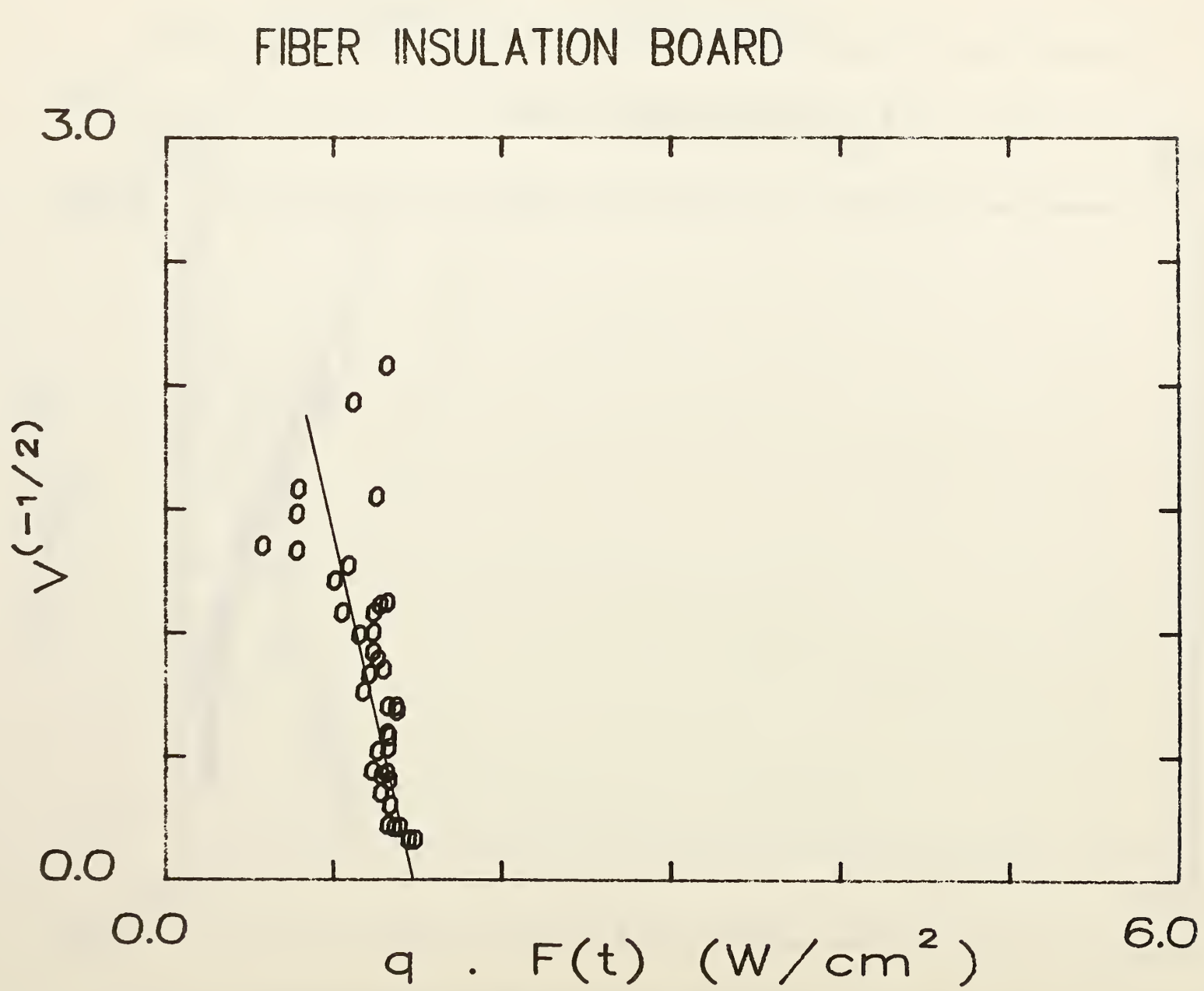

Fibure B-21. Correlation of spread velocity for fiber insulation board.

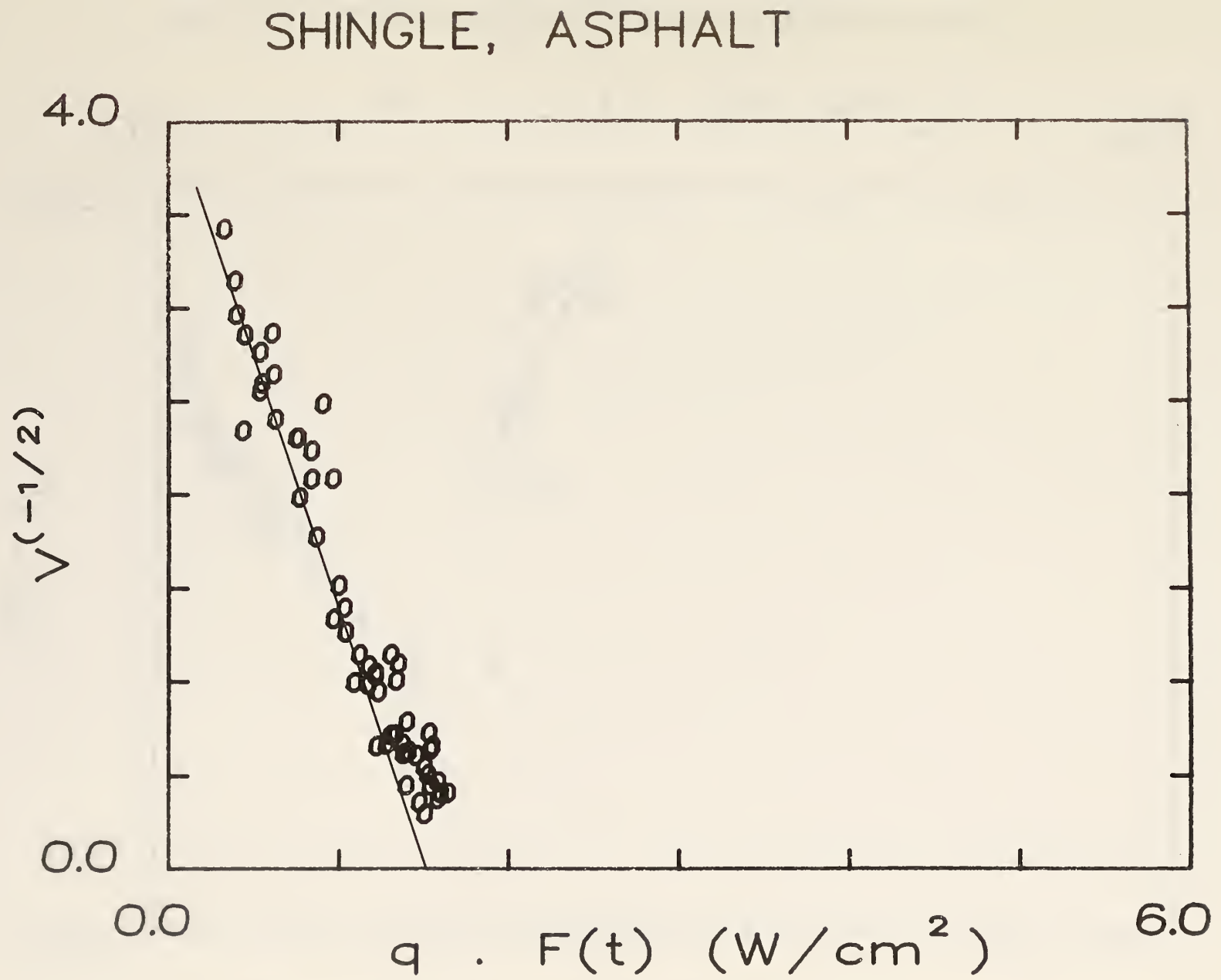

Figure B-22. Correlation of spread velocity for asphalt shingle.

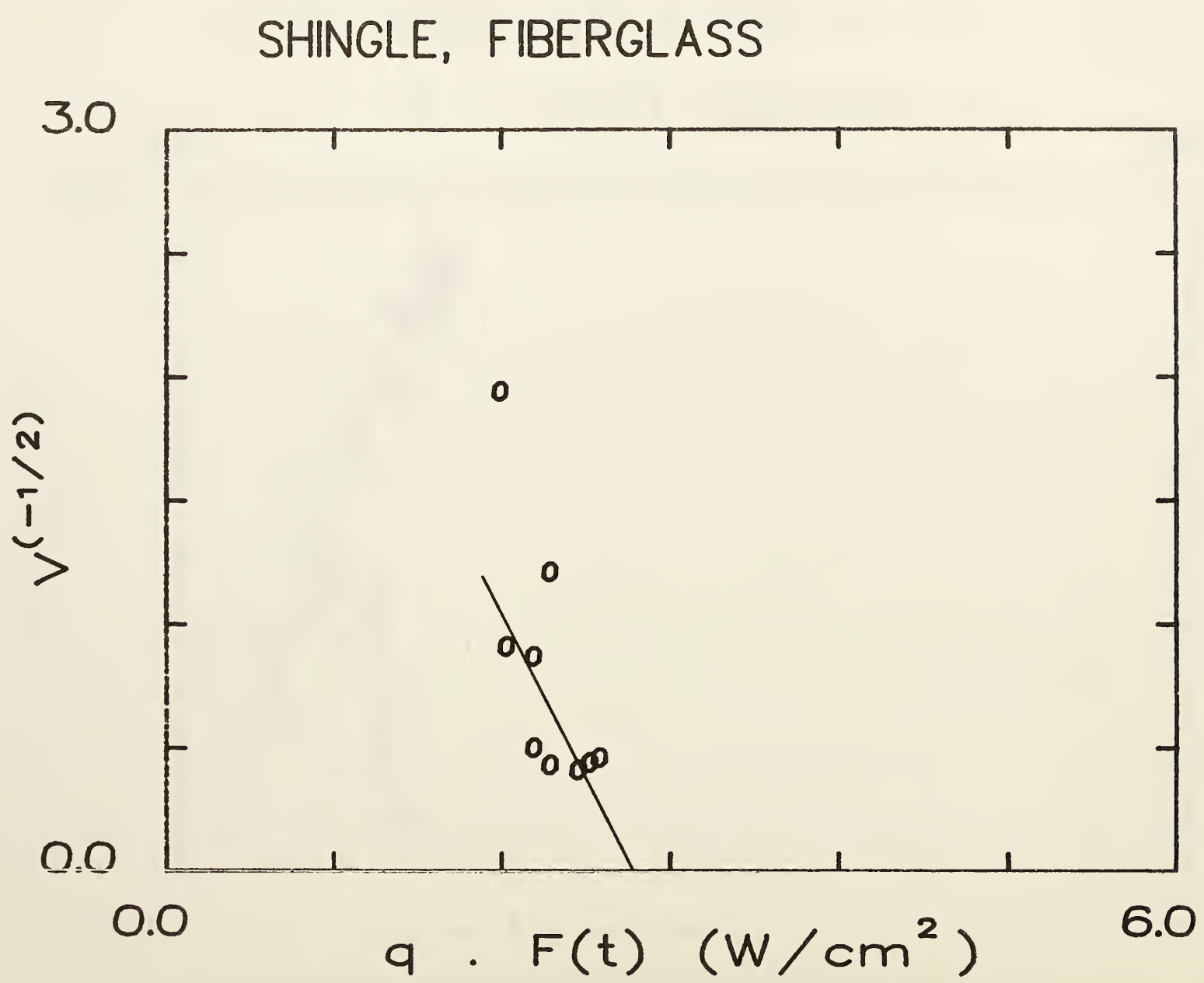

Figure B-23. Correlation of spread velocity for fiberglass shingle.

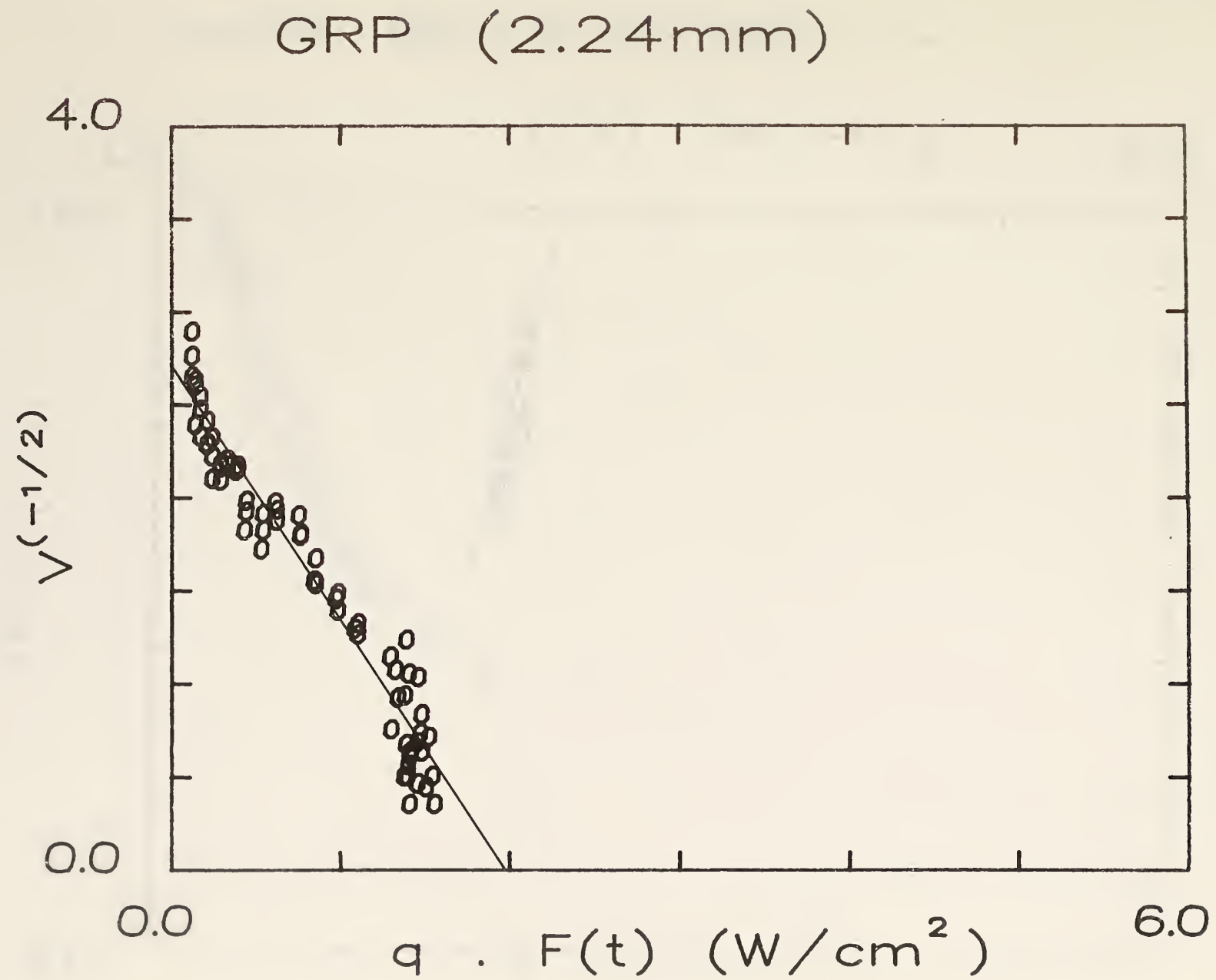

Figure B-24. Correlation of spread velocity for GRP (2.24 mm).

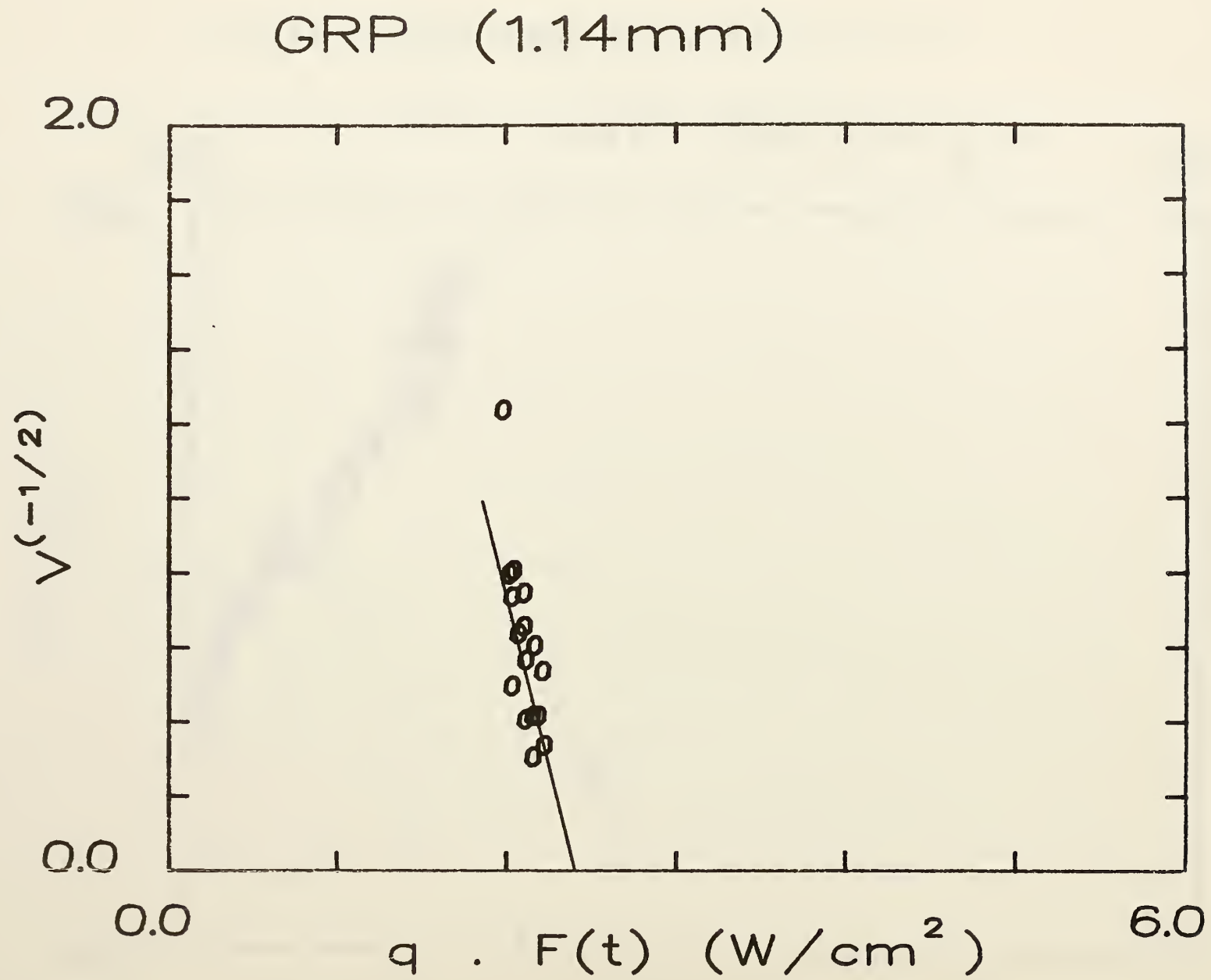

Figure B-25. Correlation of spread velocity for GRP (1.14 mm).

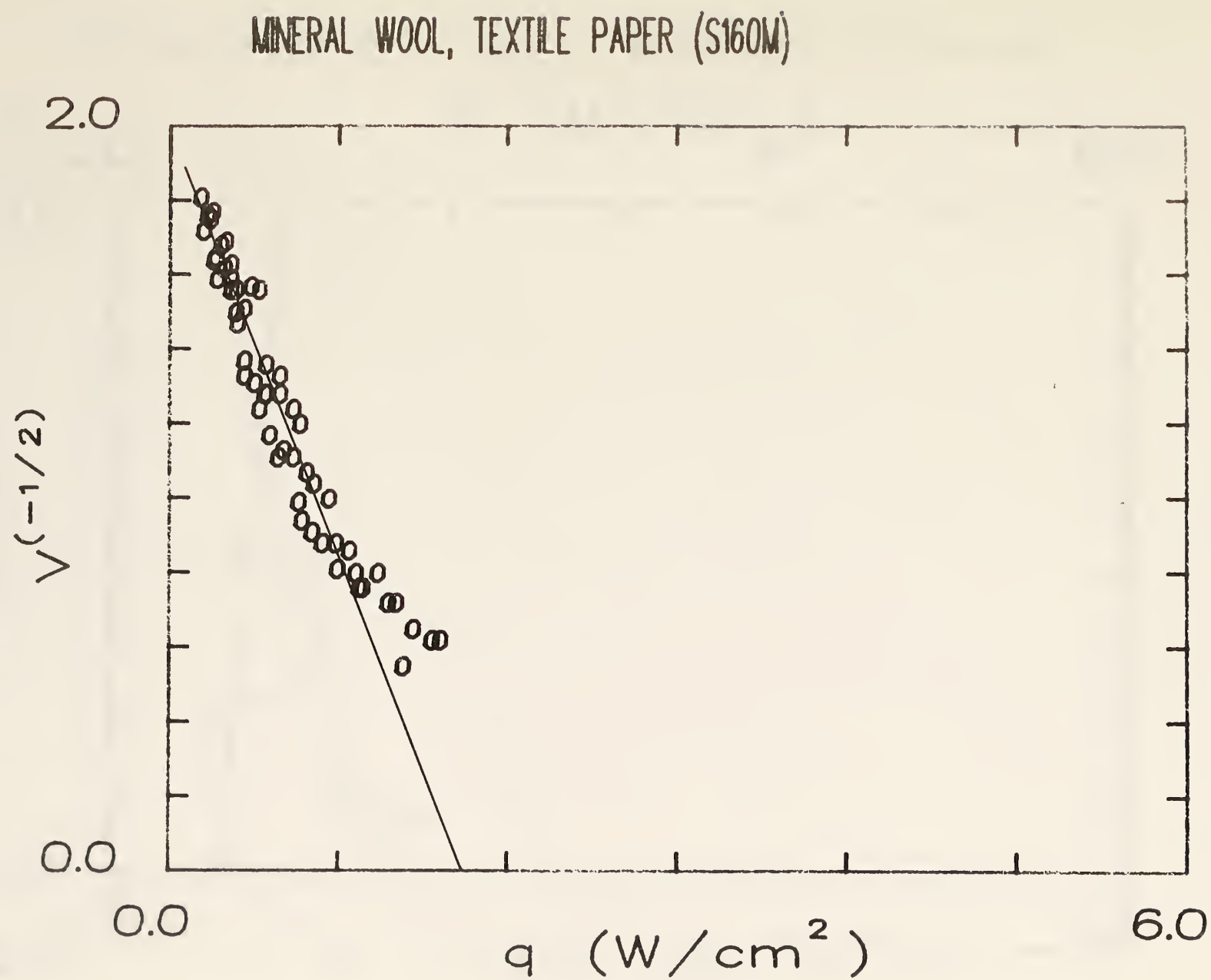

Figure B-26. Correlation of spread velocity for mineral wool, textile paper (S160).

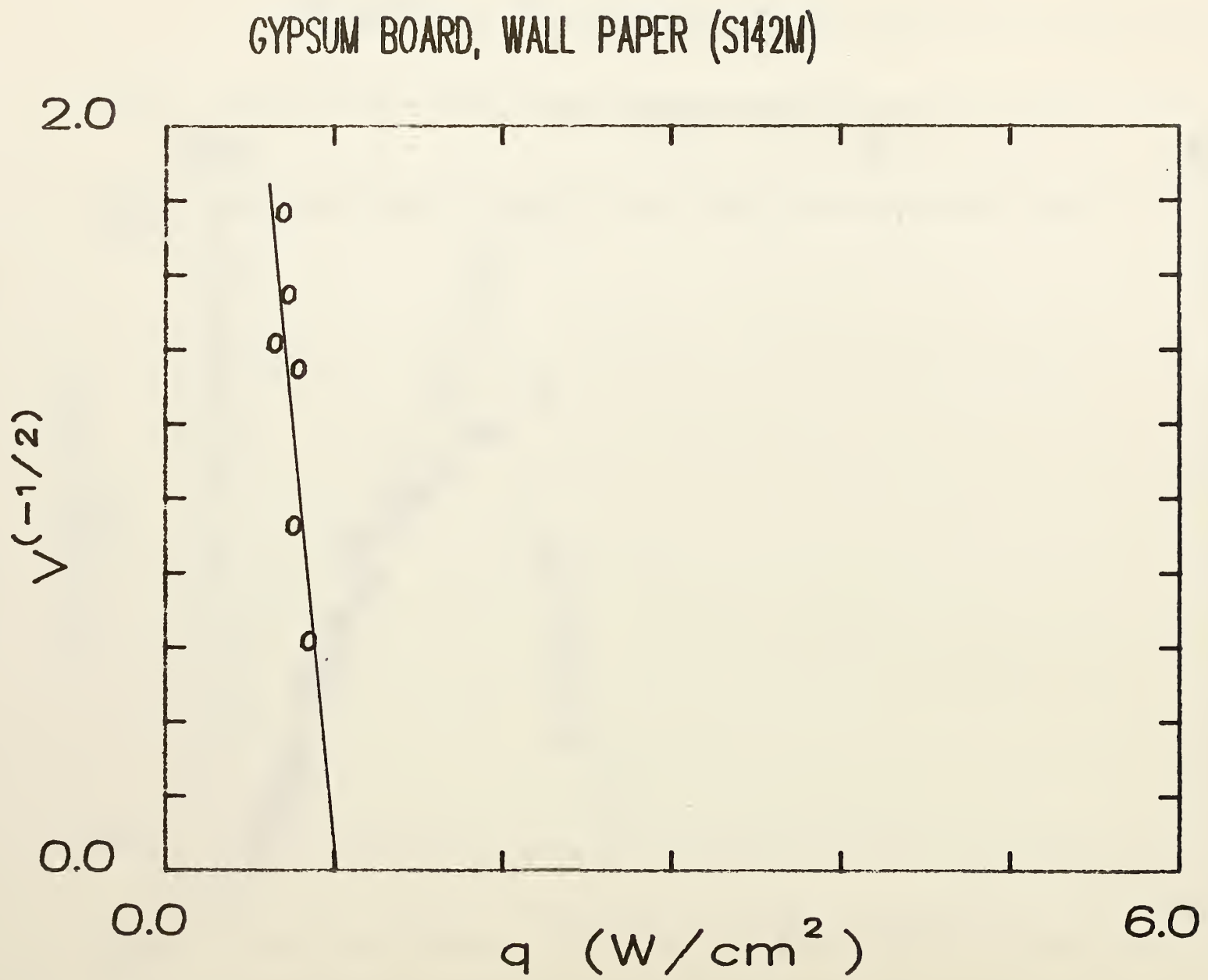

Figure B-27. Correlation of spread velocity for gypsum board, wallpaper (S142M).

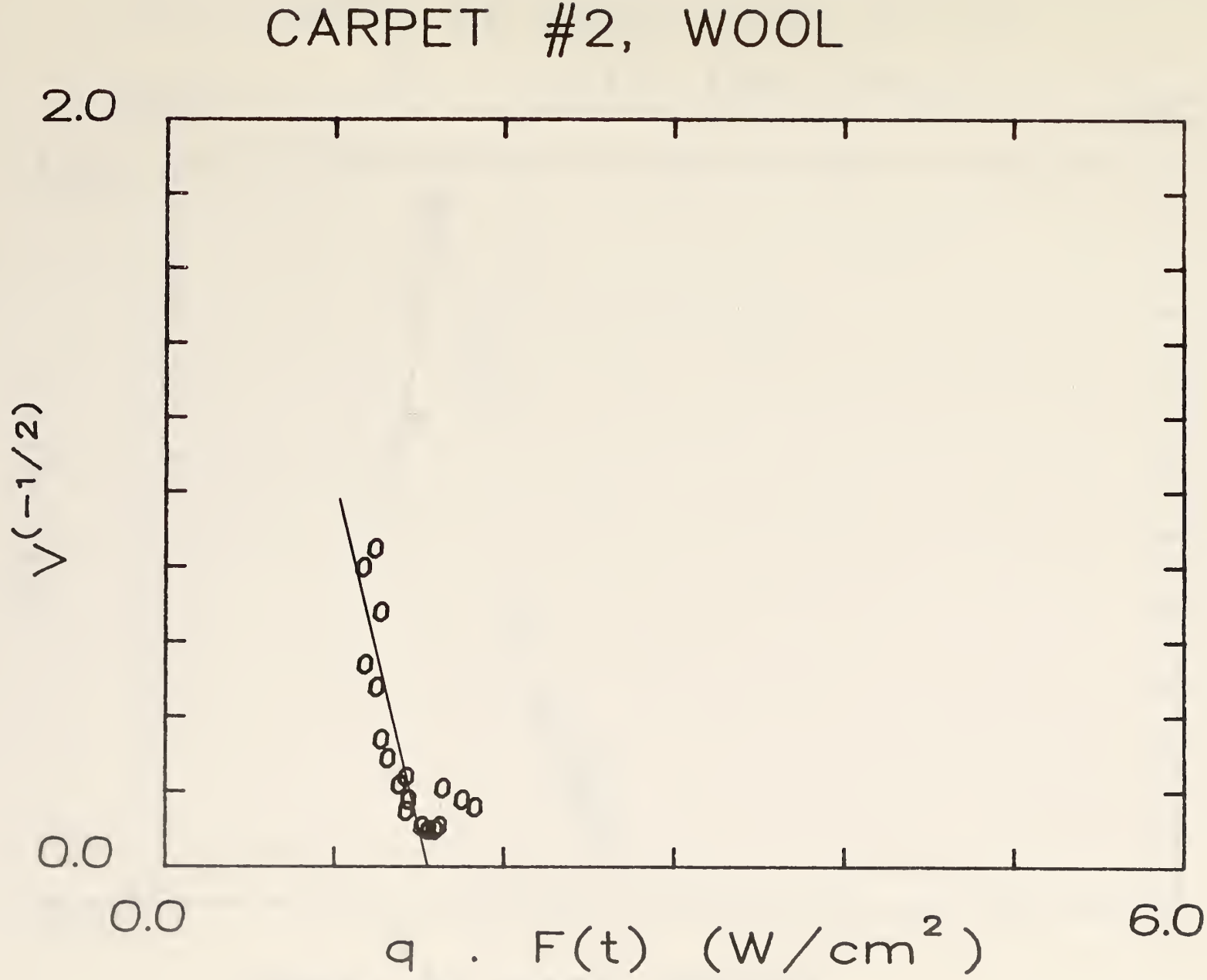

Figure B-28. Correlation of spread velocity for carpet #2 (wool).

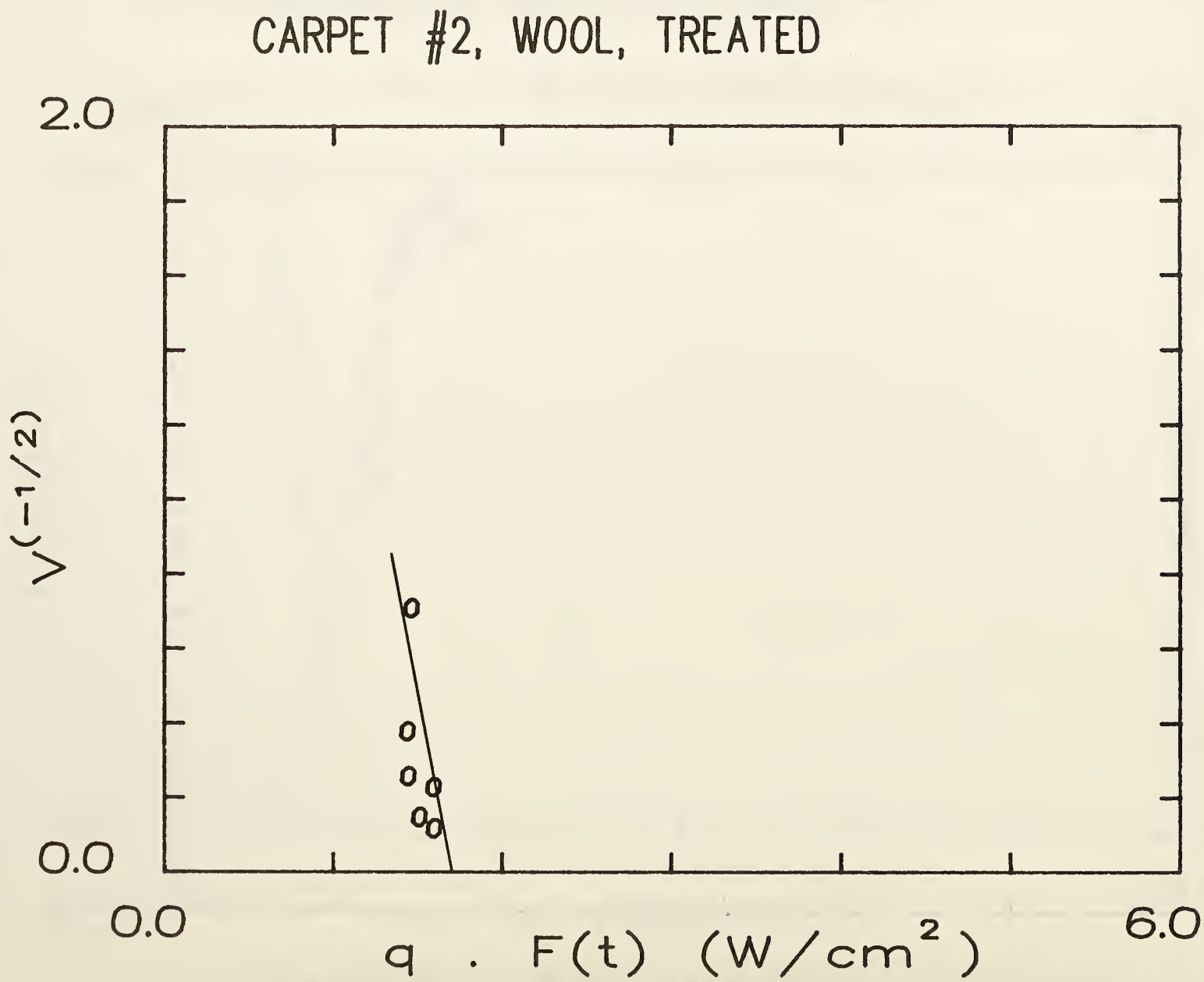

Figure B-29. Correlation of spread velocity for carpet #2 (wool treated).

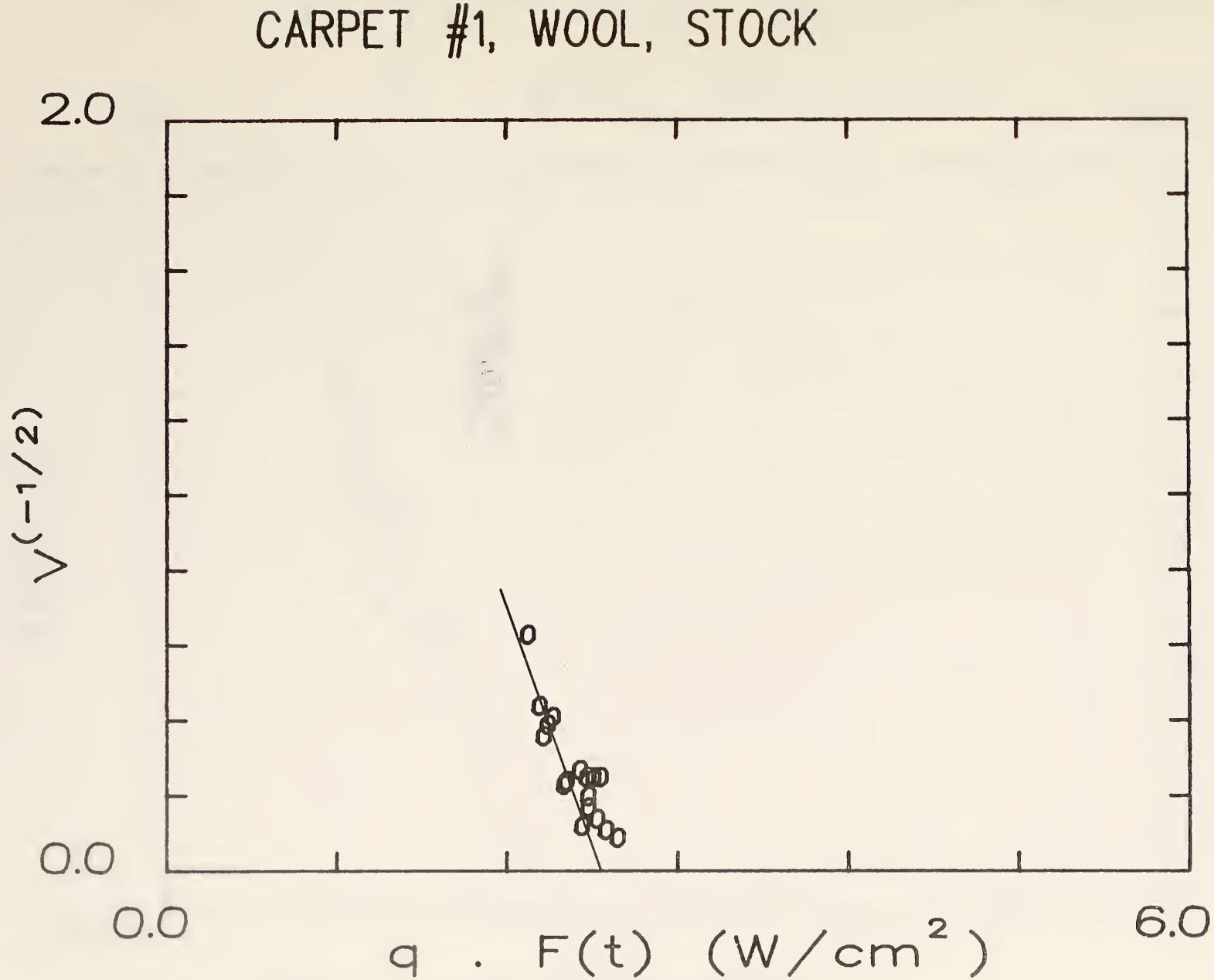

Figure B-30. Correlation of spread velocity for carpet #1 (wool, stock).

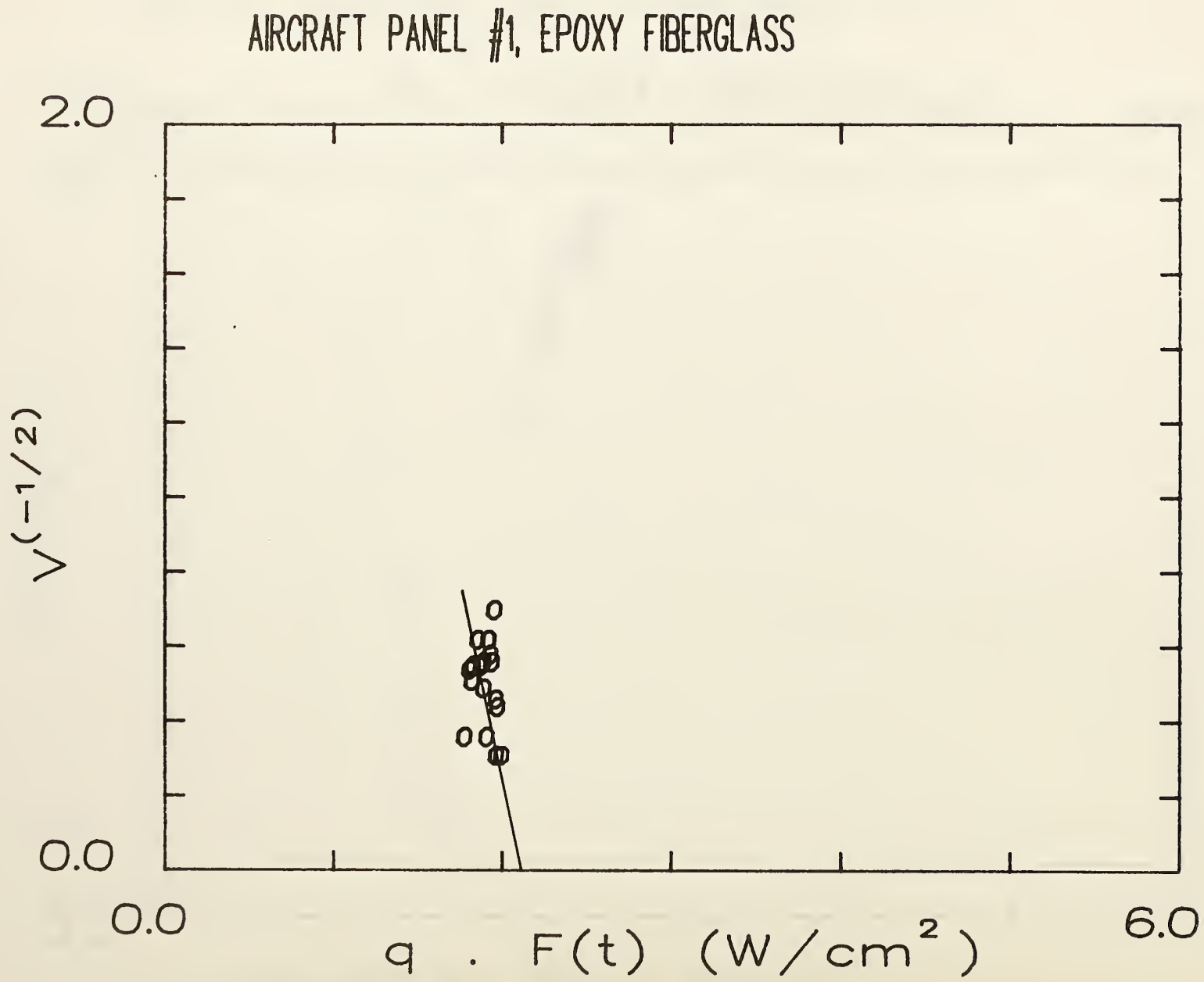

Figure B-31. Correlation of spread velocity for aircraft panel (epoxy fiberglass).

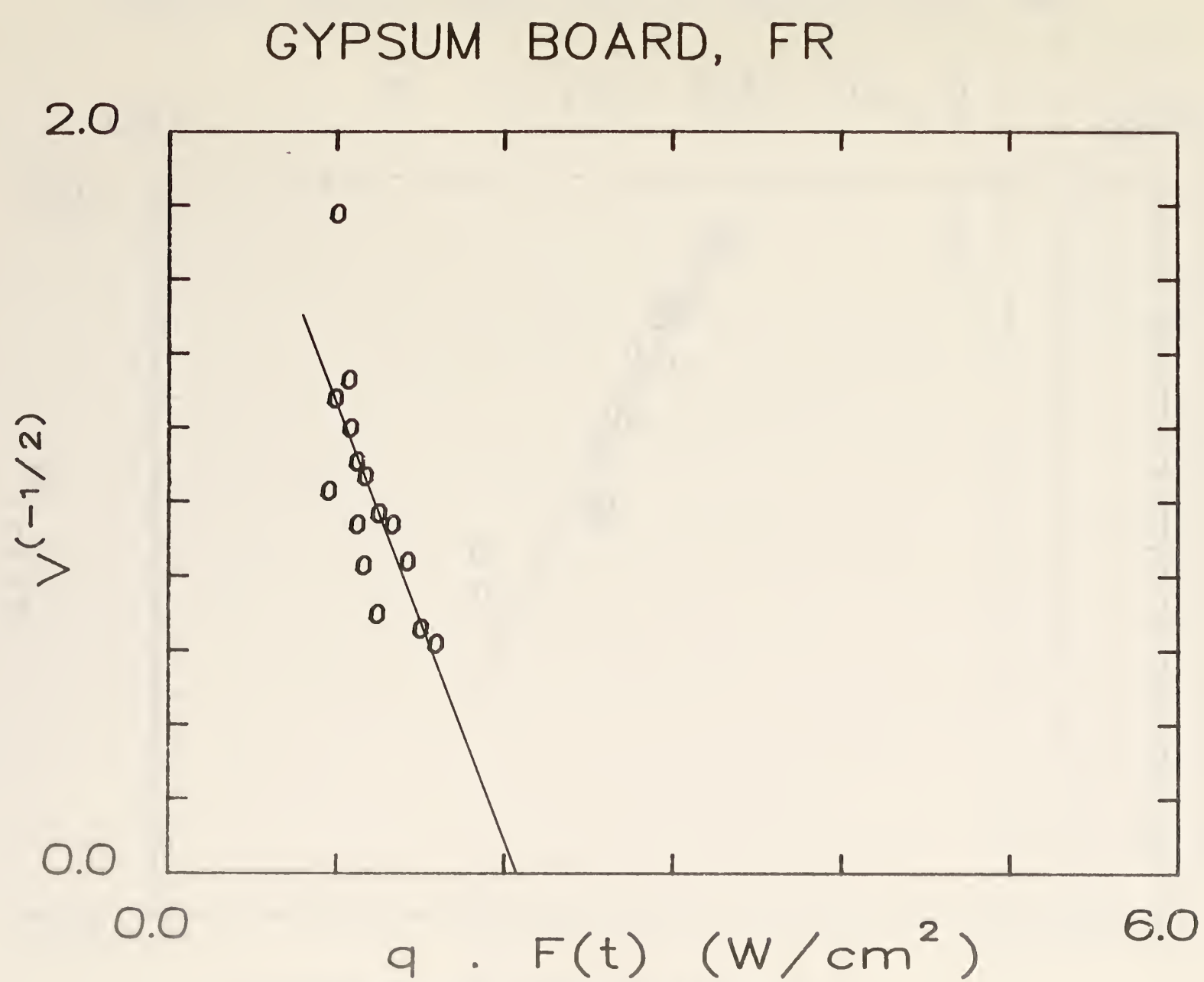

Figure B-32. Correlation of spread velocity for gypsum board, FR (1.27 cm).

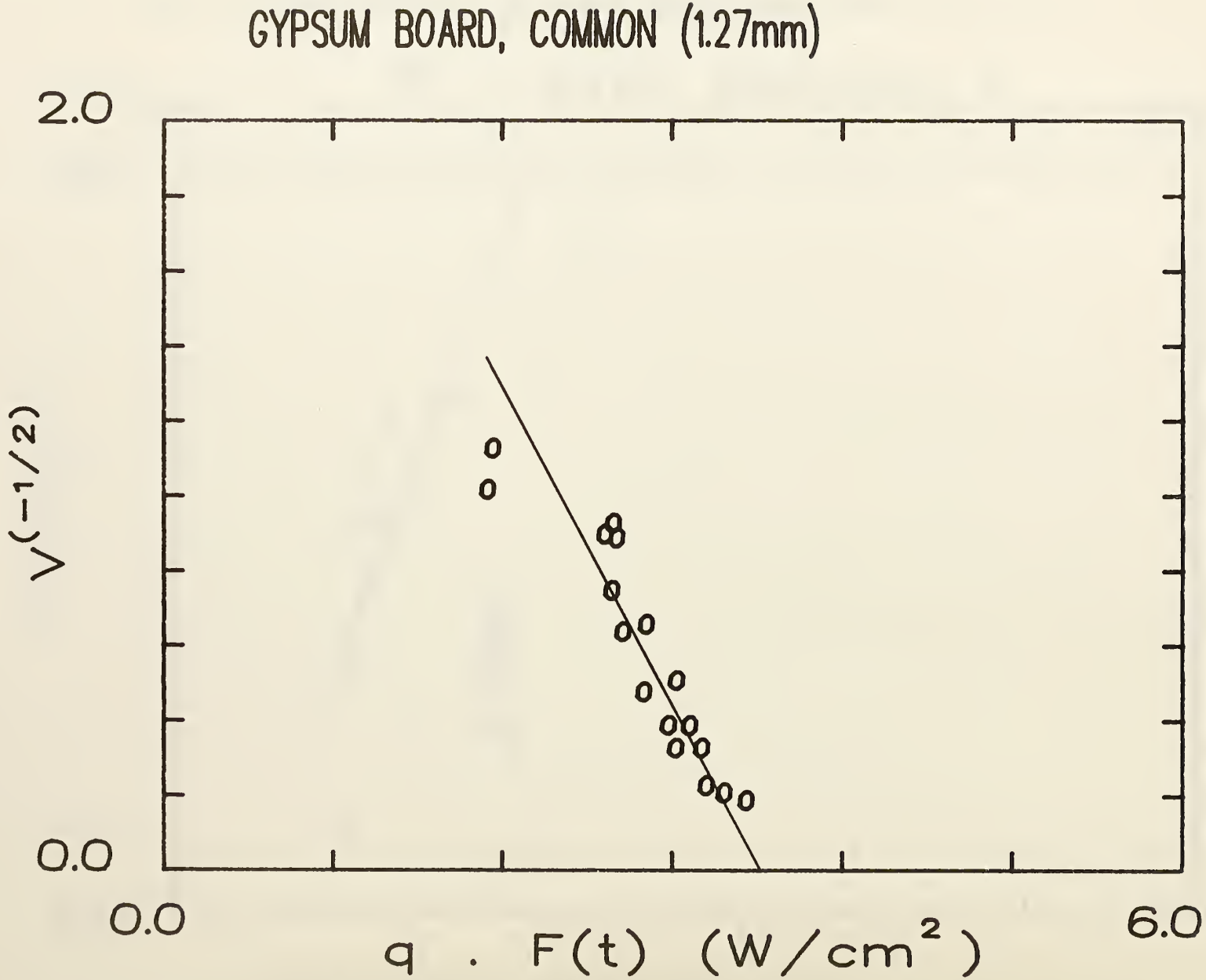

Figure B-33. Correlation of spread velocity for gypsum board (1.27 mm, common).

Appendix C. Spread and Ignition Results

Additional flammability diagrams, which plot the velocity and ignition time as a function of external flux, are shown in figures C-1 to C-3. The plotted velocity data are limited to results for which $F(t) = 1$, or $t \geq t_n$. The external flux spans the range over which opposed flow flame spread and piloted ignition is possible. Analytical curves based on the derived values of C and b are shown.

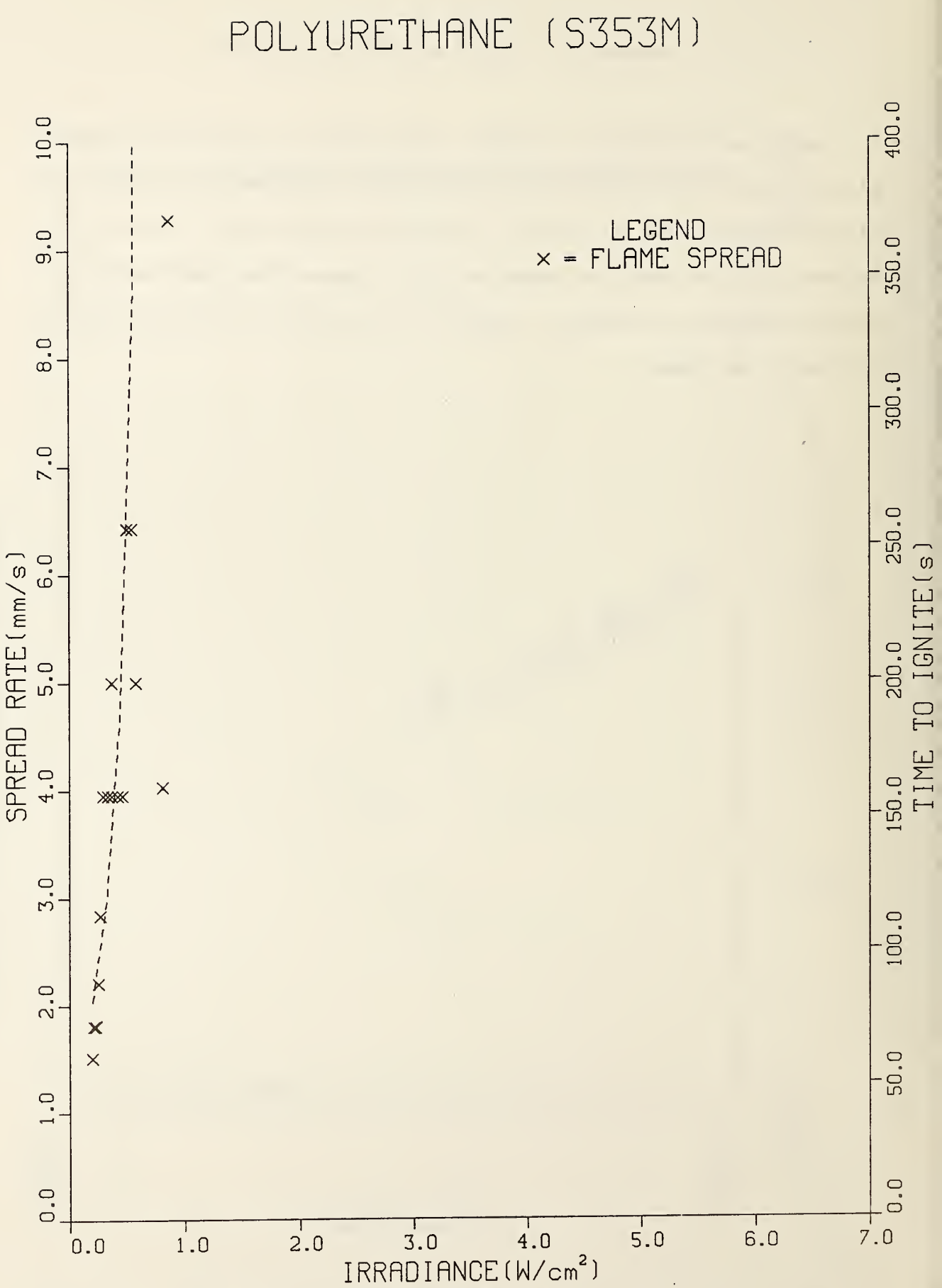

Figure C-1. Spread and ignition results for polyurethane (S353M, 30 mm).

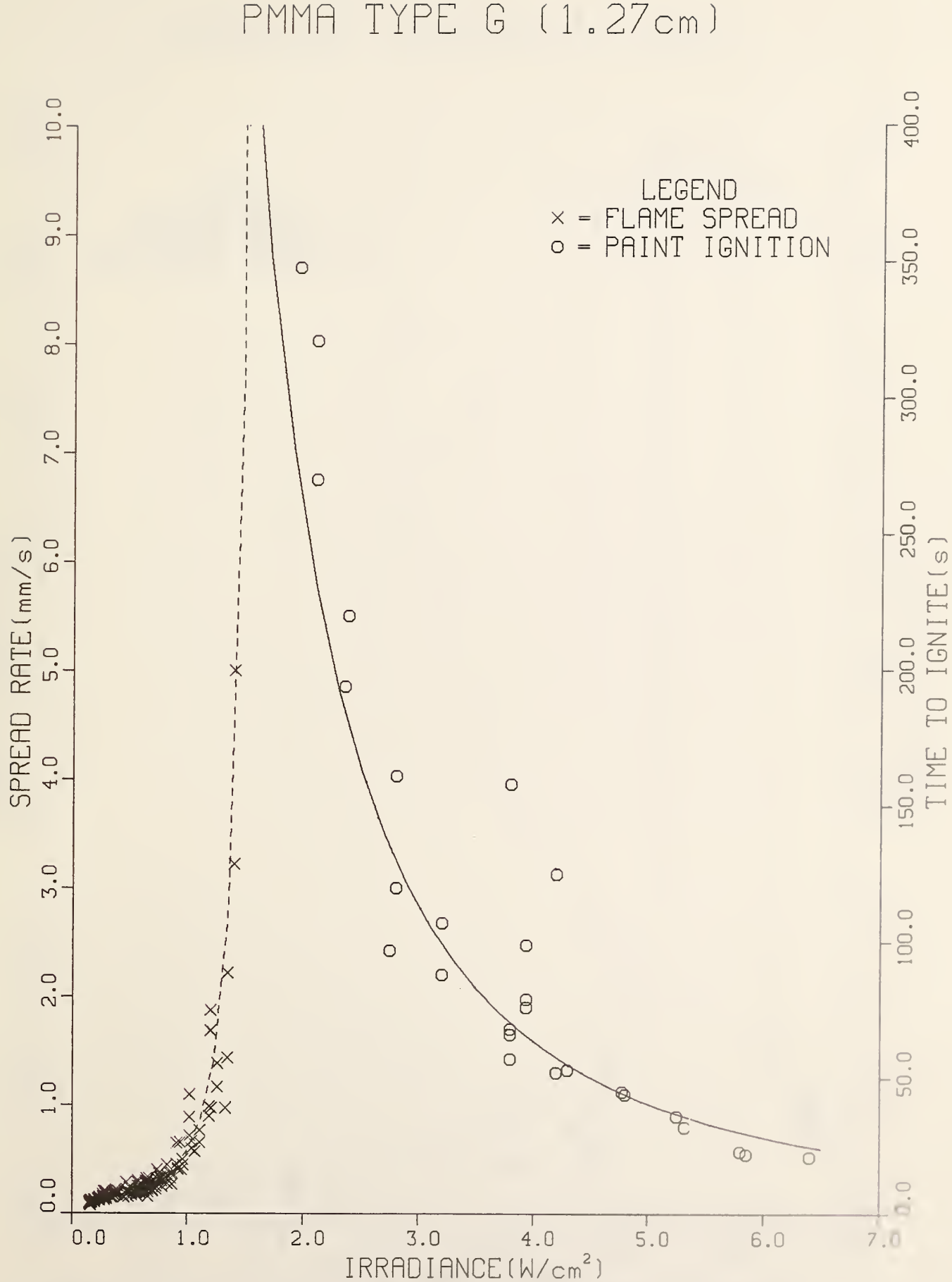

Figure C-2. Spread and ignition results for PMMA Type G (127 cm).

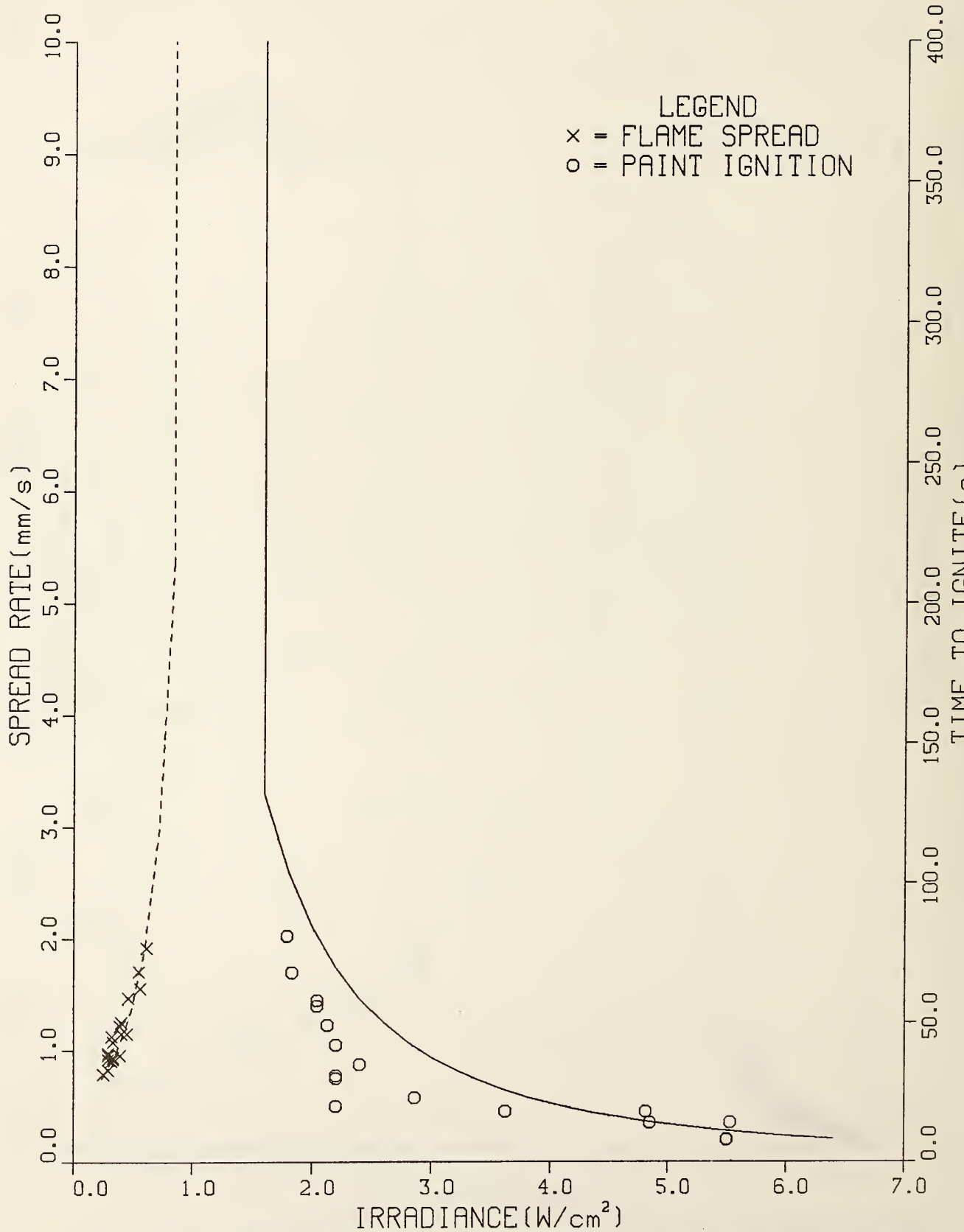

Figure C-3. Spread and ignition results for flexible foam (2.54 cm).

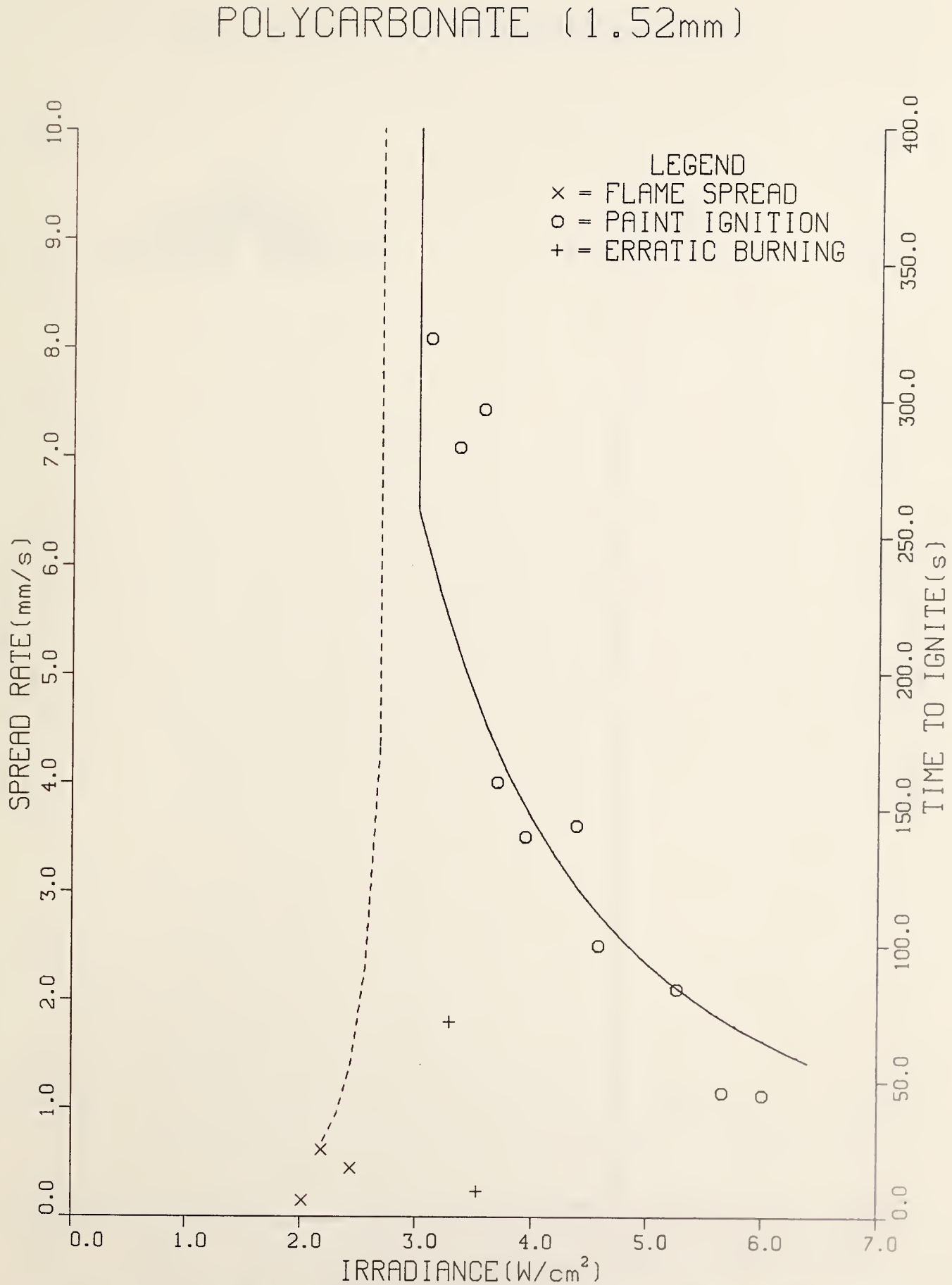

Figure C-4. Spread and ignition results for polycarbonate (1.52 mm).

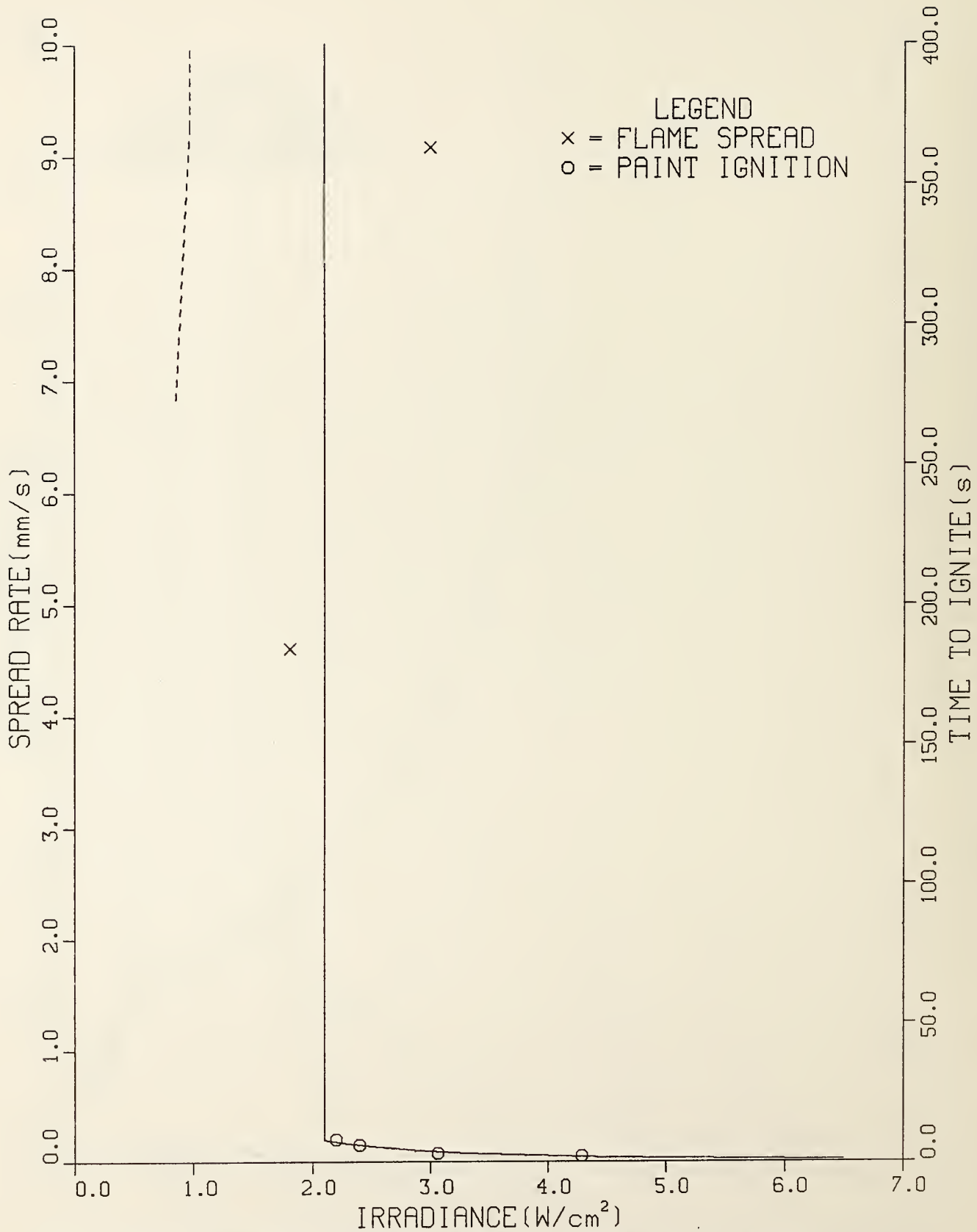

Figure C-5. Spread and ignition results for polyisocyanurate (5.08 cm).

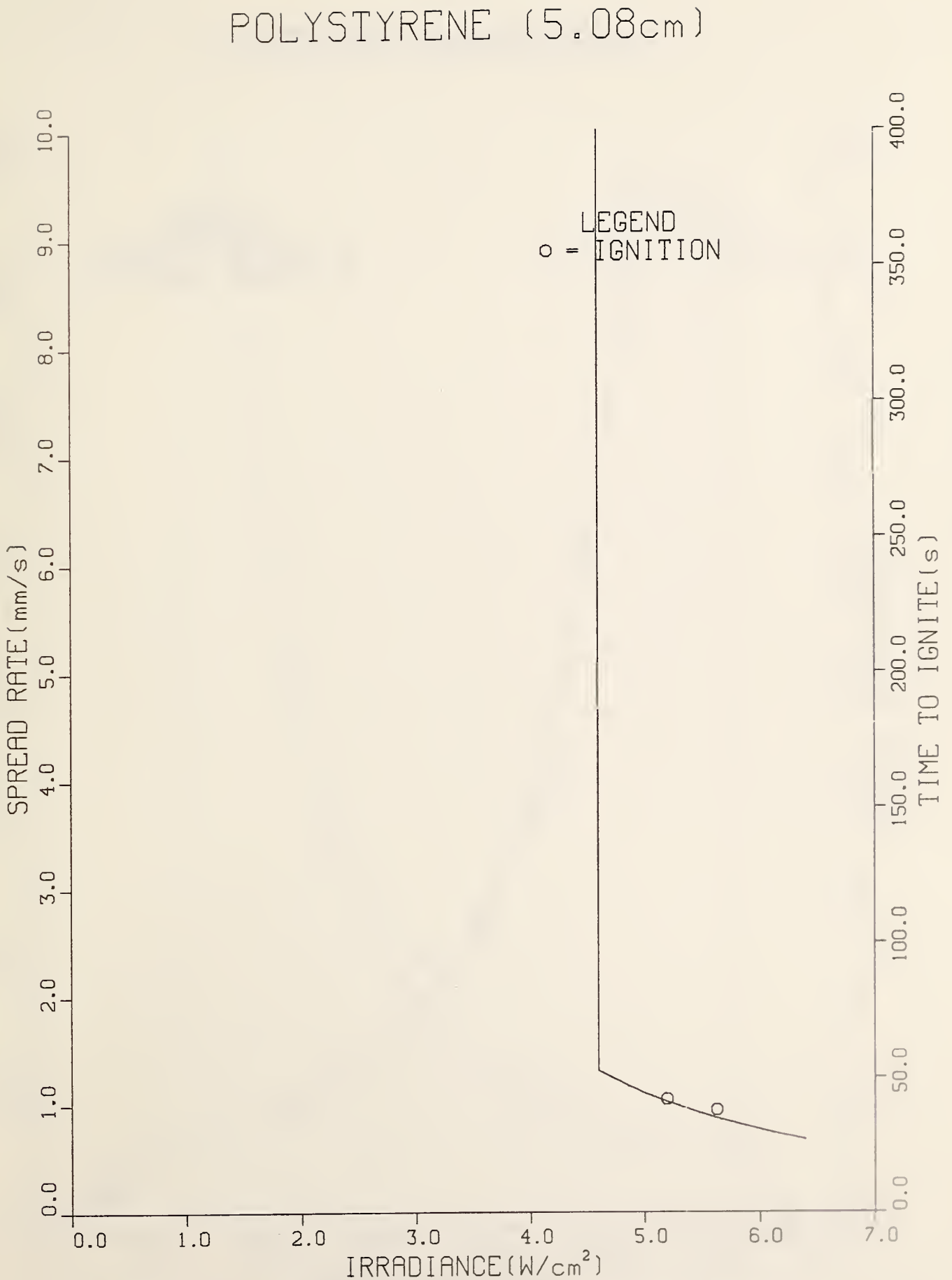

Figure C-6. Spread and ignition results for polystyrene (5.08 cm).

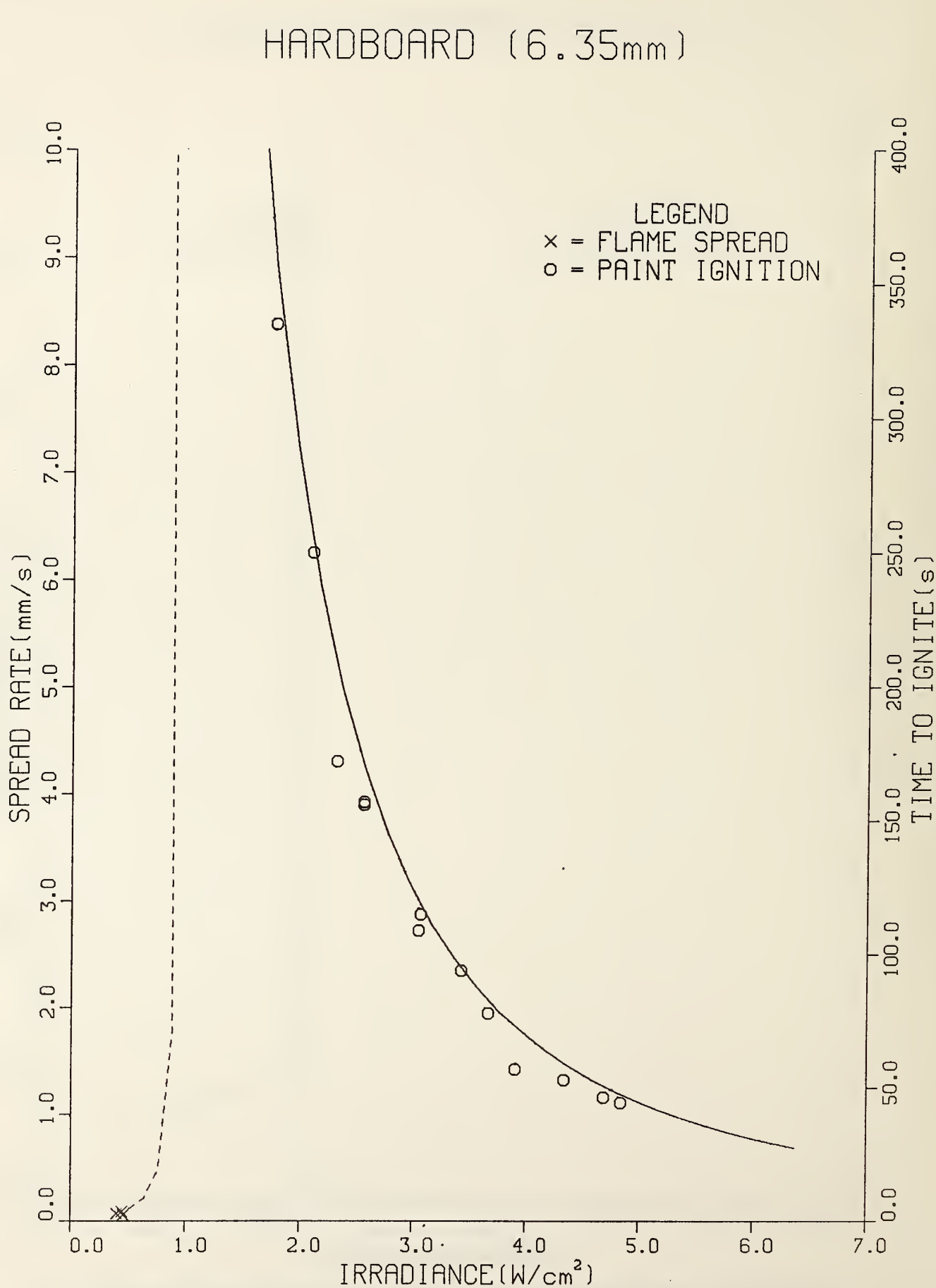

Figure C-7. Spread and ignition results for hardboard (6.35 mm).

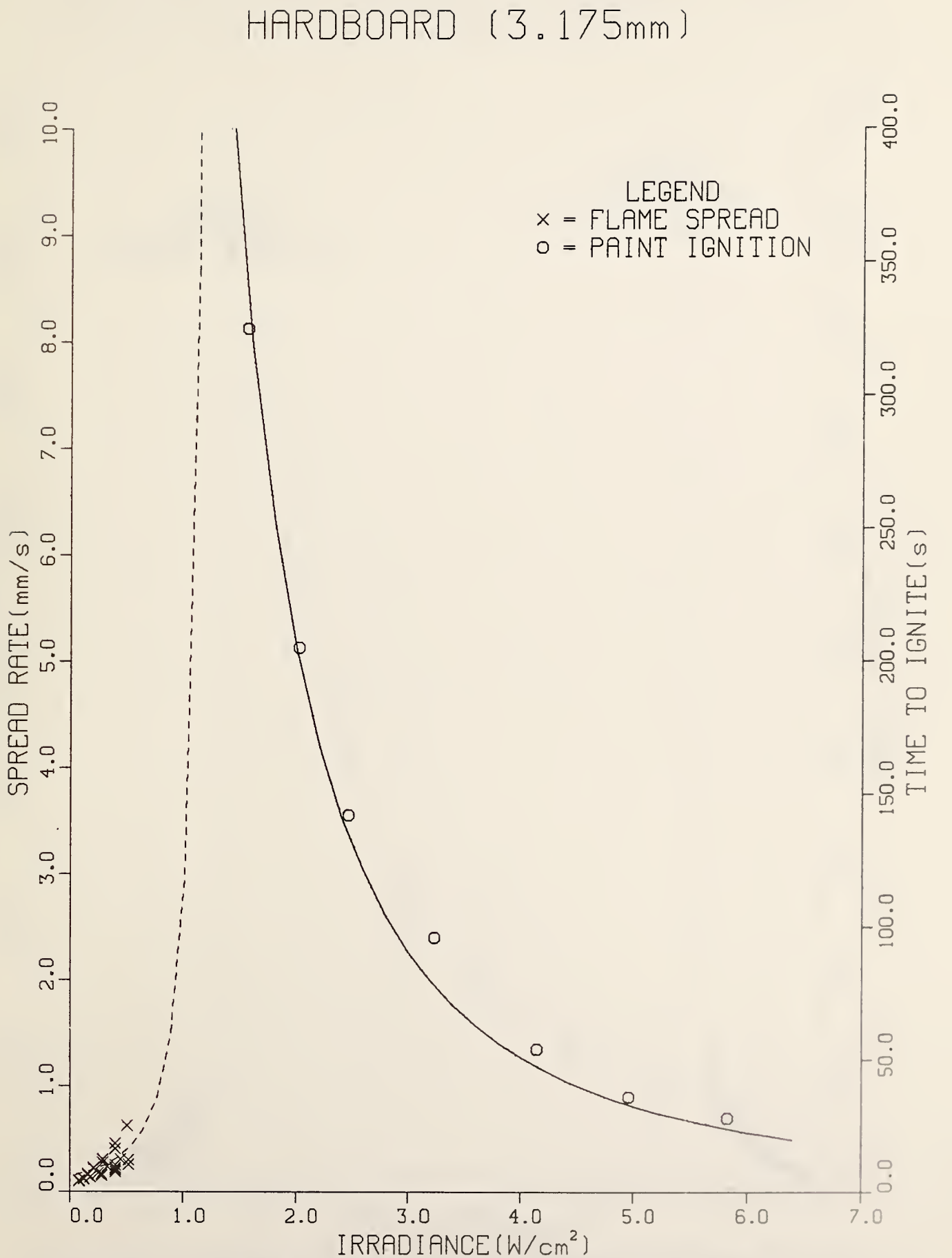

Figure C-8. Spread and ignition results for hardboard (3.175 mm).

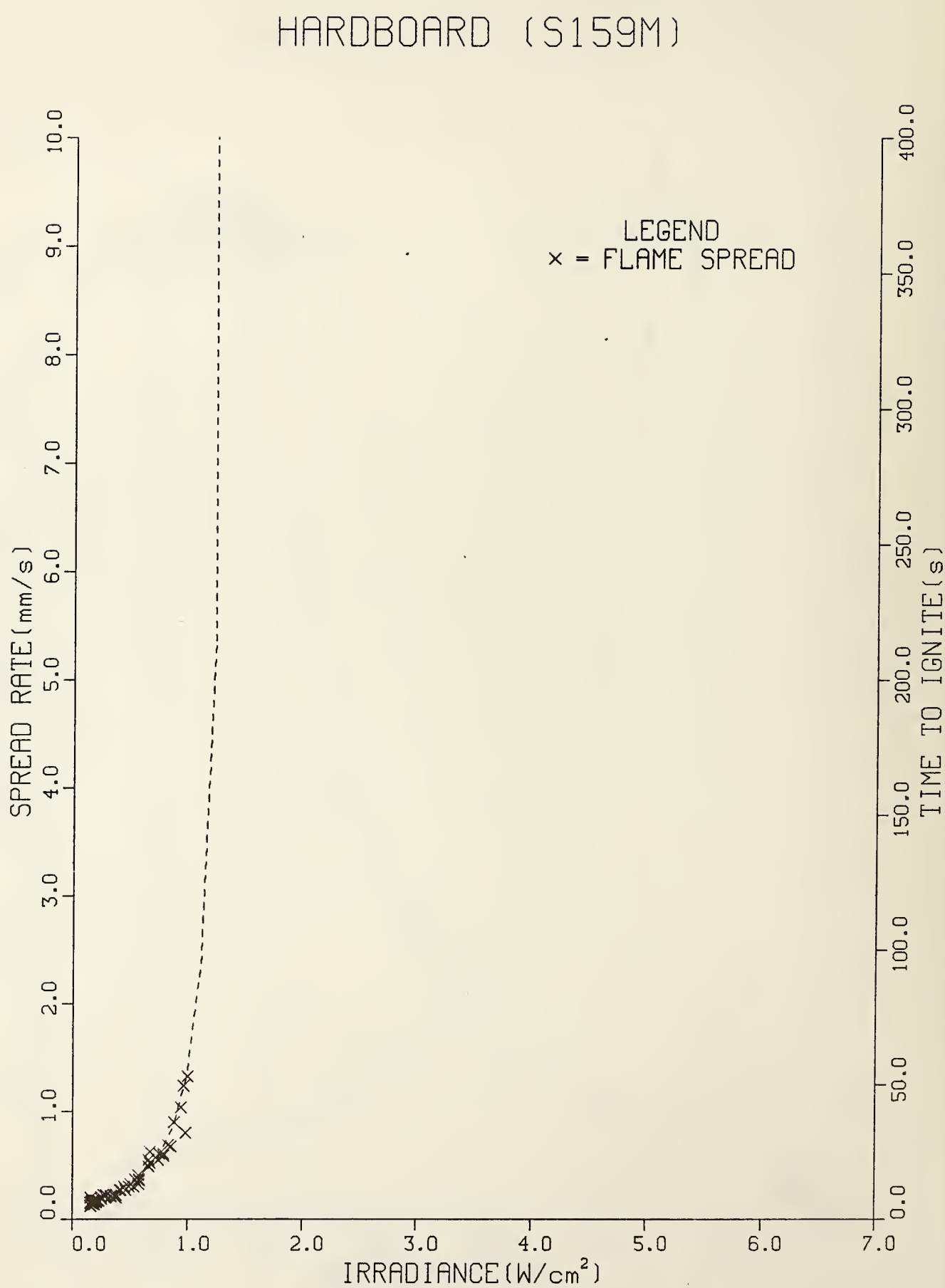

Figure C-9. Spread and ignition results for hardboard (S159M, 1.0 cm).

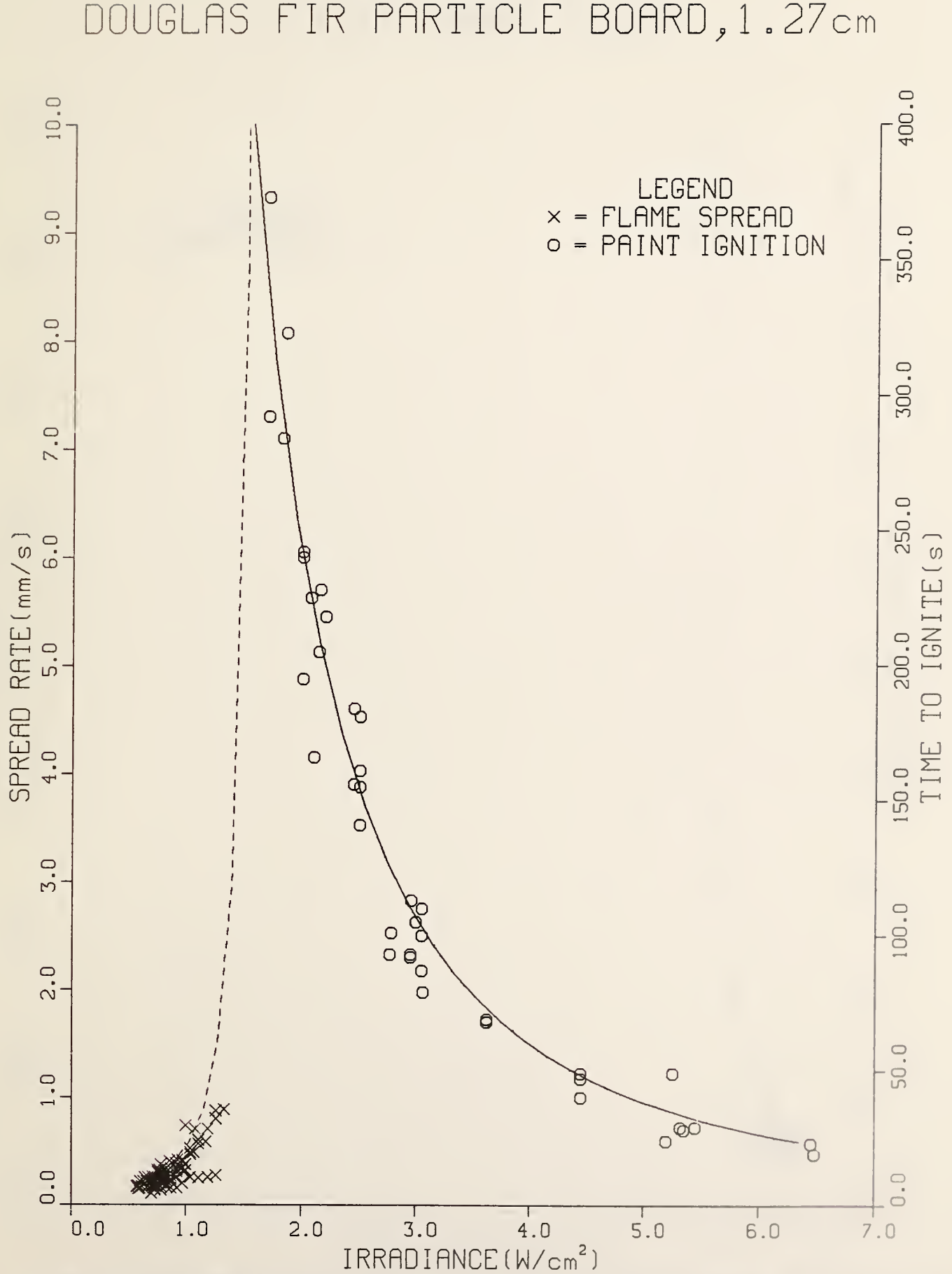

Figure C-10. Spread and ignition results for Douglas fir particle board (1.27 cm).

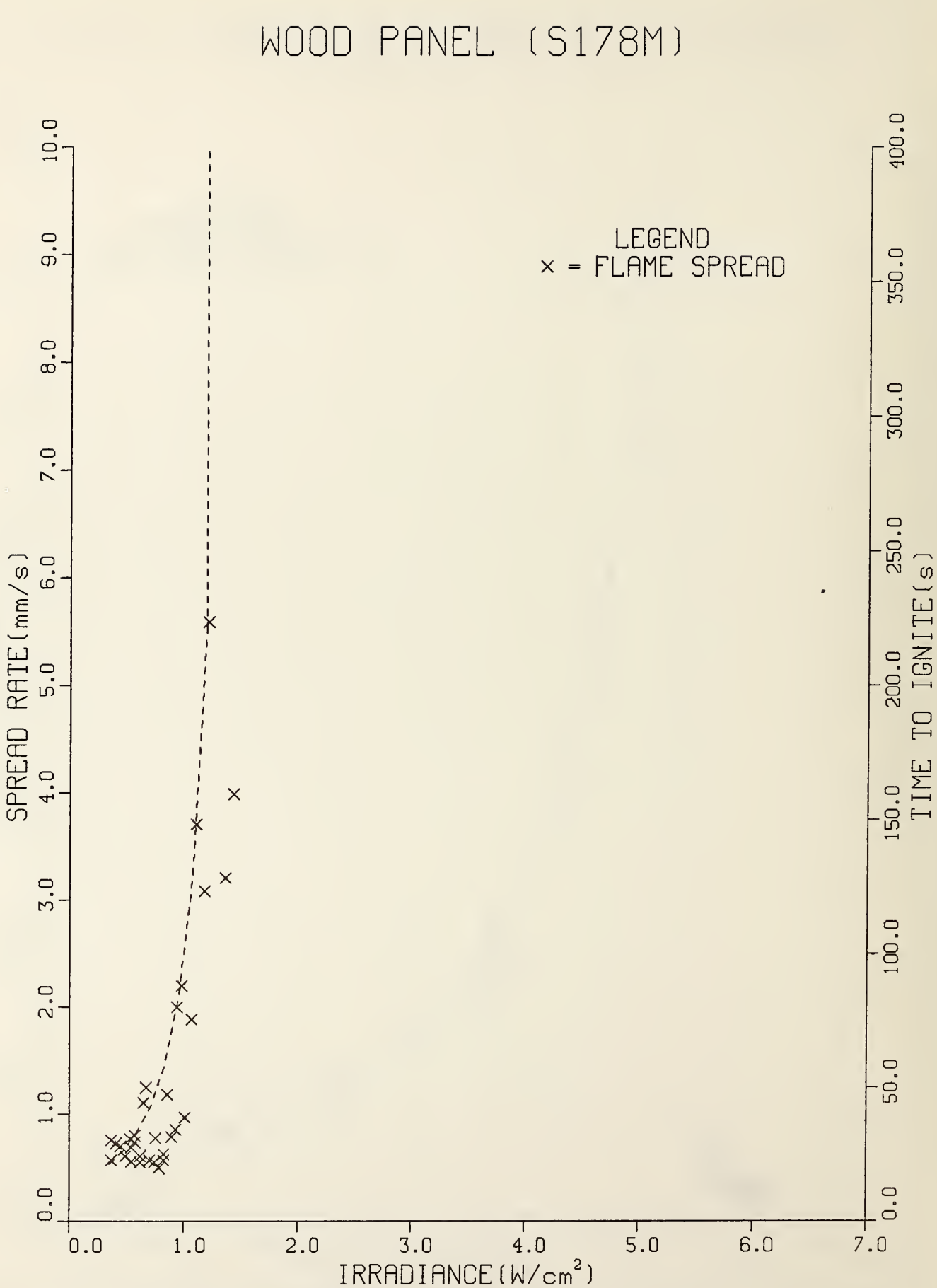

Figure C-11. Spread and ignition results for wood panel (S178M).

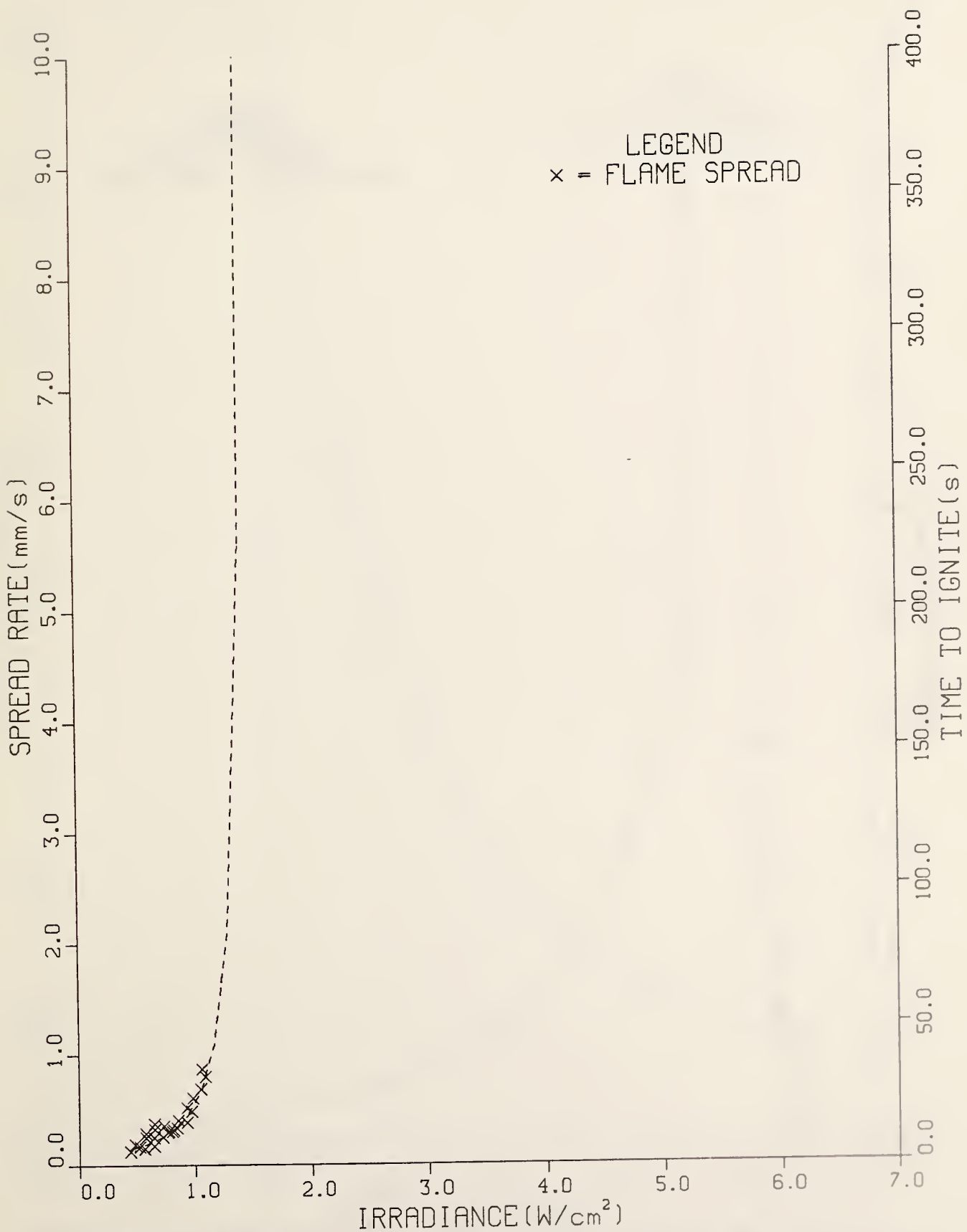

Figure C-12. Spread and ignition results for chipboard (S118M).

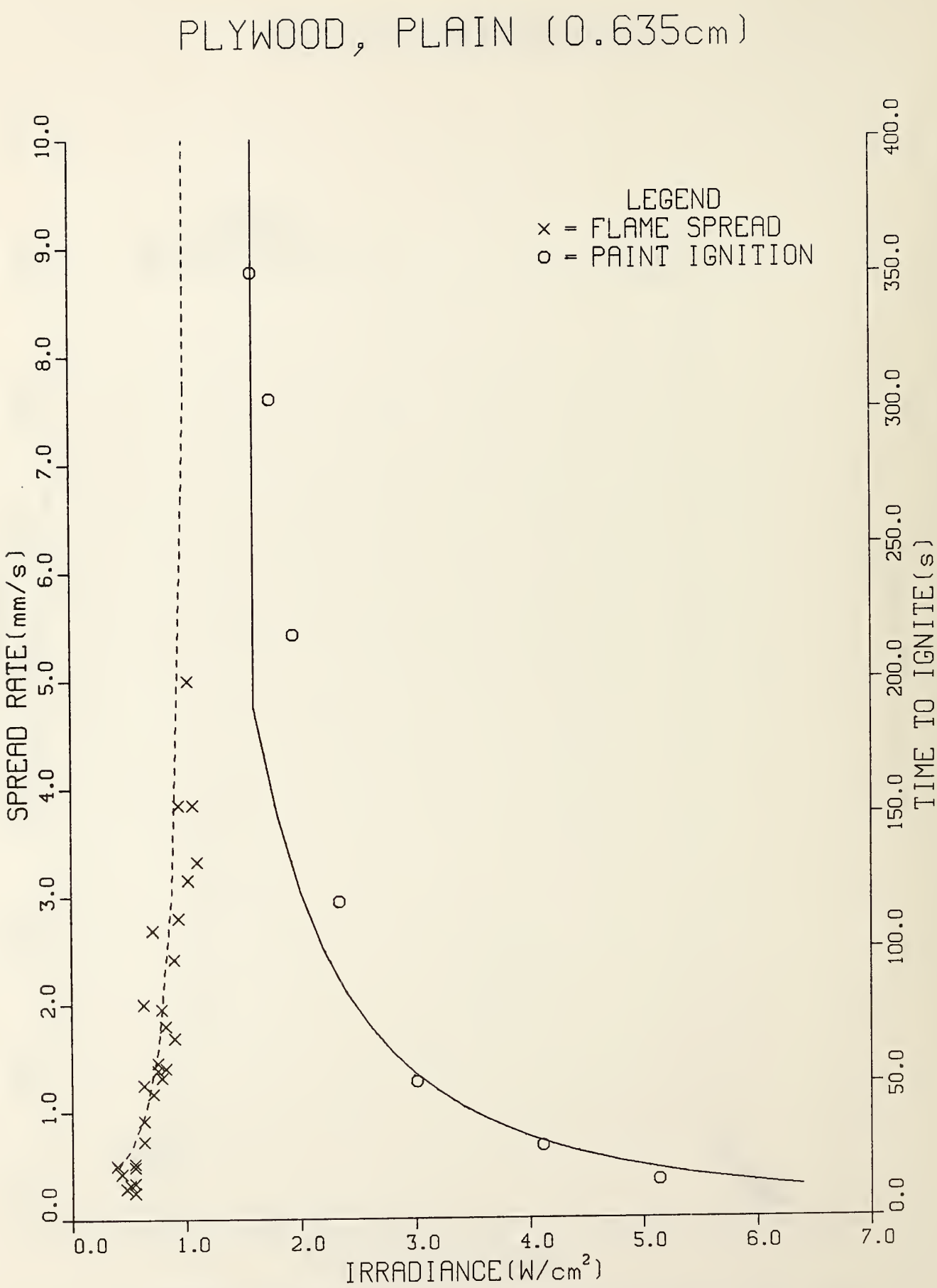

Figure C-13. Spread and ignition results for plywood, plain (0.635 cm).

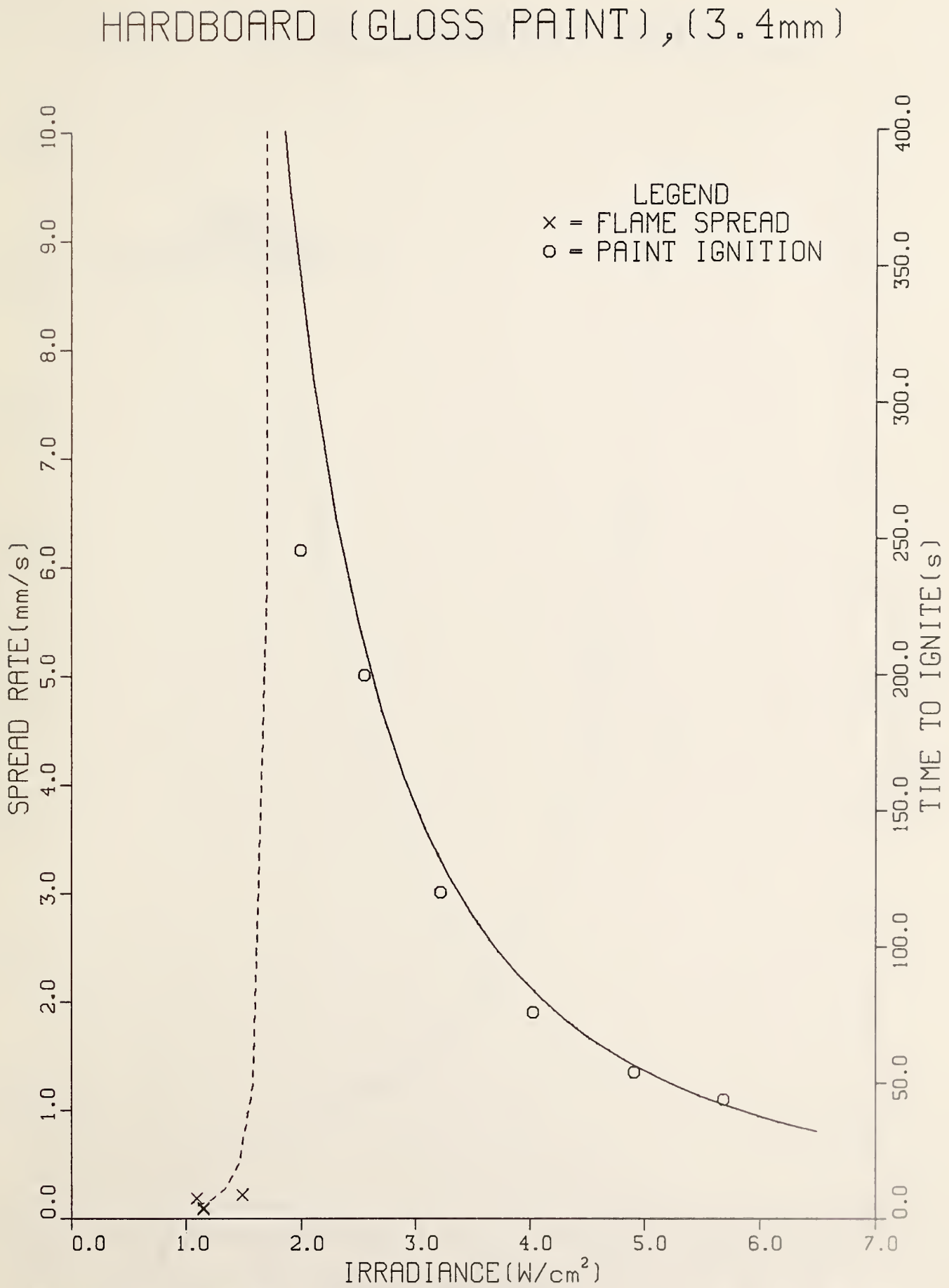

Figure C-14. Spread and ignition results for hardboard (3.4 mm, gloss paint).

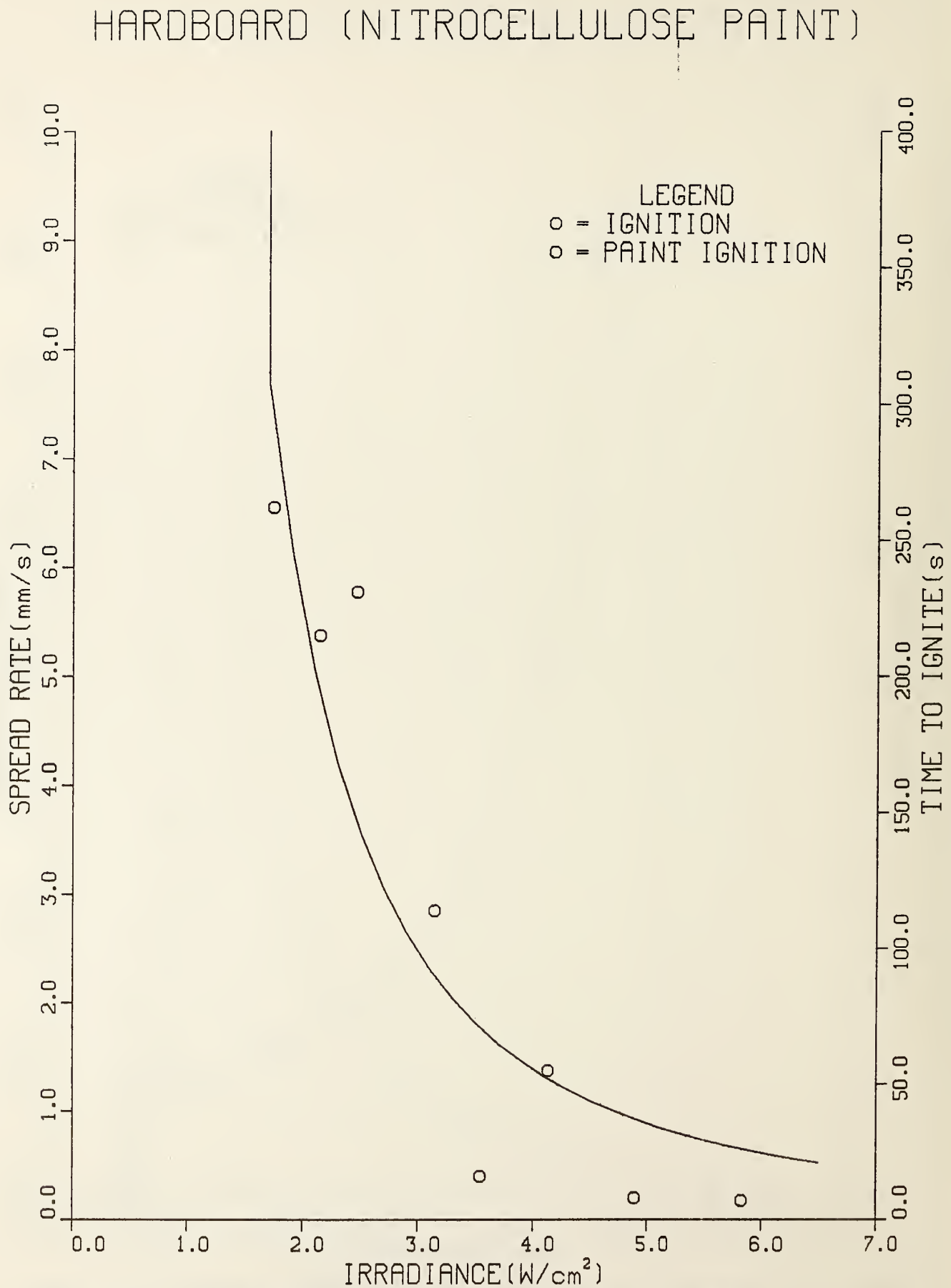

Figure C-15. Spread and ignition results for hardboard (3.4 mm, nitrocellulose paint).

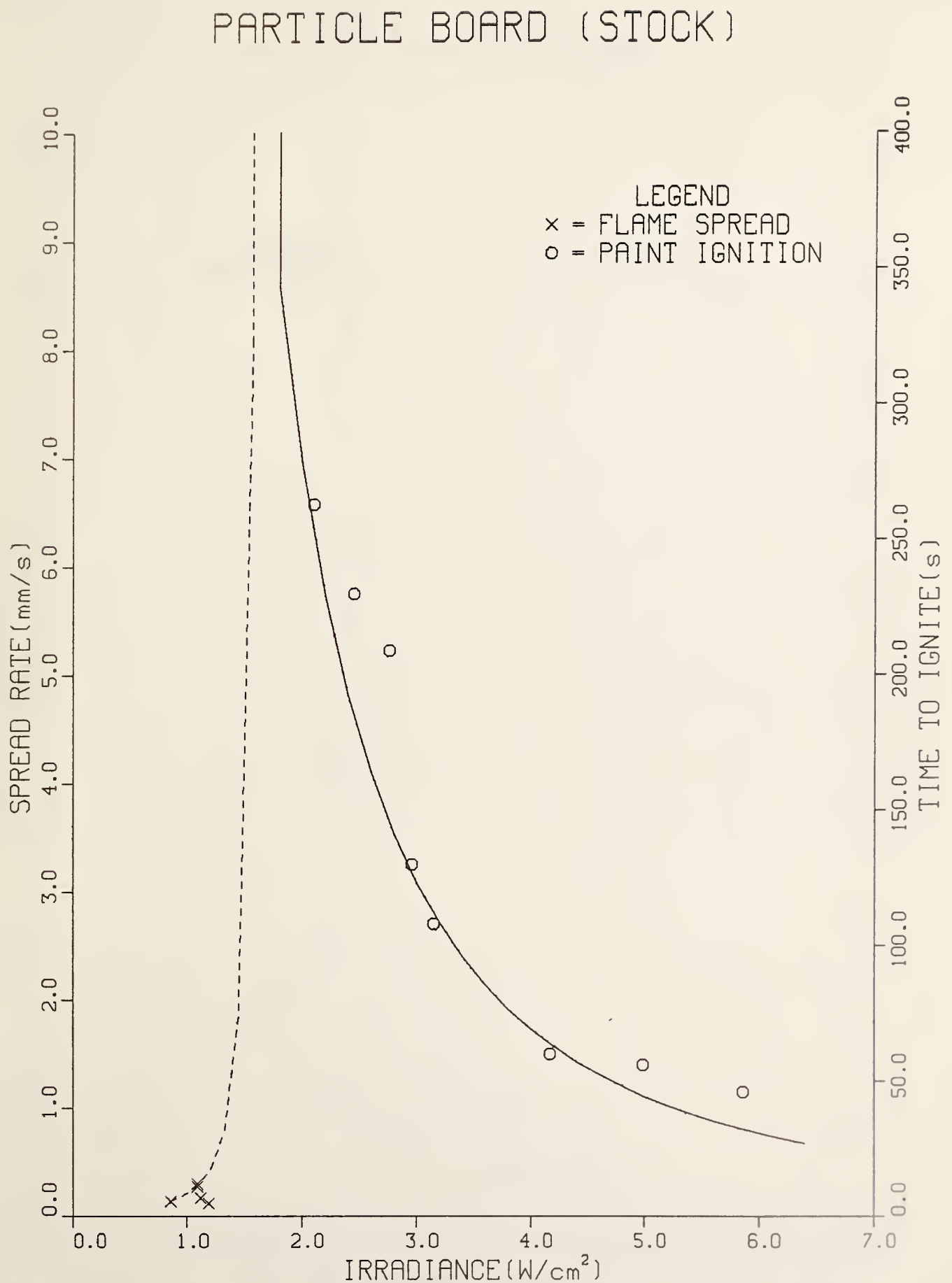

Figure C-16. Spread and ignition results for particle board (1.27 cm, stock).

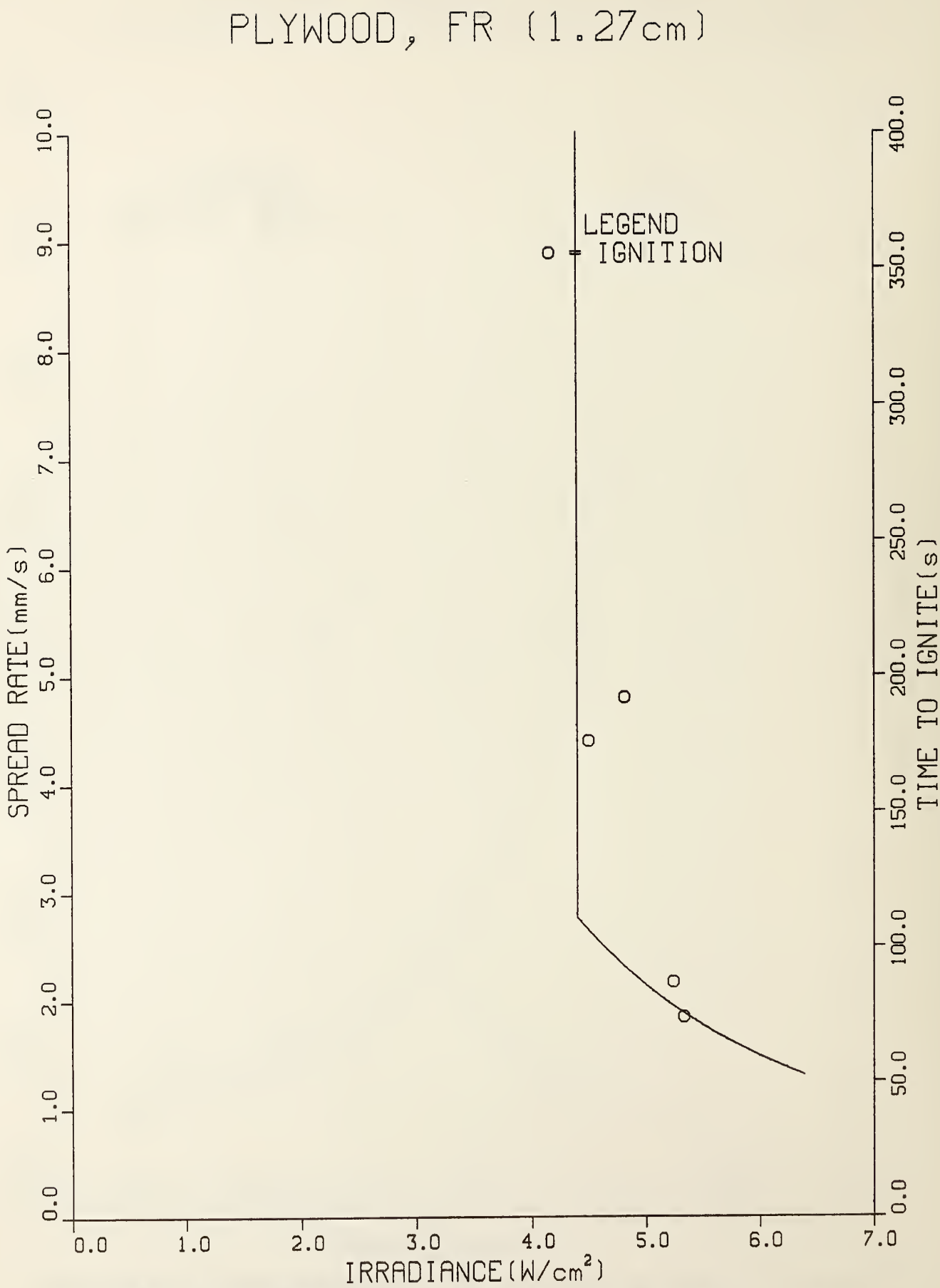

Figure C-17. Spread and ignition results for plywood, FR (1.27 cm).

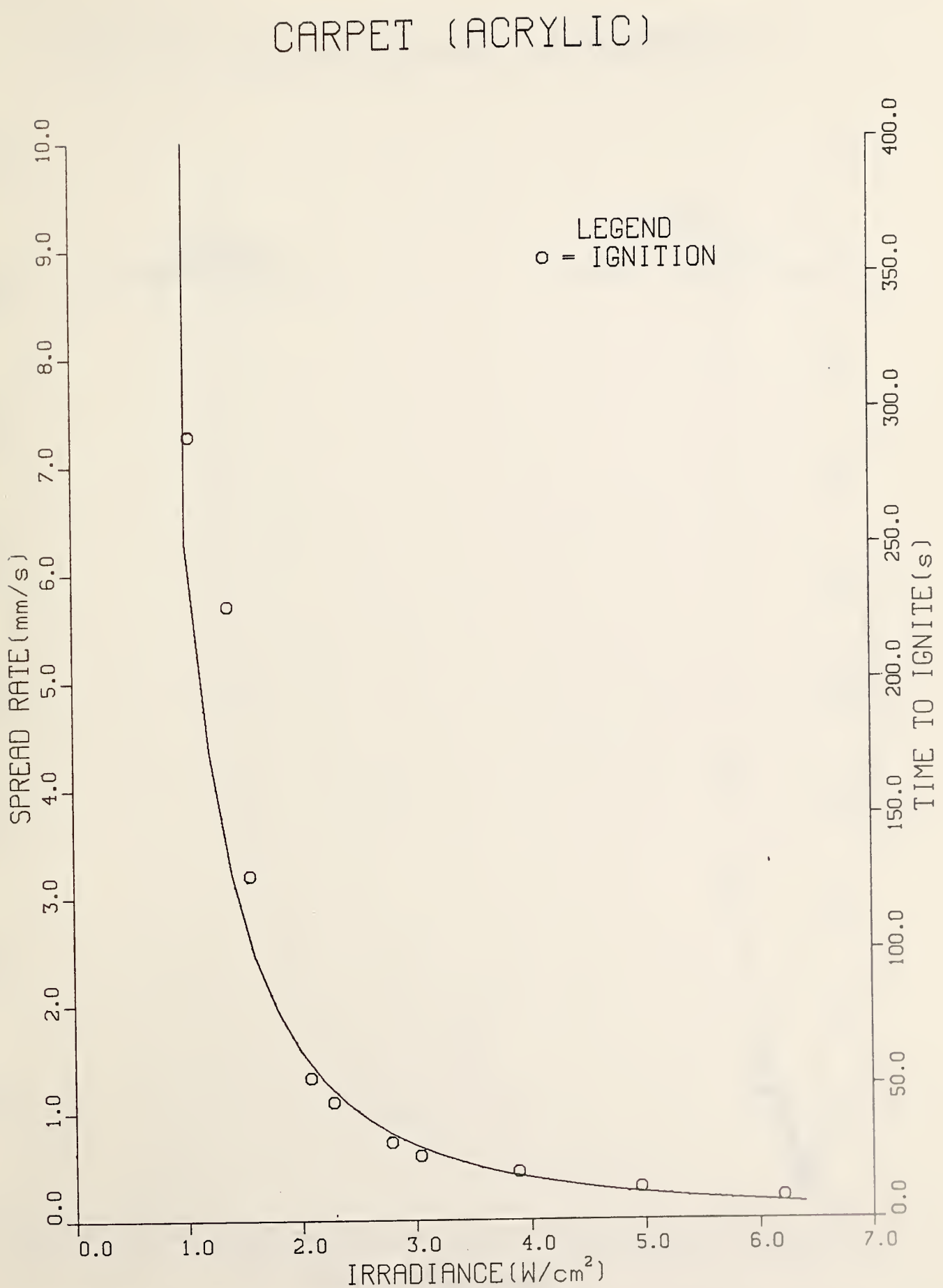

Figure C-18. Spread and ignition results for carpet (acrylic).

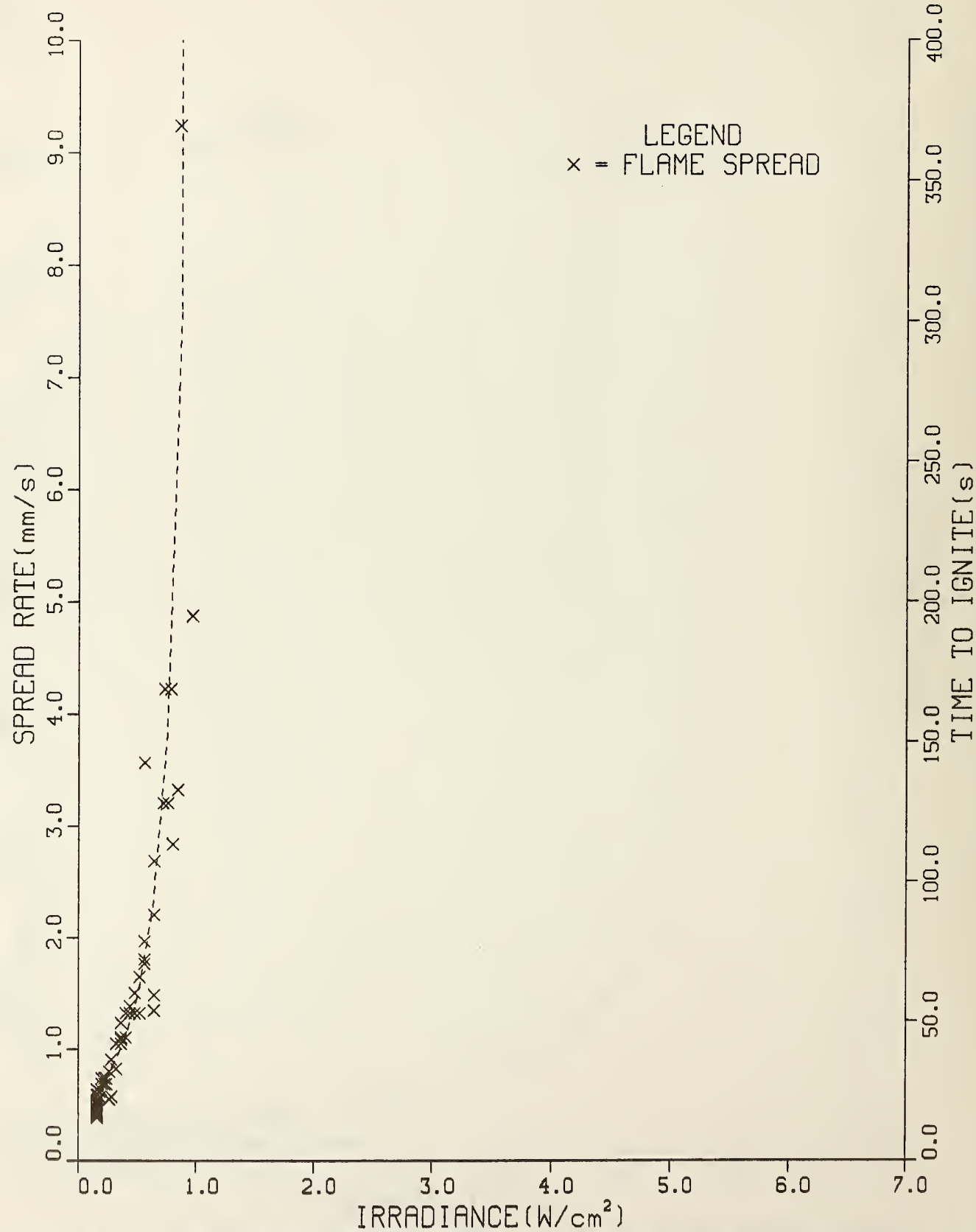

Figure C-19. Spread and ignition results for fiberboard, low density (S119M).

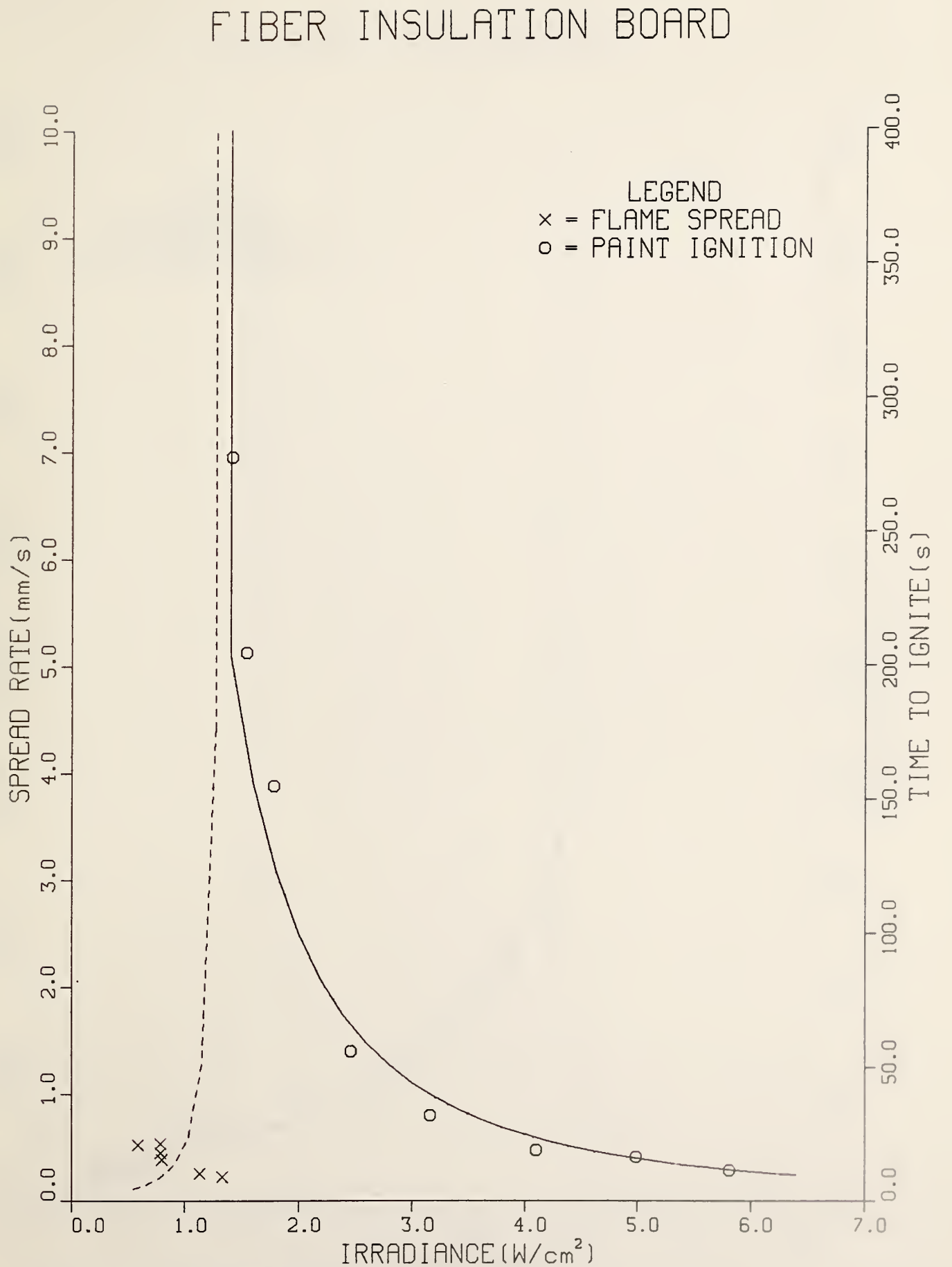

Figure C-20. Spread and ignition results for fiber insulation board.

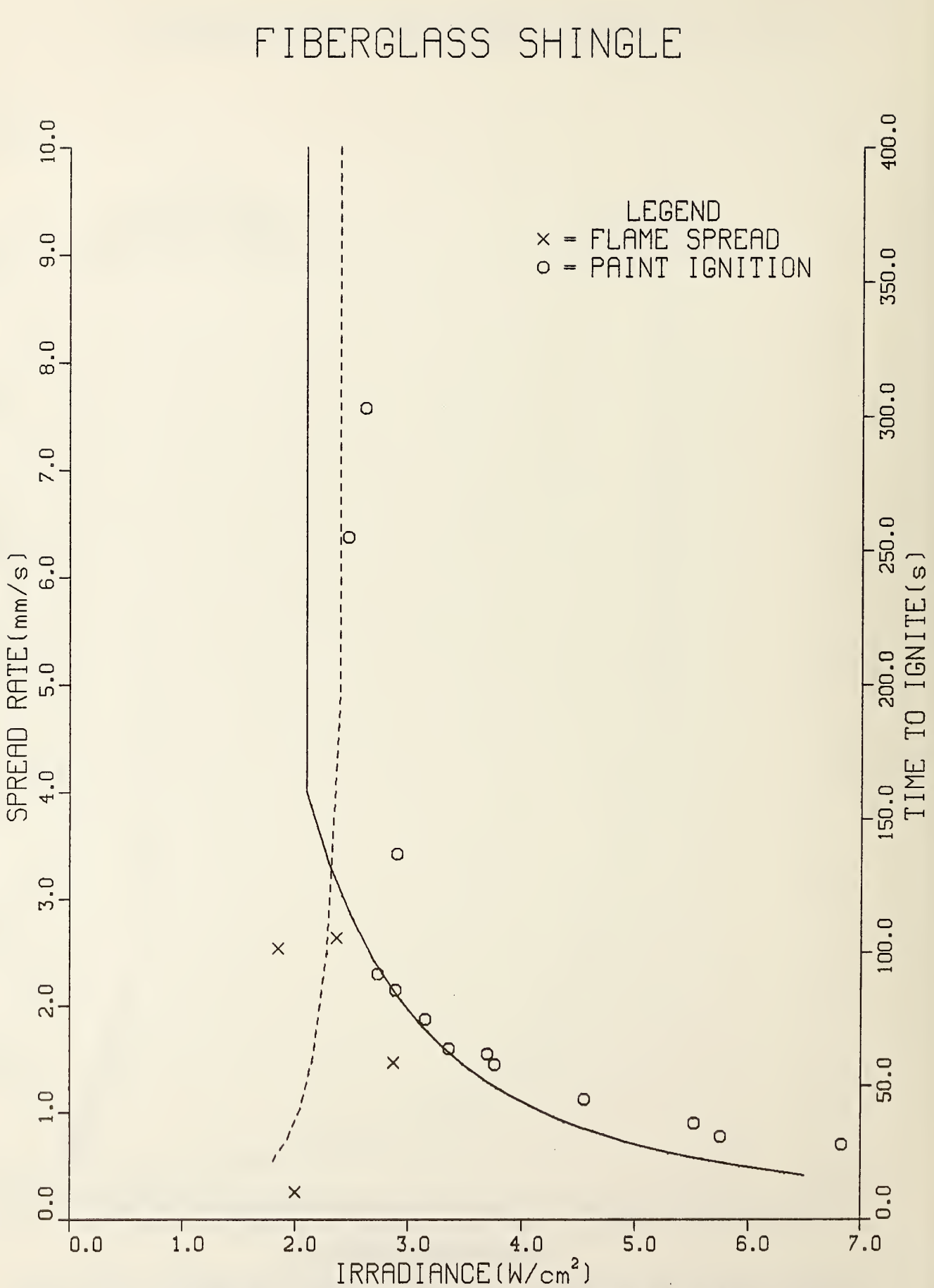

Figure C-21. Spread and ignition results for fiberglass shingle.

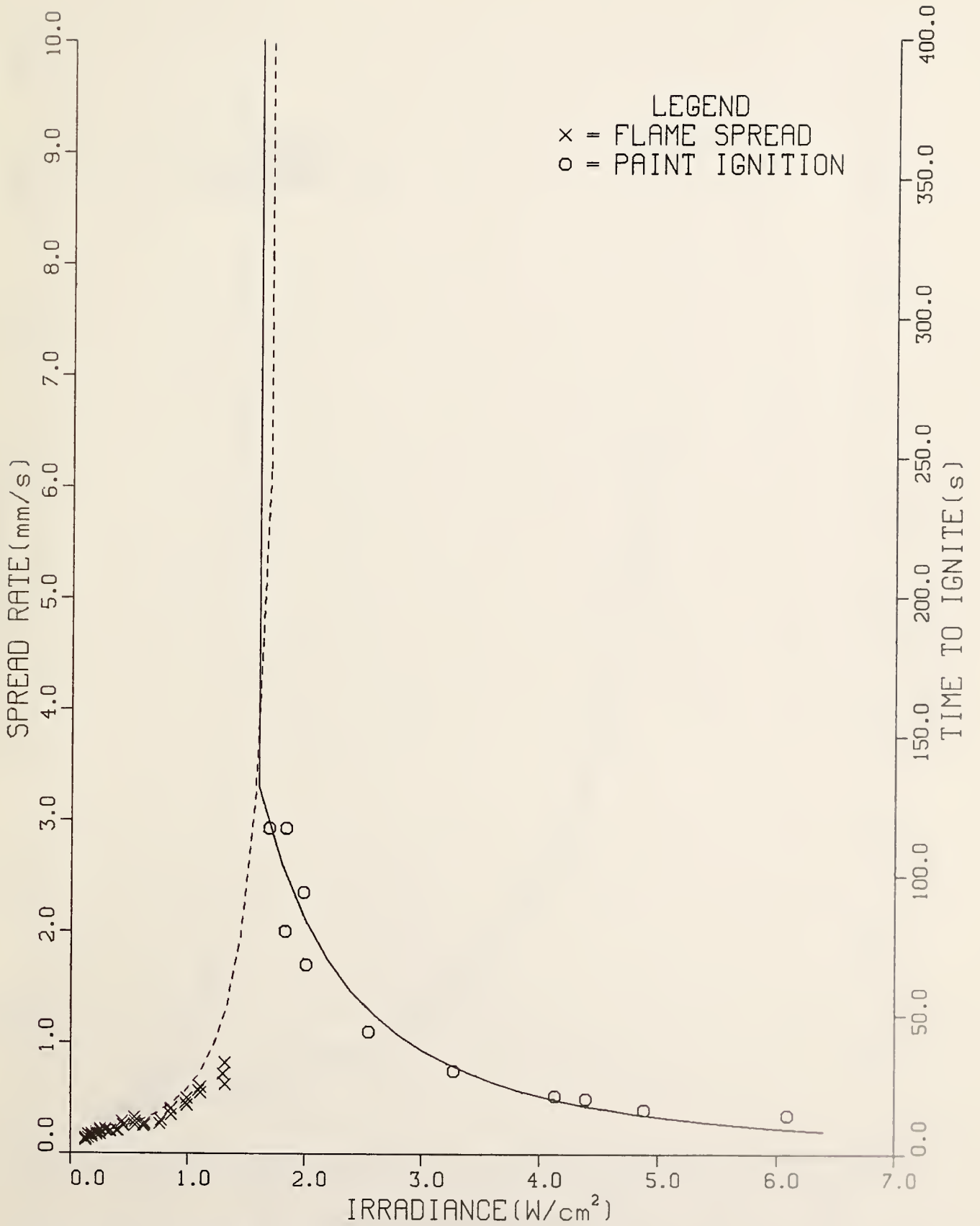

Figure 22. Spread and ignition results for GRP (2.24 mm).

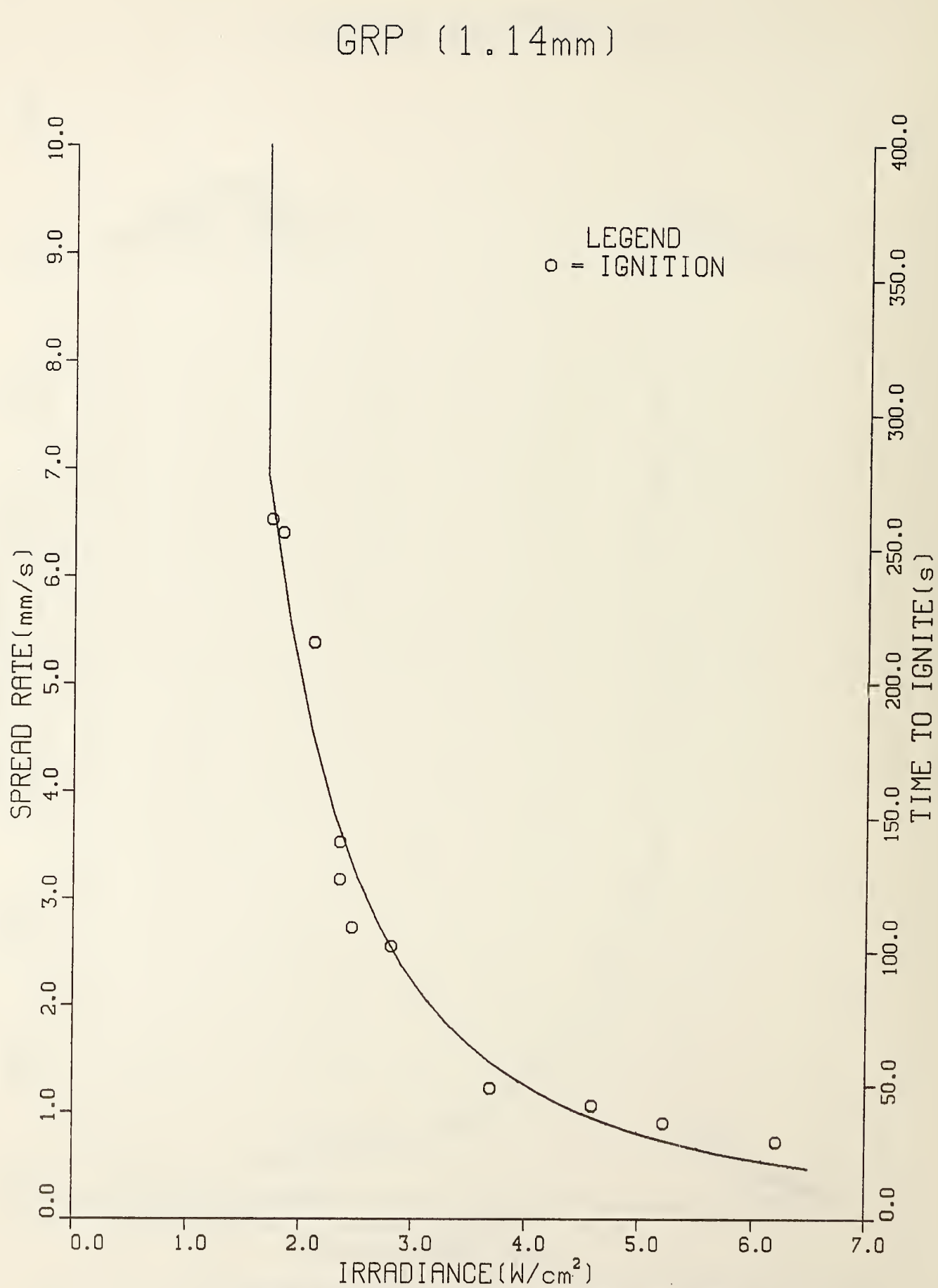

Figure C-23. Spread and ignition results for GRP (1.14 mm).

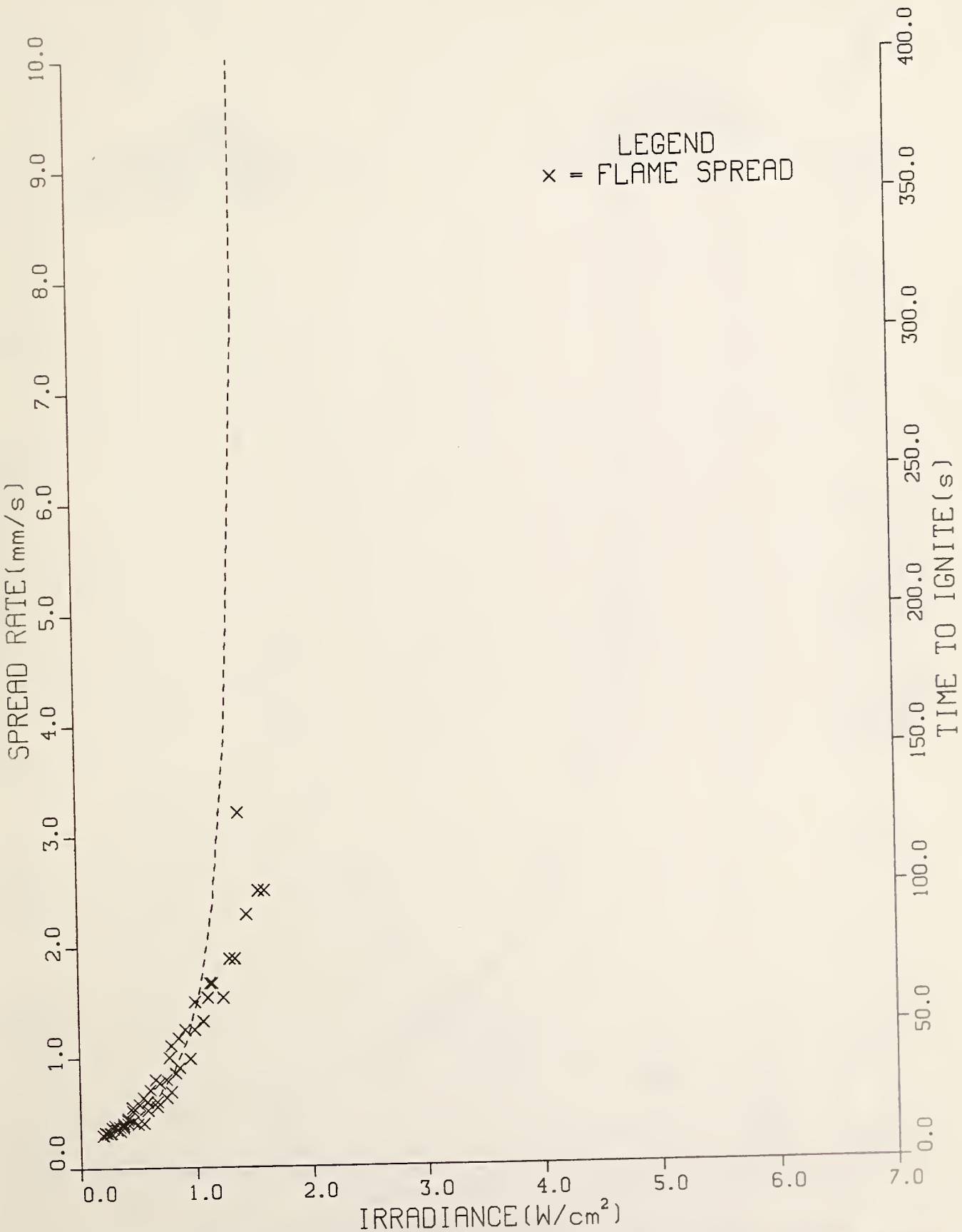

Figure C-24. Spread and ignition results for mineral wool, textile paper (S160).

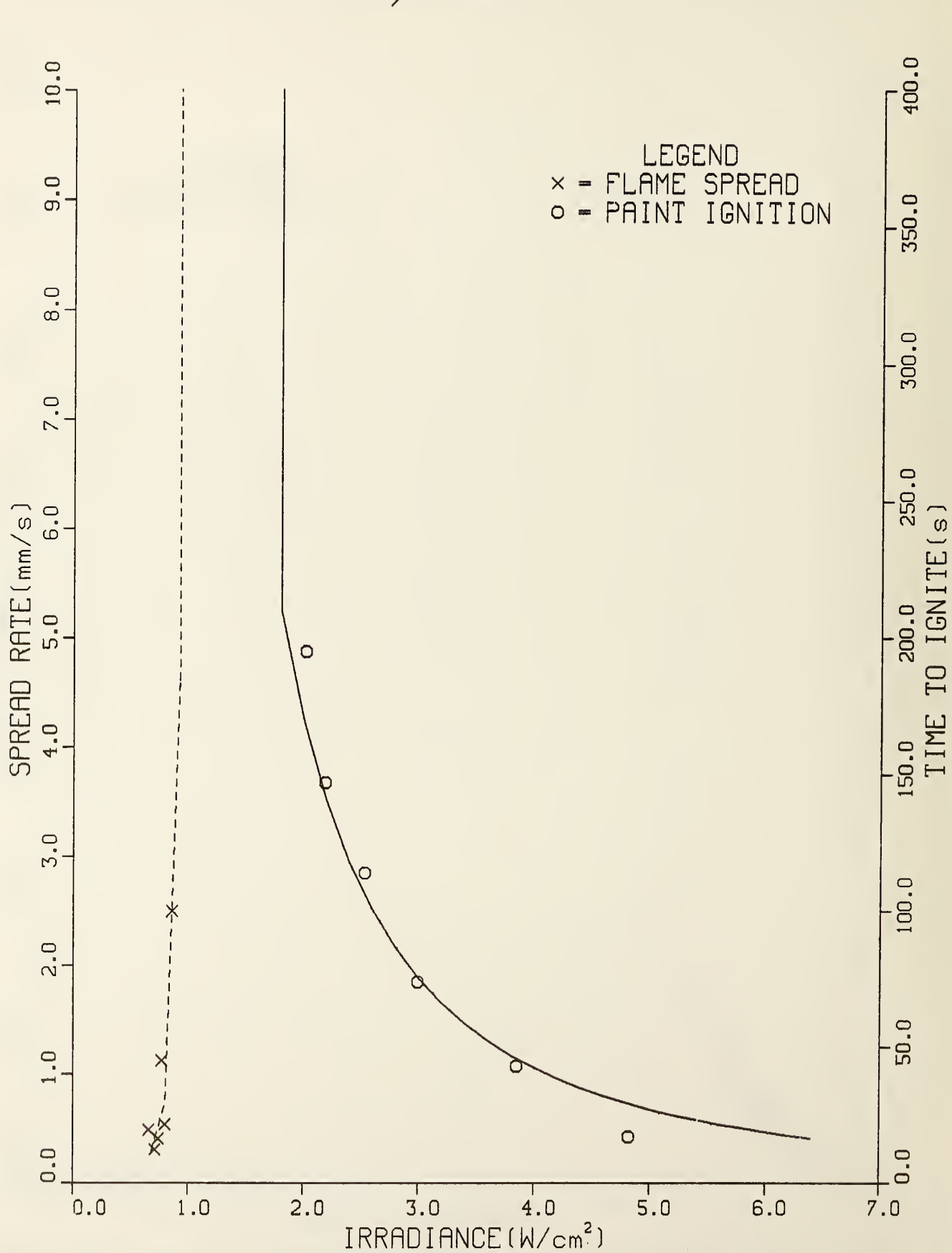

Figure C-25. Spread and ignition results for gypsum board, wallpaper (S142M).

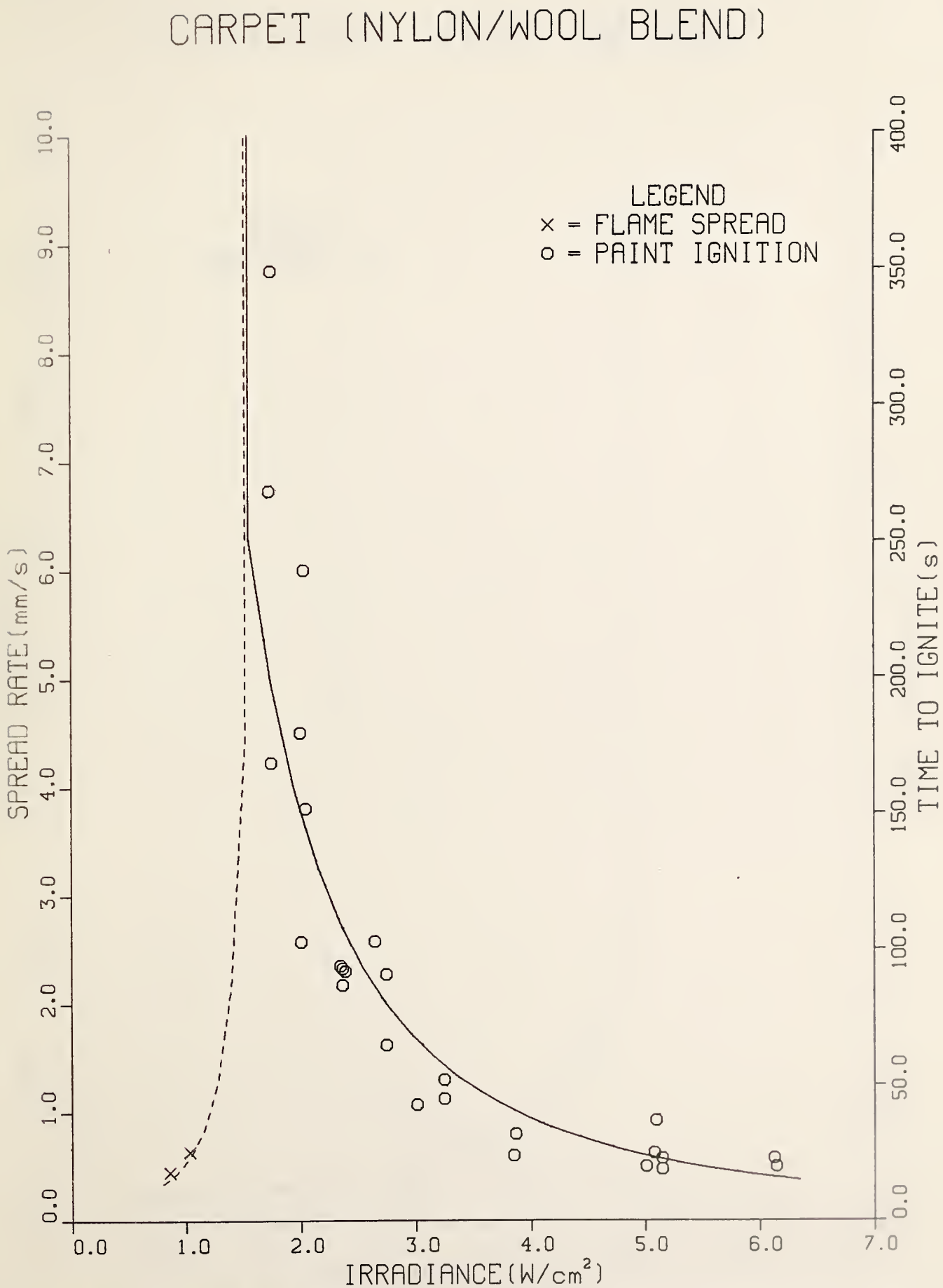

Figure C-26. Spread and ignition results for carpet (nylon/wool).

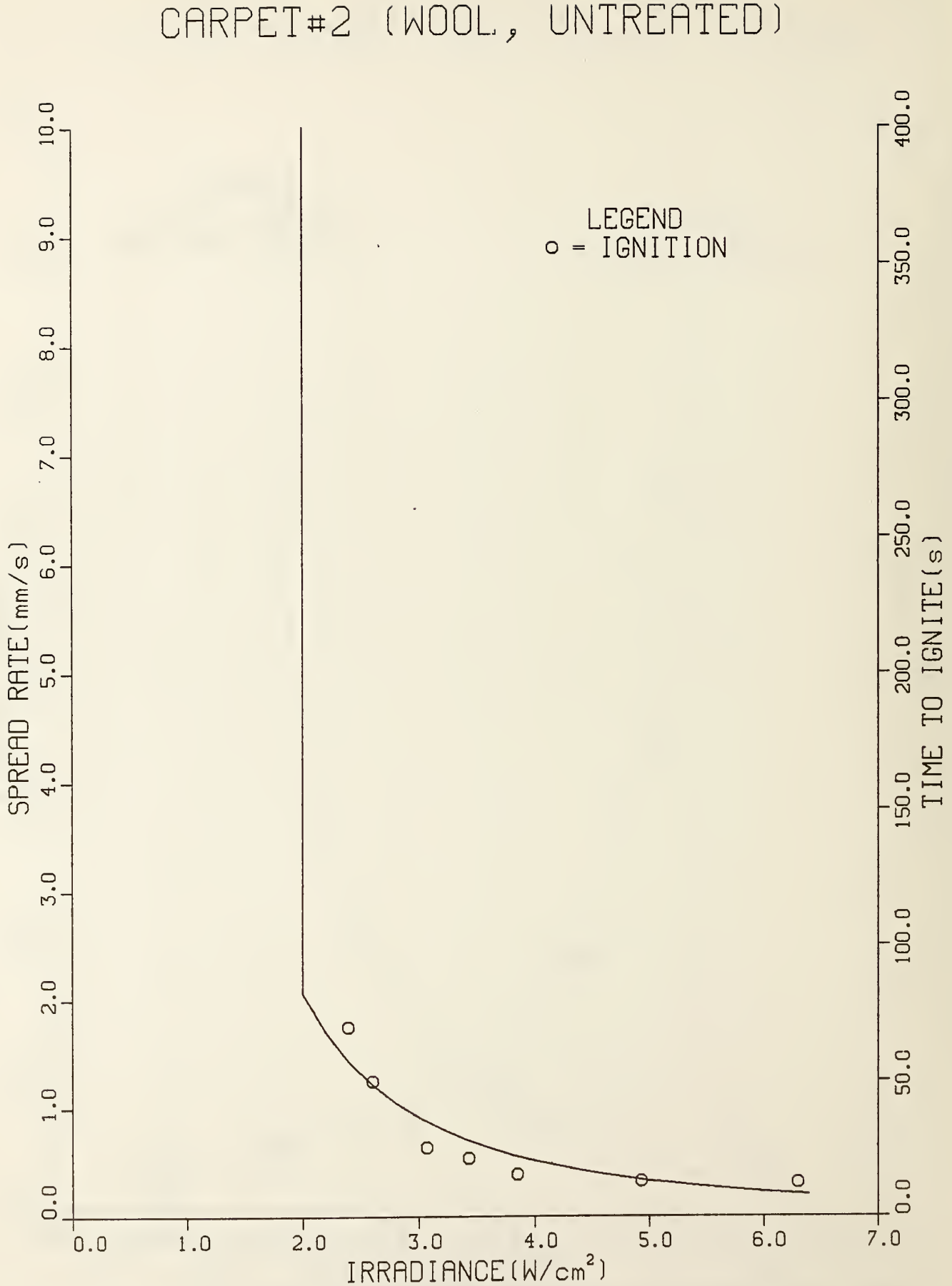

Figure Figure C-27. Spread and ignition results for carpet #2 (wool).

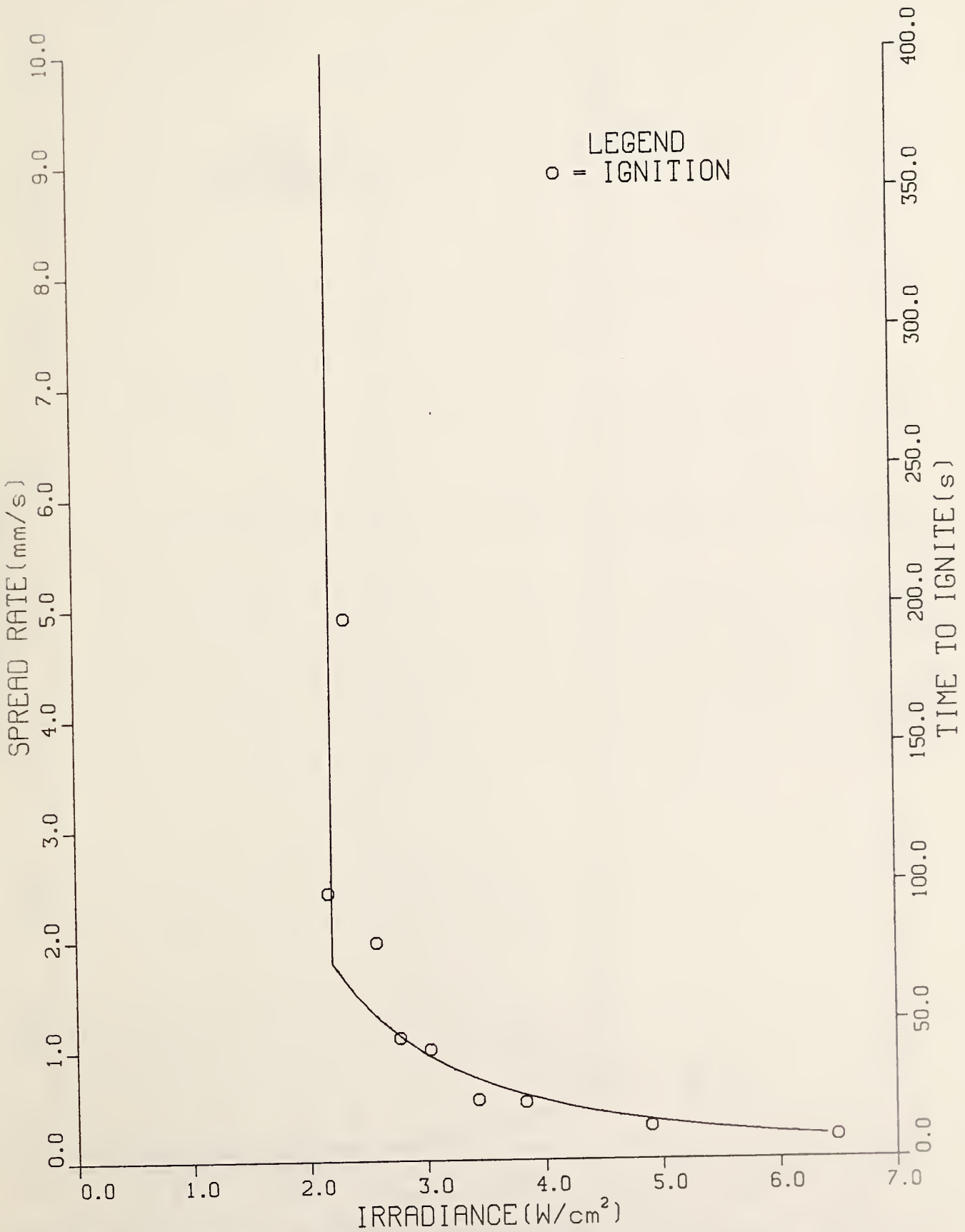

Figure C-28. Spread and ignition results for carpet #2 (wool treated).

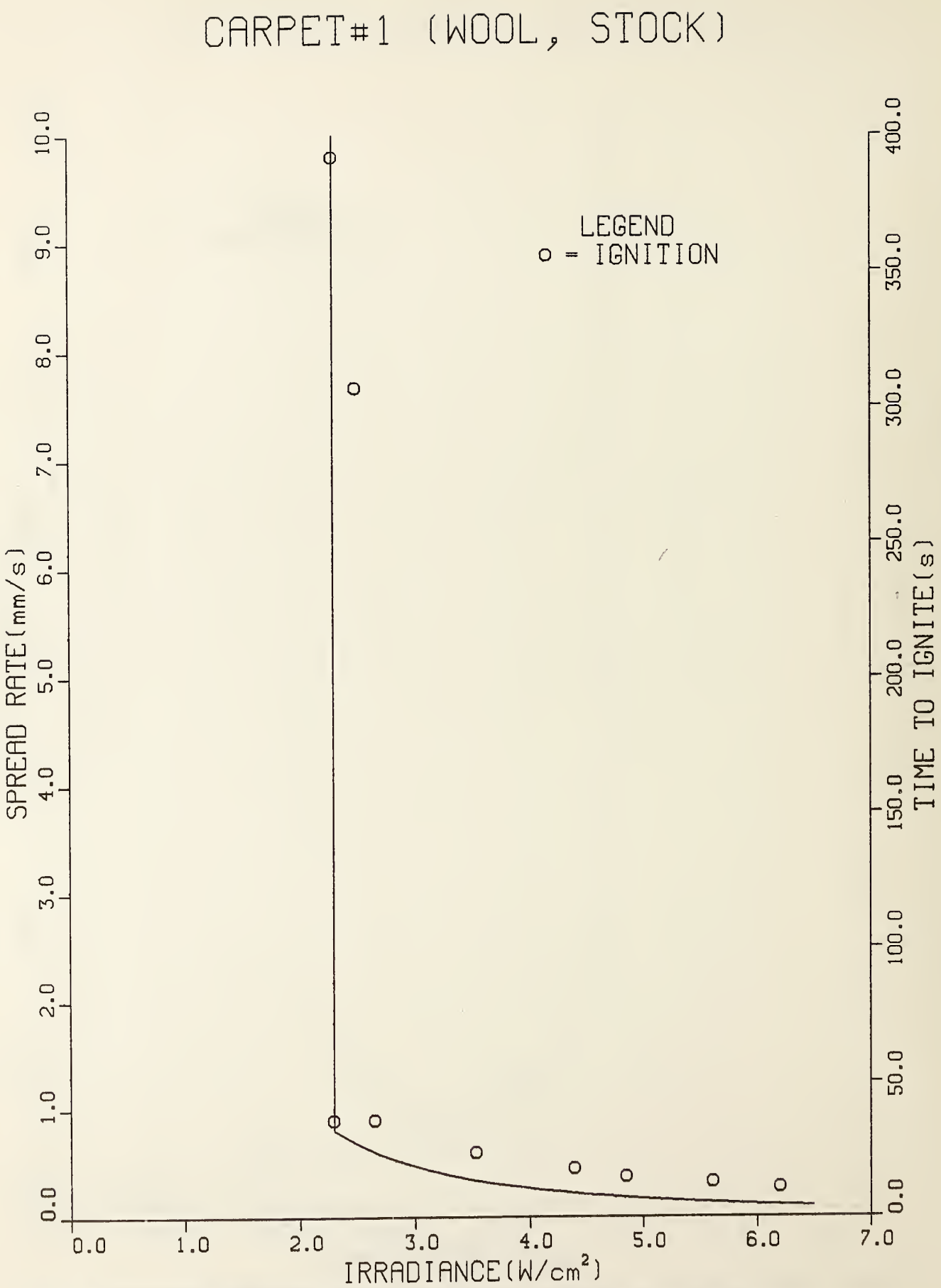

Figure C-29. Spread and ignition results for carpet #1 (wool, stock).

AIRCRAFT PANEL EPOXY FIBERGLASS

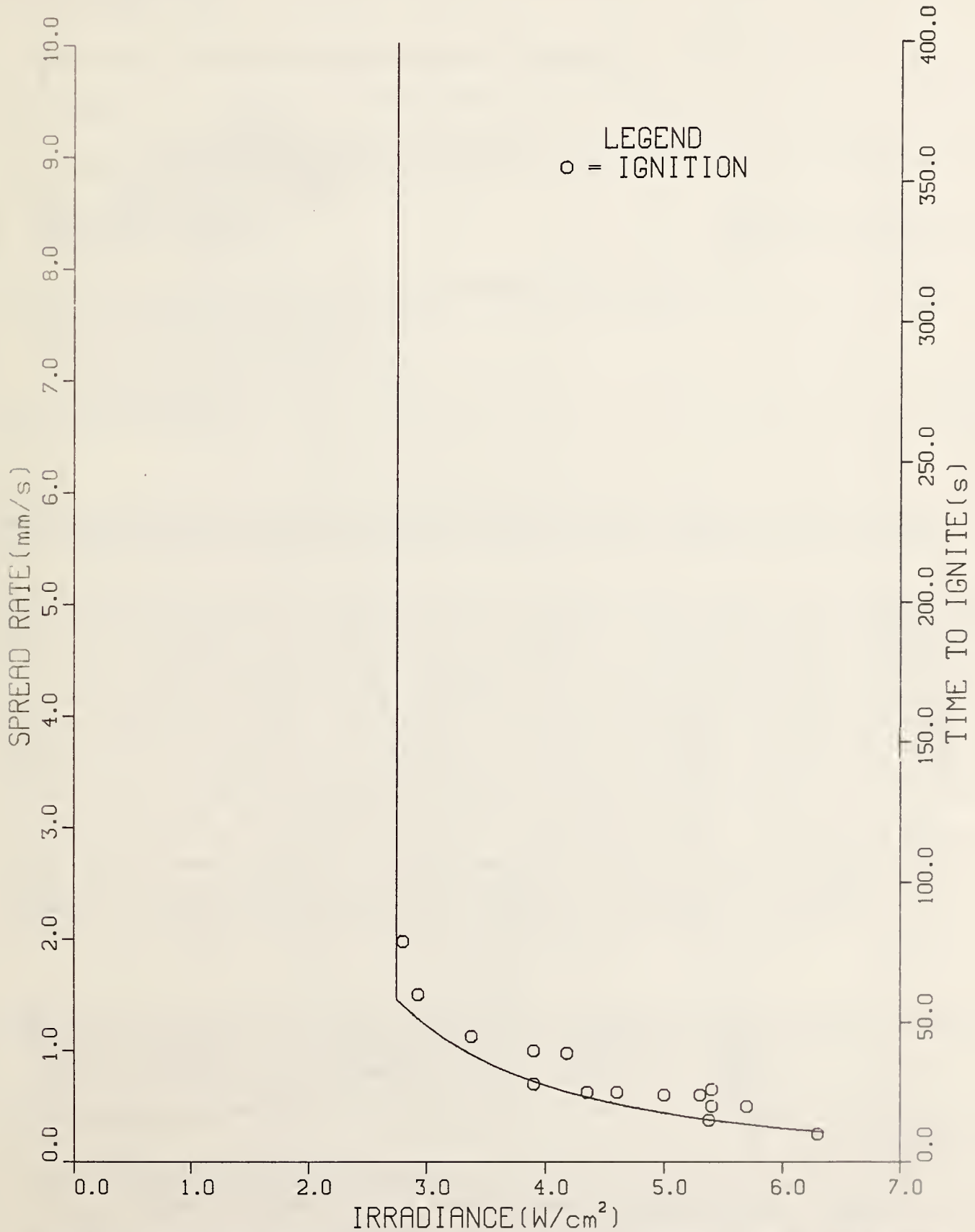

Figure C-30. Spread and ignition results for aircraft panel (epoxy fiberglass).

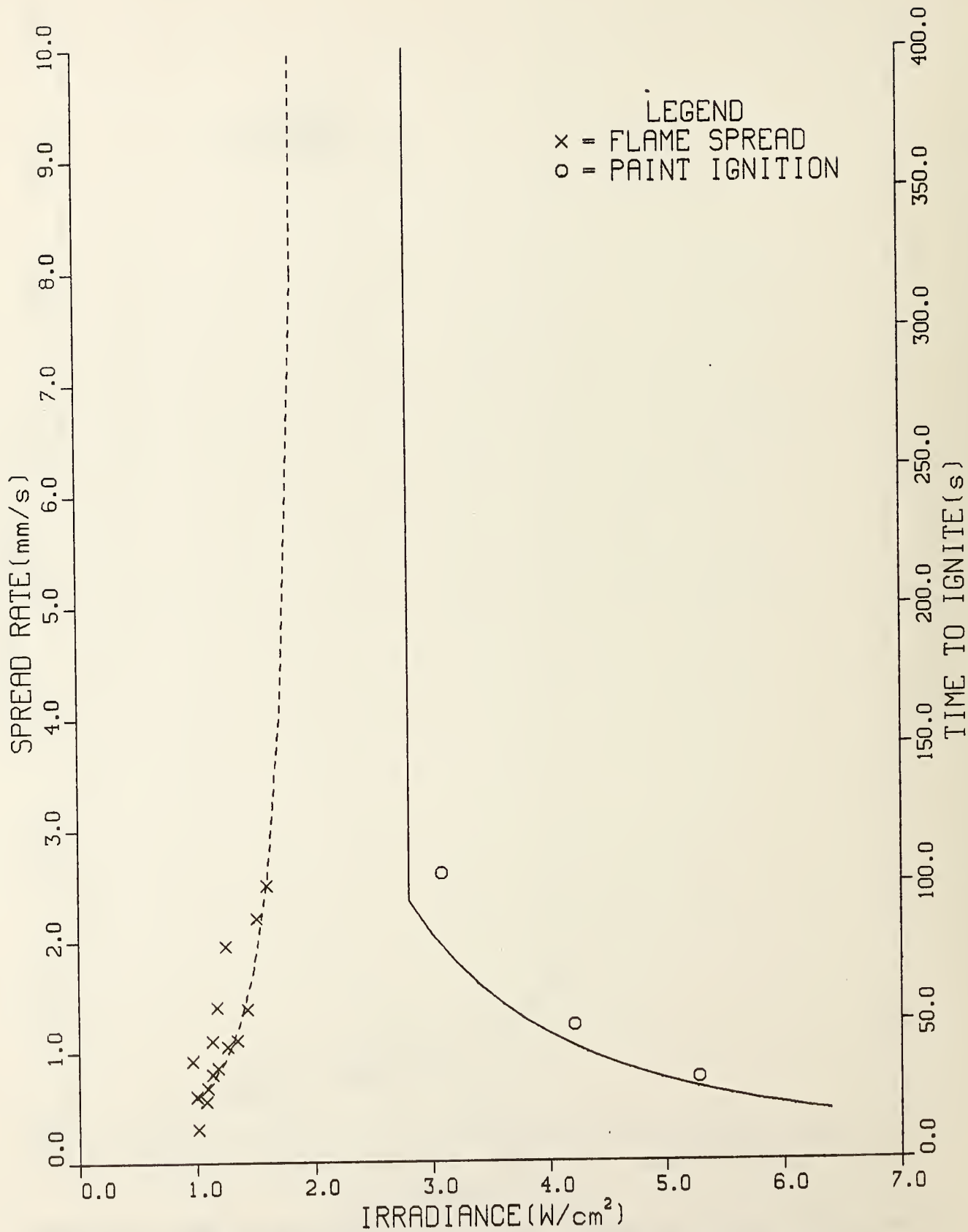

Figure C-31. Spread and ignition results for gypsum board, FR (1.27 cm).

NBS-114A (REV. 2-8C)

U.S. DEPT. OF COMM. BIBLIOGRAPHIC DATA SHEET (See instructions)	1. PUBLICATION OR REPORT NO. NBSIR 84-2943	2. Performing Organ. Report No.	3. Publication Date November 1984

4. TITLE AND SUBTITLE

New Concepts for Measuring Flame Spread Properties

5. AUTHOR(S)

J. G. Quintiere and M. Harkleroad

6. PERFORMING ORGANIZATION (If joint or other than NBS, see instructions)

NATIONAL BUREAU OF STANDARDS
DEPARTMENT OF COMMERCE
WASHINGTON, D.C. 20234

7. Contract/Grant No.

8. Type of Report & Period Covered

9. SPONSORING ORGANIZATION NAME AND COMPLETE ADDRESS (Street, City, State, ZIP)

U.S. Department of Transportation
Federal Aviation Administration
Technical Center
Atlantic City Airport, NJ 08405

10. SUPPLEMENTARY NOTES

☐ Document describes a computer program; SF-185, FIPS Software Summary, is attached.

11. ABSTRACT (A 200-word or less factual summary of most significant information. If document includes a significant bibliography or literature survey, mention it here)

An experimental procedure is described which can be used to derive data relevant to the prediction of ignition and flame spread on materials. The apparatus utilizes a radiant heat source capable of supplying up to 6.5 W/cm^2 to a vertically oriented specimen. The test results pertain to piloted ignition of a vertical sample under constant and irradiation, and to lateral flame spread on a vertical surface due to an external applied radiant heat flux. The results can be used to display the maximum velocity and ignition time as a function of irradiance. Critical or minimum irradiances for spread and ignition are determined. An empirical correlation, based on heat conduction principles, is found to correlate the ignition data and also provides a more general interpretation for the flame spread results. Further analyses of the data yield effective values for the thermal inertia of the material (kρc), its ignition temperature, and a parameter related to flame temperature. These parameters appear to be phenomenological constants for each material, rather than factors dependent on the apparatus. Results are presented for a wide range of materials. Suggestions for extending the results to other flame spread conditions are presented.

12. KEY WORDS (Six to twelve entries; alphabetical order; capitalize only proper names; and separate key words by semicolons)

carpets; composites materials; fire tests; flame spread; ignition; material properties; measurements; plastics; wood

13. AVAILABILITY

☒ Unlimited

☐ For Official Distribution. Do Not Release to NTIS

☐ Order From Superintendent of Documents, U.S. Government Printing Office, Washington, D.C. 20402.

☒ Order From National Technical Information Service (NTIS), Springfield, VA. 22161

14. NO. OF PRINTED PAGES

154

15. Price

$16.00

USCOMM-DC 6043-P80